Forschungszentrum Karlsruhe
Technik und Umwelt
Wissenschaftliche Berichte
FZKA 5929

Slow Heat-up PWR Test CORA-30: Test Results

S. Hagen, P. Hofmann, V. Noack, L. Sepold, G. Schanz, G. Schumacher

Hauptabteilung Ingenieurtechnik
Institut für Materialforschung
Institut für Neutronenphysik und Reaktortechnik
Projekt Nukleare Sicherheitsforschung

Oktober 1997

Forschungszentrum Karlsruhe
Technik und Umwelt
Wissenschaftliche Berichte

FZKA 5929

Slow Heat-up PWR Test CORA-30: Test Results

S. Hagen, P. Hofmann, V. Noack, L. Sepold,
G. Schanz, G. Schumacher

Hauptabteilung Ingenieurtechnik
Institut für Materialforschung
Institut für Neutronenphysik und Reaktortechnik
Projekt Nukleare Sicherheitsforschung

Forschungszentrum Karlsruhe GmbH, Karlsruhe
1997

Als Manuskript gedruckt

Forschungszentrum Karlsruhe GmbH
Postfach 3640, 76021 Karlsruhe

Mitglied der Hermann von Helmholtz-Gemeinschaft
Deutscher Forschungszentren (HGF)

ISSN 0947-8620

Abstract

Slow Heat-up PWR Test CORA-30: Test Results

The CORA out-of-pile experiments are part of the international Severe Fuel Damage (SFD) Program. They were performed to provide information on the damage development of Light Water Reactor (LWR) fuel elements in loss-of-coolant accidents in the temperature range 1200°C to 2400°C.

Test CORA-30 should investigate the fuel element damage behaviour with reduced initial heat-up rate of about 0.2 K/s compared to the normally used value of 1 K/s. The lower initial heat-up rate is representative for a loss-of-coolant accident which may develop after a shutdown of the reactor. The initial increase rate of the cladding temperature influences the thickness of the oxide layer reached at a given temperature. The thickness of the protective oxide layer influences the temperature time behaviour and the extent of the temperature escalation.

Test CORA-30 showed that the temperature escalation takes place also for an initial heatup rate of 0.2 K/s. The temperature at the start of the escalation was about 150 K higher than in tests with 1 K/s initial heatup. The increase rate of the temperature reached a maximum of about 2 K/s, a value much less than about 20 K/s reached for an initial temperature increase of 1 K/s. This result is important for accident management considerations.

The electric power input at the onset of the escalation was lower for CORA-30 by about 25% in comparison to the other CORA tests. In contrast to the comparable PWR tests, in which the temperature escalation proceeded downwards to 350 mm elevation, in test CORA-30 the escalation was confined to the upper half of the bundle with only a minor temperature increase to about 1250°C at 550 mm elevation.

In agreement with the axial temperature distribution the damage was limited to the upper half of the bundle. As a consequence of the longer oxidation period the absorber rod structure survived up to the 600 mm elevation, compared to 250 mm in equivalent PWR tests. This fact may be of interest for accident management considerations in connection to the criticality behaviour of a damaged core during reflood.

The liquefied material of the bundle relocated and formed two blockages between the axial elevations 500 mm to 620 mm and 800 mm to 870 mm. These elevations are 300 mm to 400 mm higher than in equivalent 1 K/s tests. The upper blockage was mainly formed by ceramic material and the lower one consisted preferentially of metallic material.

The maximum measured specific hydrogen production rate of 200 mg/s corresponds to a consumption of 27% of the steam introduced into the bundle. At the time of the escalation temperature peak the generated chemical energy is twice as large as the electric input. The totally produced hydrogen of 194 g corresponds to 20 % of the total energy input. Under the assumption that only the region with a temperature above 1400°C has contributed substantially to the oxidation, 194 g of hydrogen correspond to about 80% oxidation of the Zircaloy fuel rod cladding and shroud.

Zusammenfassung

DWR Versuch CORA-30 mit geringerer Aufheizrate: Versuchsergebnisse.

Die CORA-Out-of-pile-Experimente wurden im Rahmen des internationalen "Severe Fuel Damage" Programms durchgeführt. Sie sollten Informationen über die Schadensmechanismen bei Leichtwasser-Reaktor Brennelementen im Temperaturbereich von 1200°C bis 2400°C liefern.

Im Versuch CORA-30 sollte das Schadensverhalten der Brennelemente bei einem geringeren anfänglichen Temperaturanstieg von 0,2 K/s untersucht werden. Bei den meisten CORA-Versuchen betrug der anfängliche Temperaturanstieg des Hüllmaterials etwa 1 K/s. Der geringere Anstieg ist repräsentativ für Kühlmittel-verlust-Störfalle, die bei einem abgeschalteten Reaktor entstehen könnten. Die Geschwindigkeit des anfänglichen Temperaturanstiegs des Hüllmaterials bestimmt die Dicke der Oxidschicht bei der jeweils erreichten Temperatur. Die Stärke der schützenden Oxidschicht wiederum beeinflußt das Temperatur-Zeitverhalten und das Ausmaß der Temperatureskalation.

Der Versuch CORA-30 hat gezeigt, daß auch der langsame anfängliche Temperaturanstieg in eine Temperatureskalation einmündet. Die Temperatur zu Beginn der Eskalation lag ungefähr 150 K höher als in Versuchen mit einem anfänglichen Temperaturanstieg von 1 K/s. Die Temperatureskalation erreichte einen maximalen Wert von 2 K/s. Dieser Anstieg ist deutlich geringer als die 20 K/s Werte die beim üblichen anfänglichen Anstieg von 1 K/s erreicht wurden. Dieser kleinere Wert mag von Bedeutung bei Überlegungen zur Unfallbeherrschung sein.

Die elektrische Leistung beim Versuch CORA-30, die notwendig war um die "Starttemperatur" für die Eskalation zu erreichen, betrug ca. 25% weniger als bei den Tests mit einem Anstieg von 1 K/s. Im Vergleich zu den Standard-DWR-Versuchen, bei denen sich die Temperatureskalation bis zu 350 mm hinab ausbreitete, war im Versuch CORA-30 die Eskalation auf die obere Hälfte des Bündels beschränkt. In 550 mm Höhe bildet sich nur noch ein geringfügiger Temperaturanstieg auf 1250°C aus.

In Übereinstimmung mit dem axialen Temperaturprofil ist die Schadensentwicklung auf die obere Hälfte des Bündels beschränkt. Als Folge der längeren Oxidation blieb die Absorberstruktur bis zu einer Höhe von 600 mm erhalten im Vergleich zu 250 mm bei äquivalenten DWR-Standardtests. Dieses Verhalten ist wichtig für Überlegungen zum Kritikalitätsverhalten eines zerstörten Kerns beim Wiederfluten.

Die entstandene Schmelze erstarrte in zwei örtlich getrennten Blockaden von 870 mm bis 800 mm und von 620 mm bis 500 mm. Die Blockaden liegen damit 300 mm bis 400 mm höher als in den äquivalenten DWR-Versuchen. Die obere Blockade enthielt bevorzugt keramisches Material, während die untere im wesentlichen aus metallischen Komponenten bestand.

Die gemessene maximale Wasserstoffproduktionsrate von 200 mg/s entspricht einem maximalen Verbrauch des eingespeisten Dampfes von 27%. Die mit dieser Wasserstoffproduktionsrate verknüpfte chemische Energie ist doppelt so groß wie die zu diesem Zeitpunkt eingespeiste elektrische Leistung. Das Energieäquivalent der insgesamt erzeugten 194 g Wasserstoff entspricht etwa 20% der gesamt eingespeisten elektrischen Energie.

Unter der Annahme, daß nur Bereiche mit einer Temperatur über 1400°C an der Oxidation teilgenommen haben, entsprechen die 194 g H_2 einer Oxidation von etwa 80% des Zircaloy-Hüllmaterials und des Dampfführungsrohres in diesem Bereich.

Contents

1. Introduction

The TMI-2 accident has demonstrated that a severe fuel damage transient will not necessarily escalate to an uncontrolled core melt down accident if the design basis accident limits are exceeded. Therefore, comprehensive research programs have been initiated in various countries to investigate the relevant fuel rod bundle damage mechanisms that occur in an uncovered core, after an increase of temperature.

In the Federal Republic of Germany at the Forschungszentrum Karlsruhe (FZK) the Severe Fuel Damage (SFD) Program is now co-ordinated by the project Nuclear Safety Research (PSF) as successor of Project Nuclear Safety (PNS) and LWR Safety Project Group (PRS). As part of this program, out-of-pile experiments (the CORA-Program) were conducted at the Hauptabteilung Ingenieurtechnik (HIT). These experiments have been designed to provide information on the behaviour of Light Water Reactor (LWR) fuel elements under severe fuel damage (SFD) conditions up to meltdown. The results of the out-of-pile experiments can be used for the assessment of the SFD computer codes.

Within the framework of international co-operation the out-of-pile experiments are contributing confirmatory and complementary information to the results obtained from the limited number of inpile tests. The investigation of the basic phenomena of the damage process is supported by separate-effect tests.

The most important aspects concerning fuel rod failure and subsequent core degradation are the chemical interactions amongst the fuel element components in competition with the oxidation of the cladding in steam, which causes also the temperature escalation. Melt formation starts around 1200 °C by chemical interactions of the Inconel spacer grids and absorber materials (Ag, In, Cd) for PWRs and B_4C/stainless steel for BWRs with the Zircaloy cladding. The dissolution of the UO_2 pellets by liquid Zircaloy starts far below the UO_2 melting point.

Melt formation, relocation, blockage formation and finally fragmentation of fuel elements during reflooding characterise the degraded core and the potential of long term coolability. Furthermore the influence of internal pressure of the fuel rods (ballooning and bursting) and external pressure of the system (solid contact between pellets and cladding) on the bundle meltdown behaviour was investigated.

Further on, the investigation of the influence of pre-oxidation, initial heat-up rate, steam availability, water level in the bundle and bundle size was included in the program. The damage behaviour of WER fuel elements was the subject of the last two CORA-tests.

The tests performed in the CORA-facility are listed in the test matrix (Table 1). The original test matrix was directed towards the behaviour of PWR fuel elements only. In 1988 discussion showed that in most countries using nuclear energy, information on the behaviour of BWRs in severe accident conditions was needed. In consequence, five planned PWR experiments were replaced by BWR tests in the revised test matrix. Also the original sequence of tests was changed, as one can see from the test numbers.

In this report PWR test CORA-30 is discussed. In all CORA tests except of CORA-30 and CORA-31 the power input was chosen to start the test with an initial heat-up rate of about 1 K/s. This corresponds to the mean temperature increase of a core, if the accident develops from a reactor in operation. Probabilistic risk assessment studies have shown, that the probability for a loss of coolant accident starting from a reactor shutdown cannot be neglected. Starting from a shutdown reactor means less decay heat and with this a slower increase of temperature. The initial increase of the temperature influences the thickness of the oxide layer formed, when a given temperature is reached. The thickness of the protective oxide layer influences the time behaviour and the strength of the temperature escalation. The BWR test CORA-31 was run with an initial increase of 0.3 K/s. In test CORA-30 - discussed in this report - an initial rise of 0.2 K/s was foreseen.

2. Description of the CORA test facility

The CORA out-of-pile facility was designed to investigate the behaviour of LWR fuel elements under severe fuel damage accident conditions. In the experiments the decay heat was simulated by electrical heating. Great emphasis was placed on the fact that the test bundles contain the original materials used in light-water reactor fuel elements to investigate the different material interactions.

Pellets, cladding, grid spacers, absorber rods and channel box walls were typical of those of the investigated LWRs with respect to their compositions and radial

dimensions. In test CORA-30 the following PWR components were used: Original UO_2 pellets, Zry-4 cladding, Zry-4 and Inconel-718 spacer, and (80 Ag, 15 In, 5 Cd) absorber rods in stainless steel cladding and Zry-4 guide tubes.

Figure 1 gives a simplified flow diagram of the facility. The geometrical arrangement of the different CORA components is given in Figure 2. The central part of the facility was the fuel rod bundle. The bundle was enclosed in a Zry shroud with ZrO_2 fibre insulation. A high temperature radiation shield surrounded the bundle and shroud assembly, leaving an annular space for introduction of the quench cylinder. The bundle was connected to the power supply system at the upper and lower ends.

Below the bundle was the quench unit with a water filled quench cylinder, which can be raised around the bundle at a controlled speed. The cylinder was guided by three rods, which also connected the electric power to the bundle lower end.

The bundle upper end was fixed in the bundle head plate. The plate was connected by a funnel shaped tube to the surge condenser. The surge condenser was double-walled, leaving access to the bundle end fittings above the bundle head funnel.

The steam was produced in the steam generator, superheated and guided to the lower end of the bundle. The steam not consumed within the bundle was condensed in two parallel condensers and the hydrogen produced was fed into the off-gas system after dilution by air to a low H_2 concentration.

Bundle design:

The bundle and its surroundings are shown in Figure 3 and 4. The bundle horizontal arrangement is given in Figure 5 and the bundle components in Figure 6a. Characteristic data of the bundle are presented in Tables 2, 3 and 4. The bundle consisted of 16 heated rods, 7 unheated rods and 2 absorber rods inside the Zry guide tube.

The heated fuel rod simulator was sheathed with standard Zry-4 cladding tube, containing UO_2 annular pellets with a central heater. The heater consisted of a 1024 mm long tungsten rod (6 mm diameter), the upper electrode (300 mm molybdenum; 689-770 mm copper) and the lower electrodes (300 mm molybdenum; 183-219 mm copper). The electrodes have a diameter of 9 mm. The electrodes are flame-sprayed with 0.2 mm thick layer of ZrO_2. Large flexible copper cables provided

the connection to the electrical system. The resistance of the flexible cables to the points of voltage measurement for the determination of the power was less than 1 mΩ per rod (recommended value: 0.5 mΩ).

The resistivities R of tungsten, molybdenum and copper are given respectively in the following three equations:

$$R_w = 2.61 \bullet 10^{-2} + 2.63 \bullet 10^{-4} T_w + 2.20 \bullet 10^{-8} T^2_w$$

$$R_{Mo} = 2.29 \bullet 10^{-2} + 5.36 \bullet 10^{-5} T_{mo} + 1.38 \bullet 10^{-7} T^2_{Mo} - 2.22 \bullet 10^{-11} T^3_{Mo}$$

$$R_{cu} = 7.89 \bullet 10^{-3} + 9.90 \bullet 10^{-5} T_{cu} - 5.49 \bullet 10^{-8} T^2_{Cu} + 3.16 \bullet^{-11} T^3_{Cu}$$

with T in [Kelvin] and R in [$\Omega mm^2/m$].

The unheated fuel rod simulators consisted of solid UO_2 pellets and Zry cladding. The unheated rods extended to about -200 mm elevation, i.e. to about 20 mm above the initial water level of the quench cylinder (-220 mm). Zry-4 spacers were used at 880 mm and -5mm elevation and an Inconel 718 spacer of + 496 mm (Figure 3).

The absorber rods (Figure 6a) were built from original components: (80 Ag, 15 In, 5 Cd; wt%) absorber alloy in 10,2/11,2 mm stainless steel cladding. The rod was surrounded by the 12,2/13,8 mm Zry-4 guide tube.

The fuel rod simulators and the absorber rods were screwed into the bundle head plate, sealing it hermetically. The bundle head plate thus gave the fixed elevation for the axial thermal movement of the rods.

For upper end bundle cooling the heated rods (the copper electrode inside the Zry-4 cladding) and the connectors for the pressure capillaries and the thermocouples of the unheated rods were surrounded by water. The water was cooled by a heat exchanger. Argon was blown against the lower surface of the plate to protect the sealing in the bundle head plate.

At the lower end the heated fuel rod simulators were cooled by the water of the quench cylinder. The initial water level was at the -220 mm elevation. The unheated rods were in contact with the water of the quench cylinder only by the thermocouple connections. The gross volume of water inside the quench cylinder (230 mm ID) was about 70 l.

The bundle was surrounded by a Zry-4 shroud of 1.22 mm thickness. The shroud conducted the steam through the bundle. The steam entered at an orientation of 180° into the lower end (0 mm elevation). To minimise the heat losses form the shroud, it was surrounded by a 19 mm (0.75 inch) thick insulating layer of ZrO_2 fibre. On account of the low heat conductivity and heat capacity of the ZrO_2 fibre the shroud temperature could follow the bundle temperature closely. The shroud participated in the interaction with steam. The resulting oxidation energy contributed substantially to bundle heat-up.

The connection between steam inlet at 0 mm elevation and shroud was made by a stainless steel steam distribution tube. This tube extended down into the water of the quench cylinder thus forming a lower closure. The time history of the water level in the quench cylinder showed that there is no net condensation of steam in the quench cylinder.

At an elevation of 36 mm the steam distribution tube joined into the shroud. From here the shroud extended in vertical direction for 1231 mm and the insulation for 1036 mm. At 6 elevations (390 mm to 890 mm) windows of 40 mm x 30 mm in the shroud and shroud insulation allowed the bundle inspection by the video systems.

The annuli between the shroud and the high-temperature shield on one hand and high temperature shield and pressure containment of the other hand were closed at the upper end by fibre ceramic layers of 38 mm thickness.

High temperature shield:

To keep the heat losses as low as possible, the bundle was surrounded by an additional high temperature shield (HTS). The vertical and the horizontal cross-sections of the high temperature shield are given in Figures 3 and 4. The high temperature shield consisted mainly of ceramic fibre plates. The inner layer of plates consisted of ZrO_2, and the outer layer of Al_2O_3. The fibre ceramics were excellent insulators and had a low density which resulted in a low heat capacity. The thermal shock behaviour of the fibre ceramics was also extremely low.

The mechanical strength of the high temperature shield was ensured by external walls of stainless steel (0.9 mm). The fibre ceramic plates were attached to the stainless steel cover by ceramic nails. The inner ZrO_2 layer was 38 mm thick, and the

outer Al_2O_3 layer 76 mm. They were separated by a gap of 23 mm. The distance from the inner insulation surface to the centre of the bundle was 153 mm.

The high temperature shield was located within the pressure tube. In the pressure tube a large number of flanges allowed access to the bundle. Through these holes and their extensions in the temperature shield, the bundle could be inspected during the test with the help of the videoscope systems.

Heating system:

In CORA-30 16 rods were heated. The rods could be individually connected to three power systems available. In this test the intended power input was the same for all rods. Since the voltages and currents of the individual rods were measured, the power input for each rod could be determined. The power input was controlled by a computer. The time dependent power history was programmed before the test. The power was controlled by measurement of the currents of the groups, and by setting the voltage necessary to obtain the desired power.

3. Test Conduct

In the CORA experiments the following phases for the test sequence were generally distinguished (Figure 9):

1. 0-3000 s: pre-heating

2. 3000-10500 s: transient

3. > 10500: cooldown.

The pressure in the system was controlled as in all tests to 0.22 Mpa. The argon input is separated in two parts. First 8 g/s Argon is preheated and entering together with the steam at the lower end into the bundle (0 mm elevation). The second amount of 6 g/s is not flowing through the bundle and is used for the protection of the bundle head plate (4,4 g/s) and for keeping the windows of the videoscopes clean. The whole second contribution is marked with the label "videoscopes". Both amounts contribute to the dilution of the hydrogen leaving the facility.

The flow of 8 g/s preheated argon through the bundle and a low constant electric power input of about 0.52 kW increase the temperature to a level high enough to avoid condensation of steam (8 g/s) added after 3300 sec.

During the transient phase the initial temperature increase of about 0,2 K/s was produced by raising the electric power input from 6 to 22.6 kW (Figure 8). The test was terminated by turning off the electric power at 10500 s (slow cooldown by heat losses). The steam input was also stopped at 10500 s.

The boundary conditions during the test are given in detail in Figures 9 to 24. Figure 9 shows the argon flow within the facility. Figure 10 presents the constancy of the overpressure of 1,2 bar (2,2 b absolute) in the system. Figure 11 gives the total electric power input, which was produced by the voltage inputs to the three groups of rods (Figure 13) and the resulting total current (Figure 15). The electric power input is controlled by measurement of the voltages of the rod groups and the currents of the individual rods. Then the computer sets the voltages to give the power required. The total electric energy input corresponds to the time integral of the power input (Figure 14).

In Figure 16 the time dependence of the resistance of the bundle is given. Between 6000 and 7000 s a peak can be recognised. The peak is correlated in time to the temperature peak due to the escalation by the Zry/steam reaction. This behaviour reflects the strong temperature dependency of the resistance of the tungsten heater.

Comparing Figures 11, 13, 15 and 16 one can recognise, that in the region with fast changing temperature by the additional exothermal heating the resistance change is so dominant, that for linear power increase a faster voltage increase results in a current decrease.

In Figure 17 the currents of the single rods for the three groups are given. The irregularities around 6000 s are caused as consequence of the melt formation due to the temperature escalation peak. The oscillations are much smaller and are disappearing much faster than in the other tests performed. This is a hint for a smaller melt formation within the bundle.

The resistance of the rod groups and the single rods are given in Figure 18 and Figures 19-21. In all graphs the influence of temperature can be seen. The sharp spikes during power shutdown are artificial due to measurement of voltage and current at not exactly the same time.

In Figure 22 the water temperatures in the quench cylinder at -250 mm and -300 mm are given. The water level at the start of the test was at -220 mm. Due to the longer test time the maximum temperature values are higher than in the regular tests /15/. At -250 mm 116°C was reached compared to 100°C and at -300 mm the maximum value was 100°C compared to 81°C. In the regular tests with larger melt formation, we get remarkable decrease of the temperature at -250 mm and increase at -300 mm due to disturbance of the stratification in the quench cylinder by falling melt. The smooth temperature traces for test CORA-30 with only minor changes after 6000 s hint to much smaller amounts of melt falling into the water of the quench cylinder.

At -50 mm elevation (Figure 23) the temperatures are measured on the outside of the steam tube (15° and 195°) and 15 mm inside the steam tube (165° and 345°). Between 6000 s and 7000 s the temperatures measured at 165° and 195°, in the neighbourhood of the steam entrance show a formation of a minimum. In respect to time this minimum is in coincidence with the exothermal reaction in the upper part of the bundle.

The temperature of the incoming argon at the steam inlet is measured with two thermocouples (Figure 24). The resulting measurements give practically the same value. The increase of the steam inlet temperature is caused by the heat up of the walls of the connecting tube from superheater to the entrance of the bundle due to the additional heat capacity of the steam

4. Temperature measurements

The temperatures in the bundle were measured by high-temperature thermocouples of WRe5/WRe26 wires and HfO_2 insulating material. The sheath was made of tantalum and Zircaloy. Thermocouples with "Ker" in the name (Figures 35 and 40) were additionally shielded with a ZrO_2 sheath. The measurements in the high temperature shield were performed with NiCrNi-thermocouples sheathed with stainless steel. Also the compensation cables were sheathed with stainless steel. The positions of the thermocouples in the bundle are given in Table 5 and Figure 25 and 34 and those in the high temperature shield in Figures 50 and 51.

The temperature measurements of the bundle are presented as function of time in the following way: on one hand, the temperatures of the components (heated rods, unheated rods, etc.) are given in Figures 26 to 33. On the other hand - for comparison reasons - the temperature measurements for different components are grouped by axial elevations (Figures 35 to 47). The temperatures of the high temperature shield are given in Figures 52 to 65.

4.1 Temperature in the bundle

Comparing the temperatures at different radial positions for the same elevation a very flat radial temperature profile can be recognised. This is due to the bundle arrangement with the very effective ZrO_2 fibre insulation (low heat conduction and heat capacity), which allowed the Zircaloy shroud to participate in the energy production by the exothermal reaction. The temperatures at the different components show therefore the same axial behaviour and can be discussed together. The measurements at the same elevation have therefore been combined to give representative temperatures for the bundle. The results of this combination are given in Figure 48 as best-estimate temperatures of the bundle as function of time for different elevations. In Figure 49 these values are re-arranged as axial temperatures distributions for different times in the test sequence.

The contribution of the exothermal heating can be clearly seen on the time dependant temperature graphs of all components. During the - in comparison to the normal tests - much slower heat-up distinct temperature peaks have formed in the upper part of the bundle between 6000 s and 7000 s. As in tests with an initial heat-up of 1K/s the temperature escalation starts in the upper part of the bundle. In CORA-30 the escalation commences at 950 mm elevation compared to preferentially 850 mm in the normal tests. The temperature at the start of the escalation is about 150 K higher than in tests with 1 K/s initial temperature increase. But the electric power input at which this "starting temperature" is reached is much lower for CORA-30 compared to the normal tests (Figure 12). In contrast to the comparable PWR tests in which the escalation proceeds down to 350 mm elevation , in test CORA-30 at 550 mm only a minor temperature rise was found.

The explanation of the temperature peaks in the upper part of the bundle by the exothermic reaction is confirmed by the measurement of the hydrogen production

rate, which shows a pronounced peak in the same time interval (Figure 66). In Figure 67 the power corresponding to the measured hydrogen is compared to the electric power input. At the time of escalation the contribution from the exothermal reaction is more than two times larger than the electric power input. No influence of the exothermal reaction is seen in all temperature measurements at 450 mm elevation and below.

At the beginning of the transient phase the temperature of the bundle is mainly determined by the temperature of the incoming gas and steam, which is higher than 550 °C. This results in a decreasing axial temperature profile with increasing elevation with the maximum at the lower end. With increasing power input and temperature level the incoming steam and gas is cooler than the bundle and acts as coolant. The maximum of the temperature moves to the upper end of the bundle. At 5500 s a clear maximum of about 1200°C has formed at 950 mm. At this elevation the temperature escalation is started, but the highest temperature is reached at 1050 mm elevation, where the escalation started about 100 s later. The temperature escalation developed to about 1150 mm at the upper end and to about 650 mm at the lower end. At 1250 mm and 550 mm only minor temperature peaks were formed.

The strong axial asymmetry is demonstrated in Figure 46. In the upper picture the temperature at 50 mm above (1050 mm)and 26 below (-26 mm) the heated region (tungsten heater) are compared. At 1050 mm the maximum temperature of about 2200°C has developed by the influence of the exothermal reaction and at the lower position the temperature has only reached about 600°C, far below the temperature to start an escalation. The primary reason for this asymmetry is the convective cooling by steam and gas entering at 0 mm elevation. A secondary effect results from the temperature dependence of the axial electric power profile ($P_{el} = I^2R$), which is determined by the dependence of tungsten resistance. The higher temperature in the upper part results in a higher specific power input. The same asymmetric behaviour is seen in the lower picture of Figure 46 where the temperatures 250 mm above (1250 mm) and 250 mm below (-250 mm) are compared.

4.2 Temperatures of the High Temperature Shield

In Figures 52 to 55 the time dependant temperature at the different elevations are given for the inside surface of the HTS (153 mm radius), inside the insulation

(192 mm and 255 mm radius) and on the outer surface (293 mm radius). At 153 mm radius (Figure 52) the influence of exothermal reaction can be seen in the temperature peaks down to 390 mm, though in the bundle the temperature peak had developed only down to 550 mm elevation. After 19 mm of ZrO_2 fibre insulation and 0,9 mm of stainless steel, the temperature peaks are broadened (Figure 53; r = 192 mm). At 255 mm and 293 mm radius the peaks have disappeared.

In Figures 56 to 60 temperatures are compared at equivalent positions on opposite sites in the high temperature shield. As can be seen at 153 mm radius for 990 mm and 890 mm and at 192 mm radius for 950 mm and 750 mm the temperatures at the positions 75° and 175° in the neighbourhood of the steam inlet (180°) are higher before the escalation and lower after the escalation than at the equivalent position (255° + 345°) at the opposite site of the high temperature shield. At 550 mm elevation (Figure 61) the same behaviour is found for the two positions 165°/345°. At 150 mm elevation the temperature is for the whole time of the test higher at 165° than at 345°.

In Figures 63 to 65 at 950 mm, 550 mm and about 150 mm the temperatures at the four radial positions are shown. A steep temperature gradient in the insulation can be recognised. At 150 mm the temperature at 293 mm is higher than at 255 mm. The thermocouple at 255 mm is positioned inside the insulation, while at 293 mm the thermocouple is fixed to the outer stainless steel sheet. The heat conduction in the stainless steel sheet from the upper much hotter elevations must be responsible for the higher temperature.

5. Failure of the absorber and fuel rod simulators

For the absorber rod 6.2, the three unheated rods 4.4, 6.4, 6.6 and the heated rod 3.3 the internal pressure was registered to determine the time of rod failure. The results are shown in Figures 68 and 69. In Figure 70 the failure time of the absorber rod is compared with the times of first melt movement, seen in the videoscope investigations. The temperature traces of the absorber rods and guide tubes (Figure 71) allow by these irregularities to conclude on the time of failure and also on the temperatures at which this failure takes place. The temperature graphs of heated and unheated rods in the time span of failure (Figure 72) give the failure temperatures of the unheated and heated fuel rods.

From Figure 69 it can be seen, that the absorber rod 6.2 failed between 5620 and 5630 s. In test CORA-30 the data in the main test time are taken at an interval of 10 s. So the decrease of the pressure within the absorber rod to the pressure of the system took place within this time span.

The same measurement intervals are used for the temperature shown in Figure 71. One can recognise that the temperature of the thermocouple within the absorber rod 6.2 at 950 mm is decreasing about 200°C also between 5620 and 5630 s. We assume that this temperature change is caused by absorber melt coming from higher cooler elevations of the absorber rod in connection with the failure of the absorber cladding. As the temperature at 950 mm elevation was in the axial maximum region, the failure of the absorber cladding is assumed to be <1350°C, the temperature of the absorber rod at the time of failure.

In Figure 70 it is shown that the first melt movement seen by the video inspection takes place at 5644 s. The delay of about 20 s can be explained by the assumption that the absorber melt had to dissolve the Zry guide tube wall before it could penetrate into the bundle.

In Figure 72 the failure times of Figure 69 were used to determine the failure temperatures of the fuel rod simulators. We assumed, that the temperatures of the unheated rod 6.4 and heated rod 5.5 at 950 mm were representative for the failure of the rods.

6. Hydrogen generation

The hydrogen produced during the test by the steam/zirconium reaction was measured with mass spectrometer systems installed at two positions, i.e. above the test section, and in the mixing chamber after the gas had passed the condenser (see Figure 1). The gas at the test section outlet could contain a high steam partial pressure and had therefore to be diluted by helium before it entered the analyser through a capillary tube. For this purpose a dilution chamber with flow meters was installed.

A schematic diagram of the probes, gas lines, and gas analysis systems is provided in Figure 7. The off-gas mixture which contained hydrogen among other gases is transported to the spectrometer via capillary tubes. It was analysed by quadrupole

mass spectrometers of the type Leybold PQ 100. The ion currents representing the concentration of the respective gases were determined. The production rate of a gas component was calculated with the ratio of the partial pressure of the particular gas to that of argon (carrier gas) and multiplied by the argon flow rate through the test bundle. The hydrogen generation rate was evaluated as follows:

$R_m = 2 \bullet p_H F_{Ar} / (22.4 \bullet p_{Ar})$ [g/s]

with

R_m = mass production rate of hydrogen [g/s]

p_H = partial pressure of hydrogen

p_{AR} = partial pressure of argon

F_{ar} = volumetric argon flow through mixing chamber [l/s]

Based on a calibration test with bundle CORA-7, in which a mixture of argon and 30% hydrogen was radially injected into the test section, the delay time of monitoring the gas was estimated to be 80 s. This time was taken into account for the measured hydrogen production in all CORA experiments. The same calibration tests, however, show lower increases in the rate of hydrogen production than would be expected from the injected gas flow. For this reason the measured data were corrected based on the actual gas concentration, i.e. on the gas input during the calibration test. A transfer function was determined and applied to the measured data. The results is a corrected curve that better represents the H_2 production rate in the test section.

For test CORA-30 the measured as well as the corrected hydrogen production rate are given in Figure 66. The measured data are obtained from the gas probes of the mixing chamber. The corrected data are based on the transfer function of the CORA-7 calibration test. The temperature escalation starts at about 5500 s (Figure 48). This corresponds to the start of the hydrogen production (Figure 66). Integral values of the hydrogen production are shown in the lower picture of Figure 66. The total produced hydrogen amounts to about 194 g. Of interest for accident management (recombiner) is the fact, that about 2/3 of the hydrogen is produced in the short period of escalation.

In Figure 67 the chemical energy produced in the exothermal reaction is calculated from the corrected measured hydrogen and compared to the electric power input. The integral 194 g hydrogen correspond to 29.5 MJ. This contribution amounts to

20% of the total power input (chemical and electric). For the time of escalation the maximum chemical power input for the length of the bundle is twice as large as the electric input. The ratio is even higher in the active region as the chemical energy is only produced in the upper half of the bundle with escalation.

To estimate the extent of oxidation from the hydrogen measured, we assume that only the region with temperatures above 1400°C has contributed substantially to the oxidation and with this to hydrogen production. For this region the measured hydrogen corresponded to 80% oxidation of fuel rod cladding and shroud. On the other hand the measured maximum hydrogen evolution rate of 200 mg/s corresponds to a consumption of 27% of the steam introduced into the bundle.

7. Posttest appearance of the bundle

The appearance of bundle CORA-30 before the test is shown in Figure 81. Three steps of the assembly process are given. Beginning at the left side, the bundle connected by the spacers can be seen. The upper and lower spacer are made of Zircaloy and the middle spacer consists of Inconel. At the lower end the steam distribution tube with its steam entrance tube can be recognised. In the middle picture the Zry shroud is added. Finally in the picture on the right side the bundle with shroud and ZrO_2 fibre insulation is shown.

The post-test appearance of the bundle is given in Figures 82 to 91. The behaviour of the ZrO_2 fibre bundle insulation can be seen form the Figures 82 to 85. The insulation has survived the test. Only in the upper part minor deformation can be recognised form the outside (Figure 82 to 84). In Figure 85 the inner side of the insulation is presented. In accordance with the axial temperature distribution the attack on the shroud insulation has developed only above 700 mm elevation. The damage of the insulation can be recognised up to 1200 mm.

The damage to the shroud is shown in Figures 86 to 87. In the accordance with the axial temperature profile the shroud has kept its original shape with only minor oxygen uptake below 500 mm elevation. The oxidation between 500 mm and 700 mm has increased so much that above 700 mm elevation the embrittled shroud broke away during the removal of the insulation up to about 1200 mm. Figure 85

shows that a strong interaction between Zry shroud and ZrO_2 fibre insulation has taken place between 750 mm and 1200 mm.

The high temperature level in bundle and shroud up to 1150 mm is reflected in the strong interaction between shroud and shroud/insulation.

The post-test appearance of the bundle is given in a diagonal view in Figure 86, in four side views in Figure 87 and in close ups in Figure 88 to 91. The upper Zry spacer (838 mm to 880 mm) has generally survived, though strong deformation can be recognised, especially on the 30° side. A stronger oxidation has developed in the region above the spacer (880-1090 mm) compared to the region below. In the upper region one can recognise preferentially the smooth flowered oxide layers, while below the spacer one can see some deformation. On the bundle sides in 300°, 210° and 120° the absorber rods are positioned on the first internal row and can therefore be seen from the outside (the cross section above the picture can be used for location). Strongly deformed guide tube can be recognised. The cross sections discussed in the next section show that only the oxidised outer shell, which was not dissolved by the absorber material, has survived.

The damage in the bundle can best be seen from the horizontal and vertical cross sections. To enable the cutting of the cross sections, a Lucite box was set around the bundle for encapsulation with epoxy resin. The lower end of this box was closed by a paraffin layer which was produced by refreezing paraffin floating on the water of the quench cylinder. Rutapox 0273 with the hardener LC (Bakelite GmbH, Iserlohn) was used as epoxy. This epoxy was chosen, as its reaction time was slow enough that the shrinkage effect is negligible. The hardening time was one week. The bundle was filled starting from the bottom through the steam inlet. A saw with 2.3 mm thick diamond blade of 500 mm OD (mean diamond grain size 138 µm) was used to cut the bundle at 3200 rpm. The horizontal and vertical cross sections are given in Figures 92 to 103 and Figures C1 to C9.

From the cross sections in comparison to the post-test photographs one can obtain the following information:

- In accordance with the temperature profile damage to the bundle was found from about 500 mm to above 1170 mm, the cross section at the highest elevation

(Figures 92, 95, C1-C5): In the cross sections at 481 mm and 494 mm only minor changes can be seen on some rods inside the thin outer oxide layer of the Zry cladding. This may possibly be the result of melt containing absorber material, which had formed at higher elevations by interaction and had moved downwards within the cladding. This effect was seen in all CORA experiments. The Inconel spacer has survived the test as can be seen from the cross sections at 481 mm and 494 mm.

- From the horizontal cross sections (Figures 93 and 94) it can be seen, that both absorber rods have survived undestroyed at least to 495 mm elevation. The vertical cross section in Figure 95 shows that for absorber rod 4.6 the full density in the rod after the test is found up to 520 mm, while a voided filling of absorber 4.6 has remained up to 600 mm. In the region of the absorber rod 6.2 in the vertical cross section (Figure 96) above 495 mm elevation only voided refrozen material can be recognised up to the elevation of about 600 mm.
- In Figure 97 the vertical cross sections of CORA-30 are compared to those of test CORA-5. In CORA-5 the absorber rod has only survived below about 250 mm elevation. This may partly be caused by the axial temperature distribution to lower elevations. But also in the cold-lower-end test CORA-10 with a similar axial temperature distribution as in CORA-30, the absorber rod only survived above 290 mm. The survival of the absorber structure in CORA-30 to this high elevation must be caused mainly by the stronger oxidation of the guide tube, in consequence of the much slower heatup.
- The gap between absorber rod and guide tube is filled at least down to 442 mm. Partly filling of the gap can be seen down to 300 mm and 143 mm elevation. In the cross section at the highest elevation (1171 mm) the absorber rods have completely disappeared and major damage to cladding has developed.
- The horizontal cross sections of Figures C1 to C4 confirm the appearance seen in the bundle photographs: In the upper region above the upper spacer the well oxidised cladding of the outer fuel rod simulators have developed a pronounced "flowering". In the region below the spacer the generally less oxidised cladding show a less pronounced "flowering".

- The horizontal cross sections show that in the damaged region there is a stronger oxidation of the outer compared to the inner rods of the bundle. This effect is more pronounced in region above the spacer compared to the region below the spacer. In the inner region the oxidation of the bundle has to compete with the interaction of the cladding and the absorber material. In addition the oxidation may be influenced by the blockage which had formed just below the spacer and its influence on the steam flow distribution.
- The vertical and horizontal cross sections (Figures 95 and C3) show, that two blockages have formed within the bundle: The upper blockage from about 800 mm to 870 mm elevation. The lower blockage has formed from about 500 mm to 620 mm. This double blockage is confirmed by the determination of volume and mass distribution of the bundle after the test discussed in chapter 8.

The upper blockage has formed within and below the upper spacer (838 - 880 mm) and the lower above the mid spacer (454-496 mm). The cross section at 493 mm elevation - with the still intact spacer and the small amount of relocated material shows, that the relocation of the material in the region just above the spacer must be determined mainly by the axial temperature distribution. Also the melt refrozen in the upper blockage, has formed preferentially in the region of highest temperature (900 to 1100 mm) and then penetrated the upper spacer and relocated to the region below the spacer. The upper blockage is more of ceramic nature, while the lower is preferentially of metallic nature, with a high content of the absorber material.

Of interest is the comparison of the blockage formation of CORA-30 to CORA-5. CORA-5 was a PWR-test with 1 K/s initial increase, but otherwise equivalent conditions. Also in test CORA-5 we got the same double structure of the blockage formation. Only the two blockages formed at much lower elevations. The relocation to lower elevation is consistent with the axial temperature distribution of CORA-5. The other difference is the lower degree of oxidation due to the faster temperature increase.

8. Blockage formation and mass distribution

The relocation of molten material is also determined by measuring the axial distribution of the blocked area and bundle mass. These measurements were

performed in connection with the epoxying process. As can be seen in Figure 75 the resin is poured into the Lucite mould from the bottom end. By weighing the resin left in the supply container after each step, i.e. when the resin level has raised in the bundle by 1 cm, the difference of mass allows the calculation of the void volume of the bundle as a function of axial height. The filling process is slow enough so that the reading at the scale can be taken per cm.

The error of this measured mass distribution amounts to about 15 %. 10 % with respect to the measurement of 1 cm increments of the epoxy level and 5% due to the error of mass measurement. The error, however, is alternating, i.e. epoxy not measured at one step is certainly included in the next reading at the scale. A filtering method using a Fourier transformation, where higher frequencies were cut off by a low pass filter, was performed to deal with these errors.

A smoothed solid-line curve was obtained from the data by the filtering which is the distribution of the epoxy bundle fill-up, i.e. a complement to blockage in the bundle. Using the density of the epoxy and the cross sectional area inside the Lucite mould the structural area of the bundle end state can be evaluated. Referred to the area of the shroud, it is given in the left side of Figure 76 as "relative blockage".

The blocked area is defined as (cross section mould inside - cross section epoxy - cross-section of shroud remnants) referred to cross section of shroud inside.

As part of the shroud was removed together with the fibre insulation after the test, the remnants of the shroud which were present during the filling process were excluded in the evaluation by measuring their contribution to the cross section separately. The areas are given as percentages, where 100 % means complete blockage.

To determine the axial mass distribution, the epoxy filled bundle was cut into horizontal slices and these bundle segments were weighed. Knowing the axial epoxy distribution, the contribution of the resin is subtracted from the measured weight, to give the mass distribution of the bundle. Also this distribution is corrected for the share of the shroud. The results are given in the left side of Figure 77. These data represent the mass of the rods and spacer. The measured curve is compared with the mass distribution of the intact bundle.

The specific mass is defined as (mass of weighed samples - epoxy mass - mass of shroud remnants) referred to the pertinent axial segment.

If one compares the uncertainty of the axial mass distribution with the axial volume distribution, one can see, that the method using the weighed samples is the more accurate. The uncertainty of the measurement of the filled-in epoxy mass contains the same absolute error, however, the relative error is only one fifth, because the epoxy resin is referred to a 5 cm block compared with the reference of 1 cm for the volume method. Because of the lower density of the epoxy resin in comparison with the density of the structural material the relative error is further reduced. On the other hand in the mass distribution the resolution is reduced.

The axial distribution of mass and the blocked area in the bundle are showing the same behaviour and are in accordance with the results from the cross sections. A double structured blockage between 500 mm and 620 mm and 800 mm and 870 mm has resulted.

In comparison to the volume and mass distribution in Figures 76 and 77 also the axial temperature distribution in the bundle is given. On can recognise, that the metallic absorber material containing melt has relocated to the region with the steep gradient in the axial temperature distribution, while the more ceramic melt is refrozen at much higher temperatures.

9. Summary and discussion

Test CORA-30 should investigate the damage behaviour of the fuel bundle, for a loss of coolant accident developed from a shutdown reactor. Starting form a reactor after shutdown means less decay heat and with this a slower increase of the temperature. Therefore test CORA-30 was performed with an initial temperature increase of 0,2 K/s, instead of 1 k/s as in most of the CORA tests. A slower temperature increase means a thicker oxide layer at a given temperature. The thickness of the protective oxide layer influences the temperature time behaviour and the extent of the temperature escalation. The following behaviour was found:

Test CORA-30 showed, that the temperature escalation takes place also for an initial heatup rate of 0.2 K/S. The escalation started at a temperature of about 150°C higher than in tests with 1 K/s initial temperature rise and increased only to about

2 K/s, compared to 20 K in the other PWR tests. The temperature rise went up to about 2150°C similar to the 1 K/s temperatures increase. The electric power input at the initiation of escalation is by about 25% lower. Due to the much slower temperature increase the integral electric energy input up to the initiation of the temperature escalation is about twice as large for CORA-30 compared to the 1 K/s tests.

In test CORA-30 the region of escalation is limited to the upper part of the bundle. The escalation starts at 950 mm elevation (compared to 850 mm for normal tests) and reaches at 550 mm only a minor temperature increase (in normal test the escalation moved down to about 350 mm). The maximum escalation peak was reached at 1050 mm and this was also the elevation at which the temperature stayed at maximum to the end of the tests.

In accordance with the axial temperature profile the damage to the bundle was restricted to the upper half of the bundle from about 500 mm to above 1170 mm elevation. Due to the stronger oxidation as consequence of the slower heatup the absorber rod structure survived in a voided form even to about 600 mm elevation. In normal tests the absorber survived only to about 250 mm elevation. The presence of absorber material at higher elevations may have an influence on the criticality behaviour of a reflooded core.

The molten material had relocated within the bundle in two regions. From 800 mm to 870 mm elevation ceramic type material and between 500 mm and 620 mm preferentially metallic material have formed blockages. This blockages are found 300 mm and 400 mm higher than the equivalent blockages in the 1 K/s PWR tests.

In test CORA-30 the total produced hydrogen amounts to 194 g. 194 g hydrogen correspond to 29.5 MJ. This contribution is equivalent to about 20% of the total input (electric and chemical). But for the time of escalation the specific maximum chemical input is twice as large as the electric input for the length of the bundle. As the chemical energy is only produced in the upper half of the bundle, this ratio is even higher. Of interest for accident management (recombiners) is the fact, that 2/3 of the hydrogen is produced in the short period of escalation. To estimate the extent of oxidation from the hydrogen measured, we assume that only the region with temperatures above 1400°C has contributed substantially to the oxidation and with

this to hydrogen production. For this region the measured hydrogen corresponds to 80% oxidation of fuel rod cladding and shroud. In connection to steam availability the measured maximum specific hydrogen production rate of 200 mg/s corresponds to a consumption of 27% of the steam introduced into the bundle. At all times of the test we were far away from global steam starvation.

10. References

1. J.M. Broughton; P. Kuan, D.A. Petti; "A Scenario of the Three Mile Island Unit 2 Accident", *Nuclear Technology*, Vol. 87, 34-53 (1989).

2. S. Hagen, K. Hain: "Out-of-pile Bundle Experiments on Severe Fuel Damage (CORA-Program)", *KfK* 3677 (1986).

3. S. Hagen, P. Hofmann, G. Schanz, L. Sepold; "Interactions in Zircaloy/UO_2 Fuel Rod Bundles with Inconel Spacers at Temperatures above 1200°C (CORA-2 and CORA-3)", *KfK* 4378 (1990).

4. S. Hagen, P. Hofmann, V. Noack, G. Schanz, G. Schumacher, L. Sepold; "Results of SFD Experiment CORA-13 (OECD International Standard Problem 31)" *KfK* 5054 (1993).

5. M. Firnhaber, K. Trambauer, S. Hagen, P. Hofmann, G. Schanz, L. Sepold:ISP-31, "CORA-13 Experiment on Severe Fuel Damage GRS-106", *KfK* 5287, NEA/CSNI/R (93) 17 (1993).

6. S. Hagen, P. Hofmann, V. Noack, G. Schanz, G. Schumacher, L. Sepold; "BWR Slow Heat-up Test CORA-31: Test Results", *KfK* 5383 (1994)

7. S. Hagen, P. Hofmann, V. Noack, G. Schanz, G. Schumacher, L. Sepold; "Dry Core BWR Test CORA-33: Test Results", *KfK* 5261 (1994).

8. S. Hagen, P. Hofmann, V. Noack, G. Schanz, G. Schumacher, L. Sepold; "Behaviour of a VVER Fuel Element Tested under Severe Accident Conditions in the CORA Facility (Test Results of Experiment CORA-W1)" *KfK* 5212 (1994).

9. S. Hagen, P. Hofmann, V. Noack, G. Schanz, G. Schumacher, L. Sepold; "Behaviour of a VVER-1000 Fuel Element with Boron Carbide/Steel Absorber Tested under Severe Fuel Damage Conditions in the CORA Facility (Results of Experiment CORA-W2)", *KfK* 5363 (1994).

10. J. Burbach; "Results of SEM/EDX Microrange Analyses of the PWR Fuel Element Meltdown Experiment CORA-13", *KfK* 5162 (1993).

11. J. Burbach; "Results of SEM/EDX Microrange Analyses of the BWR Fuel Element Meltdown Experiment CORA-16", *KfK* 5282 (1994).

12. S. Hagen, P. Hofmann, V. Noack, L. Sepold, G. Schanz, G. Schumacher;" Comparison of the Quench Experiments CORA-12, CORA-13, CORA-17", *FZKA* 5679, (1996).

13. S. Hagen, P. Hofmann, V. Noack, L. Sepold, G. Schanz, G. Schumacher; "Impact of Absorber Rod Material on Bundle Degradation Seen in CORA Experiments", *FZKA* 5680 (1996).

14. S. Hagen, P. Hofmann, V. Noack, L. Sepold, G. Schanz, G. Schumacher; "Pre-oxidised BWR Test CORA-28: Test Results"; FZKA 5571 (1997)

15. S. Hagen, P. Hofmann, V. Noack, L. Sepold, G. Schanz, G. Schumacher; "Pre-oxidised PWR Test CORA-29: Test Results"; FZKA 5928 (1997)

16. S. Hagen, P. Hofmann, V. Noack, L. Sepold, G. Schanz, G. Schumacher; "Cold Lower End Test CORA-10: Test Results" FZKA 5572 (1997)

11. Acknowledgements

At the Forschungszentrum Karlsruhe a variety of support needed for preparation, conduct, and evaluation of the experiment is hereby gratefully acknowledged.
The facility was designed by K. Hain and his team. The special bundle set up was designed by Mr. H. Junker. The test rods were assembled by Mr. E. Mackert, the test bundles by Messrs. H. Gießmann and R. Röder. The authors would like to thank Messrs. H. Benz, C. Grehl and H.J. Röhling for test preparations and conduct.
Mr. K. P. Wallenfels was responsible for arrangement of camera and video systems and for the preparation of temperature measurements. Messrs. R. Huber and H. Malauschek prepared and conducted the on-line measurements of the off-gas composition.

Finally we would like to express our gratitude to Mrs. U. Ivanitsch for the careful typing of this report.

List of tables

Table 1: CORA Test Matrix

Test No.	Max. Cladding Tempera-tures	Absorber Material	Other Test Conditions	Date of Test
2	≈ 2000°C	-	UO_2 refer., inconel spacer	Aug. 6, 1987
3	≈ 2400°C	-	UO_2 refer., high temperature	Dec. 3, 1987
5	≈ 2000°C	Ag, In, Cd	PWR-absorber	Febr. 26, 1988
12	≈ 2000°C	Ag, In, Cd	quenching	June 9, 1988
16	≈ 2000°C	B_4C	BWR-absorber	Nov. 24, 1988
15	≈ 2000°C	Ag, In, Cd	rods with internal pressure	March 2, 1989
17	≈ 2000°C	B_4C	quenching	June 29, 1989
9	≈ 2000°C	Ag, In, Cd	10 bar system pressure	Nov. 9, 1989
7	< 2000°C	Ag, In ,Cd	57-rod bundle, slow cooling	Febr. 22, 1990
18	< 2000°C	B_4C	59-rod bundle, slow cooling	June 21, 1990
13	≈ 2200°C	Ag, In, Cd	OECD/ISP; quench initiation at higher temperature	Nov. 15, 1990
29*	≈ 2000°C	Ag, In, Cd	pre-oxidised,	April 11, 1991
31*	≈ 2000°C	B_4C	slow initial heat-up (≈ 0.3 K/s)	July 25, 1991
30*	≈ 2000°C	Ag, In, Cd	slow initial heat-up (≈ 0.2 K/s)	Oct. 30, 1991
28*	≈ 2000°C	B_4C	pre-oxidised	Febr. 25, 1992
10	≈ 2000°C	Ag, In, Cd	cold lower end 2 g/s steam flow rate	July 16, 1992
33	≈ 2000°C	B_4C	dry core conditions, no extra steam input	Oct. 1, 1992
W1	≈ 2000°C	-	WWER-test	Febr. 18, 1993
W2	≈ 2000°C	B_4C	WWER test with absorber	April 21, 1993

Initial heat-up rate: ≈ 1,0 K/s; Steam flow rate, PWR: 6 g/s BWR: 2 g/s;
CORA 10: 2g/s; CORA W1 + W2: 4 g/s; quench rate (from the bottom) ≈1 cm/s

Tab. 2: Design characteristics of bundle CORA-30

Bundle type		PWR
Bundle size		25 rods
Number of heated rods		16
Number of unheated rods		7
Pitch		14.3 mm
Cladding material		Zircaloy-4
Cladding thickness		0.725 mm
Rod length	- heated rods (elevation	1960 mm - 489 to 1471 mm)
	- unheated rods (elevation	1672 mm - 201 to 1471 mm)
Heated pellet stack		0 to 1000 mm
Heater material		Tungsten (W)
Heater	- length	1000 mm
	- diameter	6 mm
Fuel pellets	- heated rods	UO_2 annular pellets
	- unheated rods	UO_2 full pellets
Pellet stack	- heated rods	0 to 1000 mm
	- unheated rods:	- 199 to 1295 mm
U-235 enrichment		0.2 %
Pellet outer diameter (nominal)		9.1 mm
Grid spacer	- material	Zircaloy -4, Inconel 718
	- length	Zry 42 mm Inc 38 mm
	- location	lower (Zry) -5 mm center (Inc) +496 mm top (Zry) +880 mm
Shroud	- material	Zircaloy -4
	- wall thickness	1.2 mm
	- outside dimensions	90.4 x 90.4 mm
	- elevation	40 - 1235 mm

Tab. 2: (Continuation)

Shroud insulation	- material	ZrO_2 fibre
	- insulation thickness	19 mm
	- elevation	36 mm to 1036 mm
Mo electrode	- length	300 mm
	- diameter	8.6 mm
Cu electrode	- length	189 mm (lower end)
	- length	669 mm (upper end)
	- diameter	8.6 mm
Absorber rod	- number of rods	2
	- material and composition	80Ag, 15In, 5Cd (wt.%)
	- cladding	Stainless steel
	- cladding OD	11.2 mm
	- cladding ID	10.2 mm
	- length	1660 mm
	- absorber material	-189 mm to +1300 mm
Absorber rod guide tube	- material - OD	Zircaloy -4 13.8 mm
	- wall thickness of tube	0.8 mm
Plenum Volume	- heated rods	$12 \cdot 10^{-6}$ m^3
	- unheated rods	$87 \cdot 10^{-6}$ m^3

Table 3: Total specific mass data of bundle CORA-30

Specific mass [kg/m]	
Tungsten heater elements	8.74
UO_2	10.85
Zircaloy in rods	3.45
Zircaloy in absorber rods	0.43
Stainless steel in absorber rods	0.26
Ag/In/Cd absorber	1.59
Inconel grid spacer	0.11
Zircaloy grid spacer	0.14
Zircaloy of shroud	2.77
Total zircaloy	6.65

Table 4: Areas of bundle CORA-30

Cross section areas [m^2]	
Tungsten	$4.524\ 10^{-4}$
UO_2	$1.043\ 10^{-3}$
Zircaloy cladding	$5.252\ 10^{-4}$
Absorber, Ag/In/Cd	$1.634\ 10^{-4}$
Absorber, Stainless steel cladding	$3.36\ 10^{-5}$
Absorber, Zircaloy guide tube	$6.54\ 10^{-5}$
Zircaloy shroud	$4.22\ 10^{-4}$
Total area inside the shroud	$7.535\ 10^{-3}$

Table 5: Positions of thermocouples

Positions of thermocouples in unheated rods (CORA 30)

Slot Number	Elevation [mm]	Rod Number
131	1450	4,2
132	1350	2,6
101	1150	6,6
102	1050	2,2
103	950	6,4
104	850	2,4
105	750	4,4
221	550	2,6
222	550	6,6
223	550	2,2
224	450	4,2
225	350	6,4
231	150	2,4
232	50	4,4

Positions of thermocouples in absorber rods (CORA-30)

Slot Number	Elevation [mm]	Rod Number
106	950	6,2
107	750	4,6
233	450	6,2
234	350	4,6

Positions of thermocouples at heated rods (CORA-30)

Slot Number	Elevation [mm]	Rod Number
108	1150	5,3
109	950	5,5
110	750	3,5
226	550	5,5
227	350	5,3
228	150	3,3
235	50	3,5

Positions of thermocouples at guide tube (CORA-30)

Slot Number	Elevation [mm]	Rod Number
111	1150	4,6
112	950	6,2
113	750	4,6
229	550	6,2
230	350	4,6
241	150	4,6
236	50	6,2

Positions of thermocouples at grid spacer (CORA-30)

Slot Number	Elevation [mm]	Direction of TE
114	860	210°
115	860	30°
237	475	210°
238	475	30°
239	-26	210°
261	-26	30°

Positions of thermocouples in cer. tube,shroud+bundle

Slot Number	Elevation [mm]	Direction of TE
116	950	30°
117	950	210°
118	750	30°
119	750	210°

Positions of thermocouples at shroud in cer. tube (C:-30)

Slot Number	Elevation [mm]	Direction of TE
120	950	300°
121	750	300°
242	550	300
243	350	300°

Positions of thermocouples at shroud outer surface

Slot Number	Elevation [mm]	Direction of TE
122	1150	30°
123	950	30°
124	750	210°
244	550	210°
245	350	210°
246	150	210°
262	50	210°

Positions of thermocouples at bundle flange (CORA-.30)

Slot Number	Elevation [mm]	Direction of TE
134	1491	210°
135	1471	300°
136	1471	345°
137	1511	345°
138	1511	300°

Positions of thermocouples for gas (CORA-30)

Slot Number	Elevation [mm]	Direction of TE
125	1350	120°
126	1250	300°

Positions of thermocouples in shroud insulation(CORA-30)

Slot Number	Elevation [mm]	Direction of TE
133	1060	30°
127	950	30°
128	750	210°
247	550	210°
263	350	210°
264	150	210°
265	50	210°

Positions of thermocouples steam distribution tube

Slot Number	Elevation [mm]	Direction of TE
62	-300	180°
266	-250	300°
267	-50	15°
268	-50	195°
269	-50	165°
270	-50	345°
271	0	180°
272	0	180°
273	50	300°

Table 6: List of cross sections for test bundle CORA-30

Probe	Proben-länge	Axiale Lage unten	Axiale Lage oben	Bemerkungen
30-a1	100 mm	-157 mm	-57 mm	
Schnitt	2 mm			
30-a2	25 mm	-55 mm	-30 mm	
Schnitt	2 mm			Unterer Abstandshalter
30-07	13 mm	-28 mm	-15 mm	Querschnitt, Absorberschmelze
Schnitt	2 mm			
30-b	155 mm	-13 mm	142 mm	
Schnitt	2 mm			
30-c	155 mm	144 mm	299 mm	
Schnitt	2 mm			
30-d	140 mm	301 mm	441 mm	
Schnitt	2 mm			
30-e	35 mm	443 mm	478 mm	
Schnitt	2 mm			
30-03	13 mm	480 mm	493 mm	Querschnitt, mittl. Abst.halter
Schnitt	2 mm			
30-f	140 mm	495 mm	635 mm	Mit Längsschnitt
Schnitt	2 mm			
30-04	13 mm	637 mm	650 mm	Querschnitt
Schnitt	2 mm			
30-g	140 mm	652 mm	792 mm	Mit Längsschnitt
Schnitt	2 mm			
30-05	13 mm	794 mm	807 mm	Querschnitt
Schnitt	2 mm			
30-h	63 mm	809 mm	872 mm	Mit Längsschnitt
Schnitt	2 mm			

Table 6: (continuation)

30-06	13 mm	874 mm	887 mm	Oberer Abst.halter
Schnitt	2 mm			
30-i	140 mm	889 mm	1029 mm	
Schnitt	2 mm			Oberhalb der Heizzone
30-j	140 mm	1031 mm	1171 mm	
Schnitt	2 mm			
30-k	xxx mm	1173 mm	xxxx mm	Oberes Reststück

Table 7: Distribution of void volumes in unheated and heated rods

Void volume of one unheated rod

	elevation [mm]	volume [cm^3]	relative volume [cm^3/cm]
dishing of uranium pellets; gap between pellet stack and cladding	-201 to 1315	4.083	0.027
void volume above pellet stack	1315 to 1439	8.378	0.678
	1439 to 1456	0.711	0.419
	1456 to 1522	3.658	0.55
	1522 to 1531	0.387	0.43
	1531 to 1762	6.531	0.283
	1762 to 1764	0.084	0.419
system for pressure measurement		15.120	
total void volume		38.952	

Void volume of one heated rod

	elevation [mm]	volume [cm^3]	relative volume [cm^3/cm]
void volume below pellet stack	-369 to -334	0.826	0.236
	-334 to 0	1.391	0.0417
gap between pellet stack and cladding and between pellet stack and heater	0 to 1024	2.311	0.023
void above pellet stack	1024 to 1875	3.545	0.0417
	1875 to 1911	0.852	0.24
system of pressure measurement		10.860	
total void volume		19.785	

List of figures

22 : Water temperature in the quench cylinder

23 : Temperature in and on steam tube at -50 mm elevation

24 : Temperatures at the steam inlet

25 : Thermocouple locations within the bundle (CORA-30)

26 : Temperatures of heated rods

27 : Temperatures of unheated rods (TCs in central position)

28 : not used

29 : Temperatures between bundle and shroud measured with ceramic protected TCs

30 : Temperatures of the spacers

30a : Comparison of temperatures of the spacer at 860 mm to temperatures on the inner side of shroud at 750 and 950 mm elevation

31 : Temperatures of the guide tubes of absorber rods

32 : Temperatures in the absorber

33 : Temperatures at the bundle head plate

34 : Location of the thermocouples at shroud and shroud insulation (CORA-30)

35 : Temperatures of inner side of shroud measured with ceramic protected TCs

36 : Temperatures of outer side of shroud

37 : Temperatures of the shroud insulation

38 : Temperatures at elevations given (1511-1450 mm)

39 : Temperatures at elevations given (1250-1050,950 mm)

40 : Temperatures at elevations given (860,850,750 mm)

41 : Temperatures at elevations given (550, 475, 450 mm))

42 : Temperatures at elevations given (350, 150 mm)

43 : Temperatures at elevations given (50, 0 mm)

44 : Temperatures at elevations given (-26, -50)

45 : Comparison of temperatures 50 mm above and 26 mm below the heated region

46 : Comparison of temperatures 250 mm above and 250 mm below the heated region

47 : Temperatures of the bundle head plate and of the lower spacer

48 : Best-estimate bundle temperatures at different elevations

49 : Axial temperature distribution during the transient of test CORA-30

50 : Locations of thermocouples in the high temperature shield (CORA-30)

51 : Position of thermocouples in high temperature shield for test CORA-30

52 : Temperatures of HTS, Inner surface at 153 mm radius

53 : Temperatures of HTS, Temperatures in HT shield at 192 mm radius, 345°

54 : Temperatures of HTS, Temperatures in HT shield at 255 mm radius

55 : Temperatures of HTS, Temperatures in HT shield at 293 mm radius

56 : Temperatures of HTS, Comparison on inner surface at 153 mm radius and 990 mm elevation

57 : Temperatures of HTS, Comparison on inner surface at 153 mm radius and 890 mm elevation

58 : Temperatures of HTS, Comparison on inner surface at 153 mm radius and 90 mm elevation

59 : Temperatures of HTS, Comparison in HT-shield at 192 mm radius and 950 mm elevation

60 : Temperatures of HTS, Comparison in HT-shield at 192 mm radius and 750 mm elevation

61 : Temperatures of HTS, Comparison in HT-shield at 192 mm radius and 550 mm elevation

62 : Temperatures of HTS, Comparison in HT-shield at 192 mm radius and 150 mm elevation

63 : Temperatures of HTS, Radial dependence at 950 mm elevation

64 : Temperatures of HTS, Radial dependence at 550 mm elevation

65 : Temperatures of HTS, Radial dependence at about 100 mm elevation

66 : Hydrogen production in test, production rate (top) and integral values (bottom)

67 : Comparison of chemical and electric power

68 : Internal pressure of fuel rod simulators and absorber rods

69 : Determination of failure time by pressure loss measurement

70 : Comparison of failure time determined by pressure loss measurement or first melt movement due to video inspection

71 : Determination of failure of absorber rods 6.2 and 4.6 by irregularities in absorber and guide tube temperature measurement

72 : Temperatures at failure times of fuel rod simulators determined by pressure loss measurement (Fig. 69)

73 : Comparison of temperatures on heated and unheated fuel rods at absorber failure time

74 : Temperatures of unheated fuel rods

75 : Epoxing process of the test bundle

76 : Axial volume distribution after the test compared to the axial temperature distribution during the test

77 : Axial mass distribution after the test compared to the axial temperature profiles during the test

78 : not used

79 : not used

80 : not used

81 : Pre-test appearance of bundle, shroud and shroud insulation

82 : Post-test appearance of the entire bundle length with shroud insulation; 210°, 120°, 30°

83 : Post-test appearance of the bundle with shroud insulation; 300°, 210° orientation; 300-1100 mm

84 : Post-test appearance of the bundle with shroud insulation; 120°, 30° orientation; 300-1100 mm

85 : Post-test view of the inner side of shroud insulation; 300°, 210°, 120°, 30° orientation

86 : Post-test view of bundle CORA-30 after partial removal of shroud; 345°, 255°, 165°, 75° orientation

87 : Post-test view of bundle CORA-30 after partial removal of shroud; 300°, 210°, 120°, 30° orientation

88 : Post-test view; 345° and 255° orientation; 650 - 1100 mm elevation

89 : Post-test view; 300° and 210° orientation; 650 - 1100 mm elevation

90 : Post-test view; 165° and 75° orientation; 650 - 1100 mm elevation

91 : Post-test view; 120° and 30° orientation; 650 - 1100 mm elevation

92 : Horizontal cross sections of bundle CORA-30, top view (887 - -30 mm)

93 : Horizontal cross sections of the region of absorber rod 6.2, top view (1171 - 57 mm)

94 : Horizontal cross sections of the region of absorber rod 4.6, top view (1171 - 57 mm)

95 : Vertical cross sections through absorber rod 6.4, both sides of the cut (495 - 872 mm)

95a : Locations of the vertical cuts through samples CORA- 30-f, 30-g, 30-h

96 : Vertical cross sections through absorber rod 6.2, both sides of the cut (495 - 872 mm)

97 : Comparison of vertical cross sections CORA-30/CORA-5

98 : Comparison of cross sections of absorber regions CORA-30/ CORA-5

99 : Comparison of horizontal cross sections CORA-30/ CORA-5 (887, 663 mm)

100 : Comparison of horizontal cross sections CORA-30/ CORA-5 (872, 853 mm)

101 : Comparison of horizontal cross sections CORA-30/ CORA-5 (650, 663 mm)

102 : Comparison of horizontal cross sections CORA-30/ CORA-5 (478 mm)

103 : Comparison of horizontal cross sections CORA-30/ CORA-5 (299, 290 mm)

Appendix

A1 : Water temperature in the quench cylinder; initial heating phase

A2 : Temperature in and on steam tube at -50 mm elevation; initial heating phase

A3 : Temperatures at the steam inlet; initial heating phase

A4 : Temperatures of heated rods; initial heating phase

A5 : Temperatures of unheated rods; initial heating phase

A6 : Temperatures between bundle and shroud measured with ceramic protected Tcs; initial heating phase

A7 : Temperatures of the spacers; initial heating phase

A8 : Temperatures of the guide tubes of absorber rods; initial heating phase

A9 : Temperatures in the absorber; initial heating phase

A10 : Temperatures at the bundle head plate; initial heating phase

A11 : Temperatures of inner side of shroud measured with ceramic protected TCs; initial heating phase

A12 : Temperatures of outer side of shroud; initial heating phase

A13 : Temperatures of the shroud insulation; initial heating phase

A14 : Temperatures at elevations given; initial heating phase (1511-1450 mm)

A15 : Temperatures at elevations given; initial heating phase (1250-1050,950 mm)

A16 : Temperatures at elevations given; initial heating phase (860,850,750 mm)

A17 : Temperatures at elevations given; initial heating phase (550, 475, 450 mm)

A18 : Temperatures at elevations given; initial heating phase (350, 150 mm)

A19 : Temperatures at elevations given; initial heating phase (50, 0 mm)

A20 : Temperatures at elevations given; initial heating phase (-26, -50, -250, -300 mm)

A21 : Temperatures of HTS, Inner surface at 153 mm radius; initial heating phase

A22 : Temperatures of HTS, Temperatures in HT shield at 192 mm radius, 345°; initial heating phase

A23 : Temperatures of HTS, Temperatures in HT shield at 255 mm radius; initial heating phase

A24 : Temperatures of HTS, Temperatures in HT shield at 293 mm radius; initial heating phase

B1 : Power input during pre-heat phase

B2 : Resistance of bundle during pre-heat phase

B3 : Water temperature in the quench cylinder; pre-heat phase

B4 : Temperature in and on steam tube at -50 mm elevation; pre-heat phase

B5 : Temperatures at steam inlet; pre-heat phase

B6 : Temperatures of heated rods; pre-heat phase

B7 : Temperatures of unheated rods; pre-heat phase

B8 : Temperatures between bundle and shroud measured with ceramic protected TCs; pre-heat phase

B9 : Temperatures of the spacers; pre-heat phase

B10 : Temperatures of the guide tubes of absorber rods; pre-heat phase

B11 : Temperatures in the absorber; pre-heat phase

B12 : Temperatures at the bundle head plate; pre-heat phase

B13 : Temperatures of inner side of shroud measured with ceramic protected TCs; pre-heat phase

B14 : Temperatures of outer side of shroud; pre-heat phase

B15 : Temperatures of the shroud insulation; pre-heat phase

B16 : Temperatures at elevations given; pre-heat phase (1511-1450 mm)

B17 : Temperatures at elevations given; pre-heat phase (1250-1050,950 mm)

B18 : Temperatures at elevations given; pre-heat phase (860,850,750 mm)

B19 : Temperatures at elevations given; pre-heat phase (550, 475, 450 mm))

B20 : Temperatures at elevations given; pre-heat phase (350, 150 mm)

B21 : Temperatures at elevations given; pre-heat phase (50, 0 mm)

B22 : Temperatures at elevations given; pre-heat phase (-26, -50, -250, -300 mm)

C1 : Horizontal cross sections of bundle CORA-30 (1171, 1031, 1029 mm)

C2 : Horizontal cross sections of bundle CORA-30 (887, 872 mm)

C3 : Horizontal cross sections of bundle CORA-30 (807, 792 mm)

C4 : Horizontal cross sections of bundle CORA-30 (650, 635 mm)

C5 : Horizontal cross sections of bundle CORA-30 (493, 478 mm)

C6 : Horizontal cross sections of bundle CORA-30 (441, 299 mm)

C7 : Horizontal cross sections of bundle CORA-30 (142, -15 mm)

C8 : Horizontal cross sections of bundle CORA-30 (-30, -57 mm)

C9 : Horizontal cross sections of bundle CORA-30 (-157 mm)

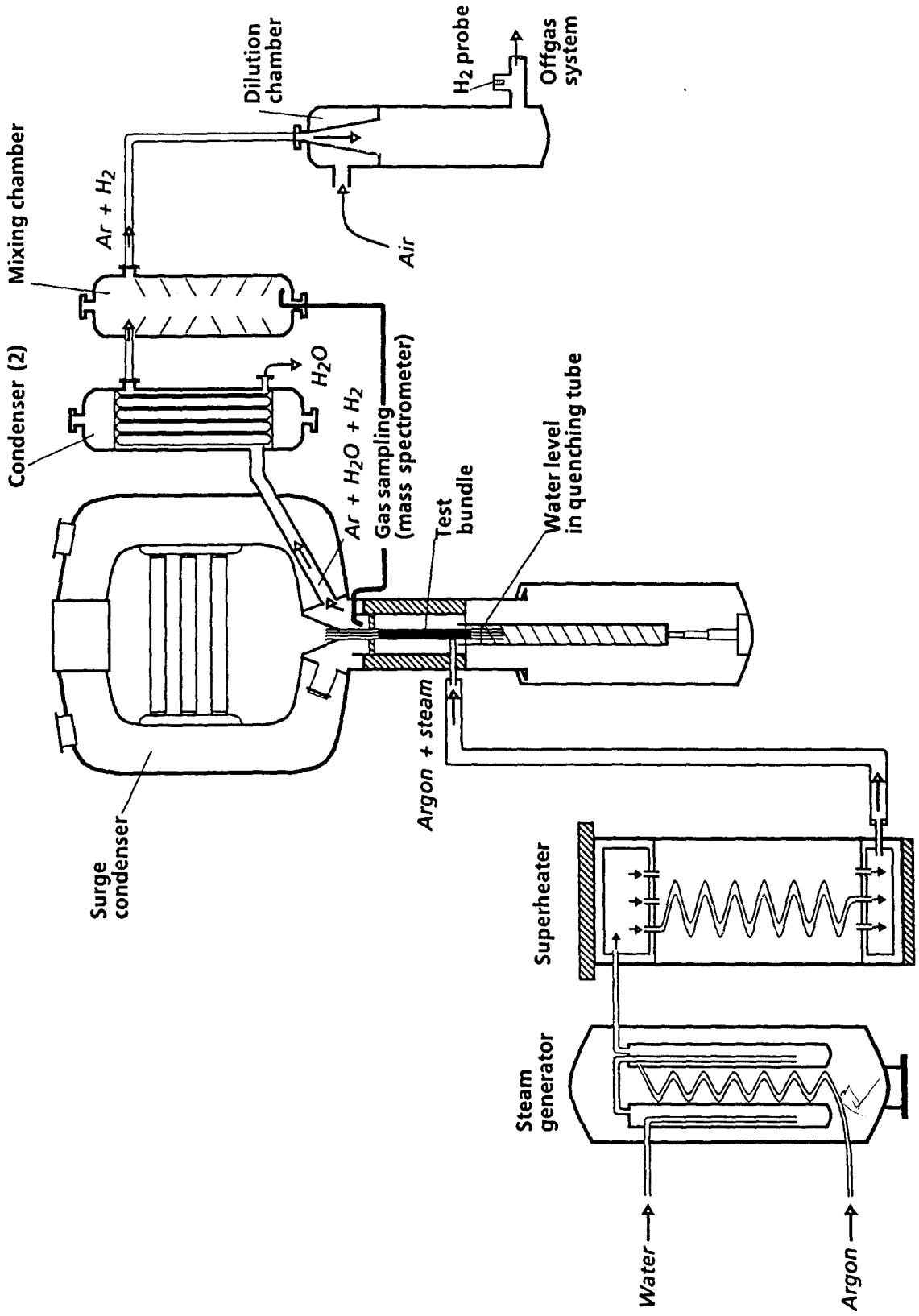

Fig. 1: SFD Test Facility (simplified flow diagram)

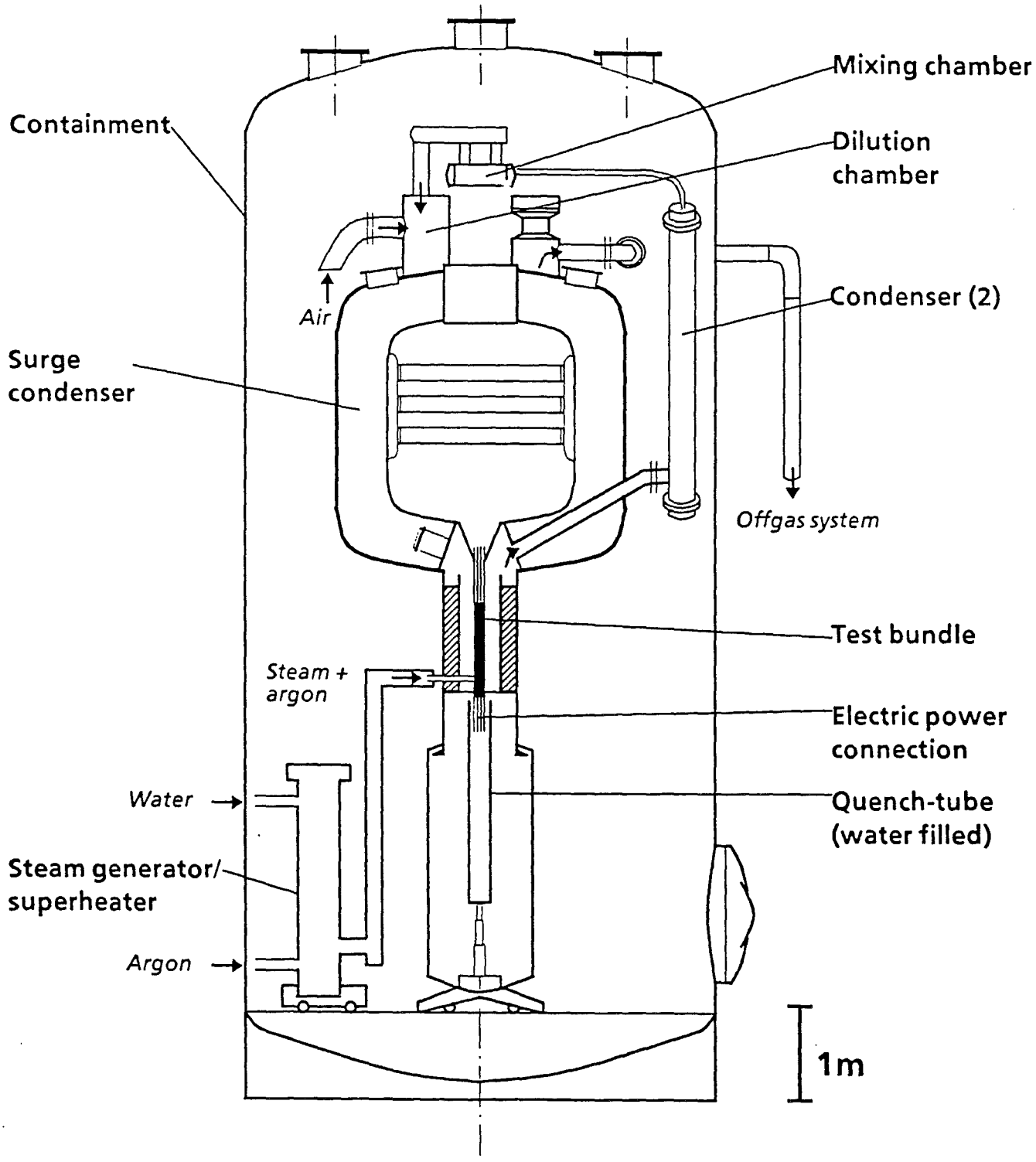

Fig. 2: SFD Test Facility CORA (Main Components)

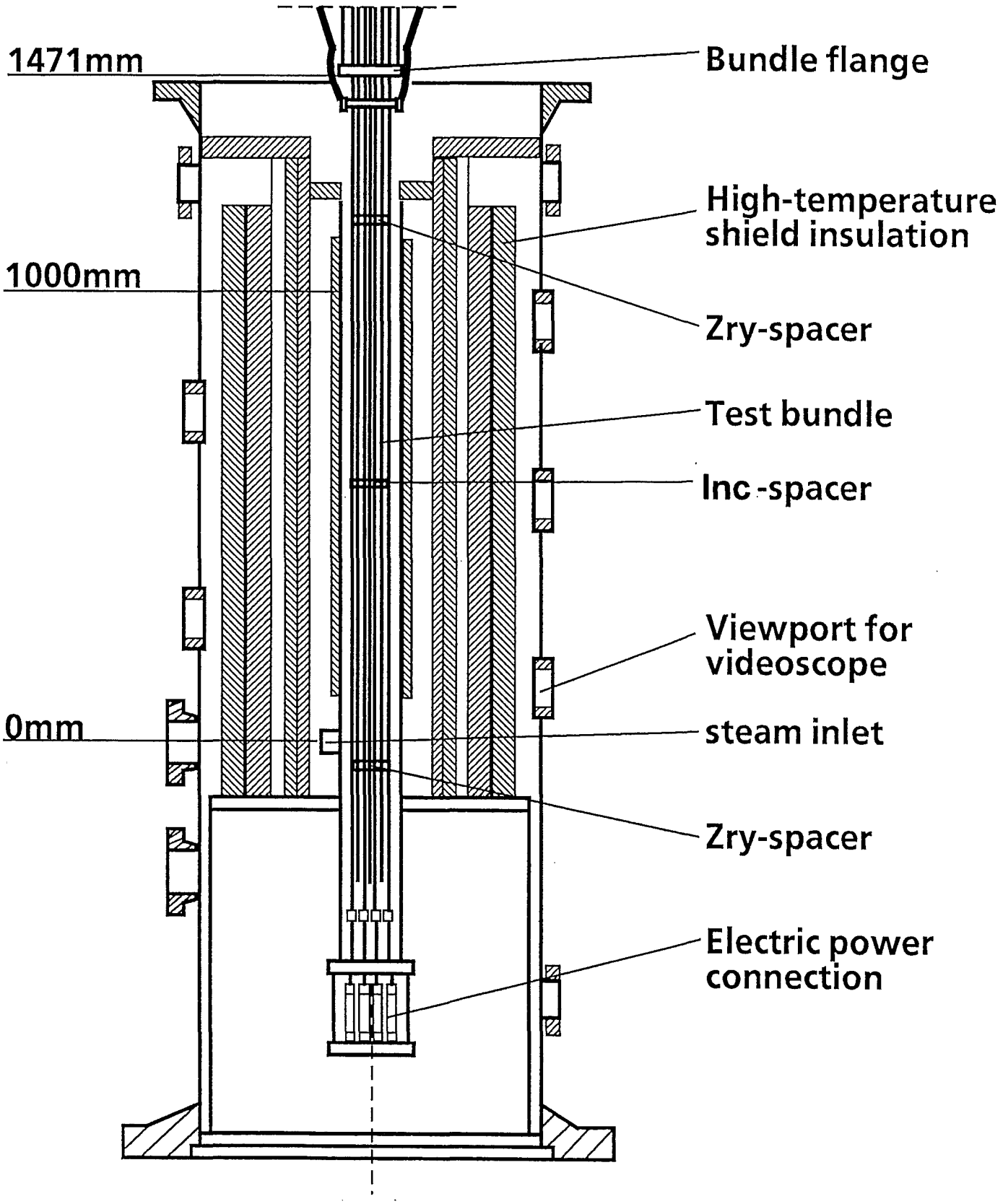

Fig. 3: CORA bundle arrangement

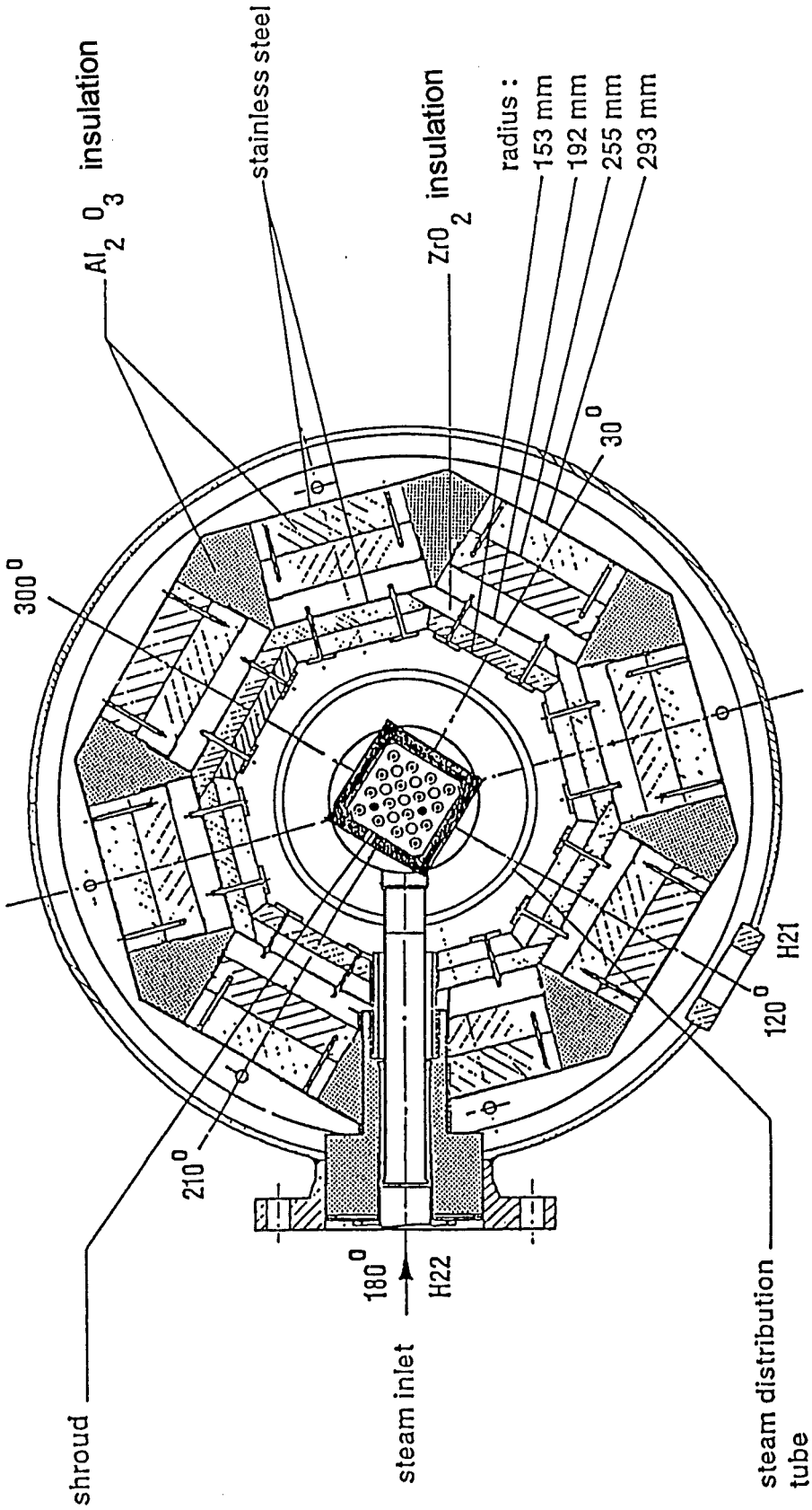

Fig. 4: Horizontal cross section of the high temperature shield

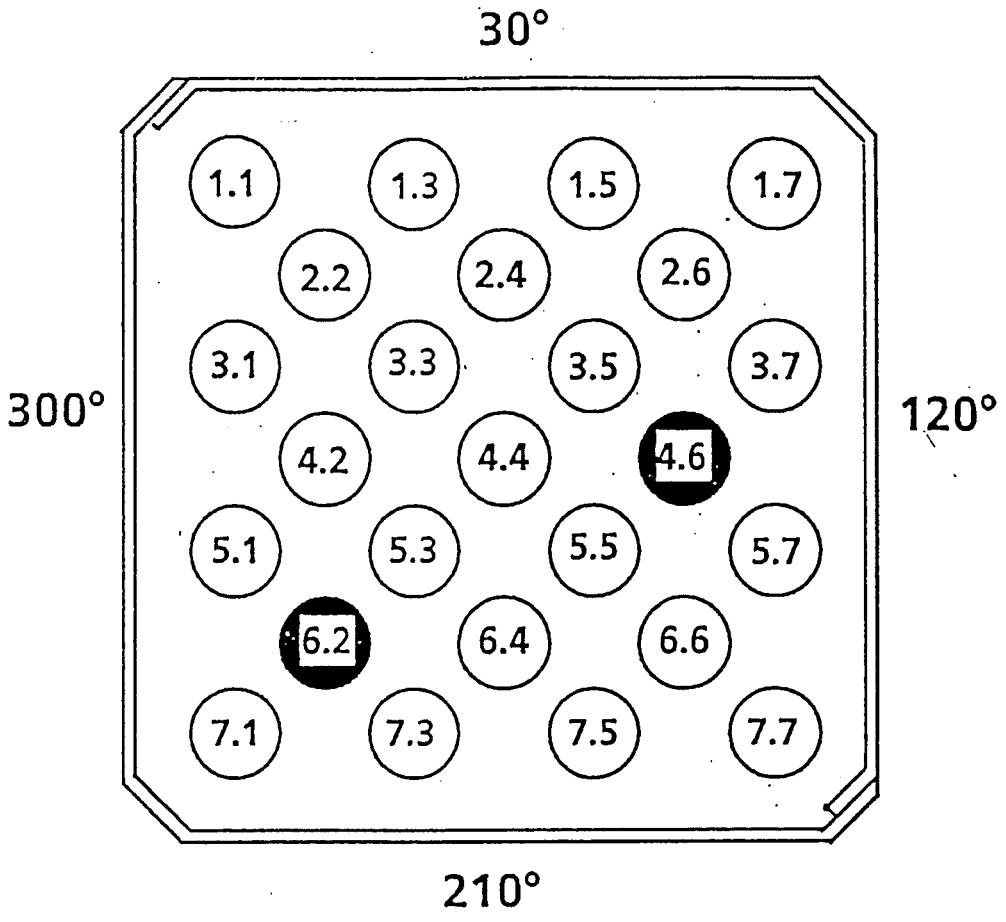

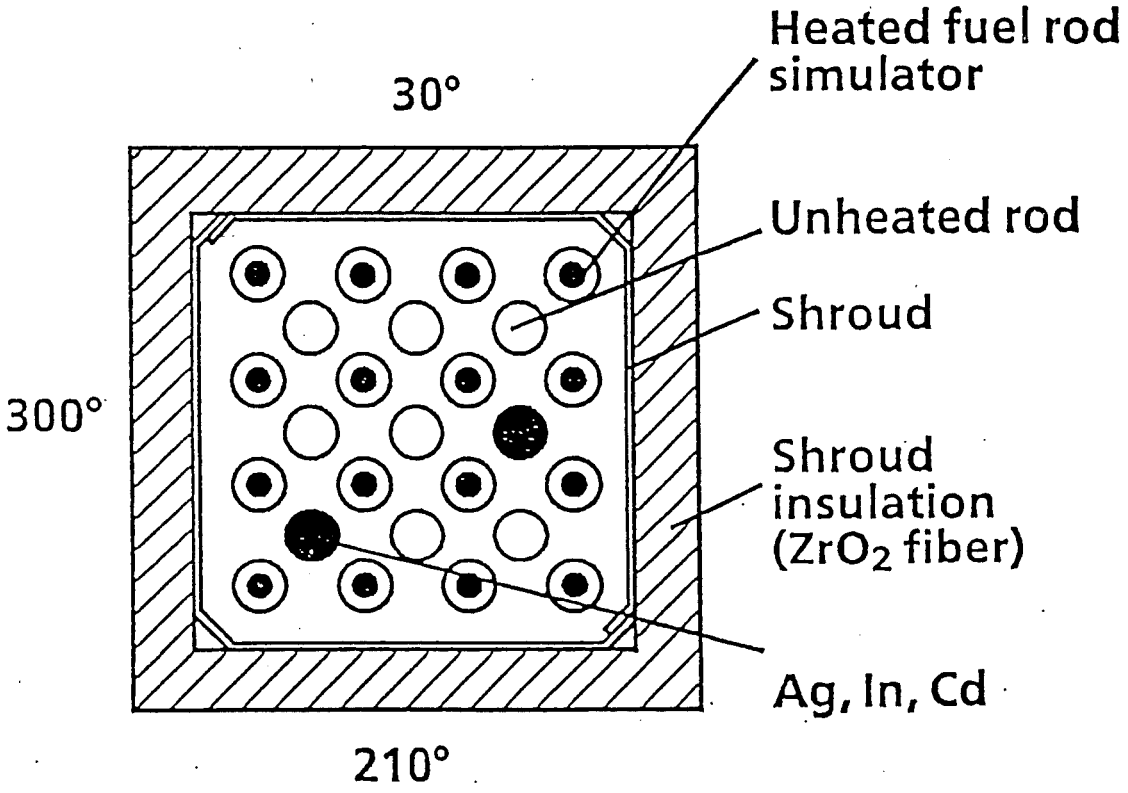

Fig. 5: Rod arrangement and test rod designation of bundle CORA-30

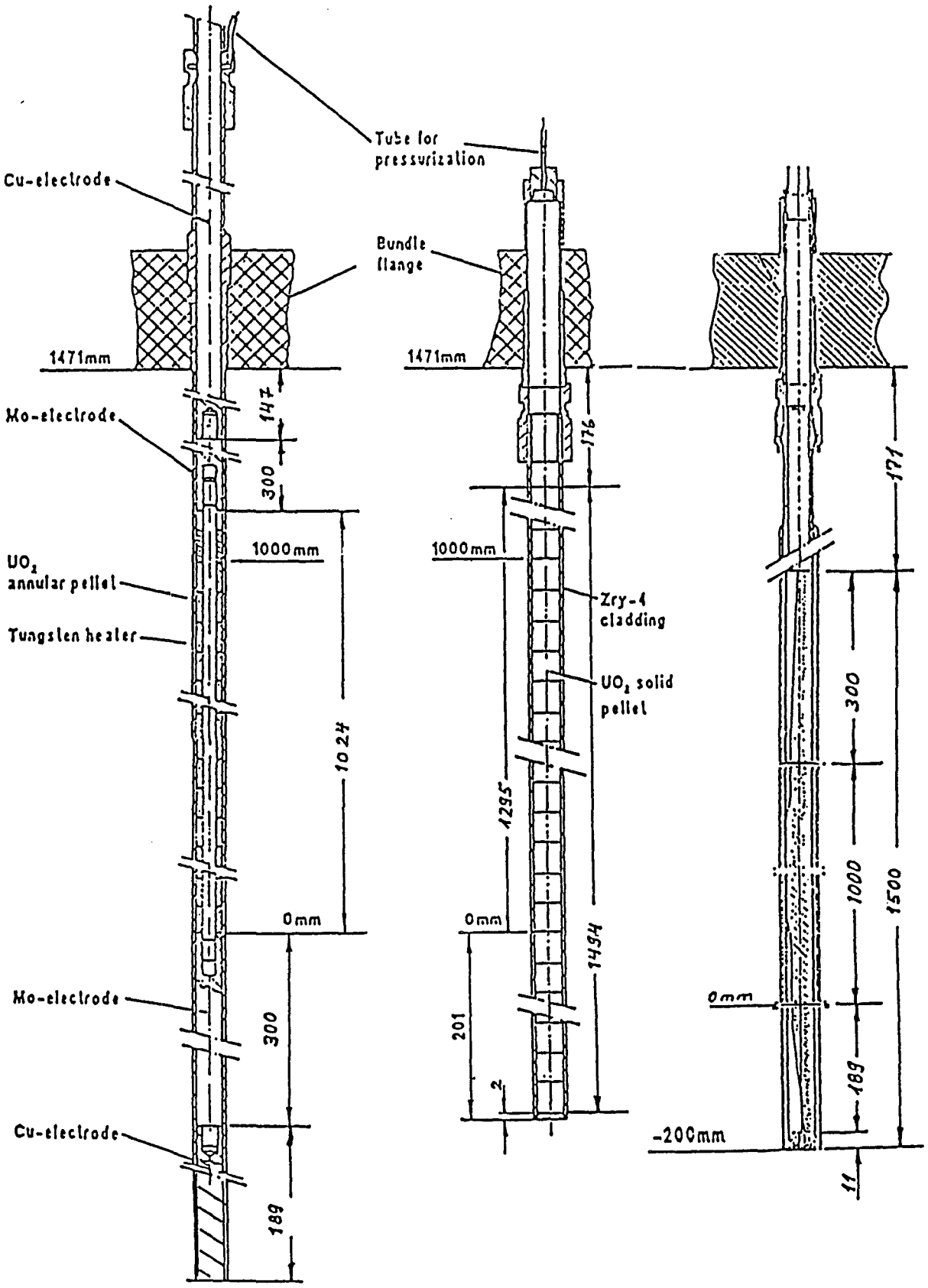

Fig. 6a: Rod types used in the CORA experiments

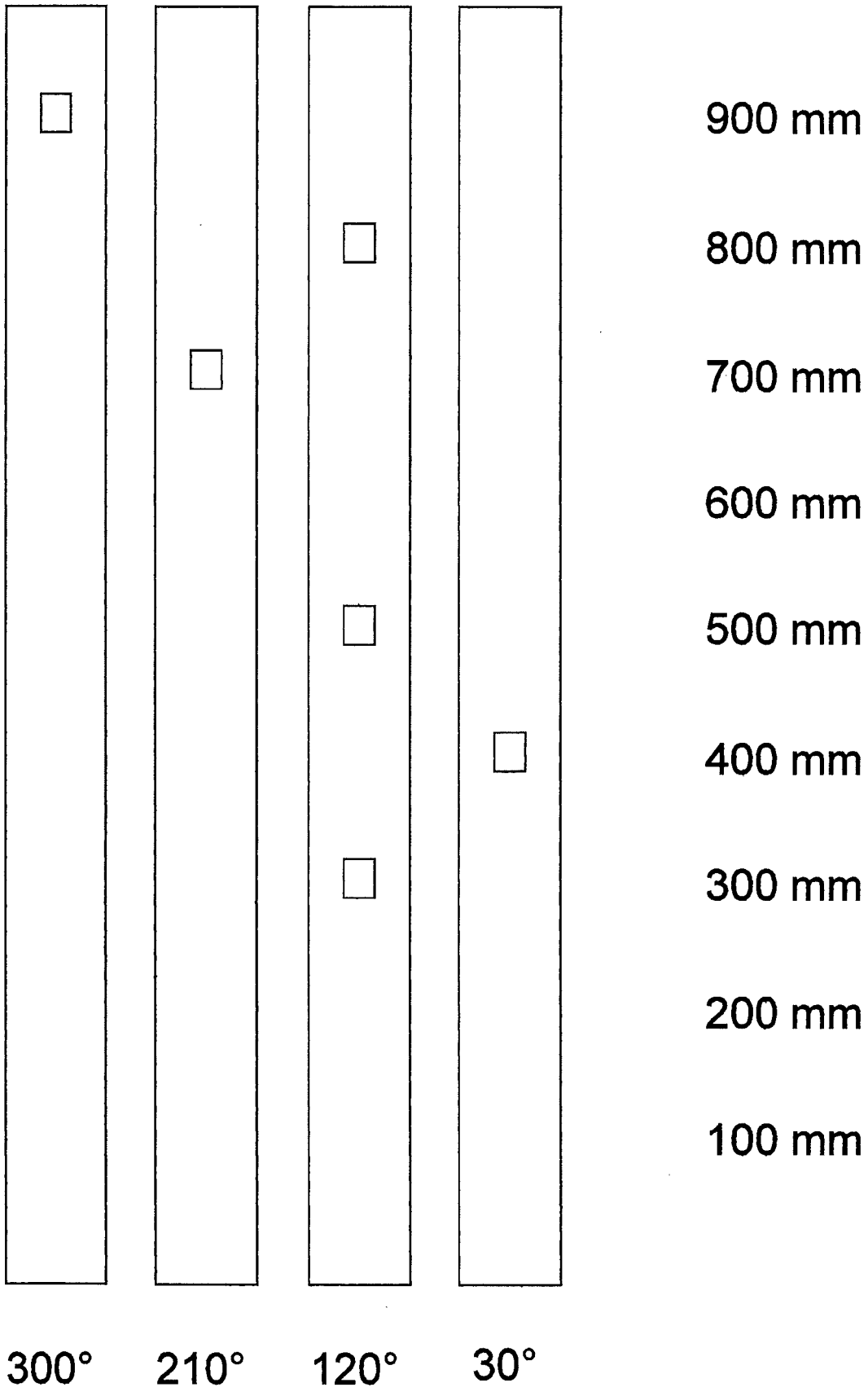

Fig. 6b: Position of windows in the shroud

(a)

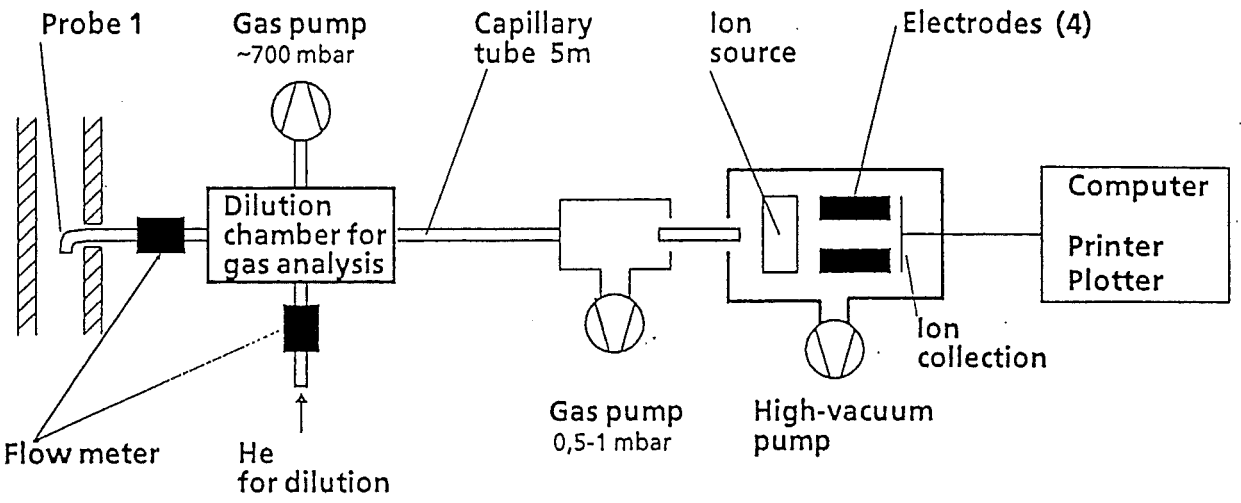

(b)

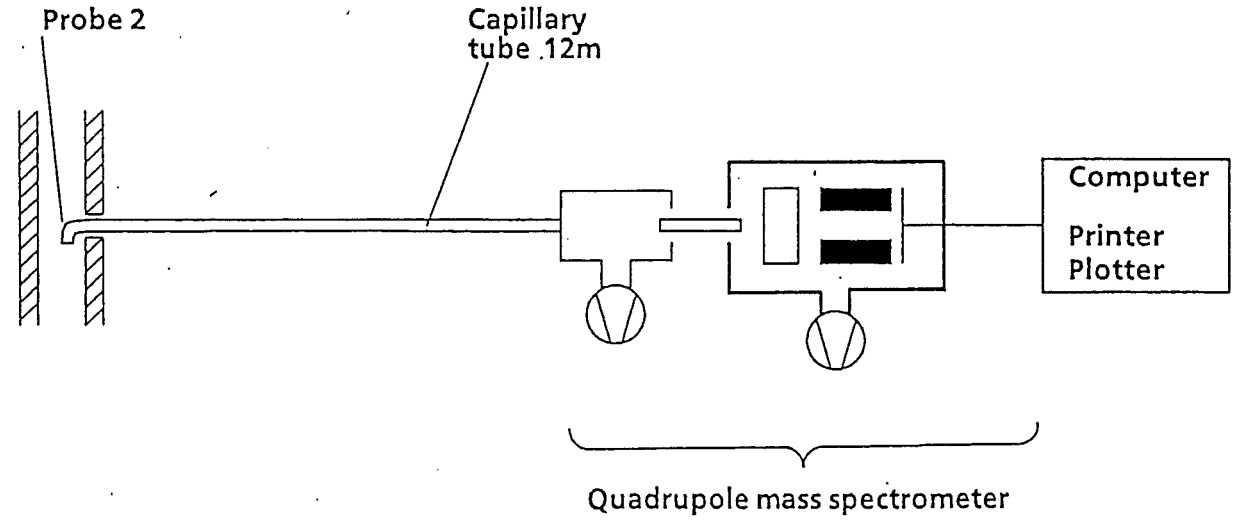

Location (a) : Outlet of test section

Location (b) : Mixing chamber

Fig. 7: Facility of hydrogen measurement

CORA-30:

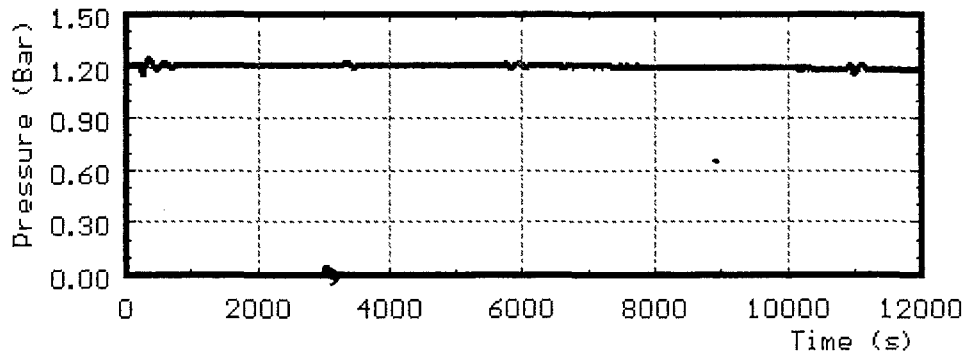

system overpressure

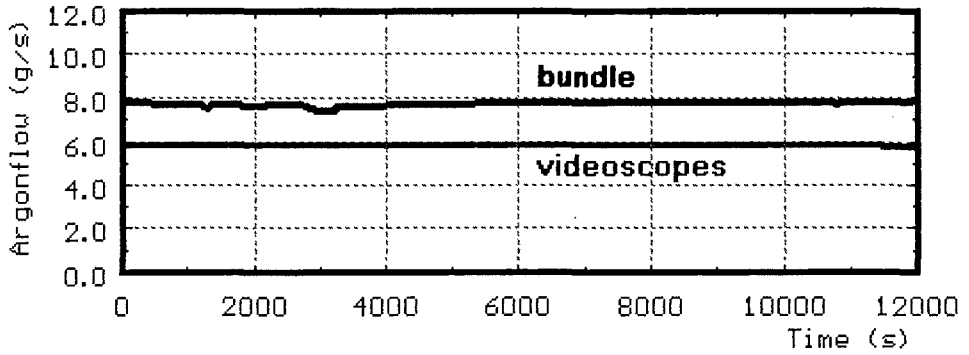

argonflow

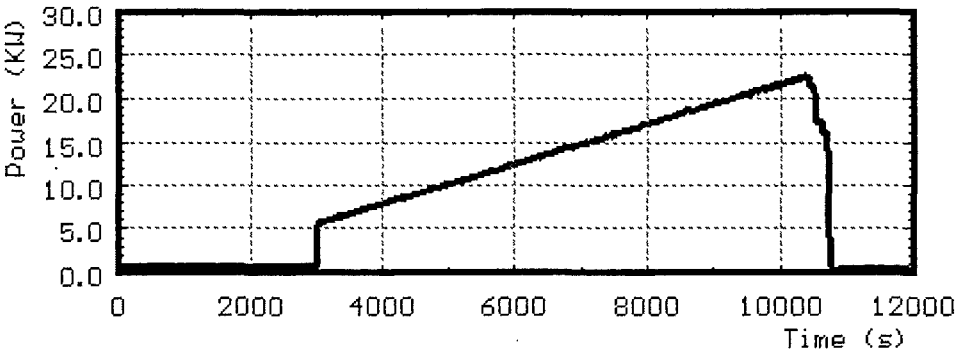

total power

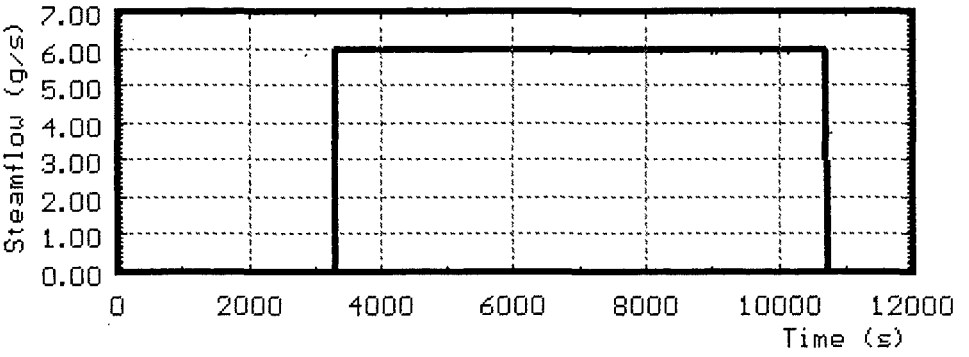

steam input

Fig. 8: CORA-30; System pressure, argon flow, steam input and power

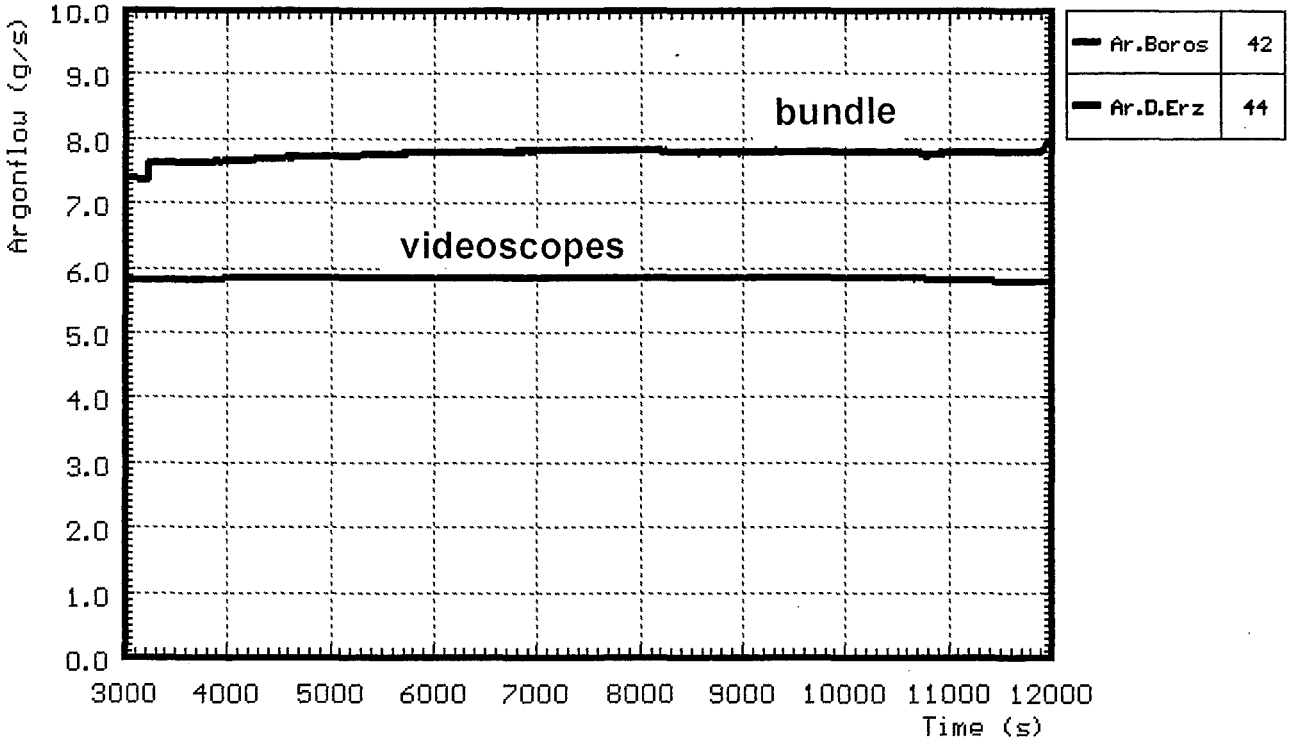

Fig. 9: CORA-30; Argon flow through bundle and videoscopes

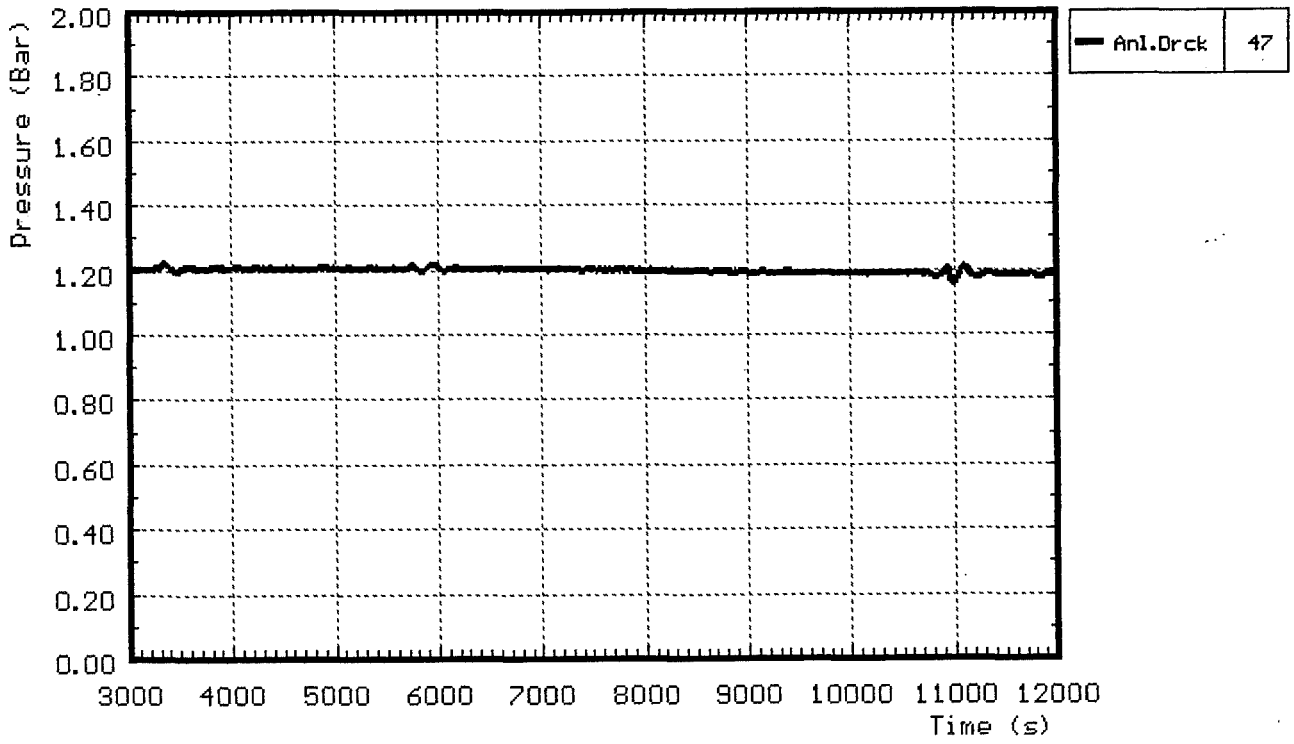

Fig. 10: CORA-30; System pressure (gauge)

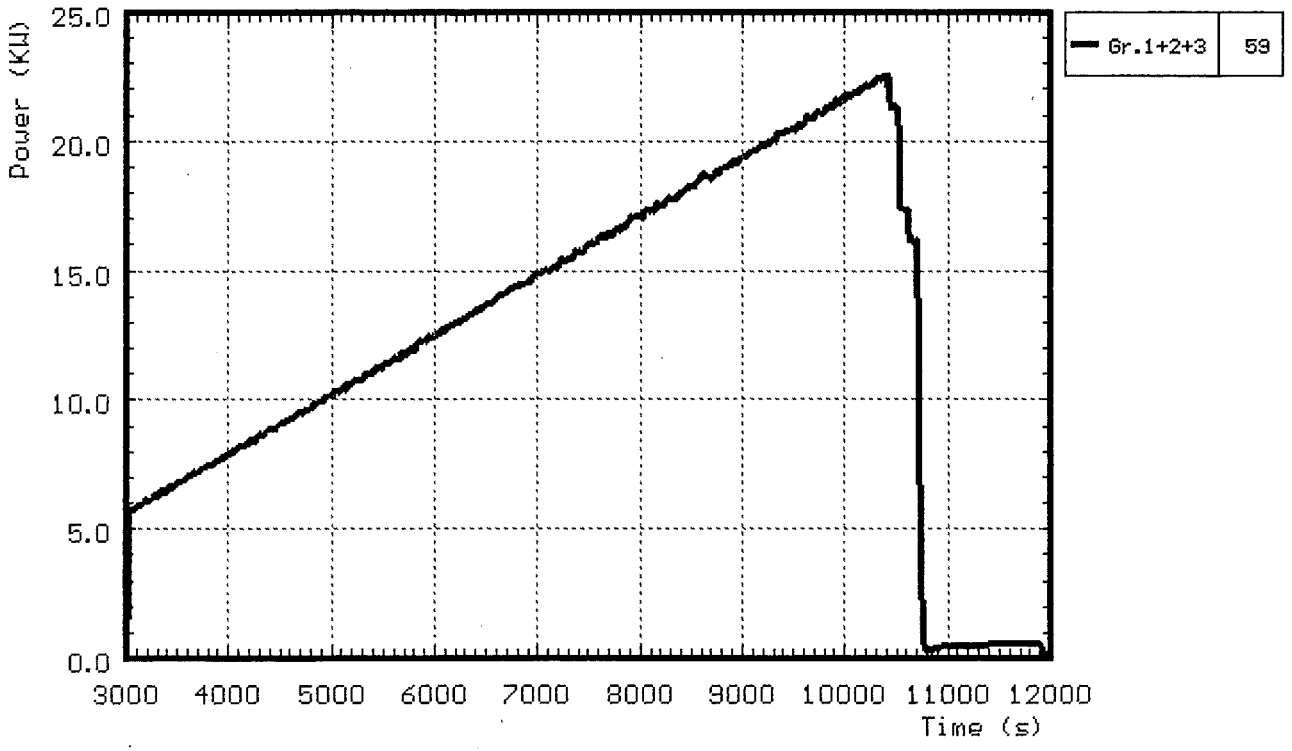

Fig. 11: CORA-30; Total electric power input

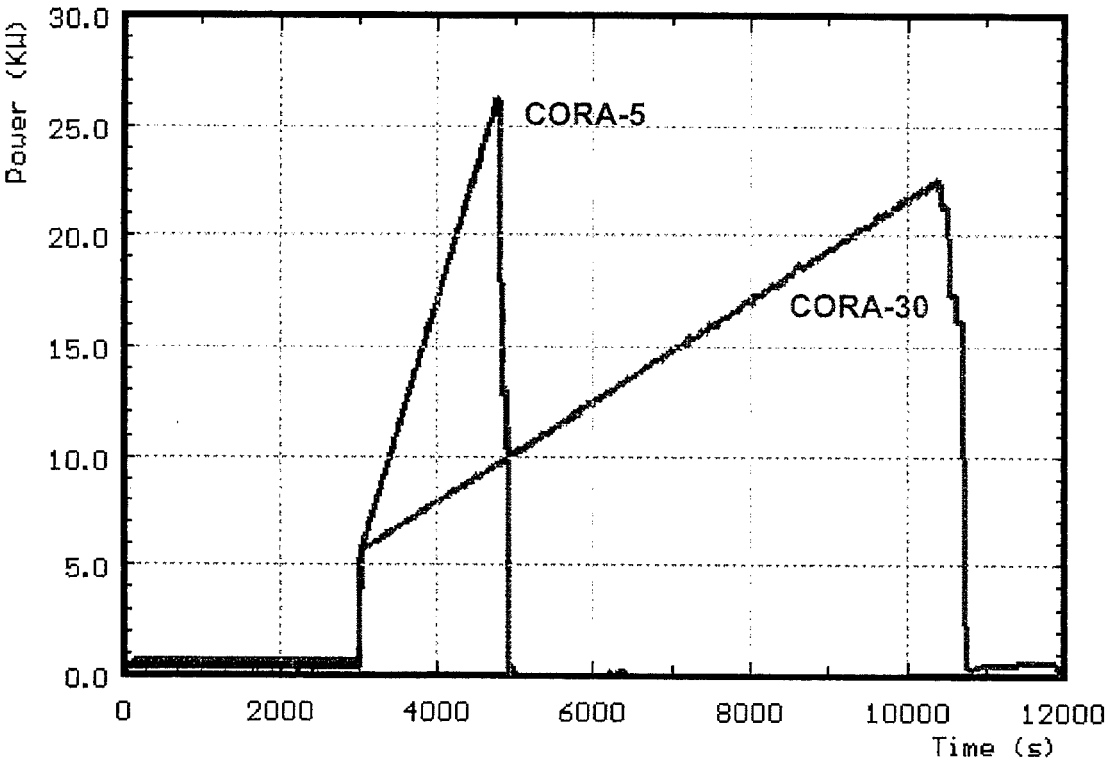

Fig. 12: Comparison of electric power input in tests CORA-30 (slow heat up) and CORA-5 (normal)

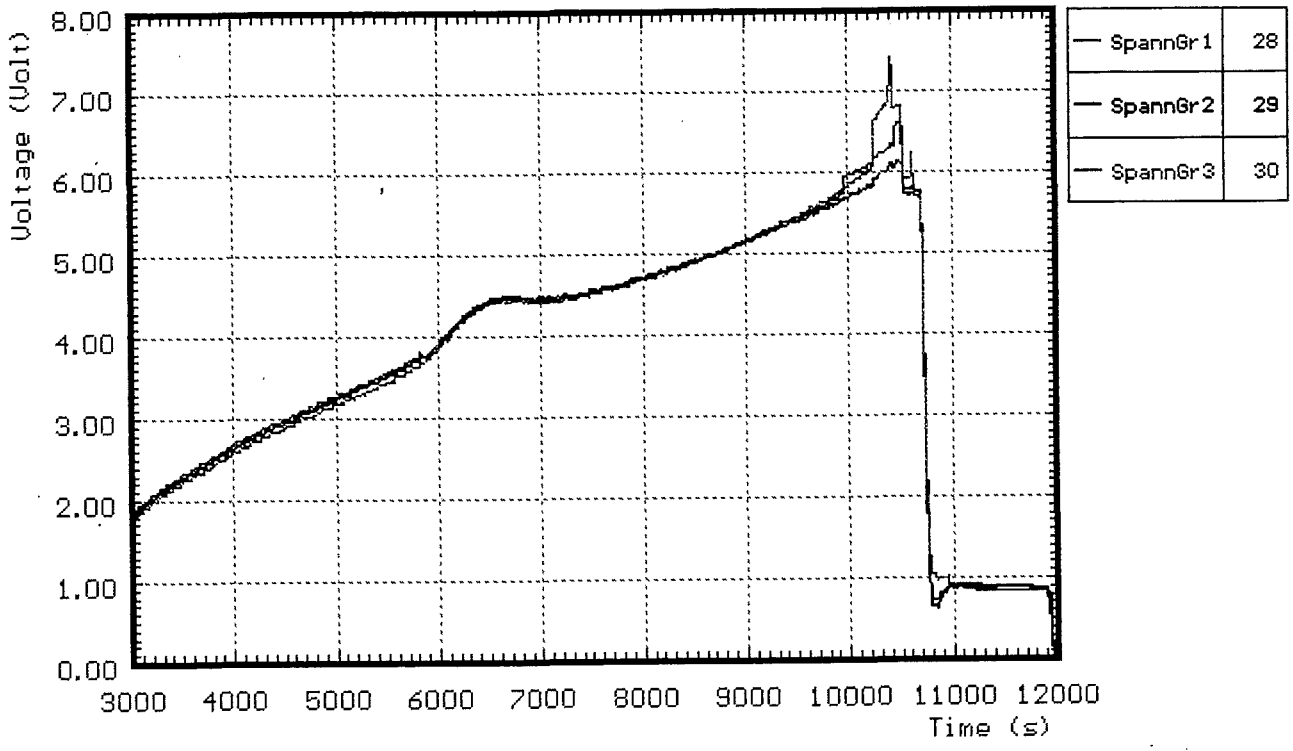

Fig. 13: CORA-30; Voltage input for the 3 rod groups

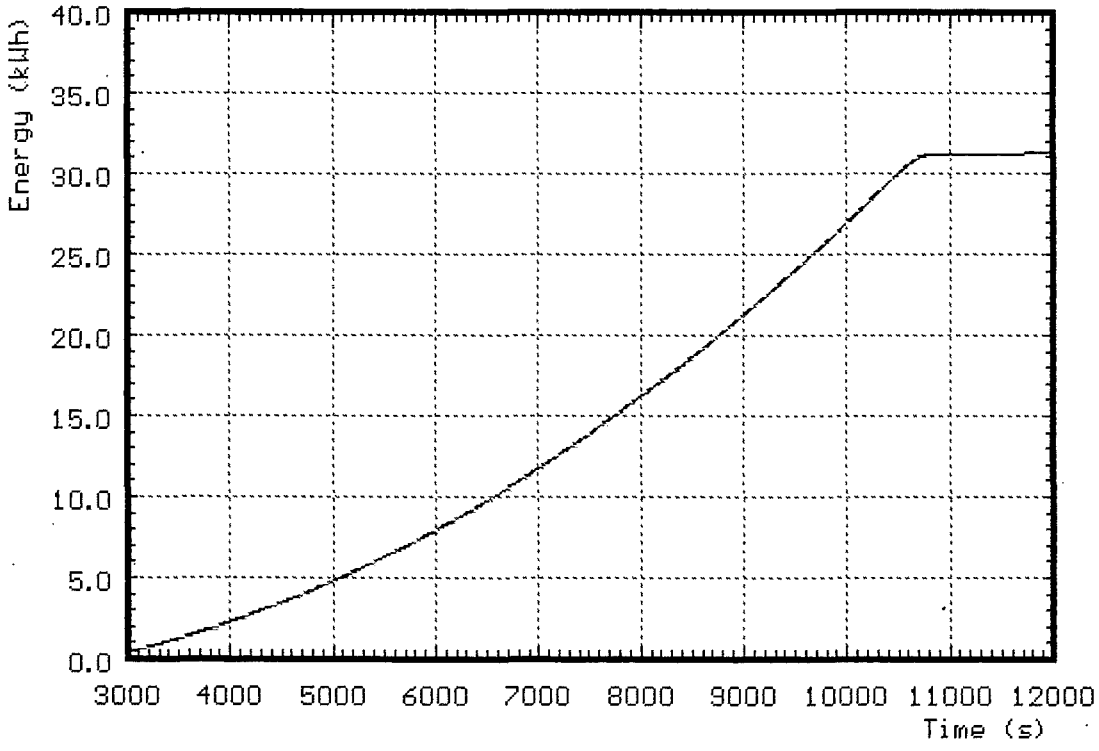

Fig. 14: CORA-30; Total electric energy input

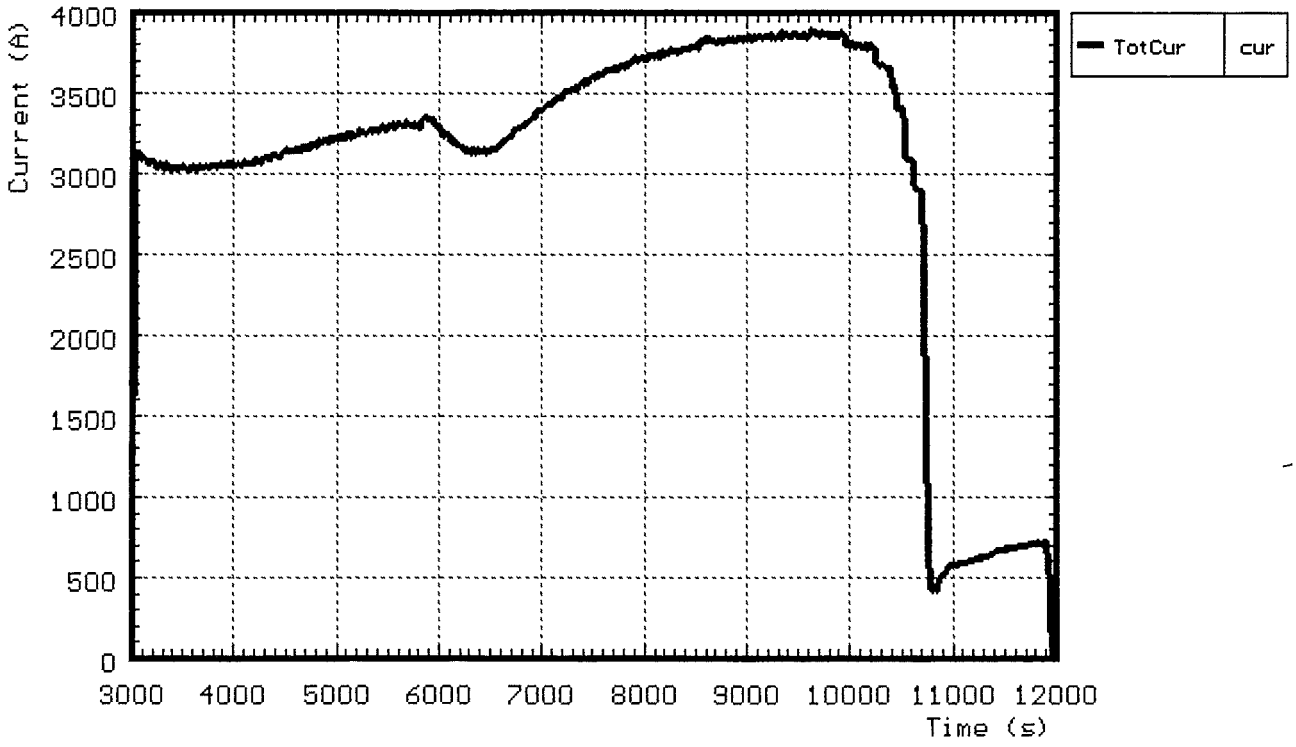

Fig. 15: CORA-30; Total current

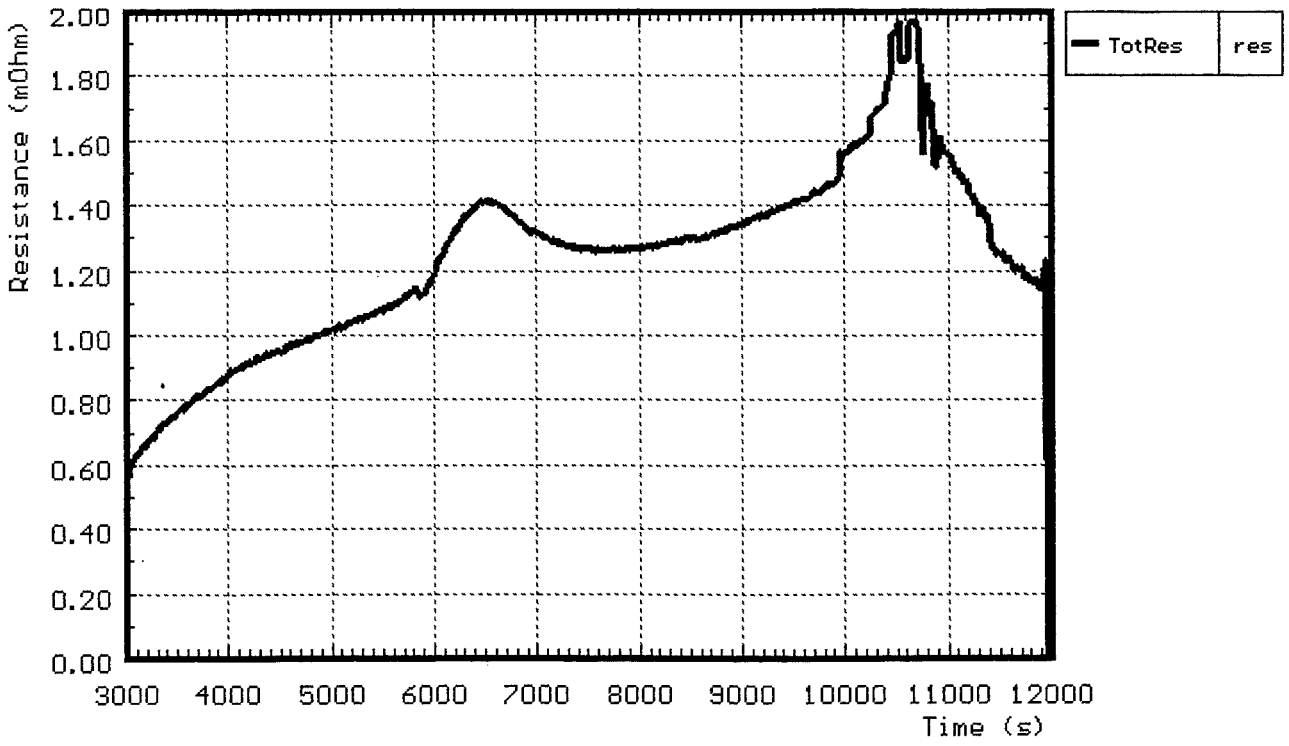

Fig. 16: CORA-30; Resistance of bundle (Voltage group 1/total current)

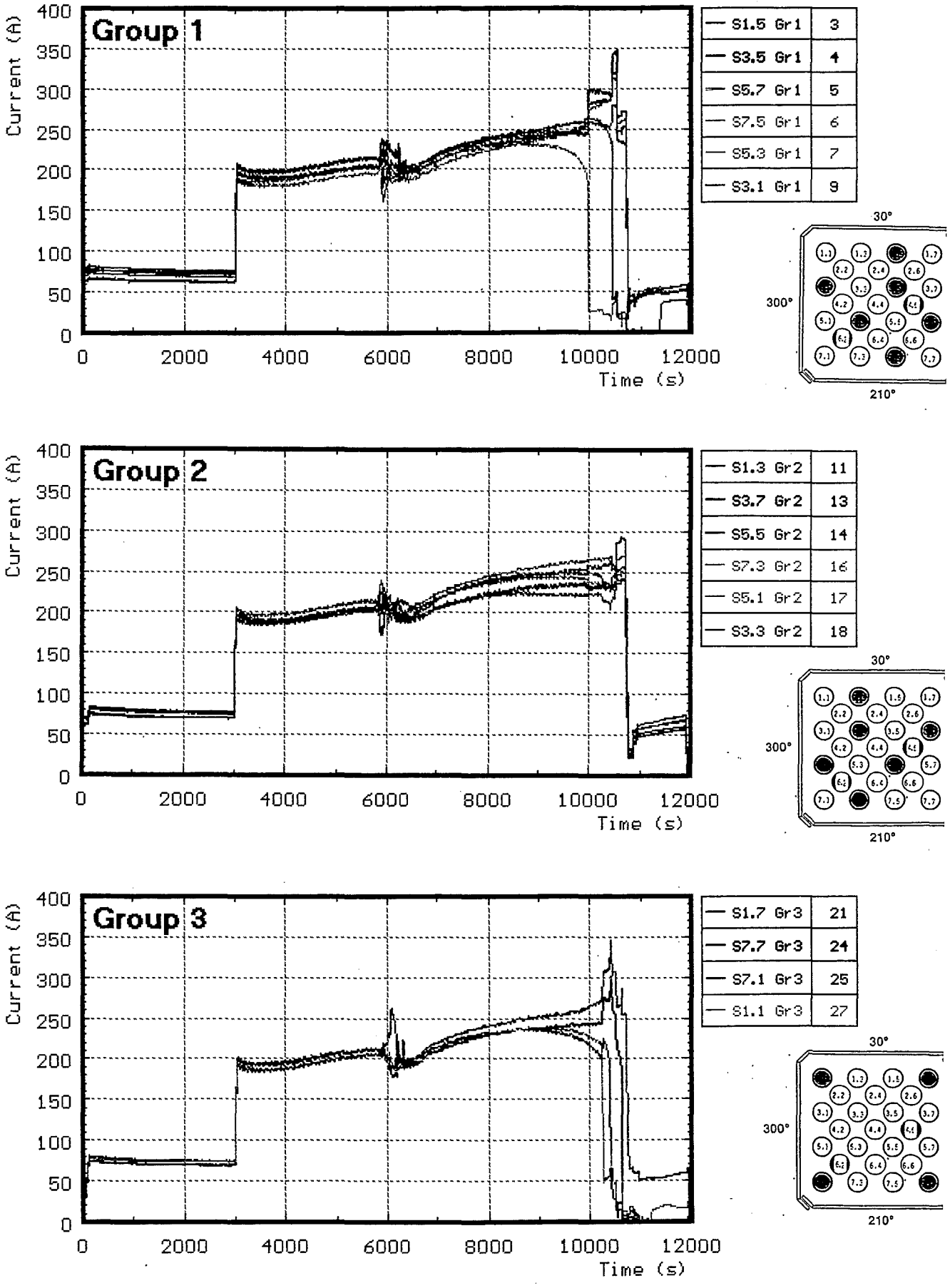

Fig. 17: CORA-30; Variations of currents within the rod groups

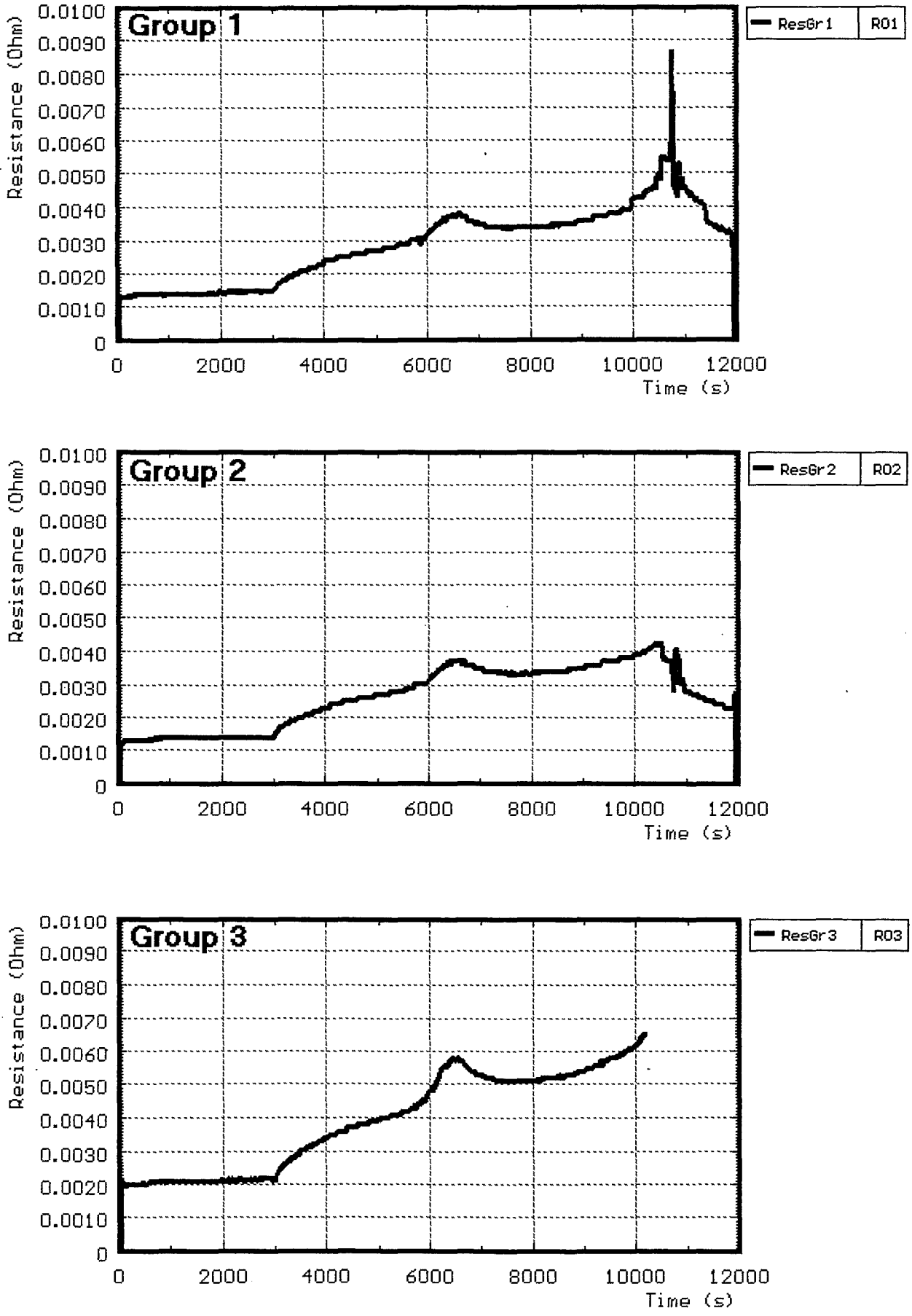

Fig. 18: CORA-30; Resistance of the rod groups

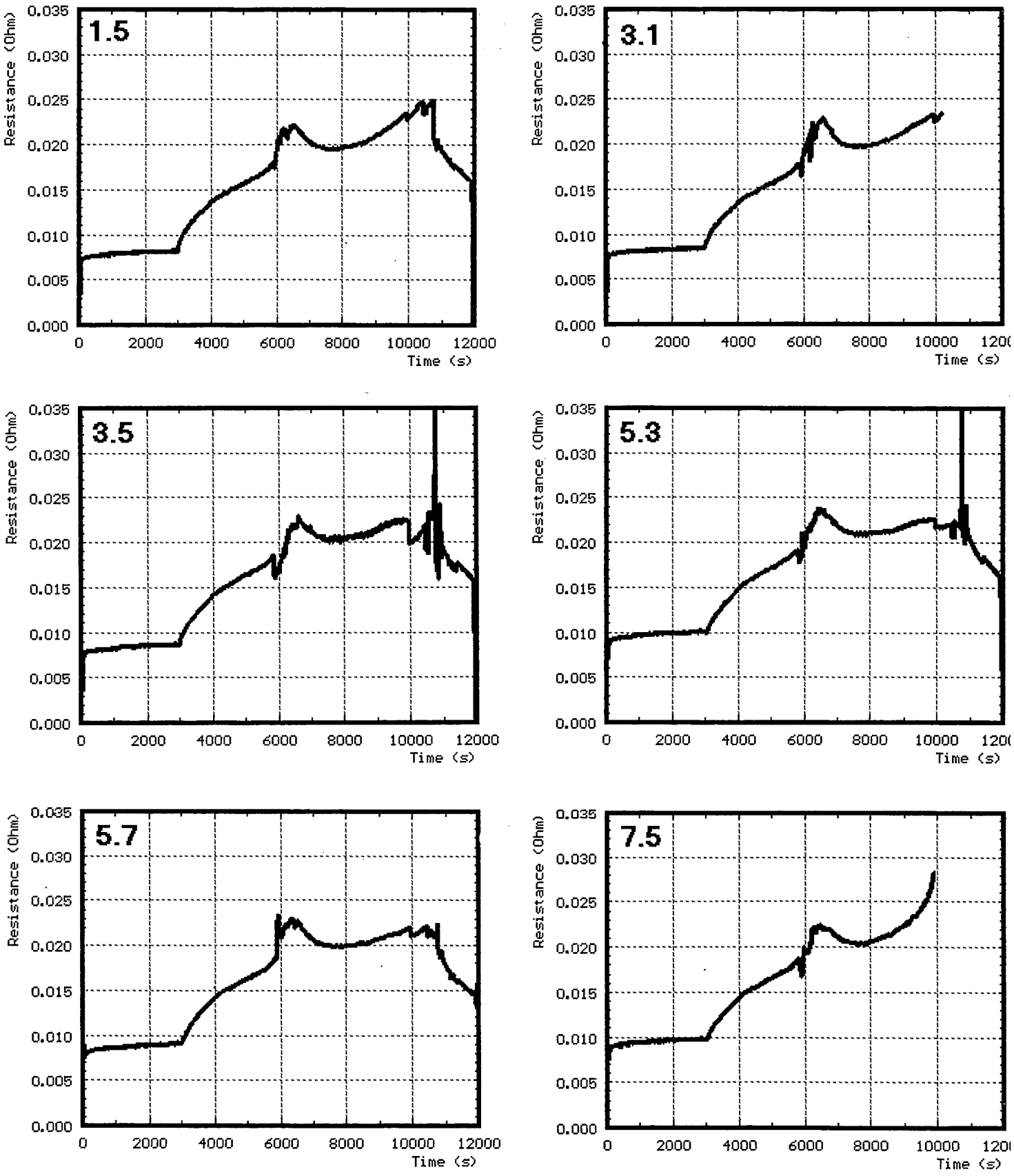

Fig. 19: CORA-30; Resistance of single rods group 1

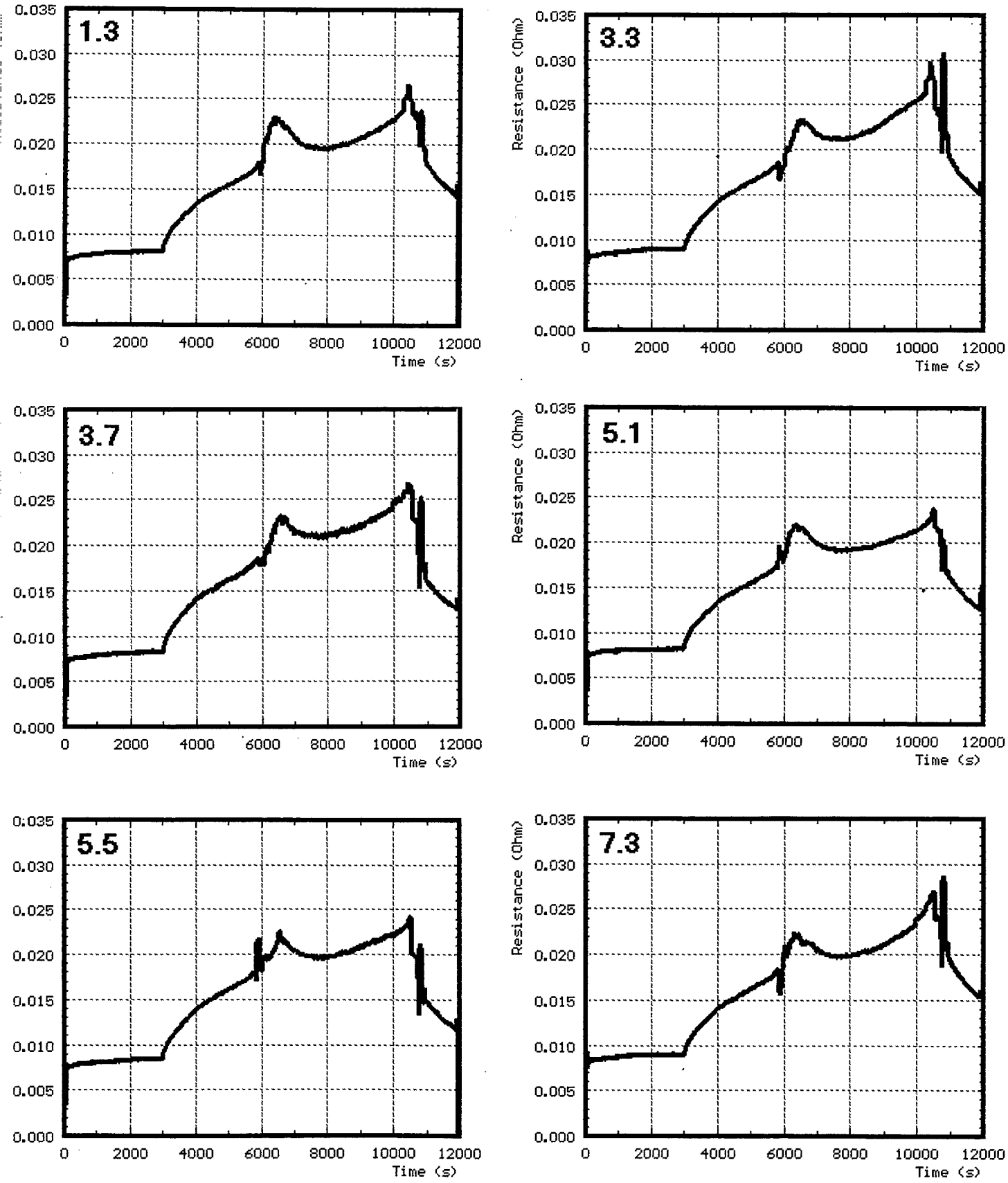

Fig. 20: CORA-30; Resistance of single rods group 2

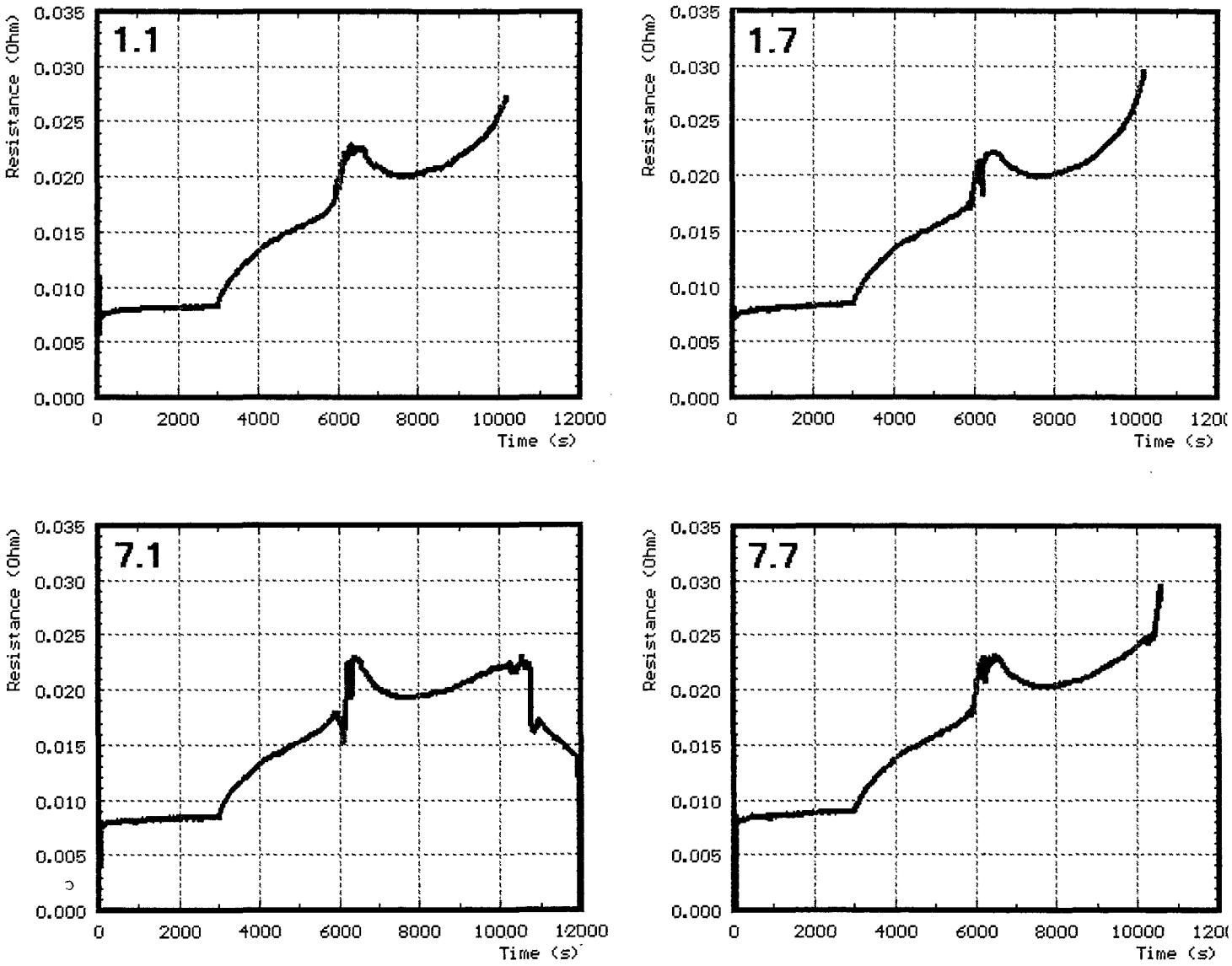

Fig. 21: CORA-30; Resistance of single rods group 3

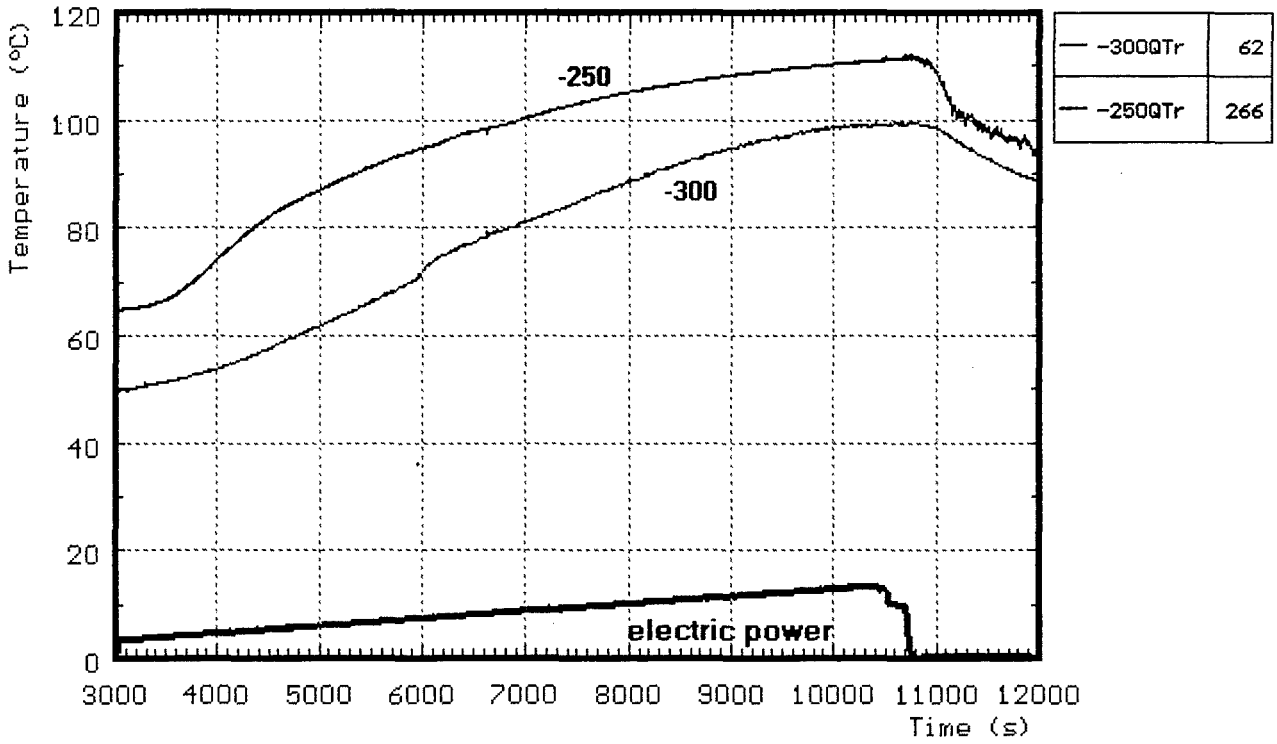

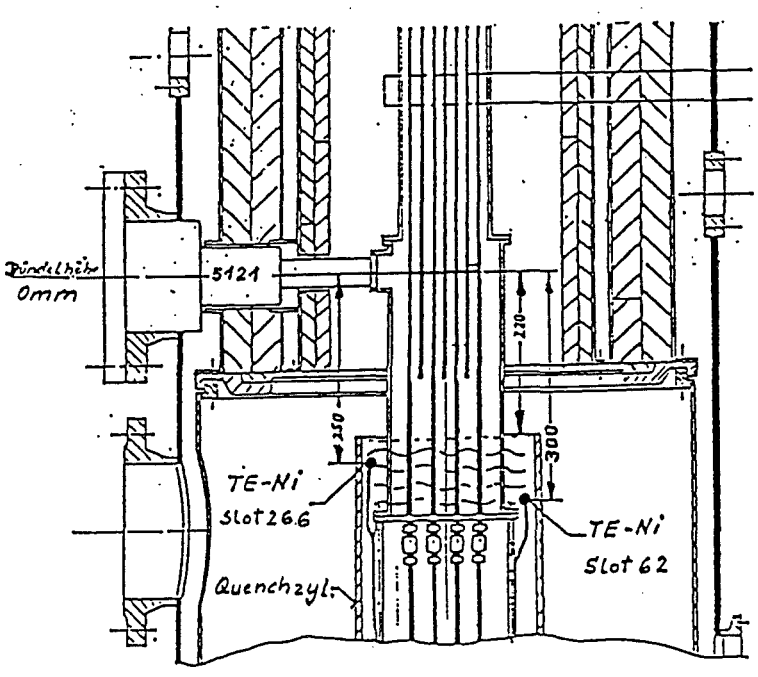

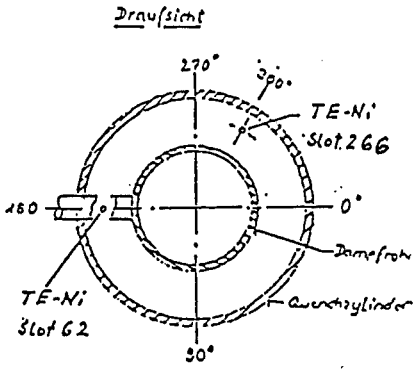

Fig. 22: CORA-30; Water temperature in the quench cylinder

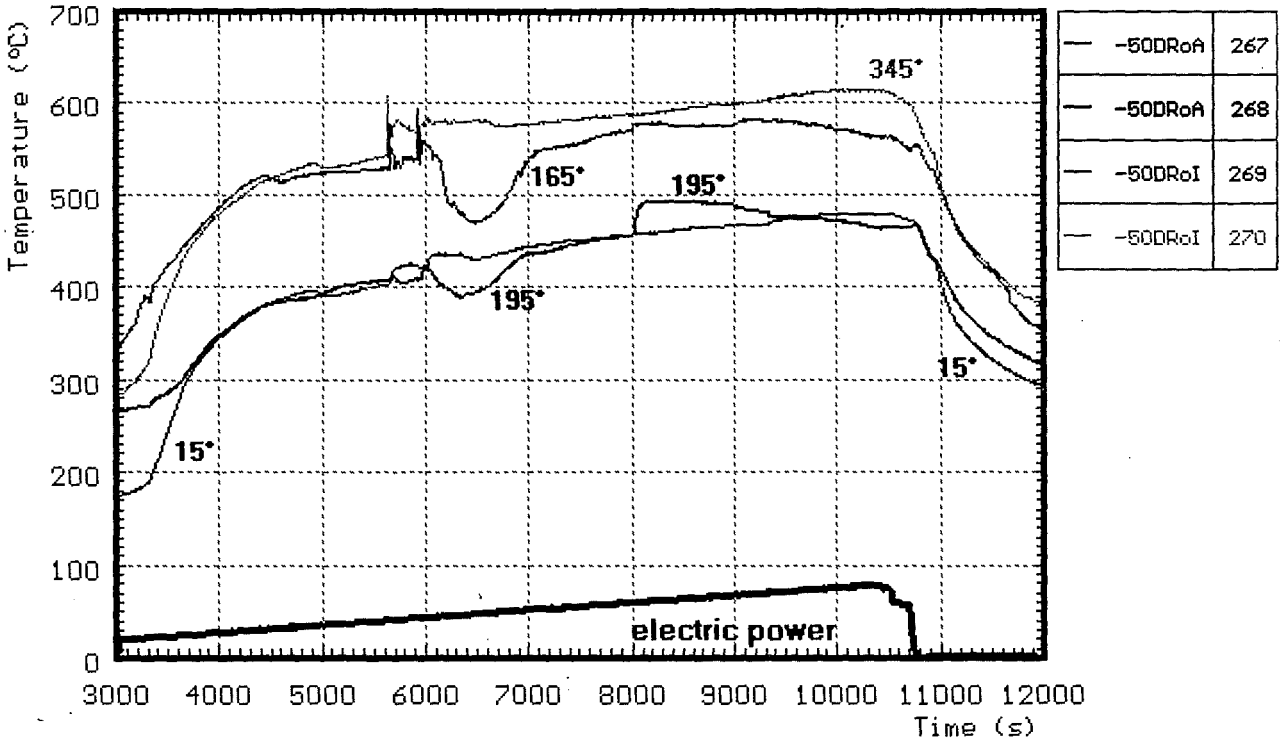

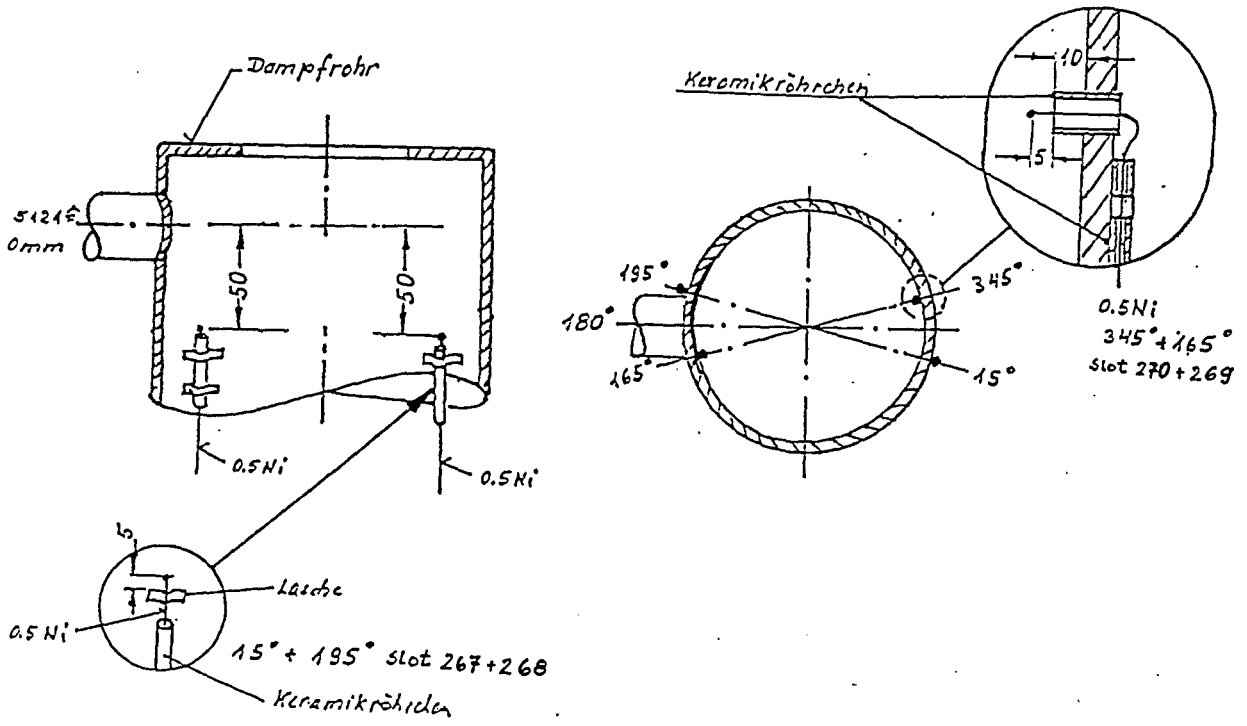

Fig. 23: CORA-30; Temperature in and on steam tube at -50mm elevation

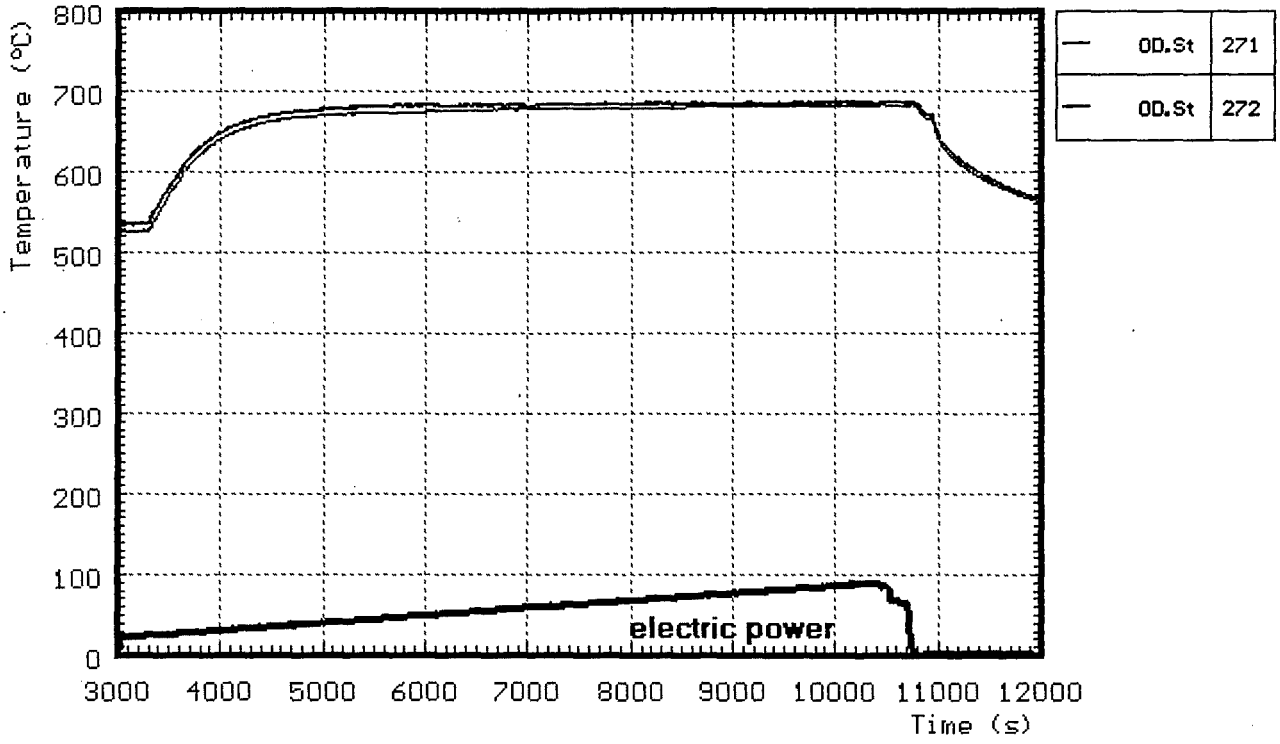

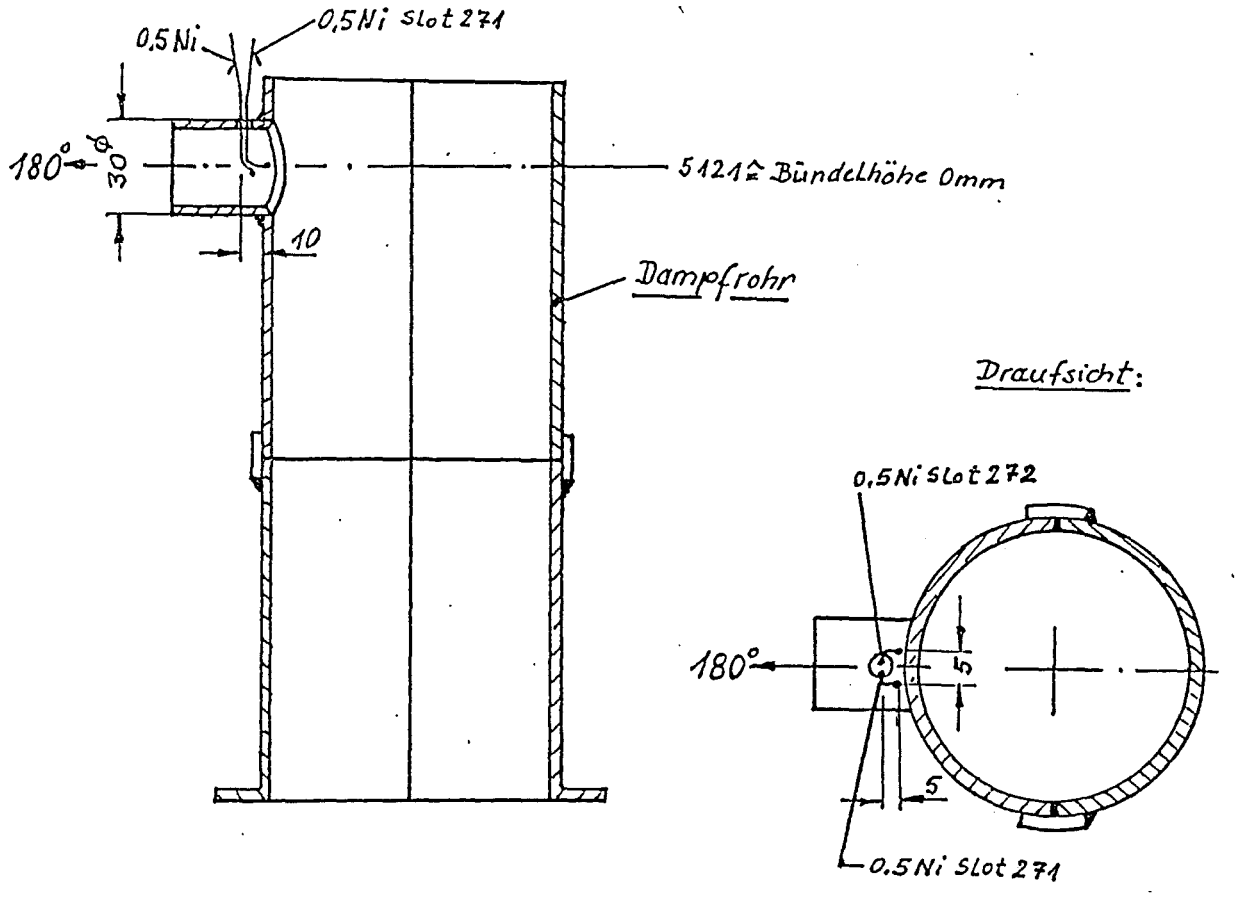

Fig. 24: CORA-30; Temperatures at the steam inlet

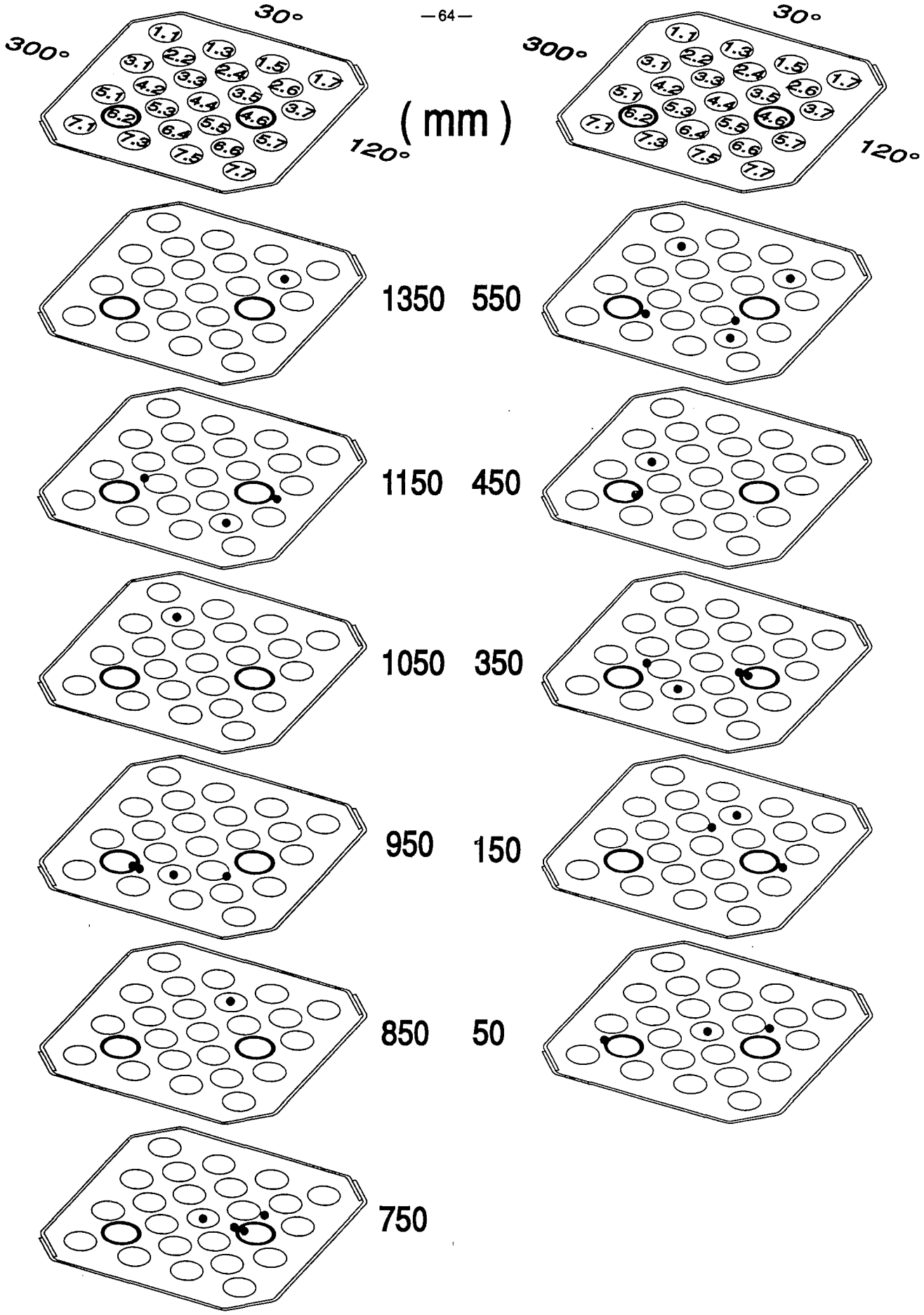

Fig. 25: Thermocouple locations within the bundle (CORA-30)

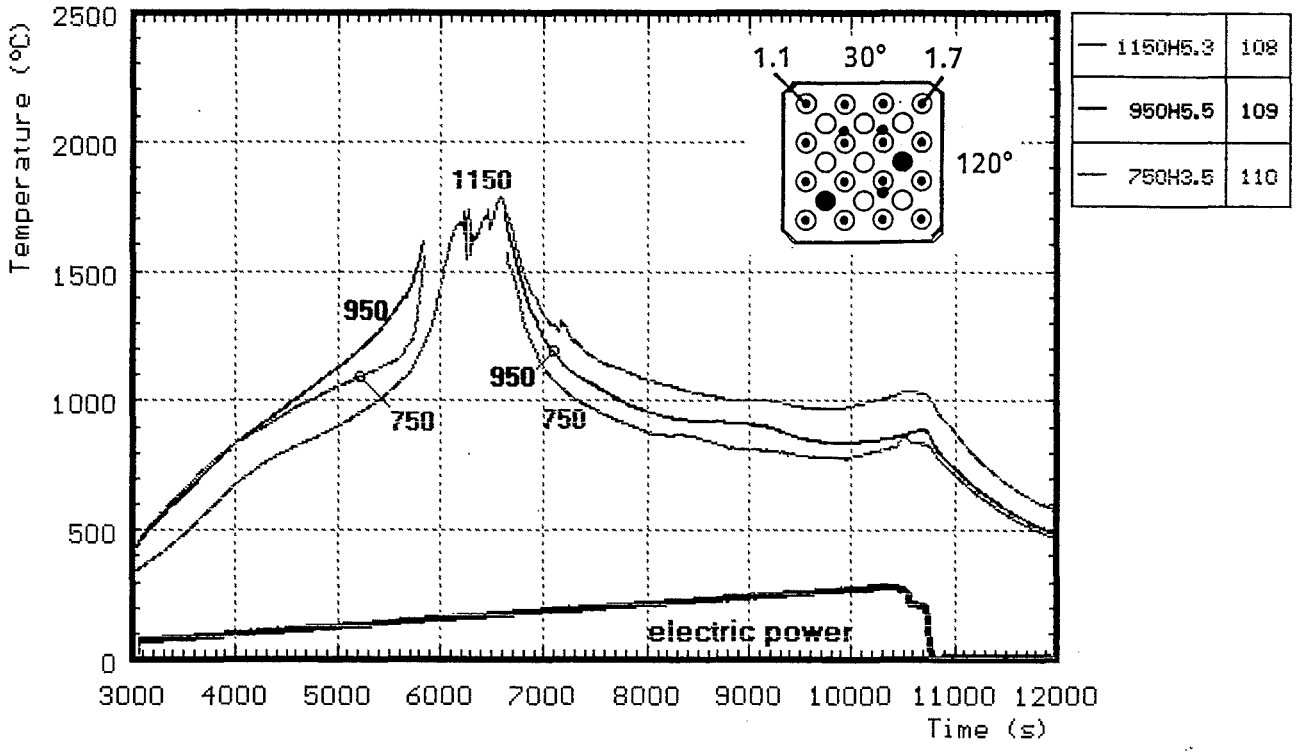

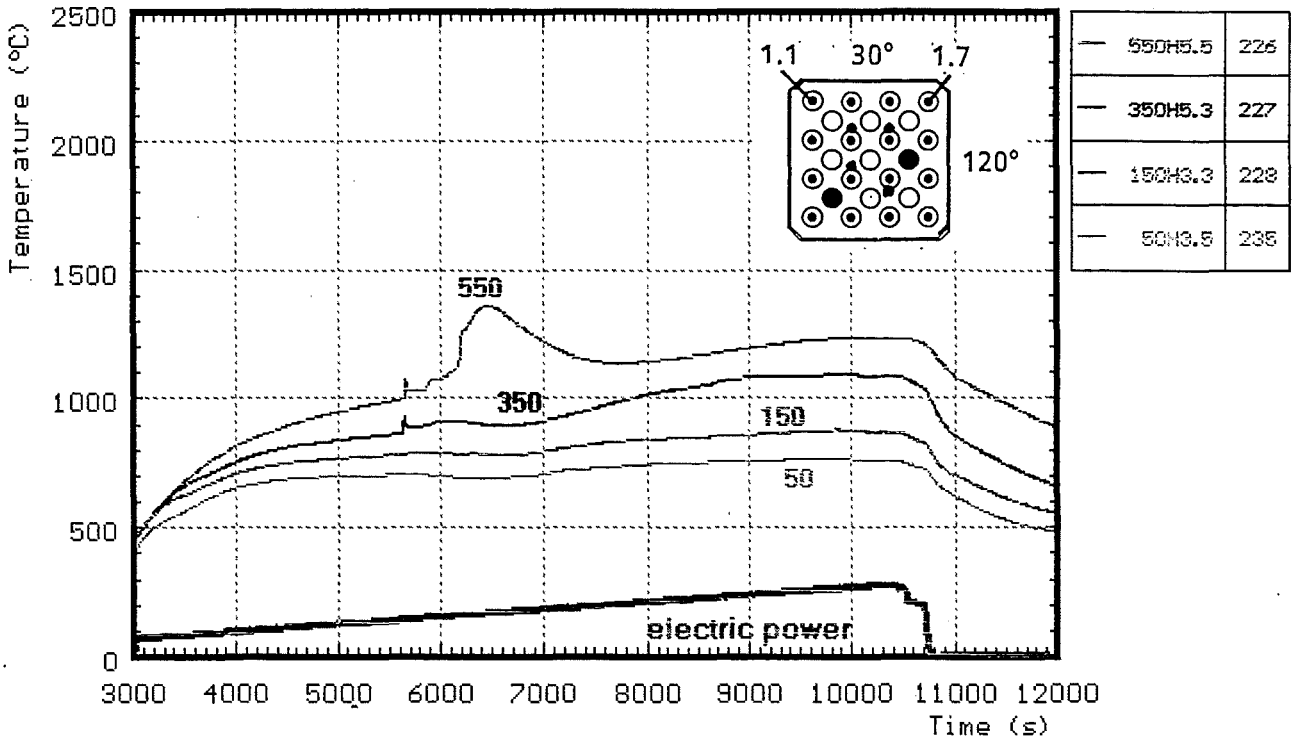

Fig. 26: CORA-30; Temperatures of heated rods

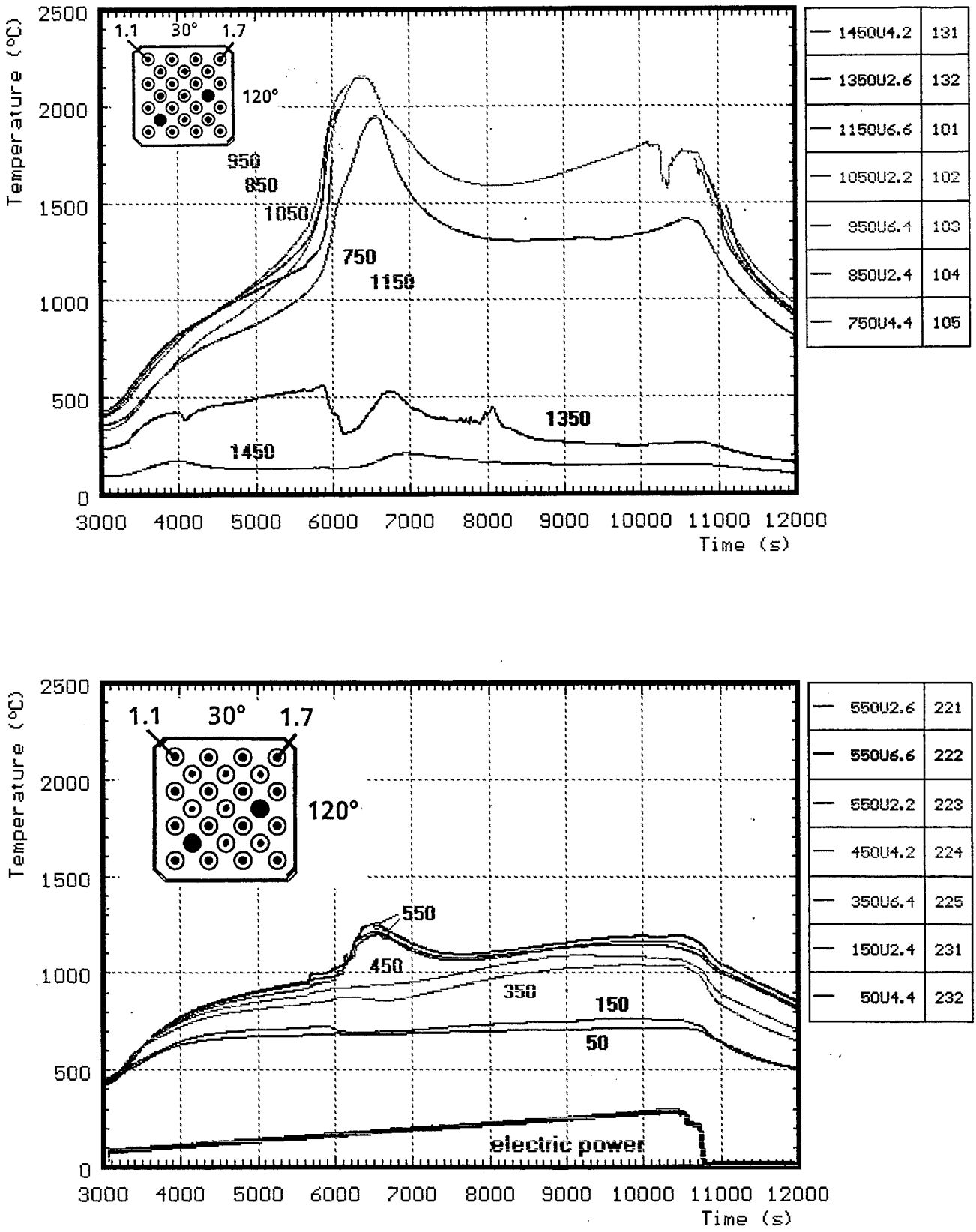

Fig. 27: CORA-30; Temperatures of unheated rods (TCs in central position)

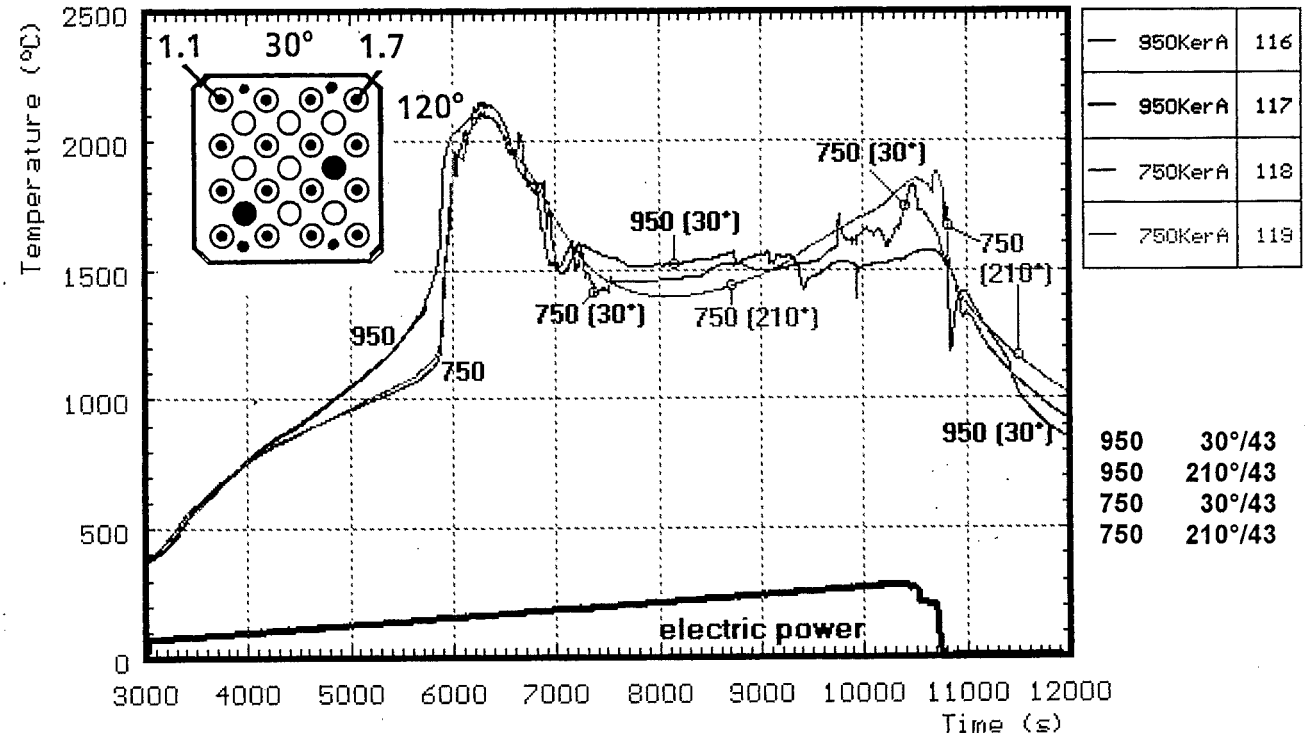

Fig. 29: CORA-30; Temperatures between bundle and shroud measured with ceramic protected TCs

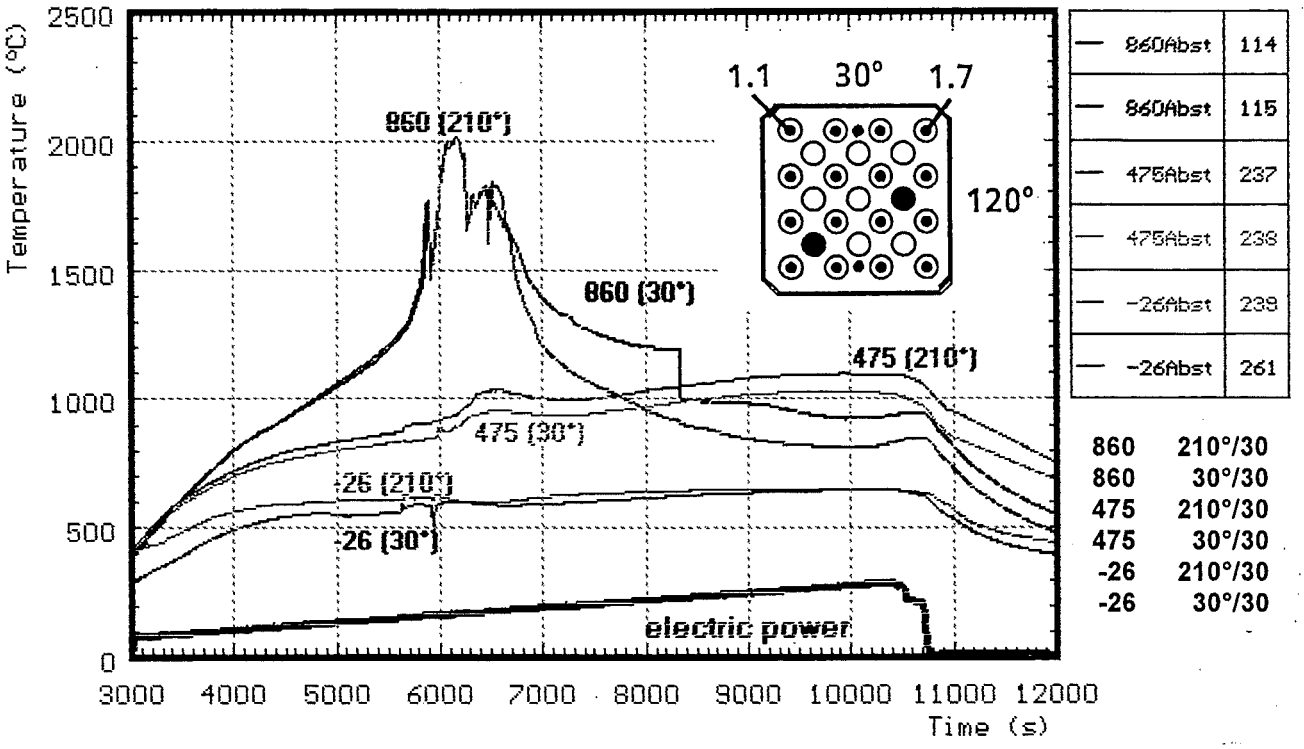

Fig. 30: CORA-30; Temperatures of the spacers

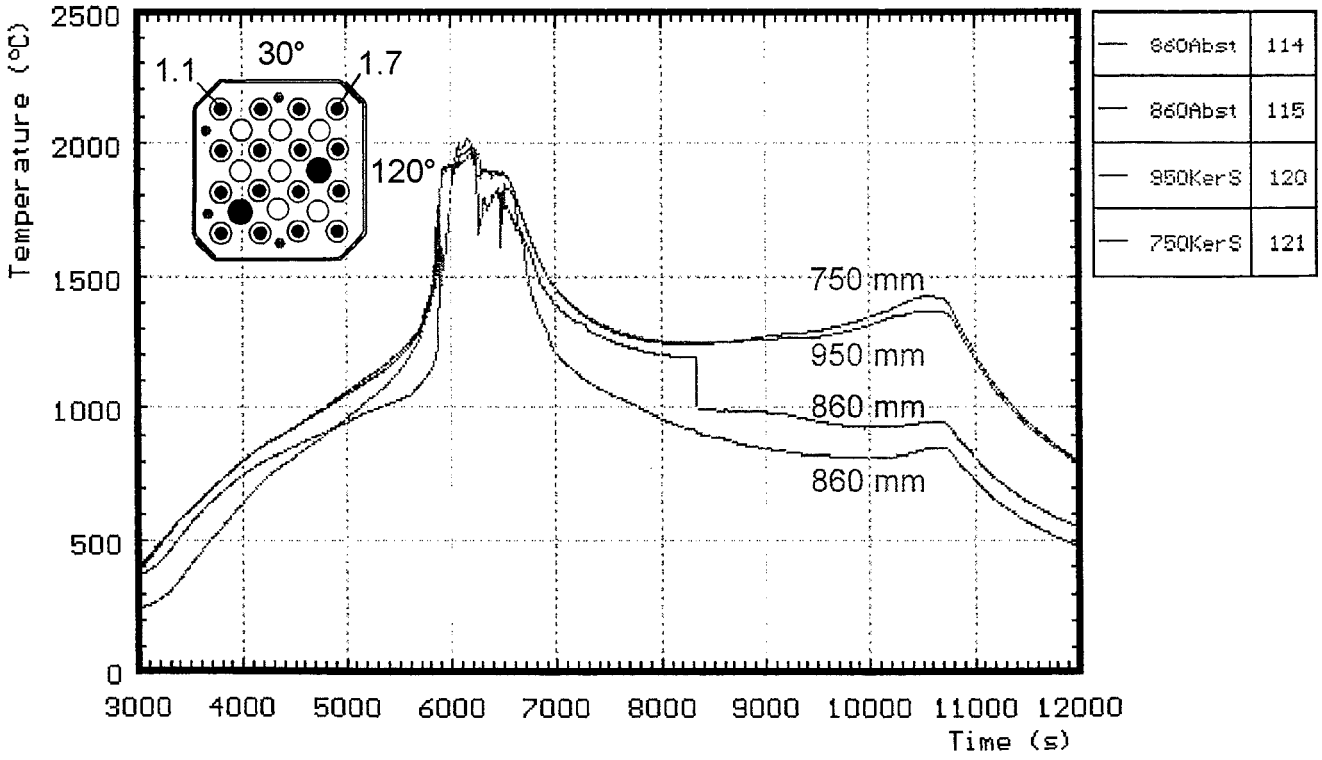

Fig. 30a: CORA-30; Comparison of temperatures of the space at 860 mm to temperatures on the inner side of shroud at 750 and 950 mm elevation

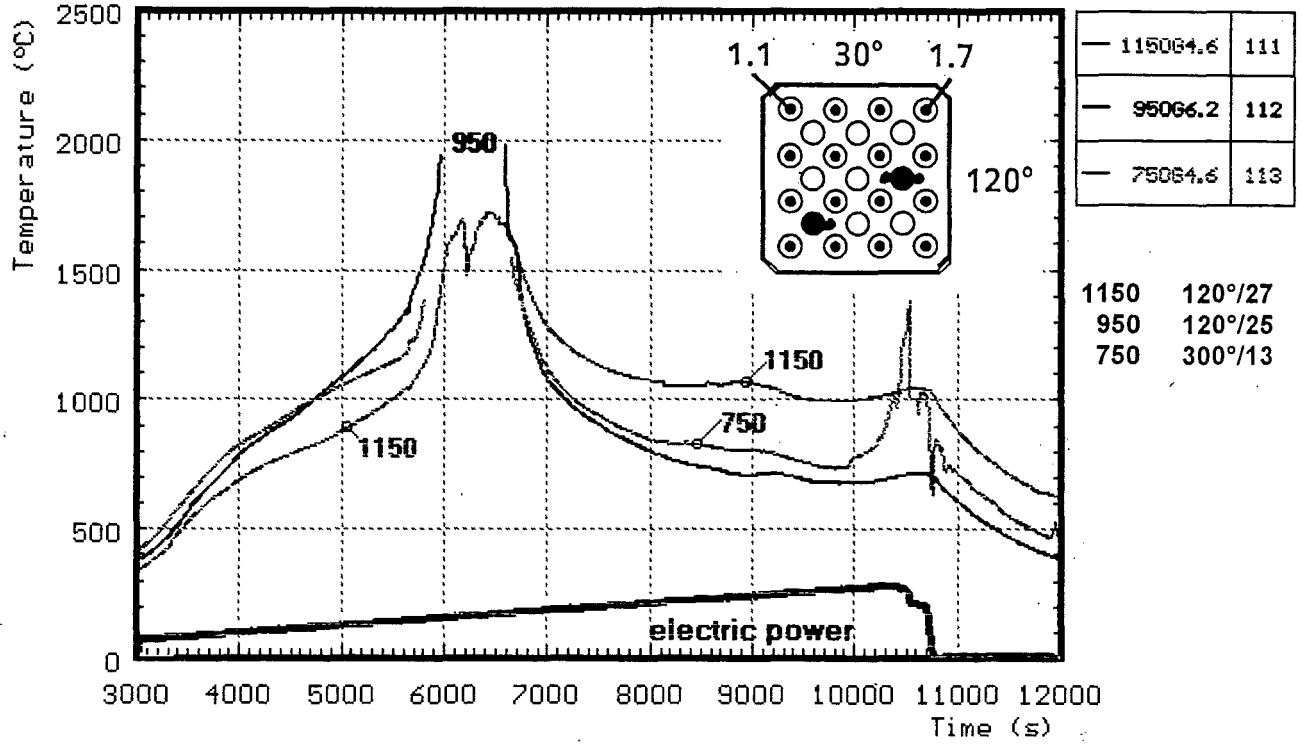

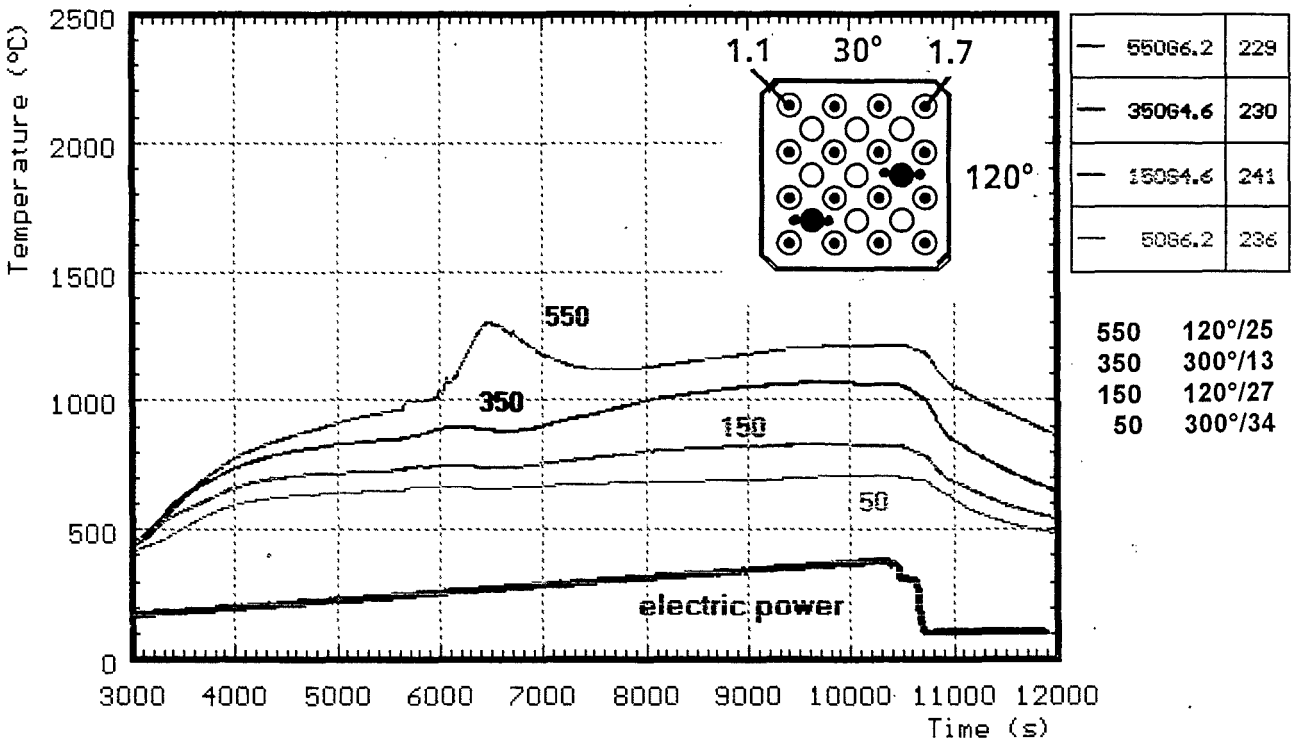

Fig. 31: CORA-30; Temperatures of the guide tubes of absorber rods

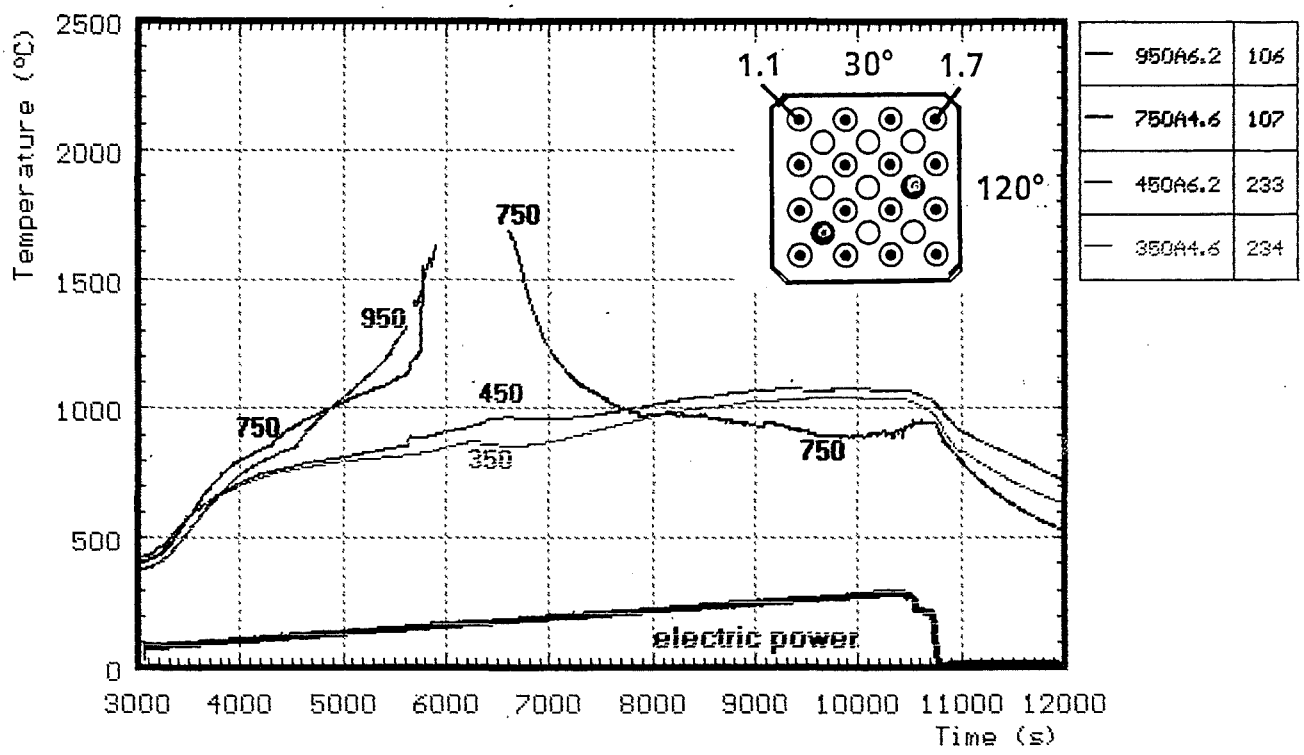

Fig. 32: CORA-30; Temperatures in the absorber

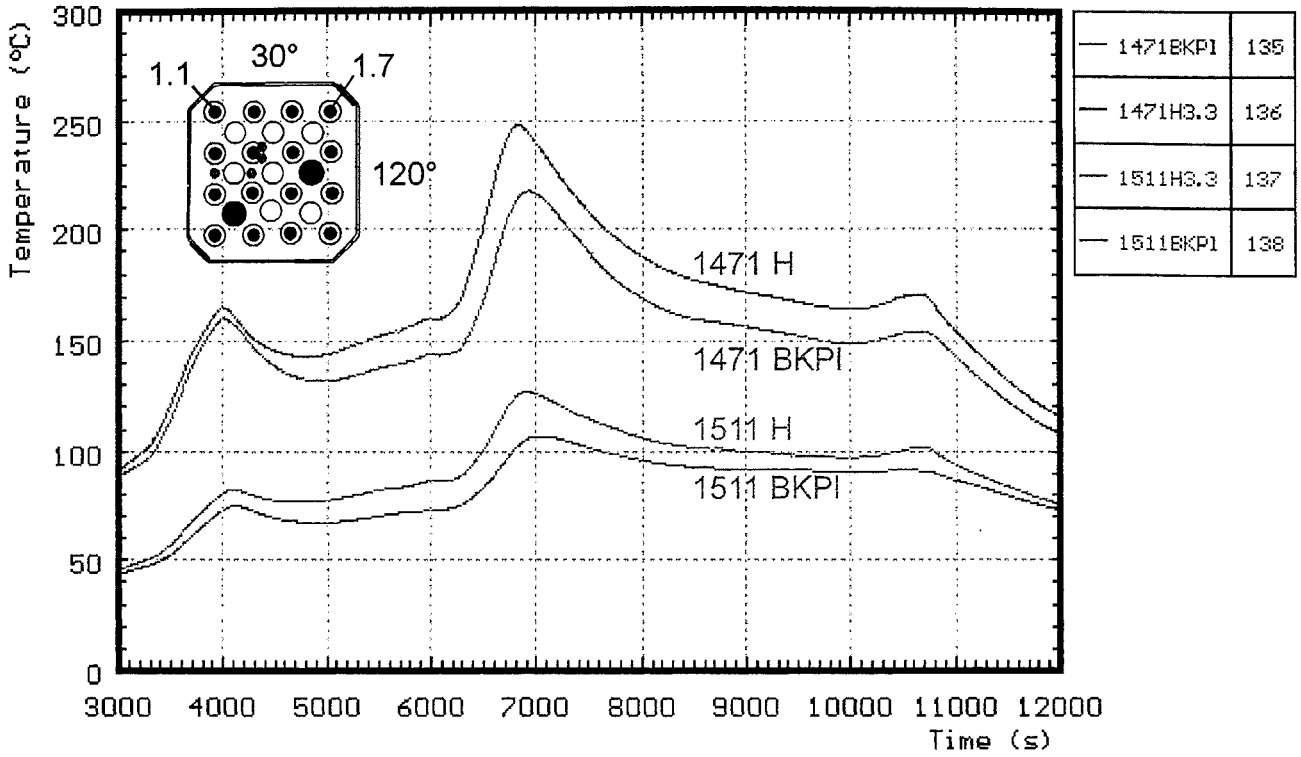

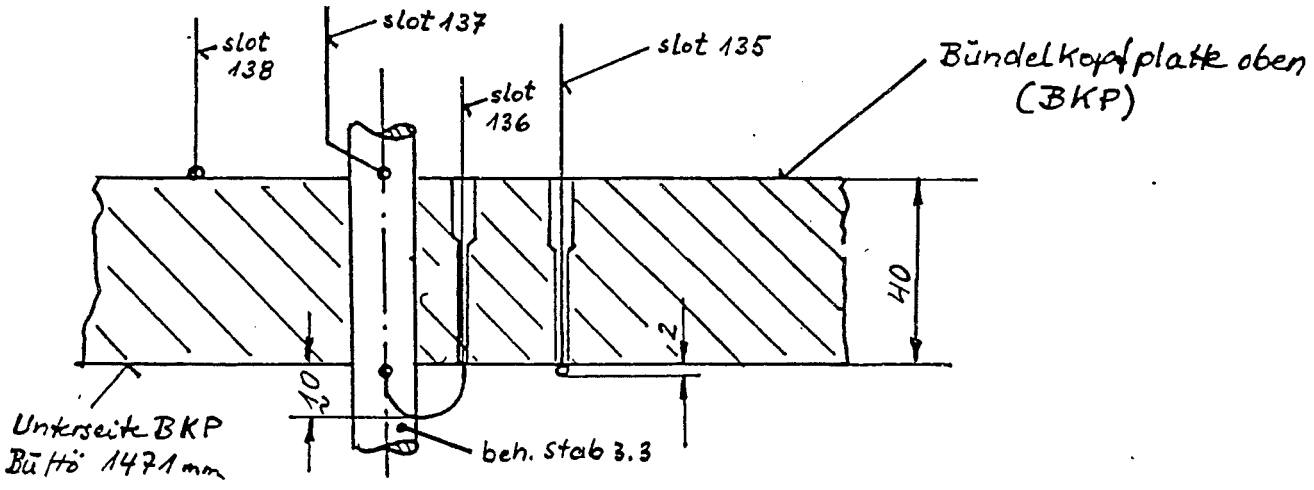

Fig. 33: CORA-30; Temperatures at the bundle head plate

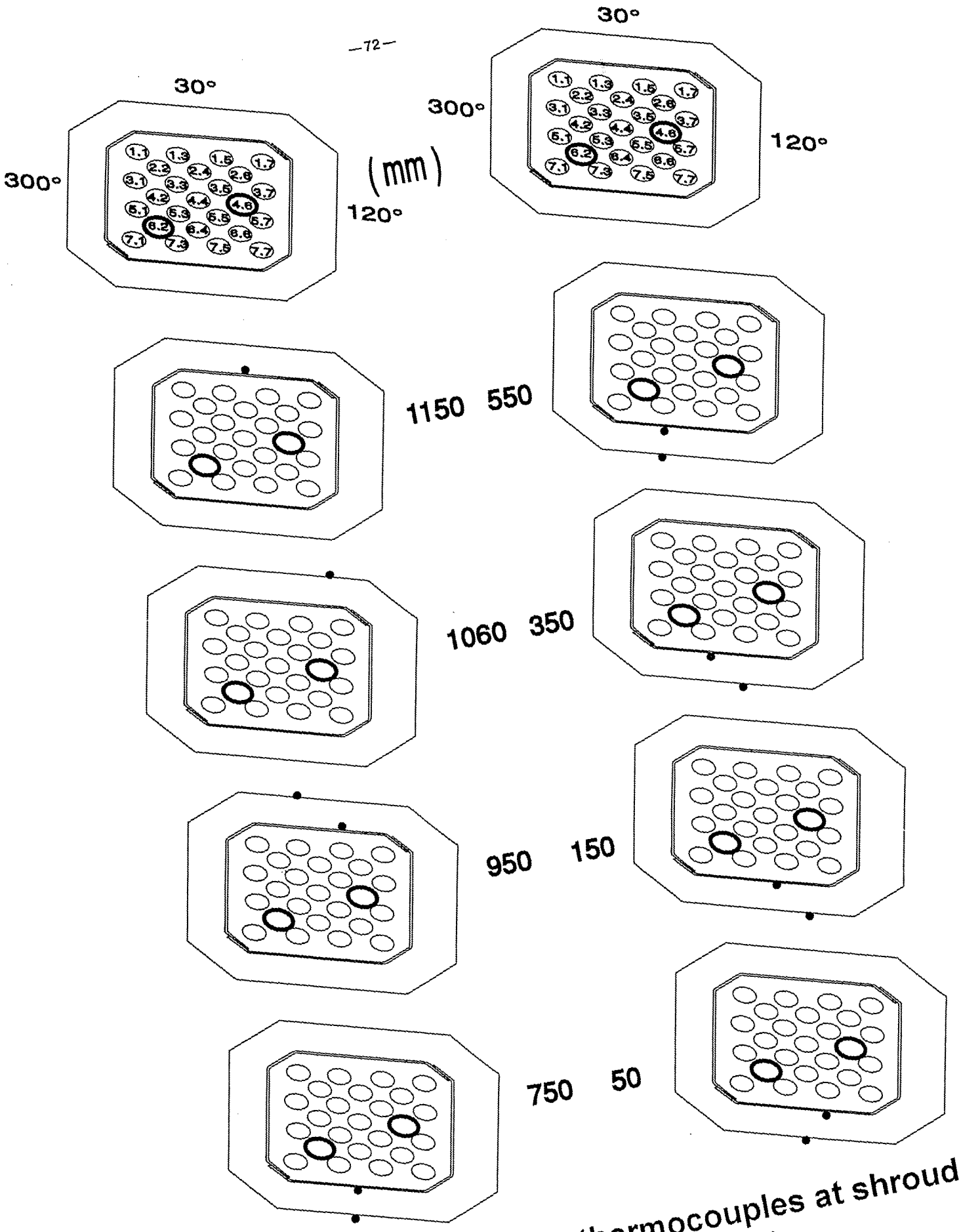

Fig. 34: Location of the thermocouples at shroud and shroud insulation (CORA-30)

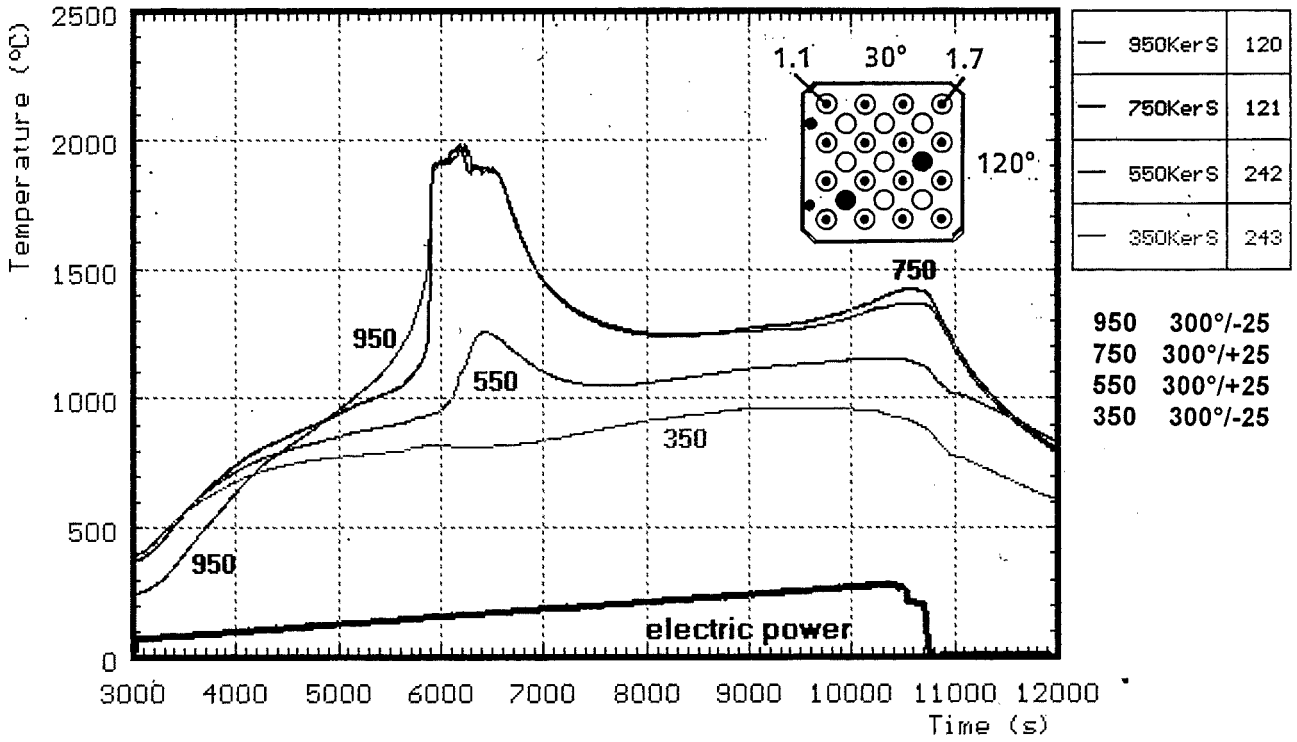

Fig. 35: CORA-30; Temperatures of inner side of shroud measured with ceramic protected TCs

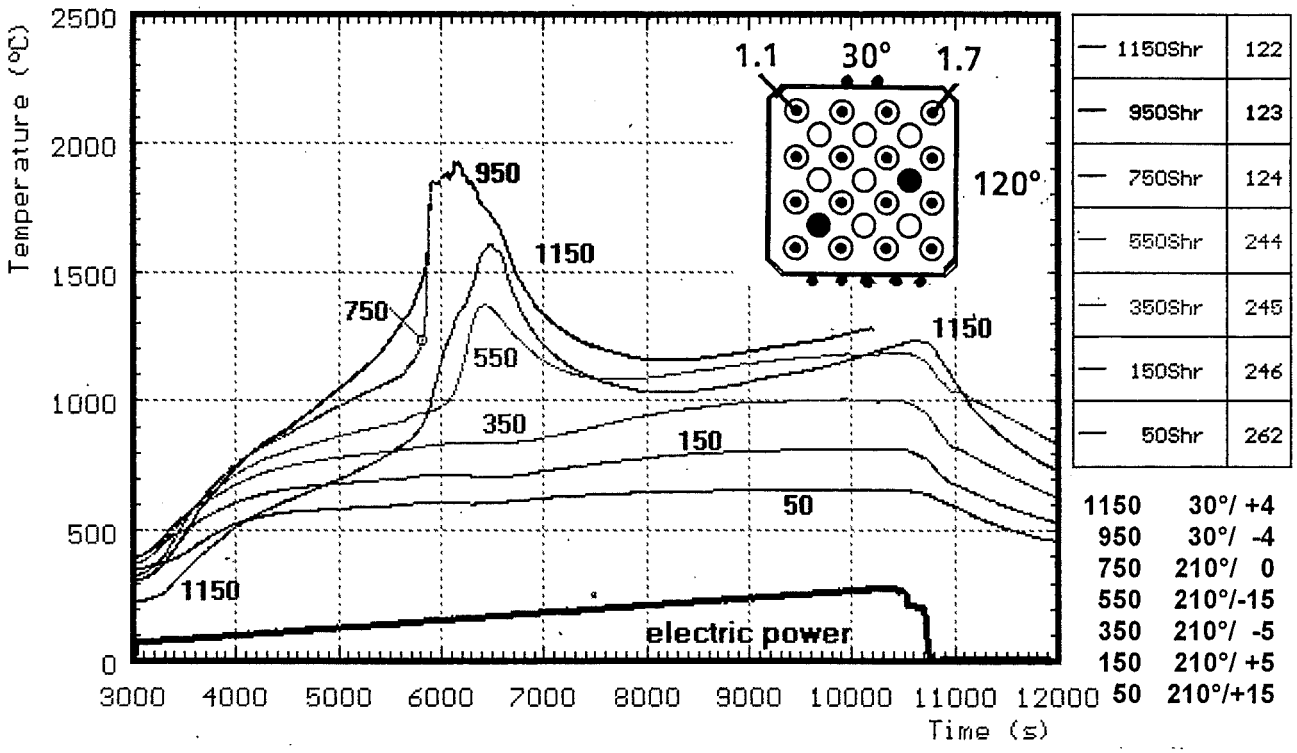

Fig. 36: CORA-30; Temperatures of outer side of shroud

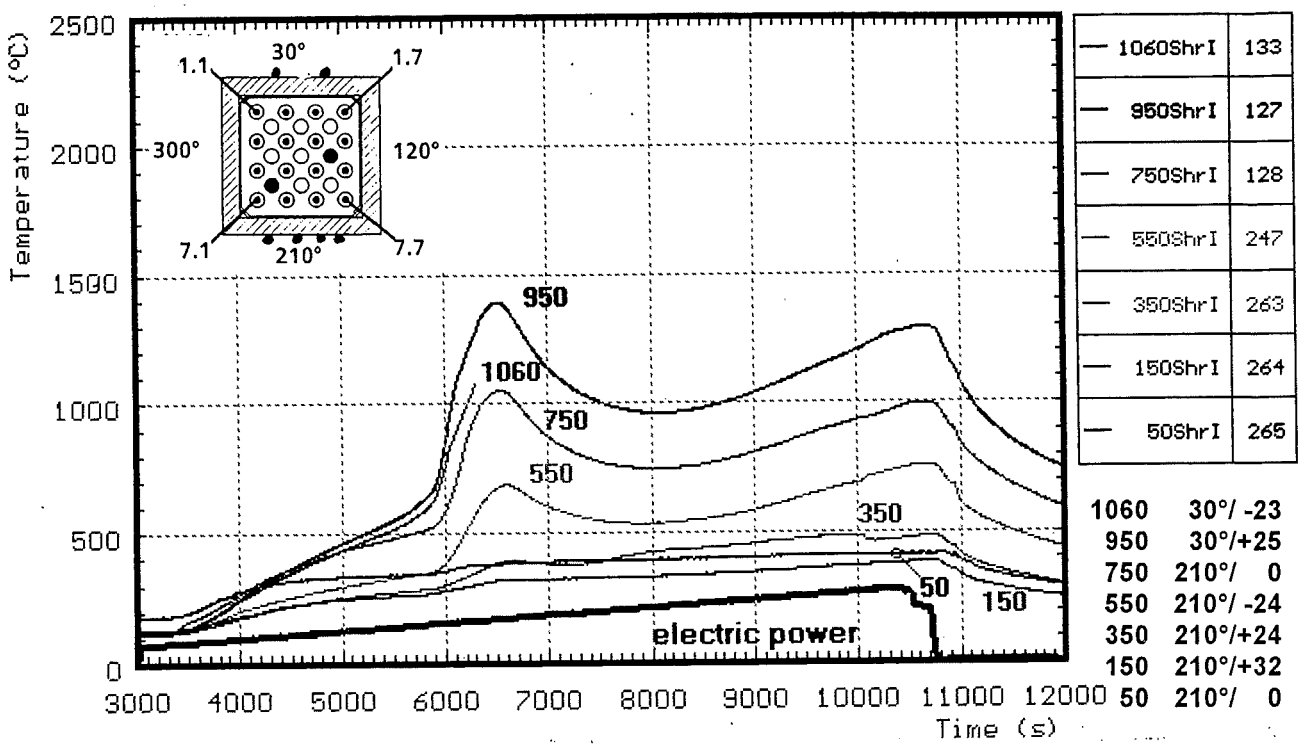

Fig. 37: CORA-30; Temperatures of the shroud insulation

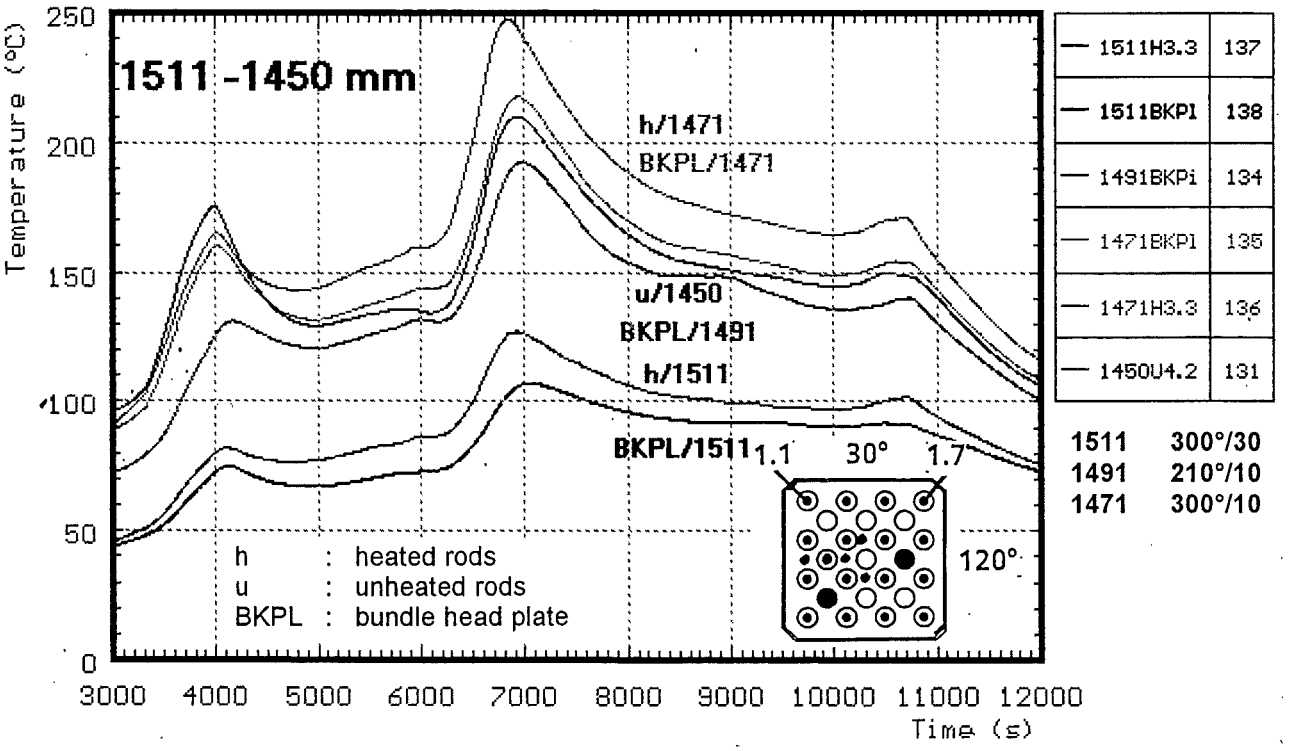

Fig. 38: CORA-30; Temperatures at elevations given (1511-1450 mm)

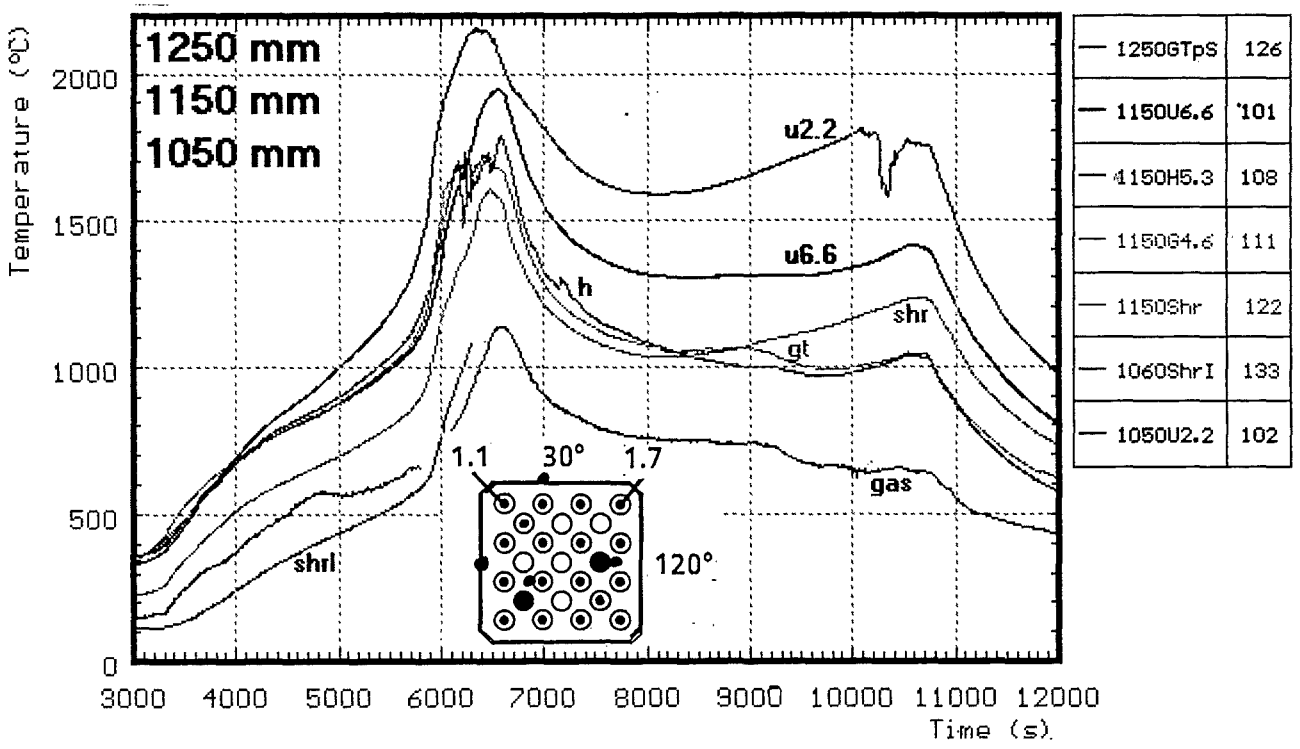

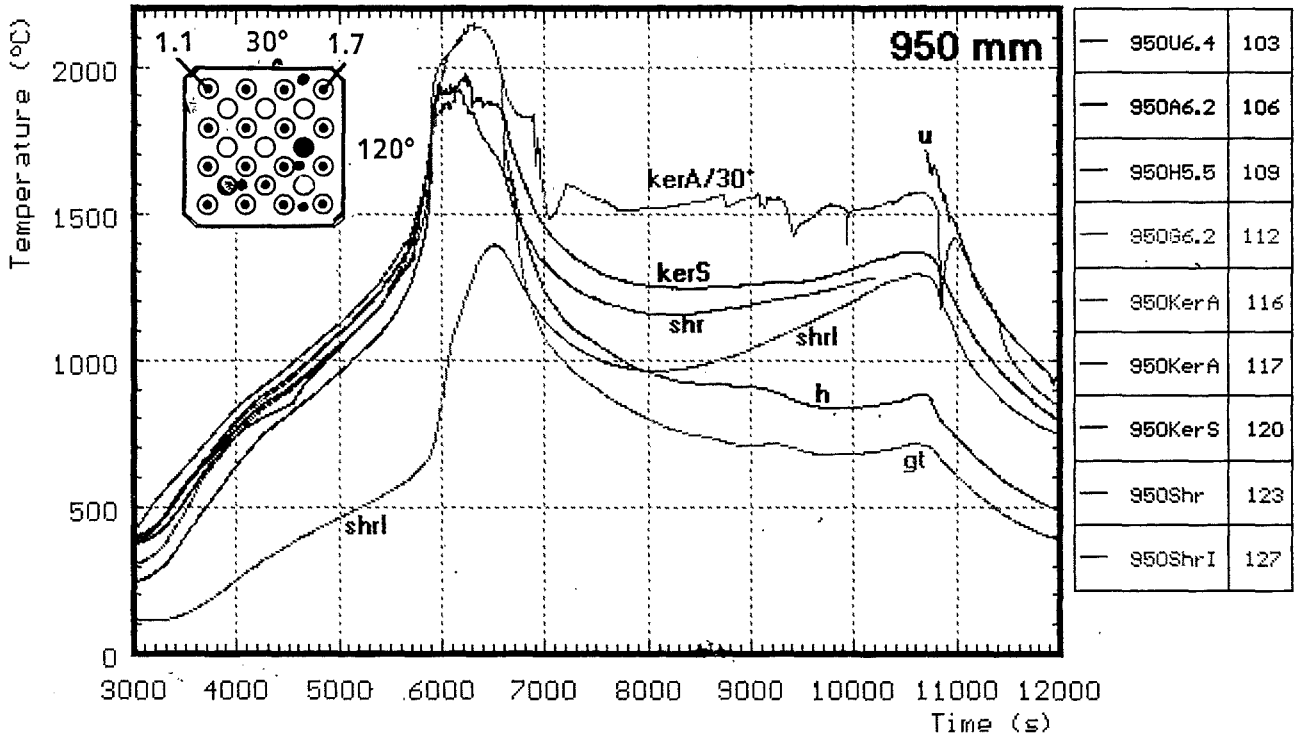

shr : on shroud
shrl : shroud insulation
gas : gas temperature
kerA : ceramic protected thermocouples

h : heated rods
u : unheated rods
gt : guide tube
kerS : ceramic protected thermocouples, inner side of shroud

Fig. 39: CORA-30; Temperatures at elevations given (1250-1050,950 mm)

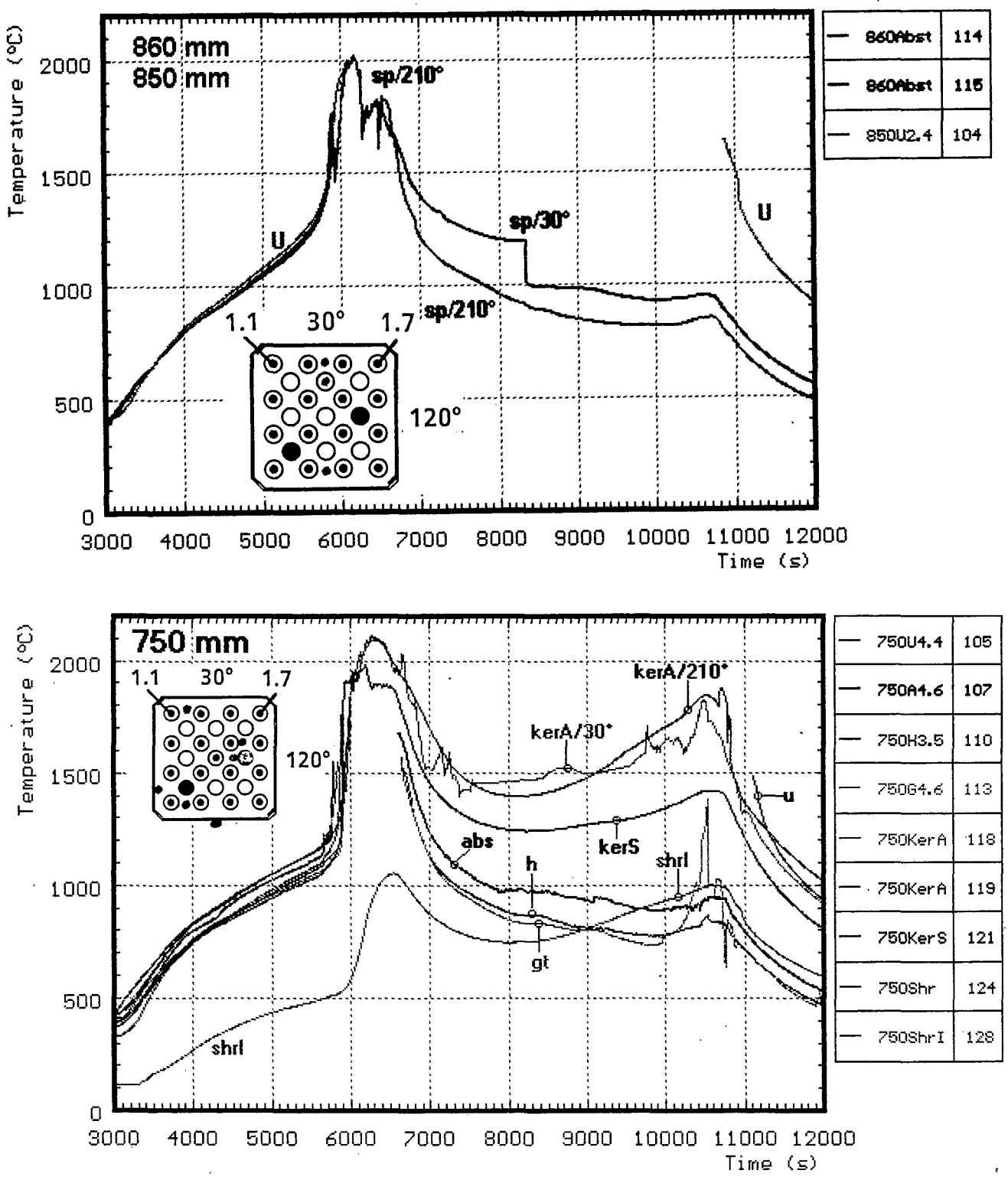

sp : spacer
shrl : shroud insulation
kerA : ceramic protected thermocouples
kerS : ceramic protected thermocouples, inner side of shroud
h : heated rods
u : unheated rods
gt : guide tube
abs : in absorber

Fig. 40: CORA-30; Temperatures at elevations given (860,850,750 mm)

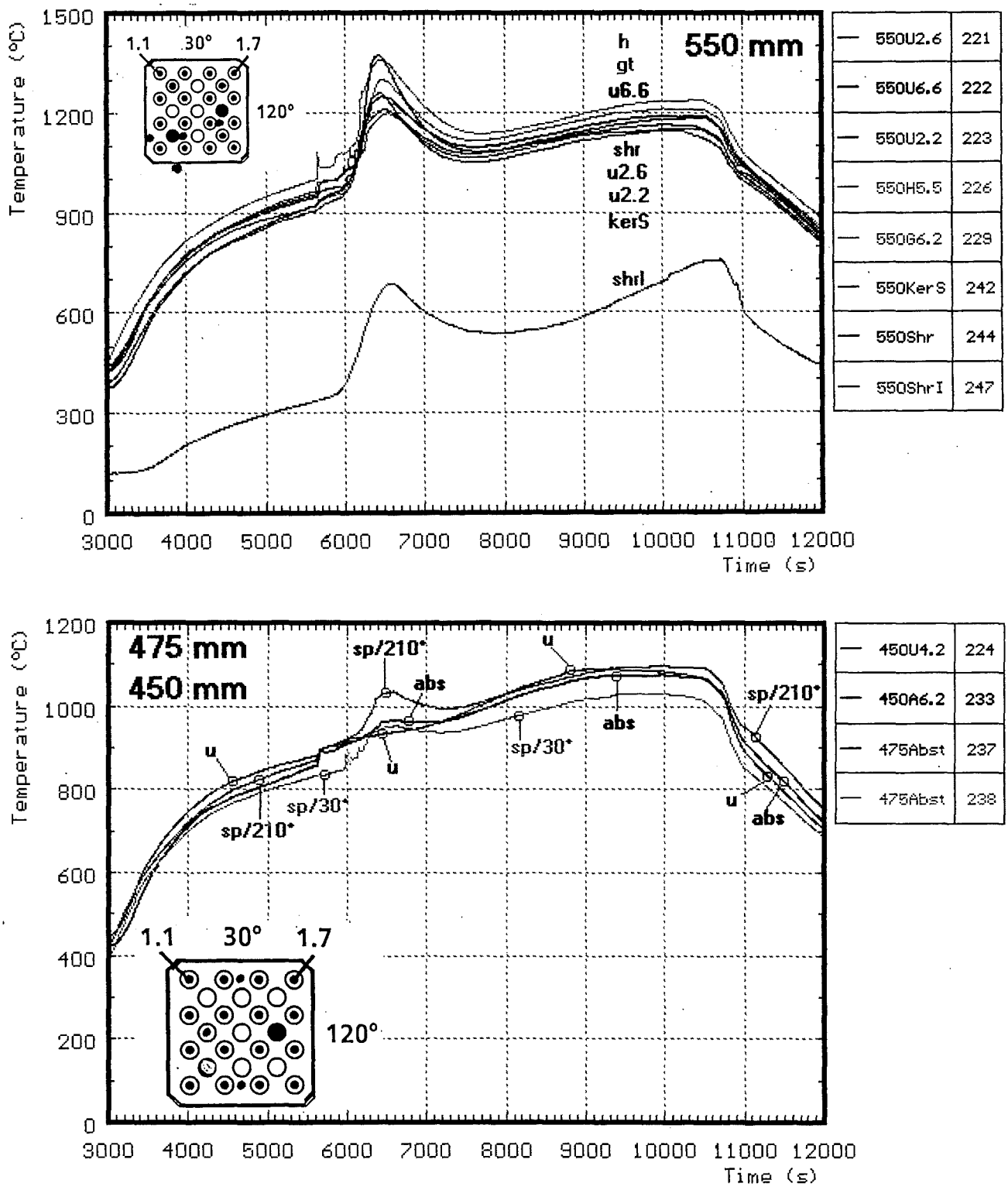

shr : on shroud
shrl : shroud insulation
kerS : ceramic protected thermocouples, inner side of shroud
sp : spacer

h : heated rods
u : unheated rods
gt : guide tube
abs : in absorber

Fig. 41: CORA-30; Temperatures at elevations given (550, 475, 450 mm)

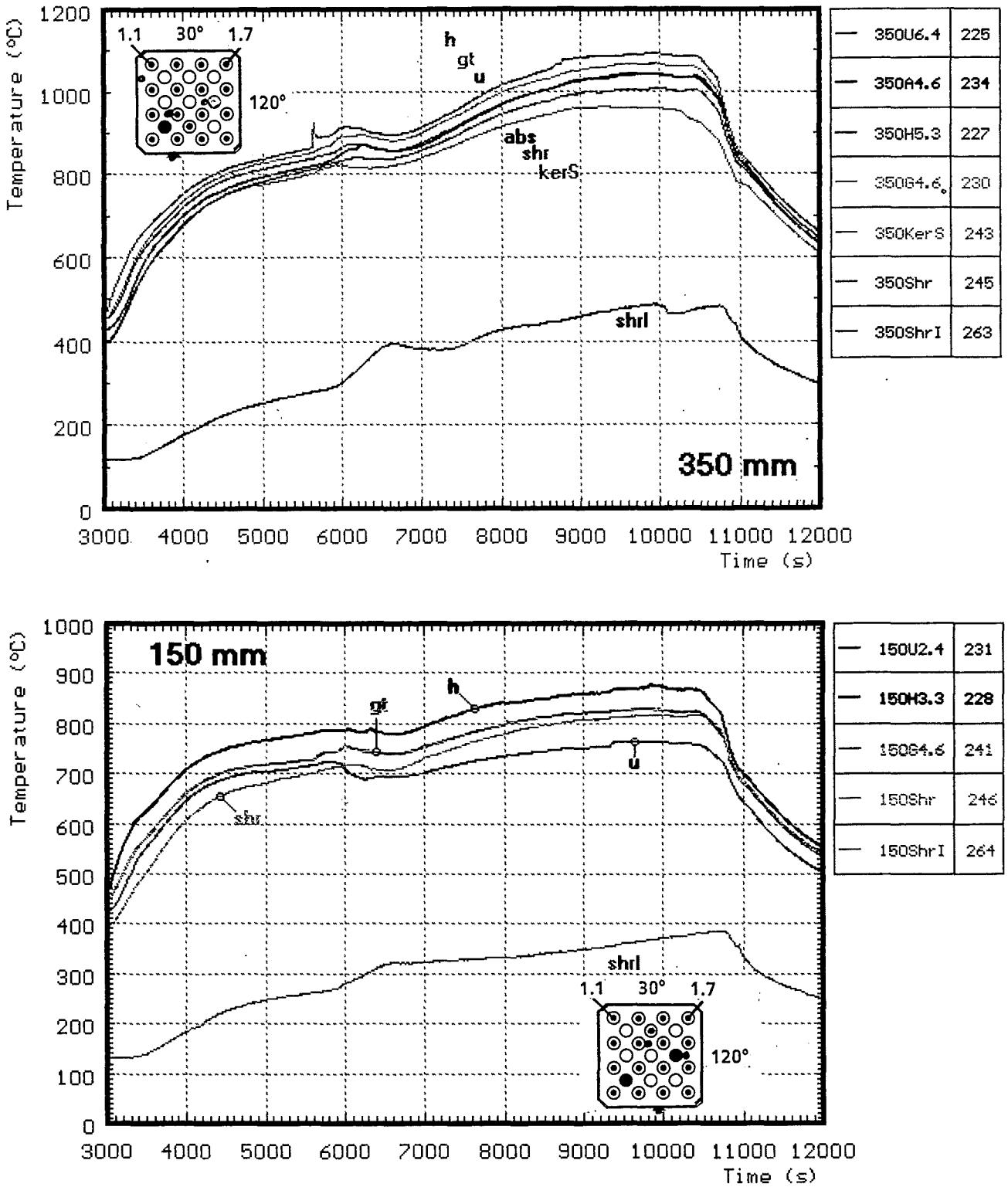

shr : on shroud
shrl : shroud insulation
abs : in absorber
kerS : ceramic protected thermocouples, inner side of shroud

h : heated rods
u : unheated rods
gt : guide tube

Fig. 42: CORA-30; Temperatures at elevations given (350, 150 mm)

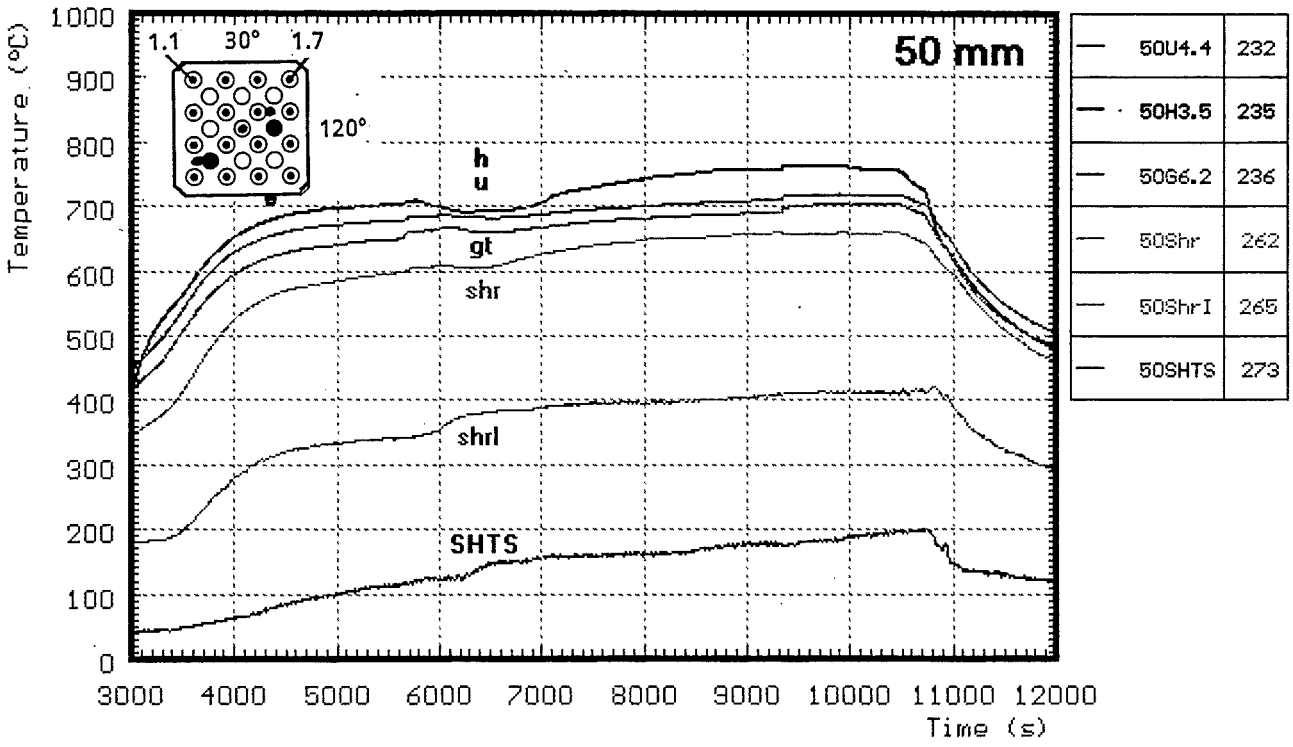

shr : on shroud
shrl : shroud insulation
SHTS : between shroud and HT shield

h : heated rods
u : unheated rods
gt : guide tube

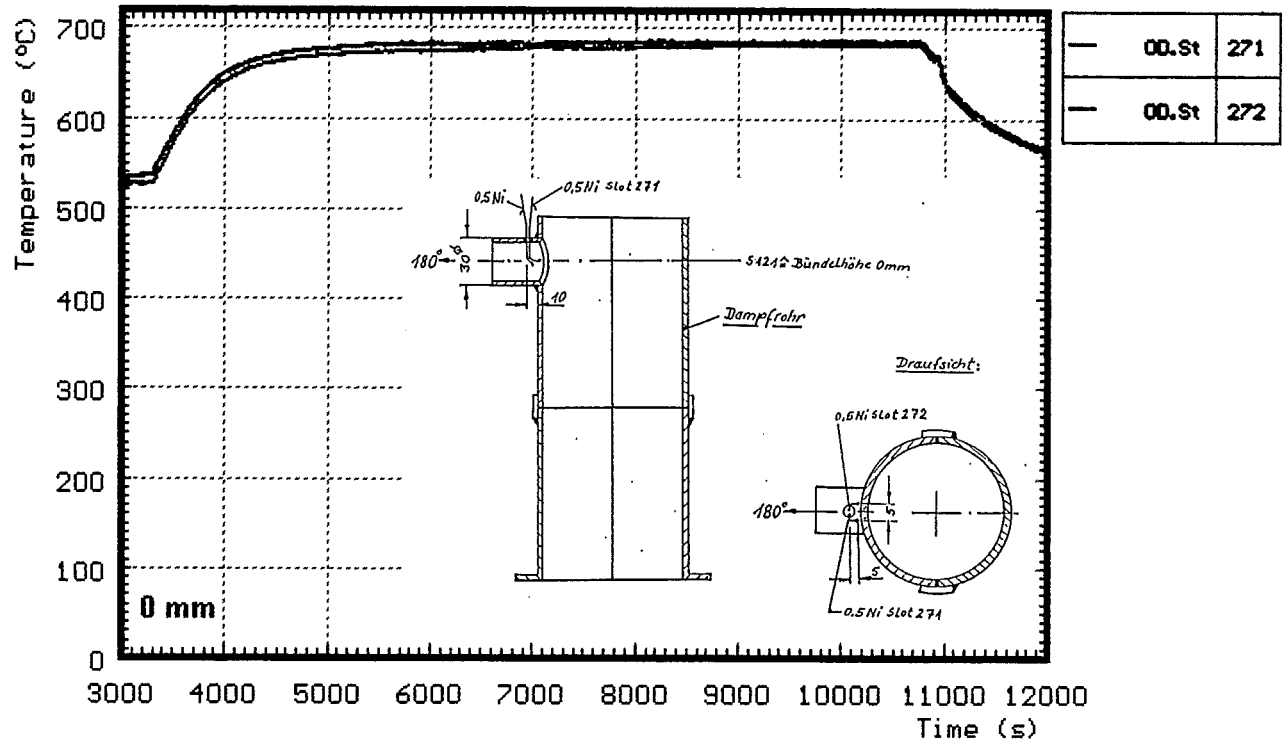

Fig. 43: CORA-30; Temperatures at elevations given (50, 0 mm)

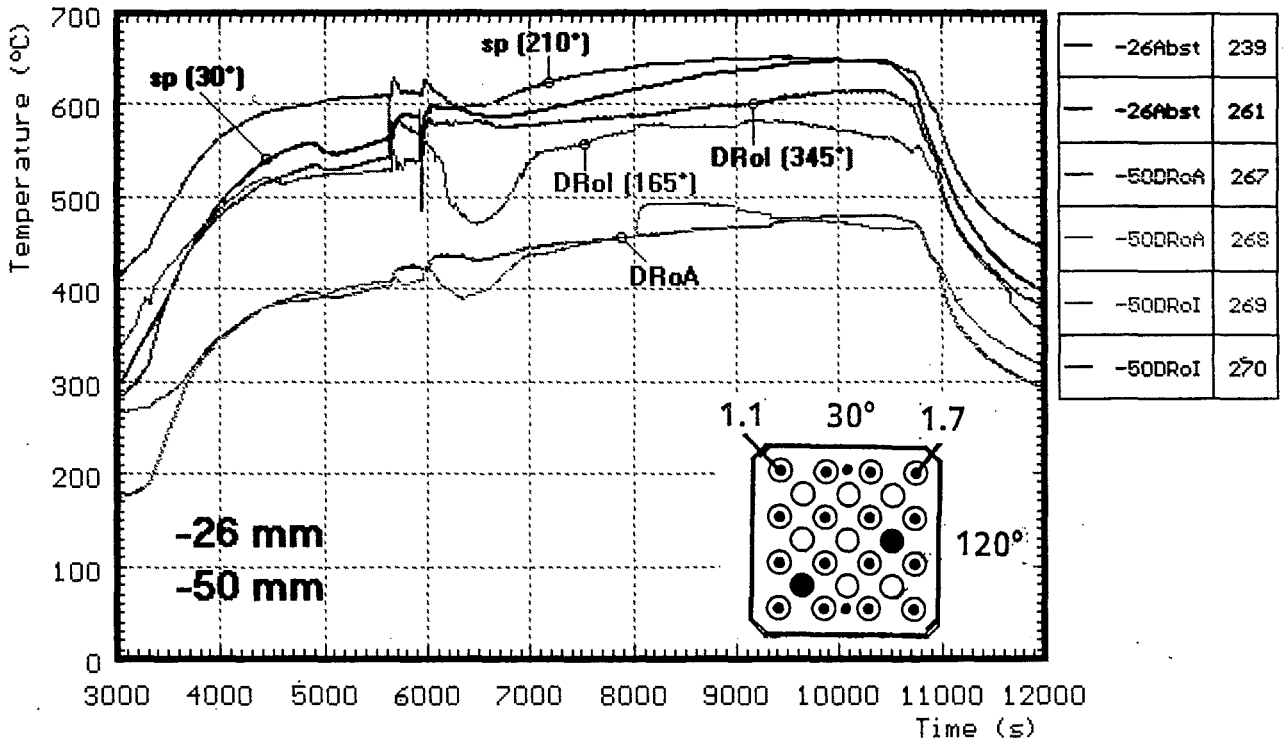

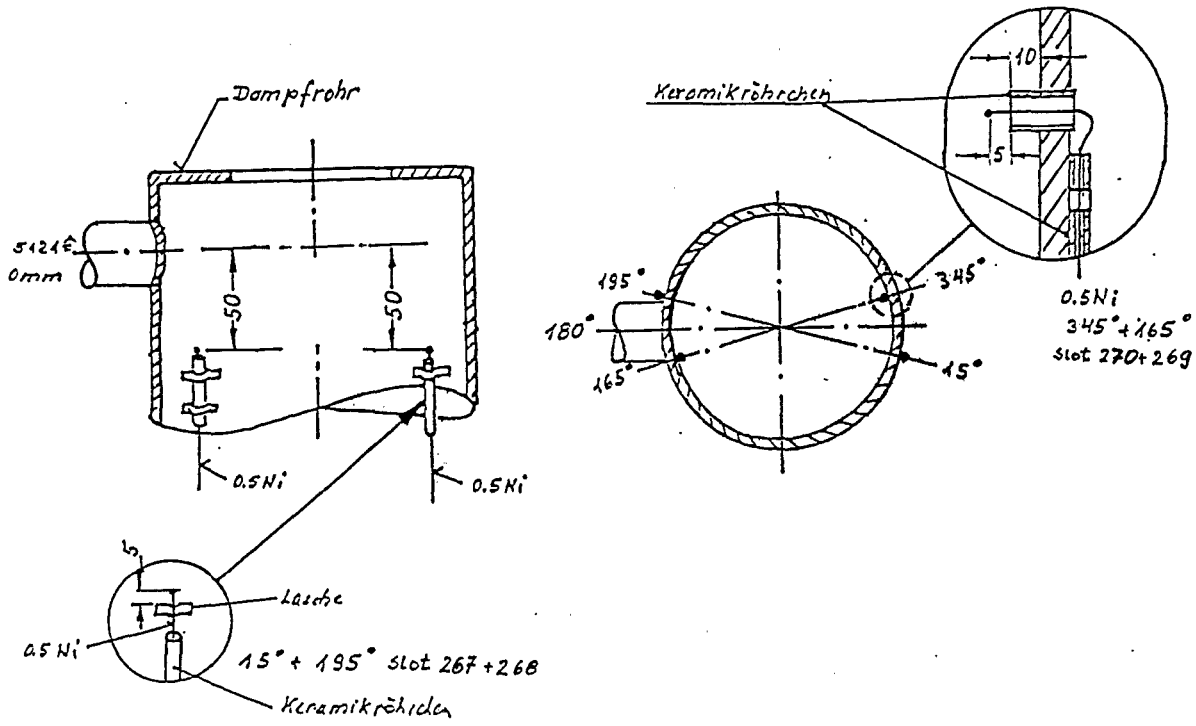

DRol : steam tube, inner side
sp : spacer

DRoA : steam tube, outer side

Fig. 44: CORA-30; Temperatures at elevations given (-26, -50 mm)

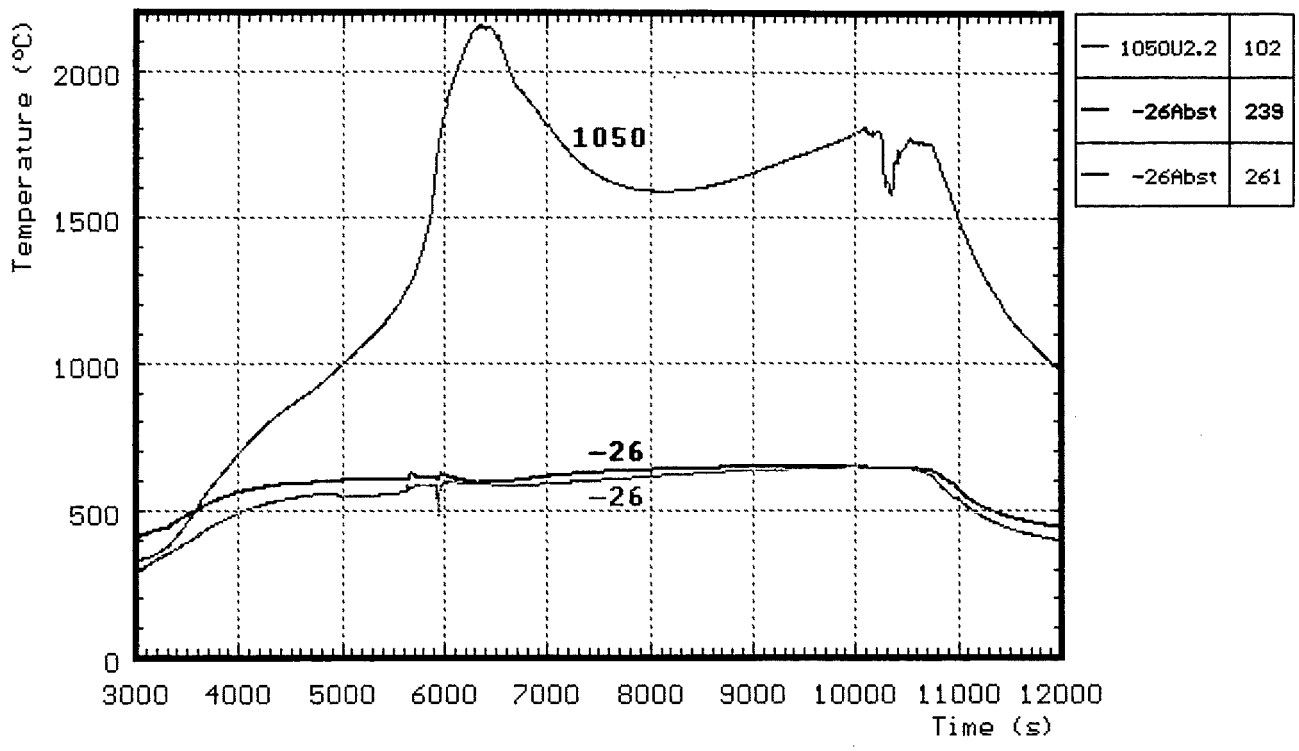

Fig. 45: CORA-30; Comparison of temperatures 50 mm above and 26 mm below the heated region

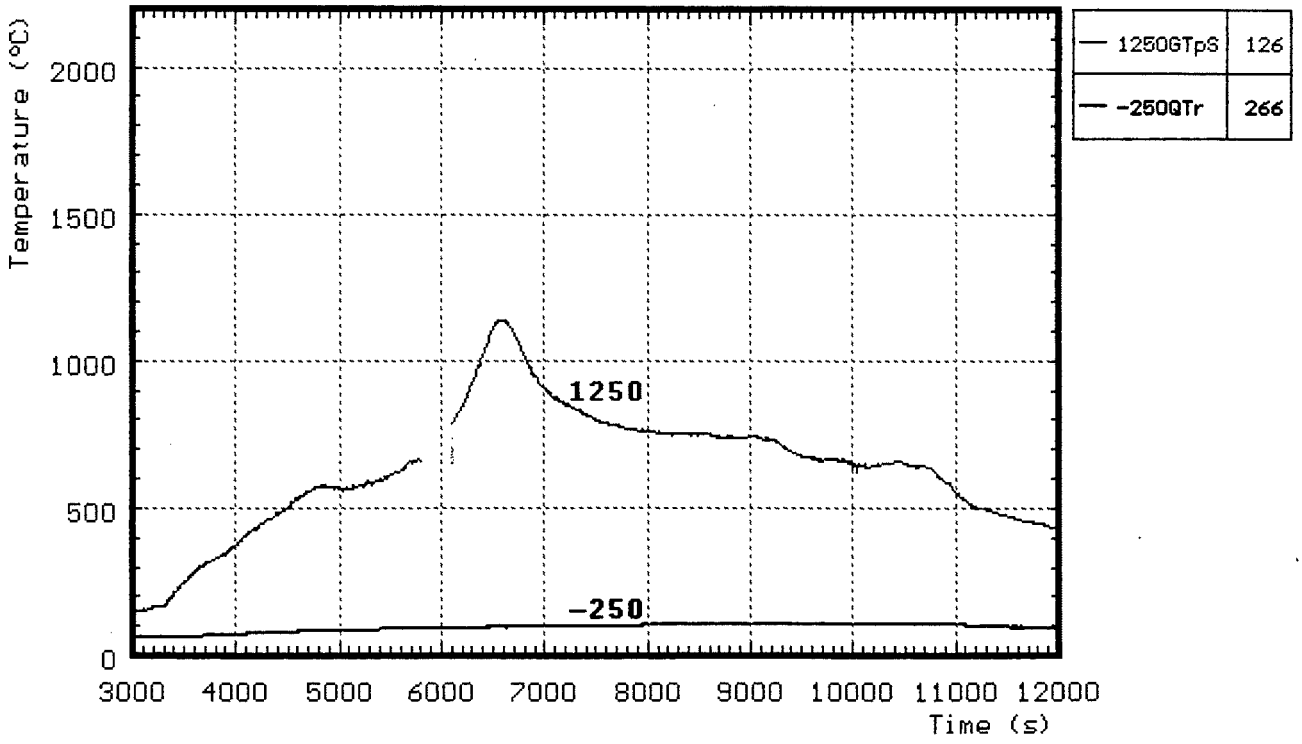

Fig. 46: CORA-30; Comparison of temperatures 250 mm above and 250 mm below the heated region

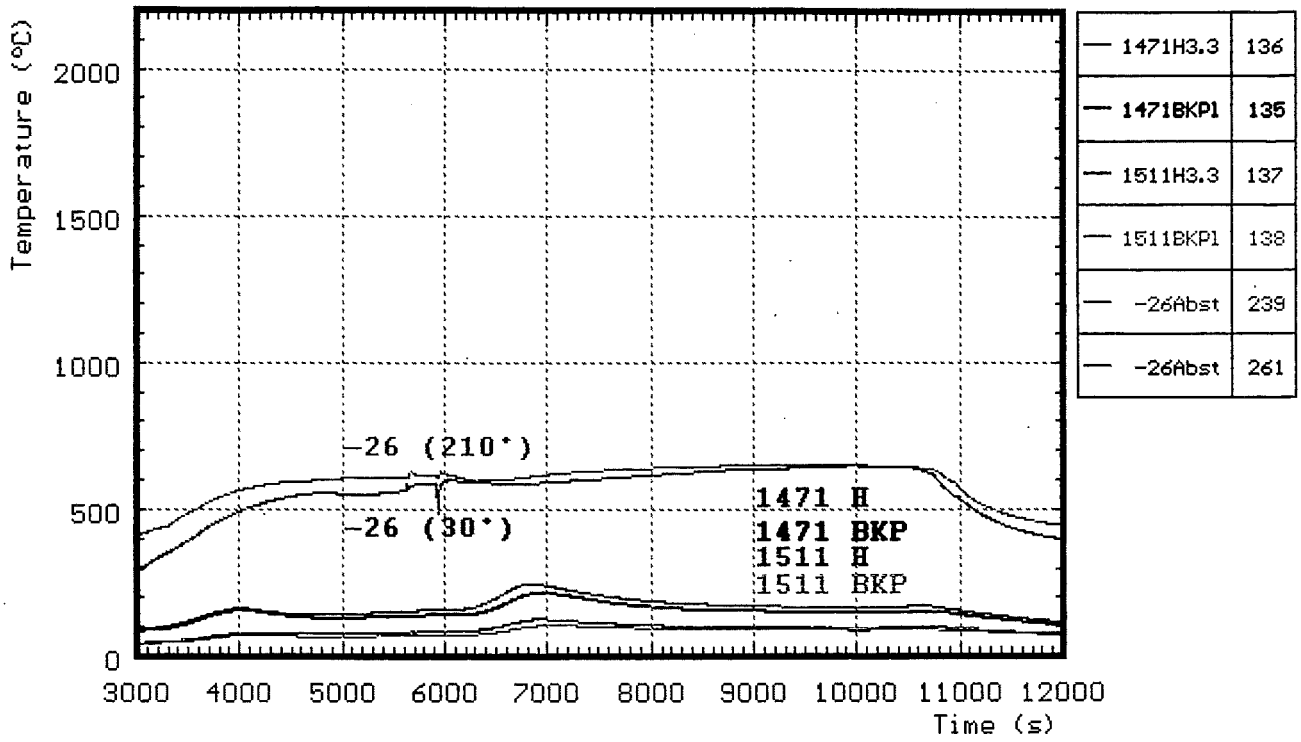

Fig. 47: CORA-30; Temperatures of the bundle head plate and of the lower spacer

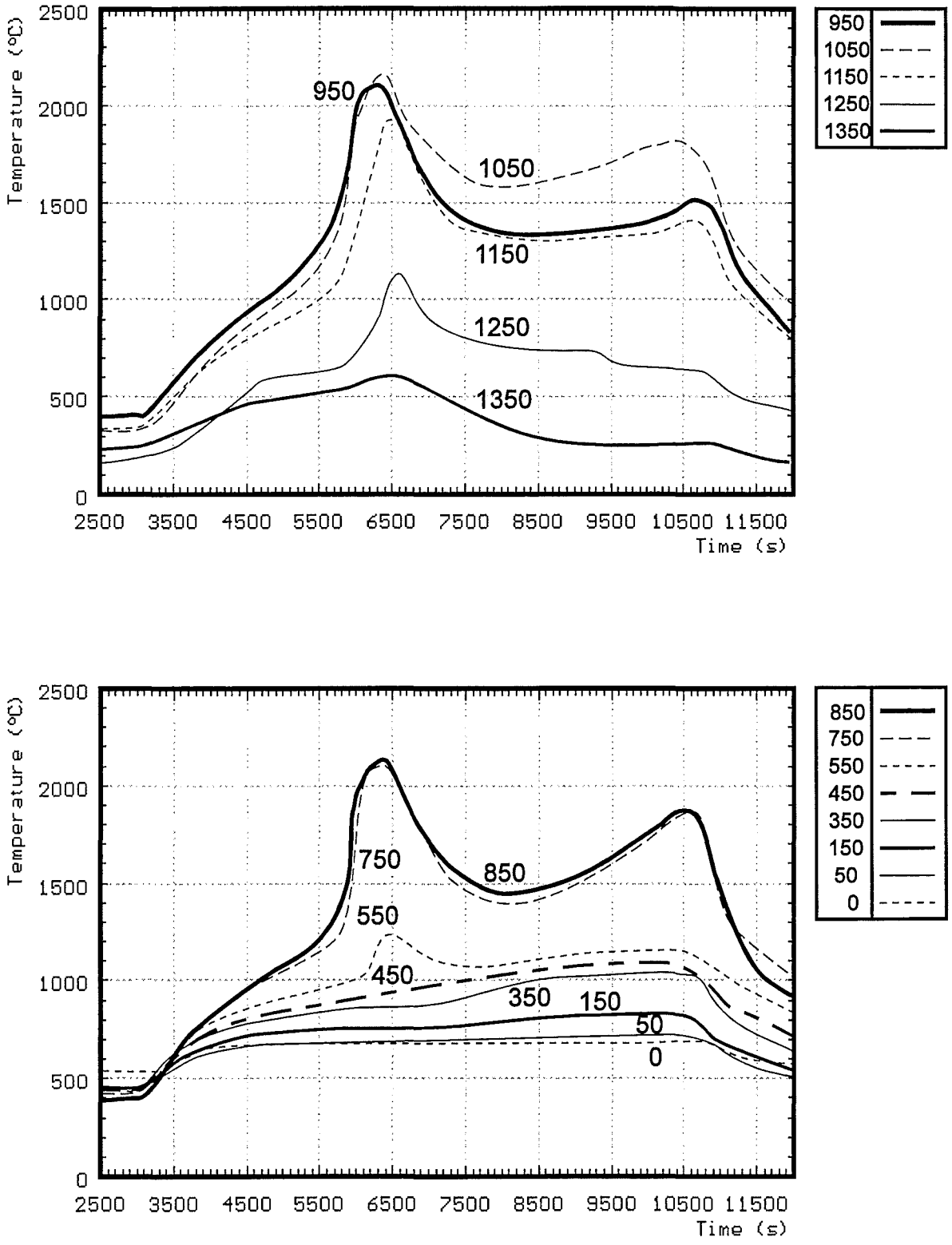

Fig. 48: CORA-30; Best-estimate bundle temperatures at different elevations

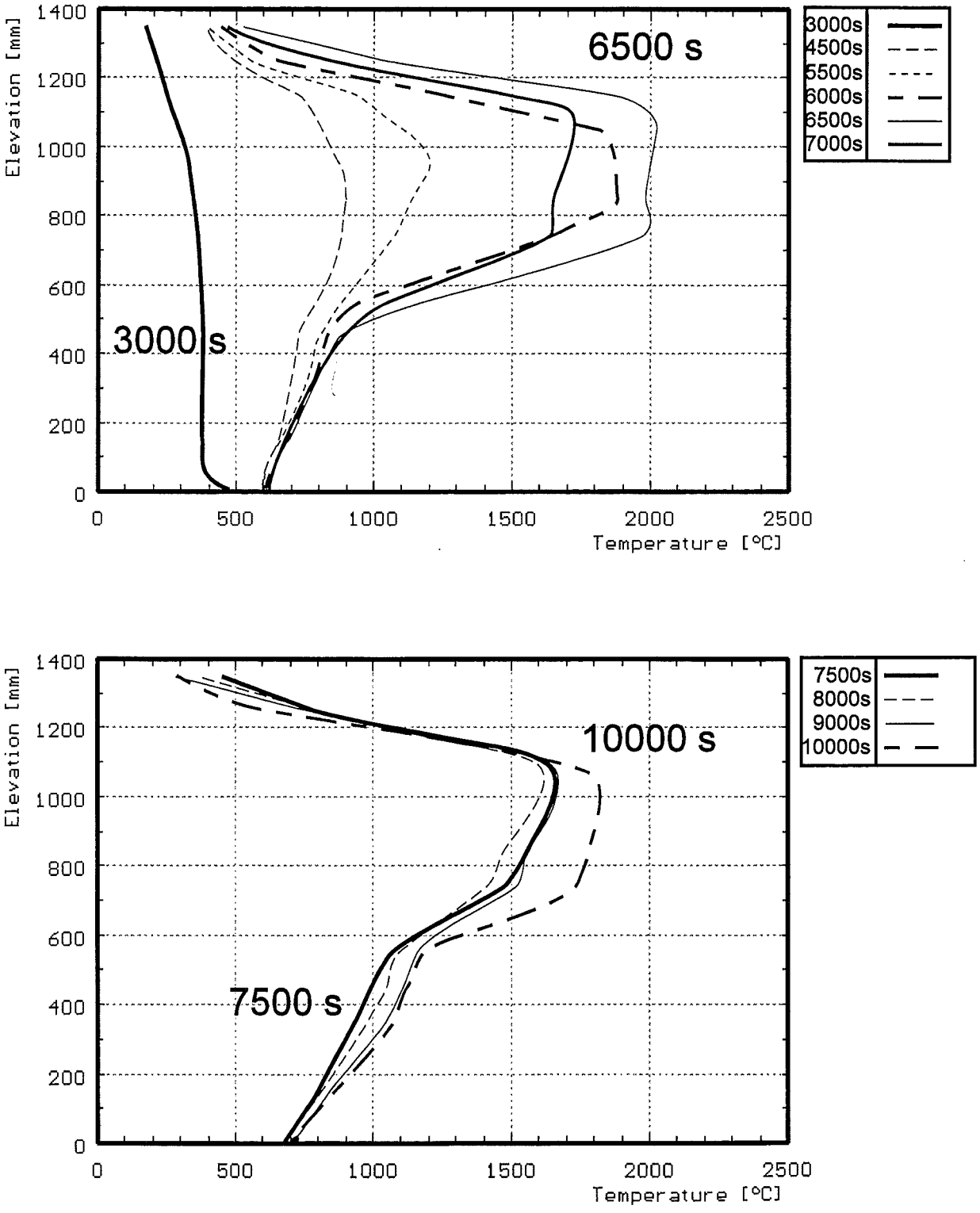

Fig. 49: Axial temperature distribution during the transient of test CORA-30

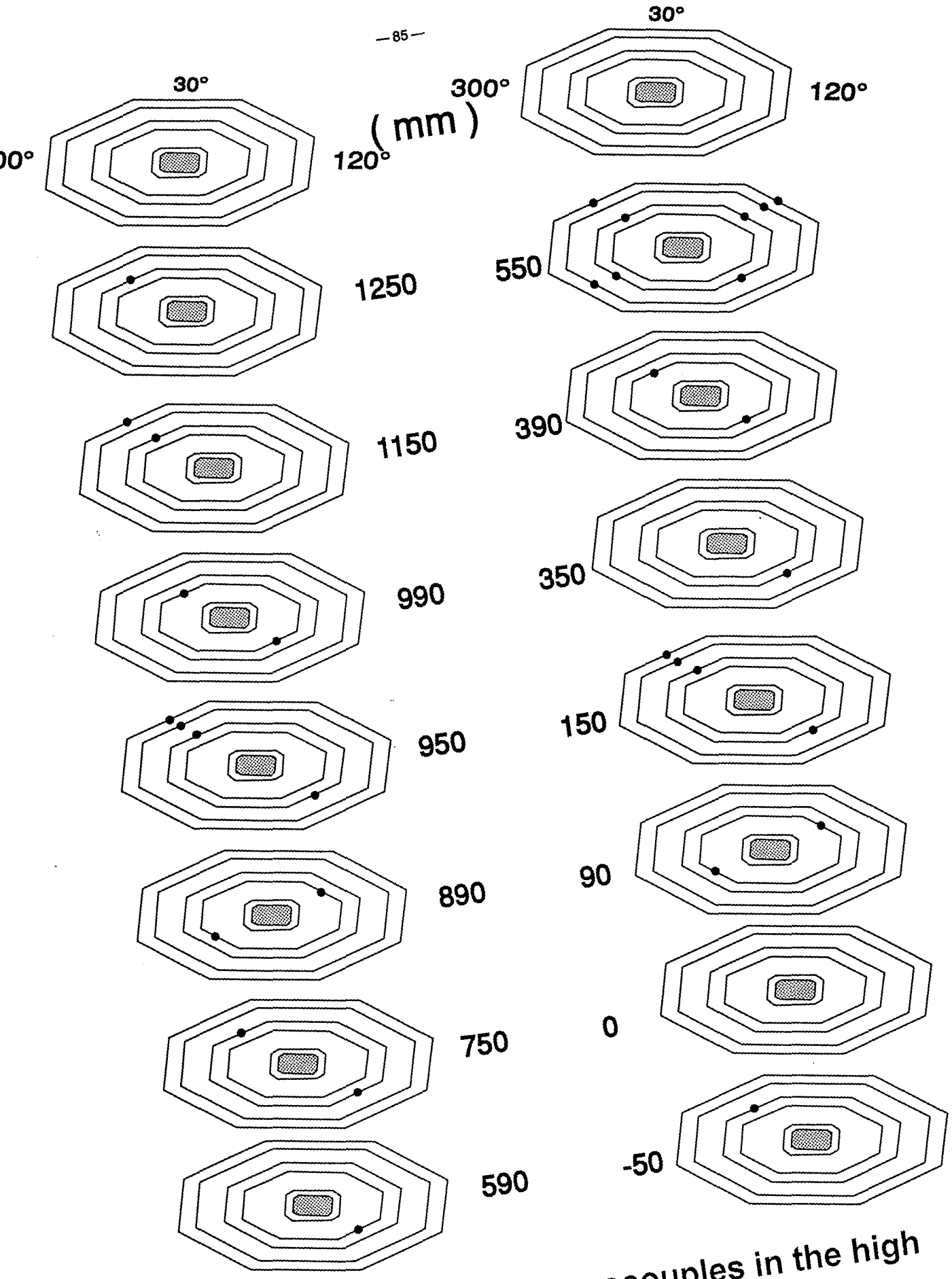

Fig. 50: Locations of thermocouples in the high temperature shield (CORA-30)

ANGLE		75°					165°		255°				345°			
RADIUS (mm)		153	172	192	255	293	153	192	153	172	192	255	153	192	255	293
ELEVATION IN BUNDLE (mm)	1250													169 234Ni		
	1150													170 235Ni		189 245Ni
	990						161 78Ni						187 1B			
	950							163 229Ni						171 236Ni	178 242Ni	190 246Ni
	890	181 20B							185 7B							
	750							164 230Ni						172 237Ni		
	590						183 21B									
	550			162 126Ni	176 130Ni	180 244Ni		165 231Ni			168 127Ni	177 131Ni		173 238ni		191 247Ni
	390						184 22B						188 23B			
	350							166 232Ni								
	150							167 233Ni						174 240Ni	179 243Ni	192 248Ni
	90	182 33B							186 26B							
	0															
	-50													175 241Ni		

Fig. 51: Position of thermocouples in high temperature shield for test CORA-30

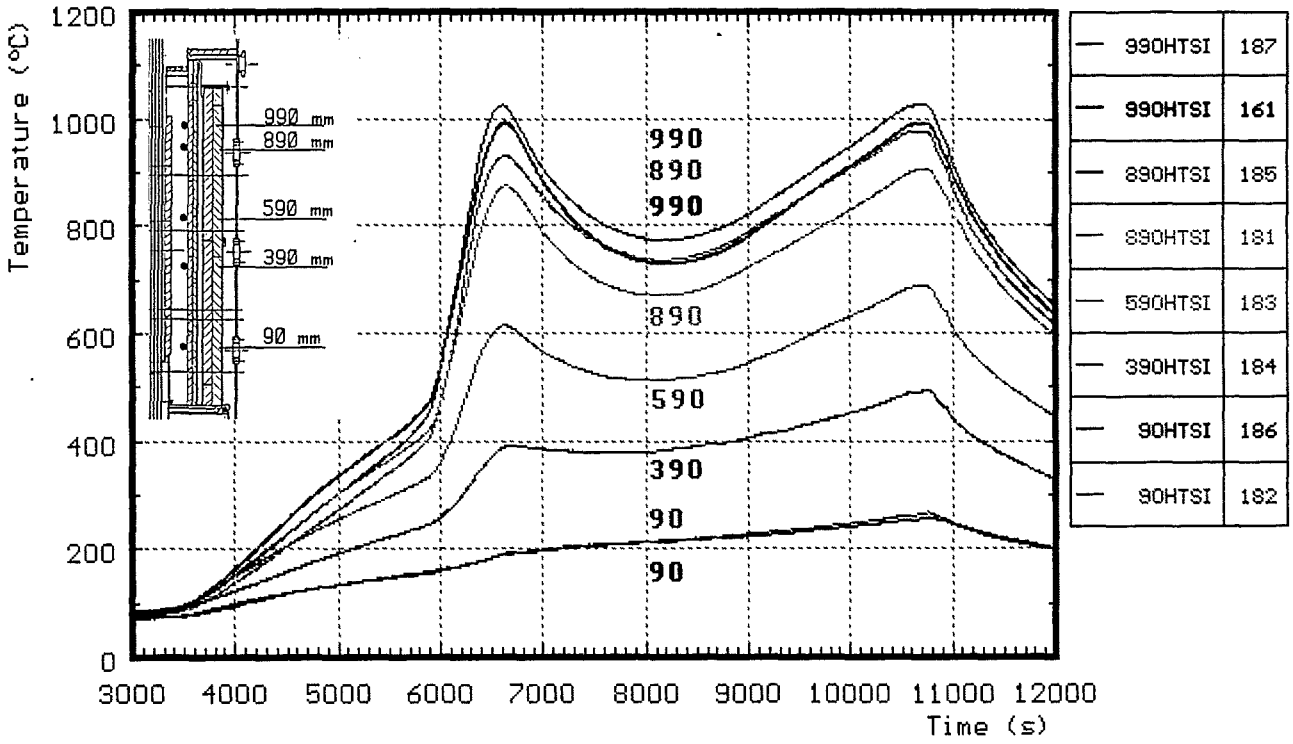

Fig. 52: CORA-30; Temperatures of HTS, Inner surface at 153 mm radius

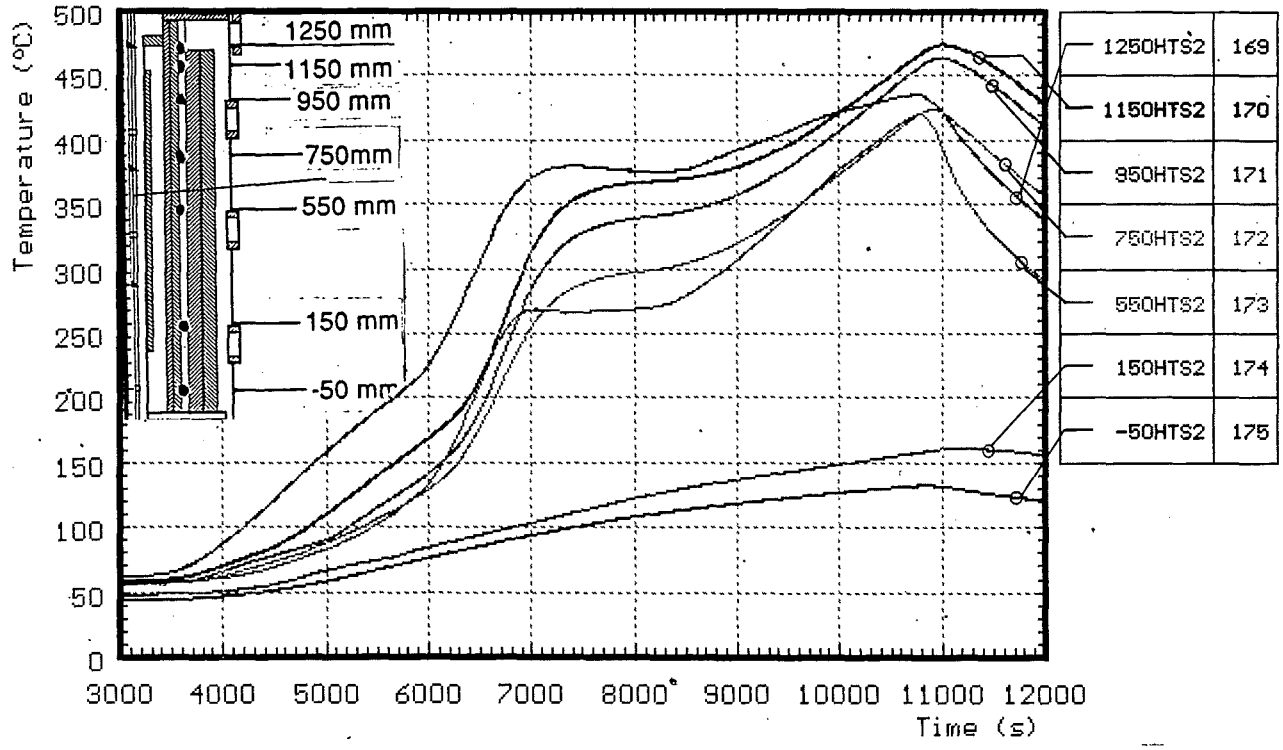

Fig. 53: CORA-30; Temperatures of HTS, Temperatures in HT shield at 192 mm radius, 345°

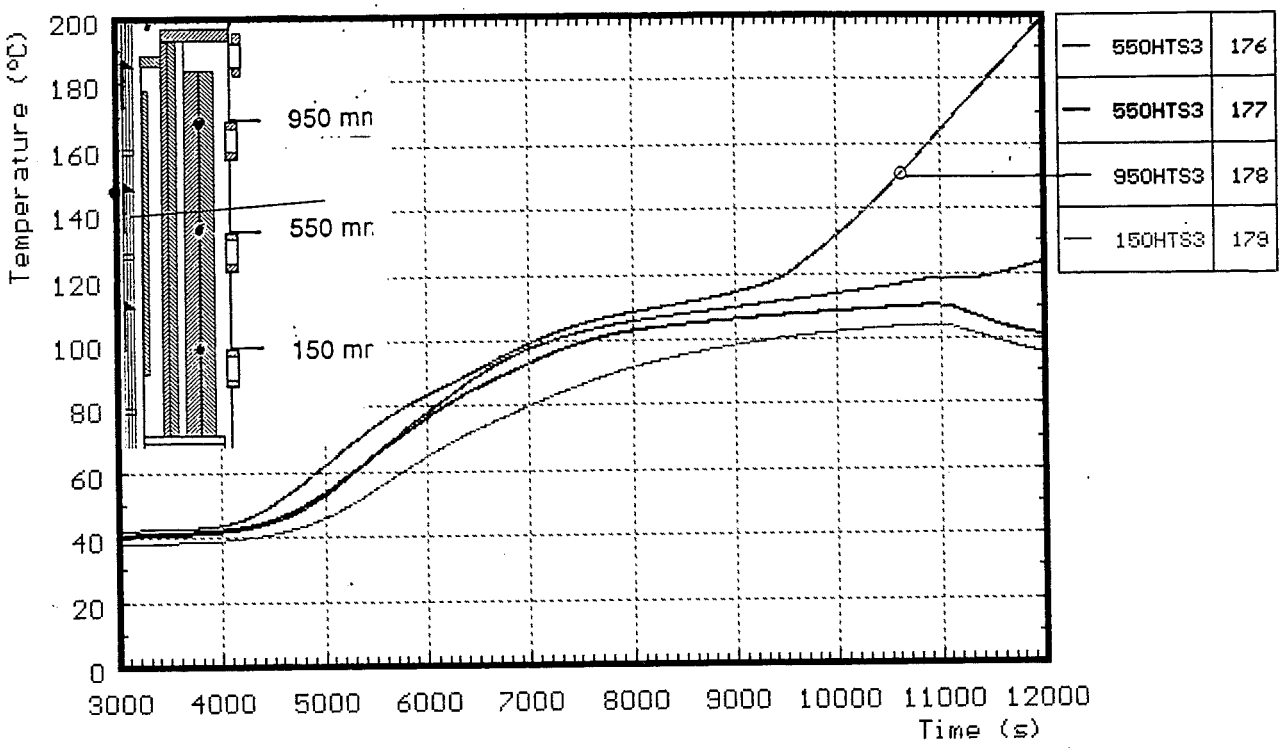

Fig. 54: CORA-30; Temperatures of HTS, Temperatures in HT shield at 255 mm radius

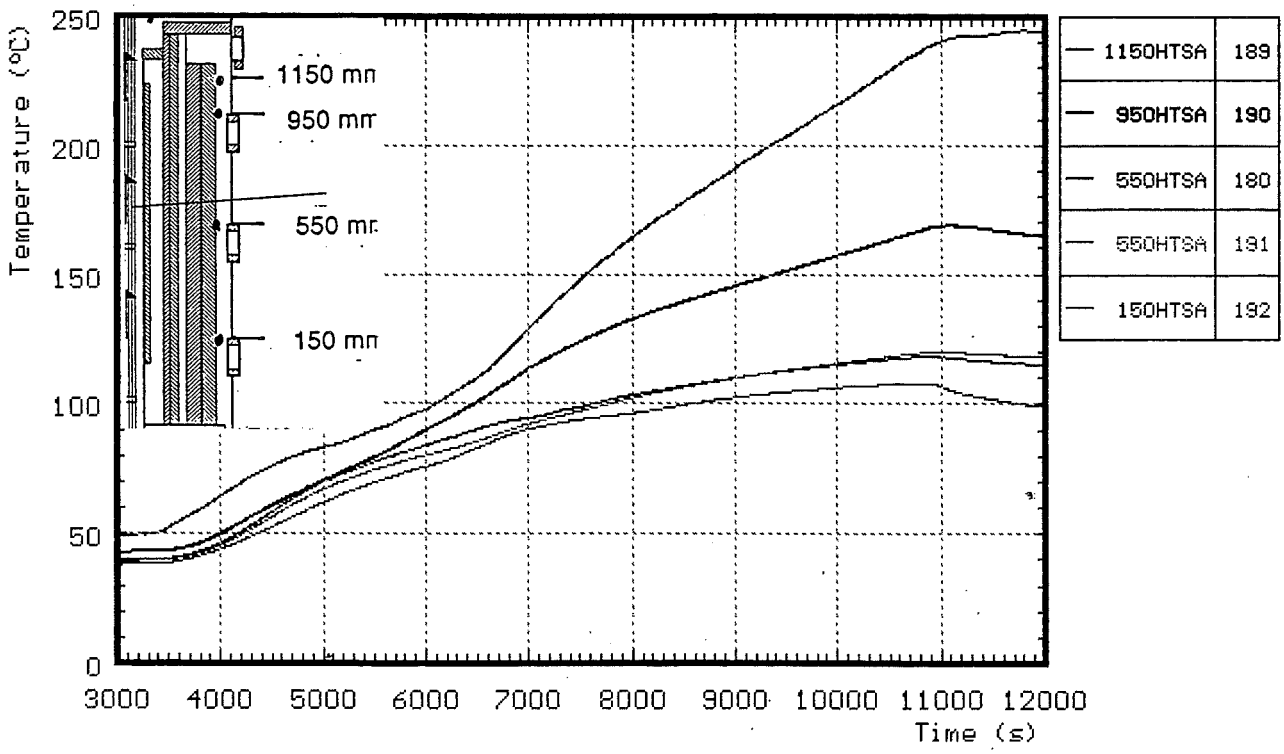

Fig. 55: CORA-30; Temperatures of HTS, Temperatures in HT shield at 293 mm radius

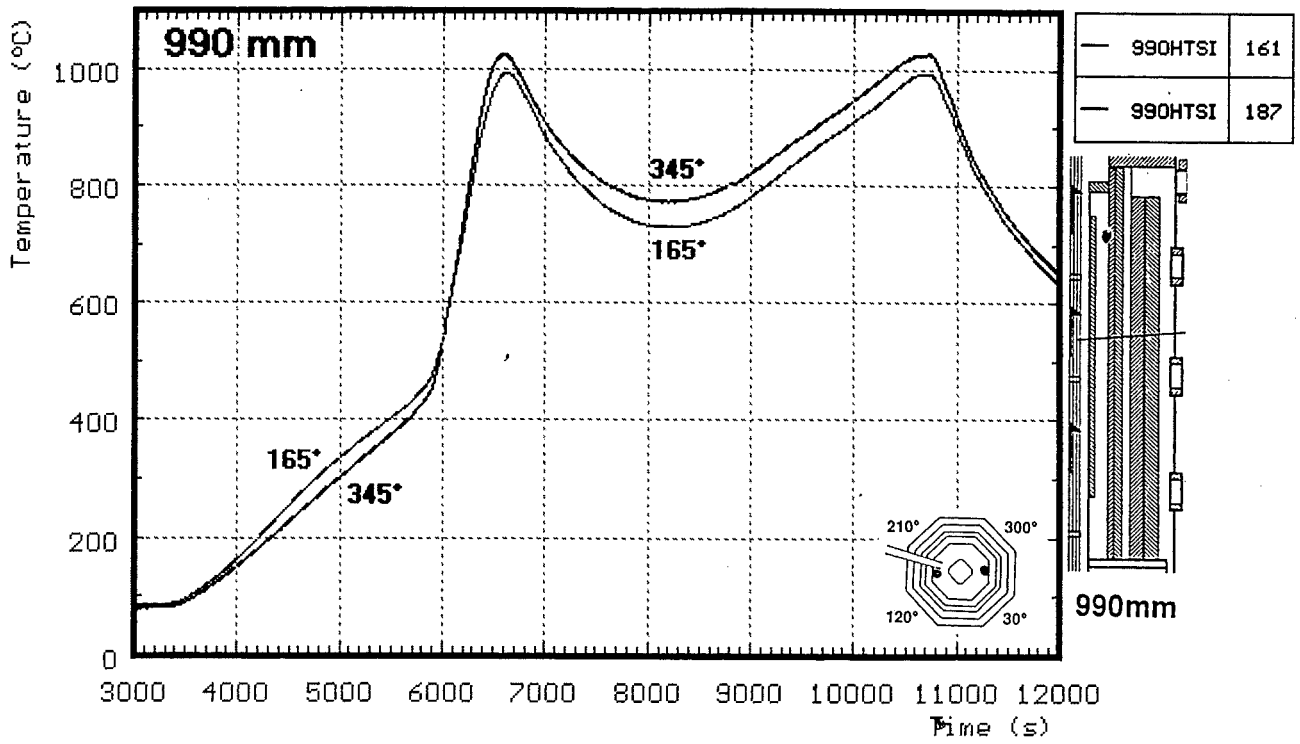

Fig. 56: CORA-30; Temperatures of HTS, Comparison on inner surface at 153 mm radius and 990 mm elevation

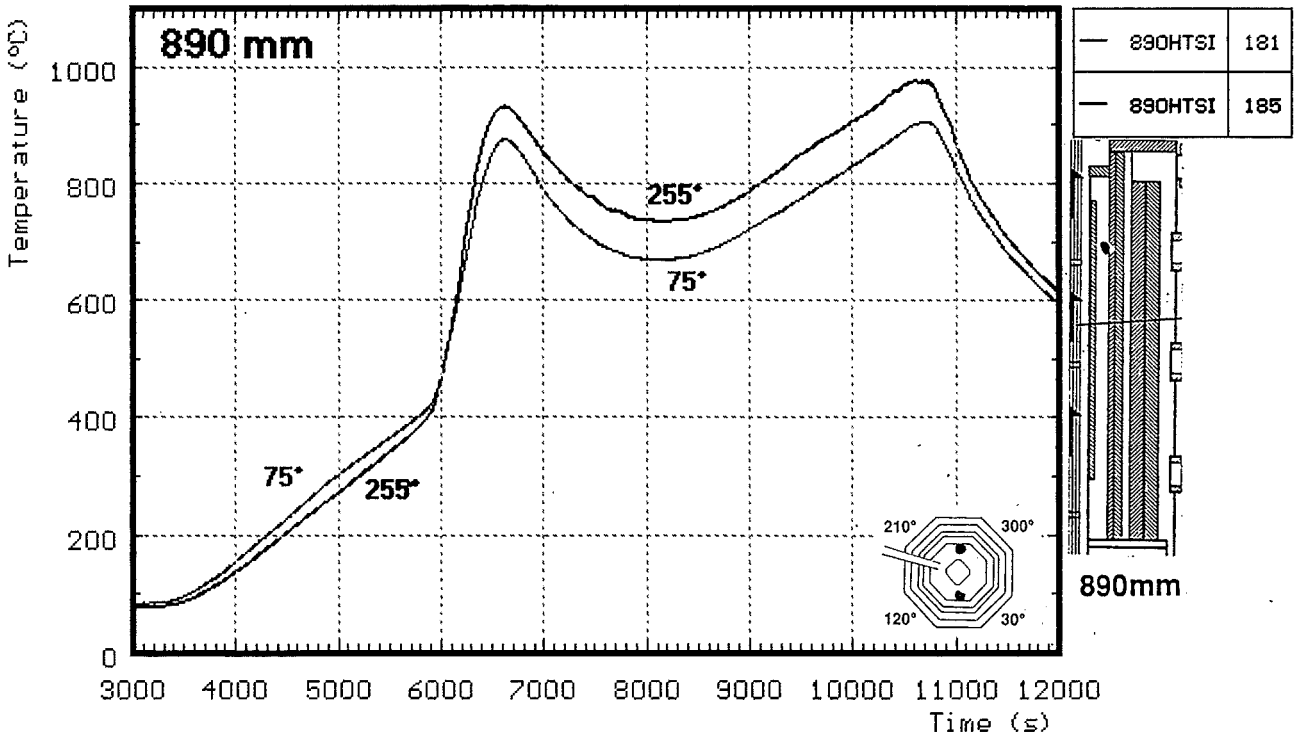

Fig. 57: CORA-30; Temperatures of HTS, Comparison on inner surface at 153 mm radius and 890 mm elevation

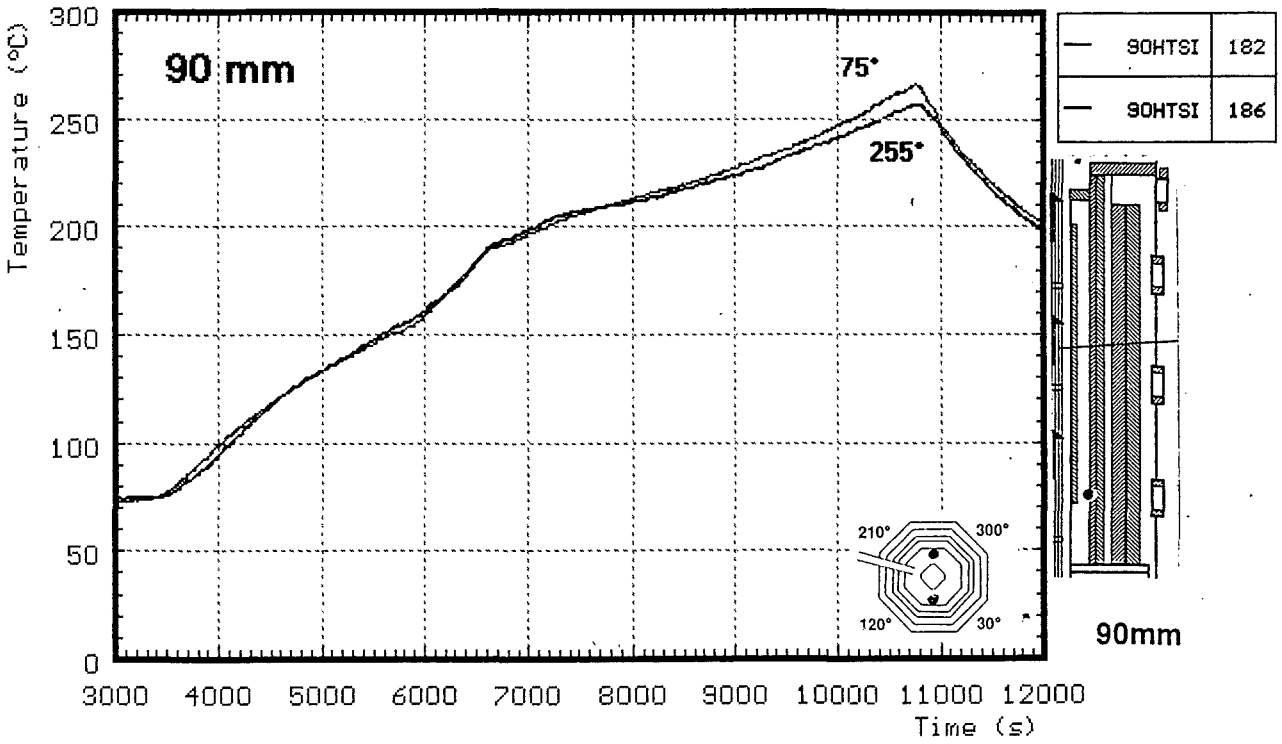

Fig. 58: CORA-30; Temperatures of HTS, Comparison on inner surface at 153 mm radius and 90 mm elevation

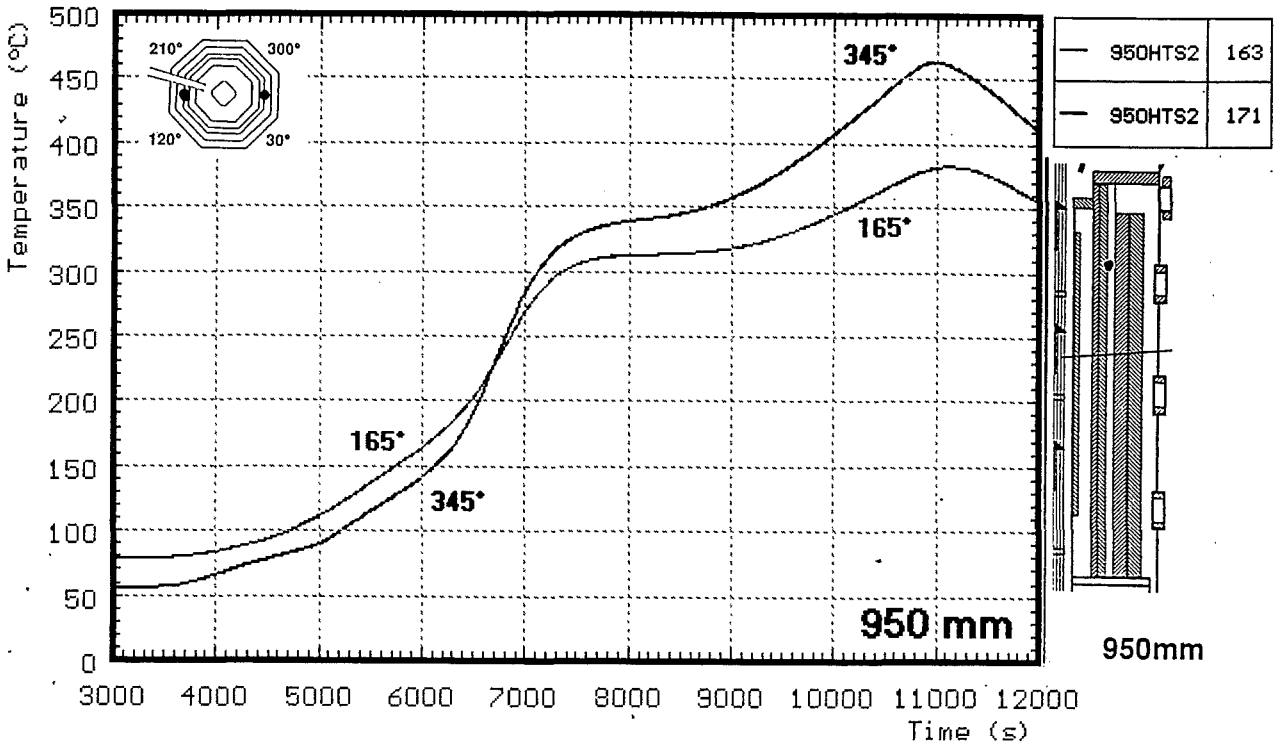

Fig. 59: CORA-30; Temperatures of HTS, Comparison in HT-shield at 192 mm radius and 950 mm elevation

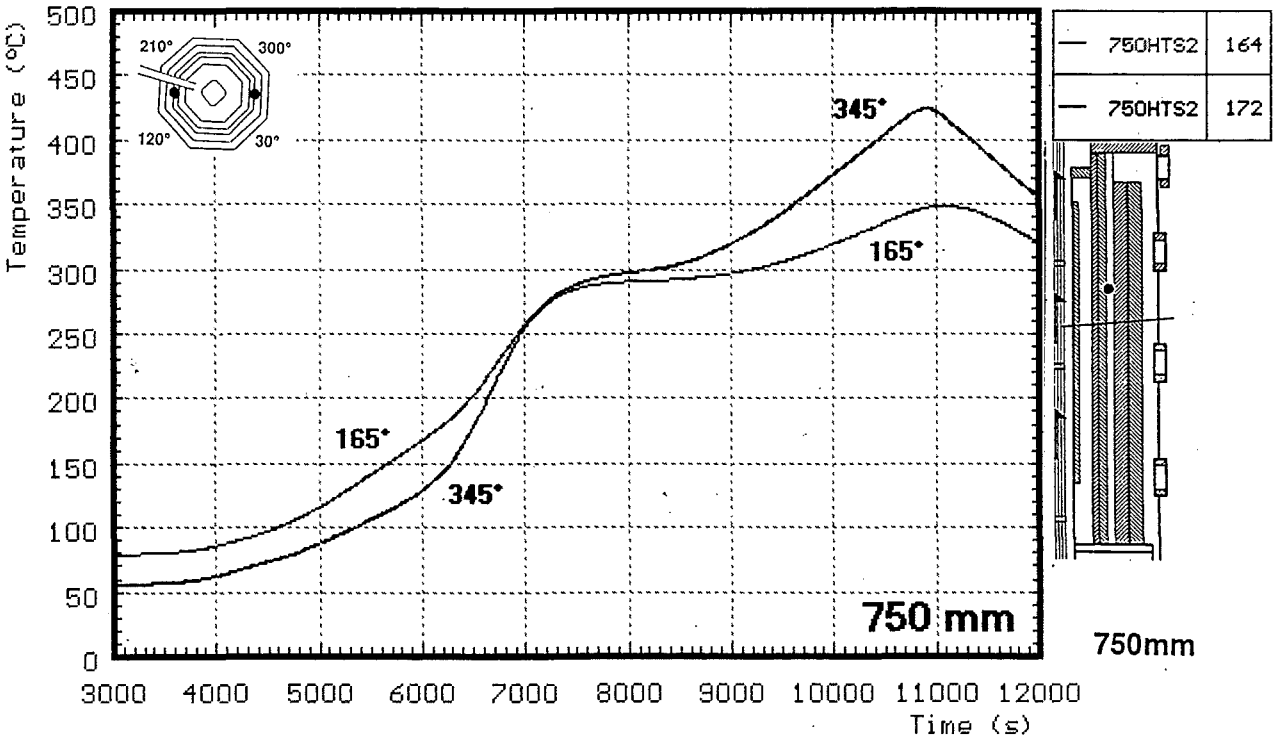

Fig. 60: CORA-30; Temperatures of HTS, Comparison in HT-shield at 192 mm radius and 750 mm elevation

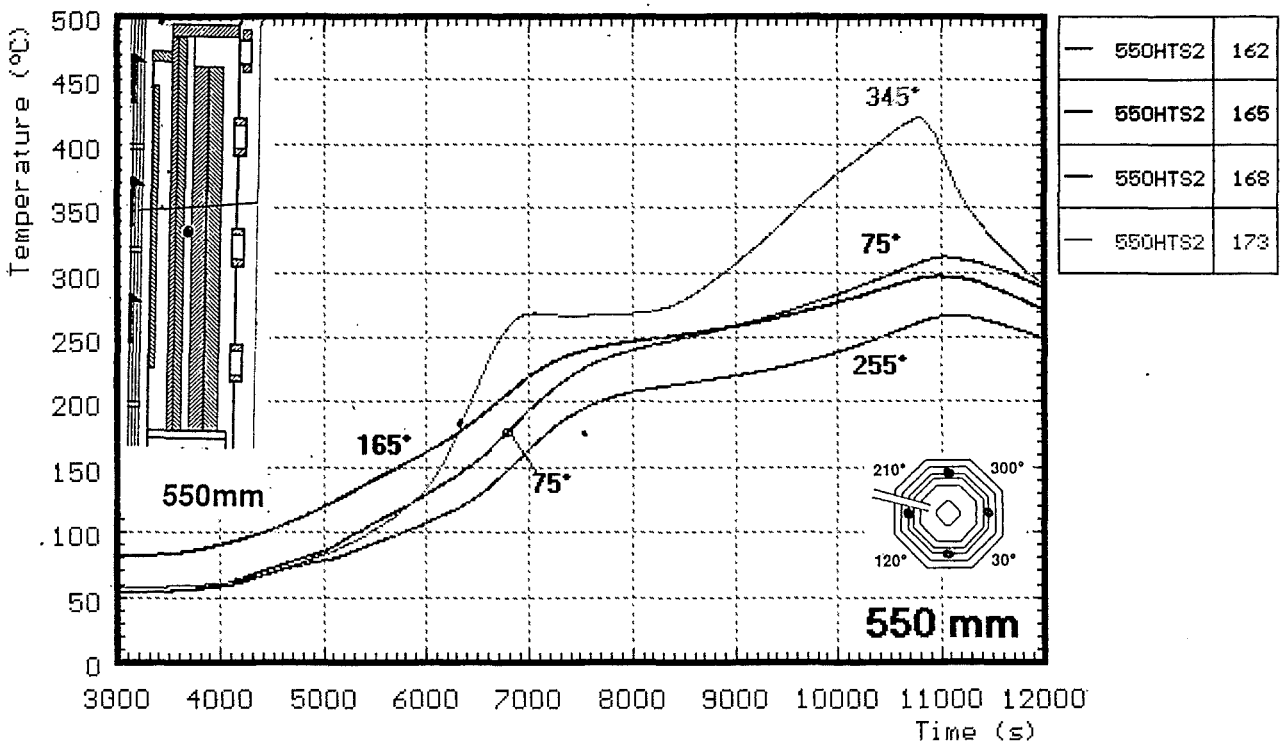

Fig. 61: CORA-30; Temperatures of HTS, Comparison in HT-shield at 192 mm radius and 550 mm elevation

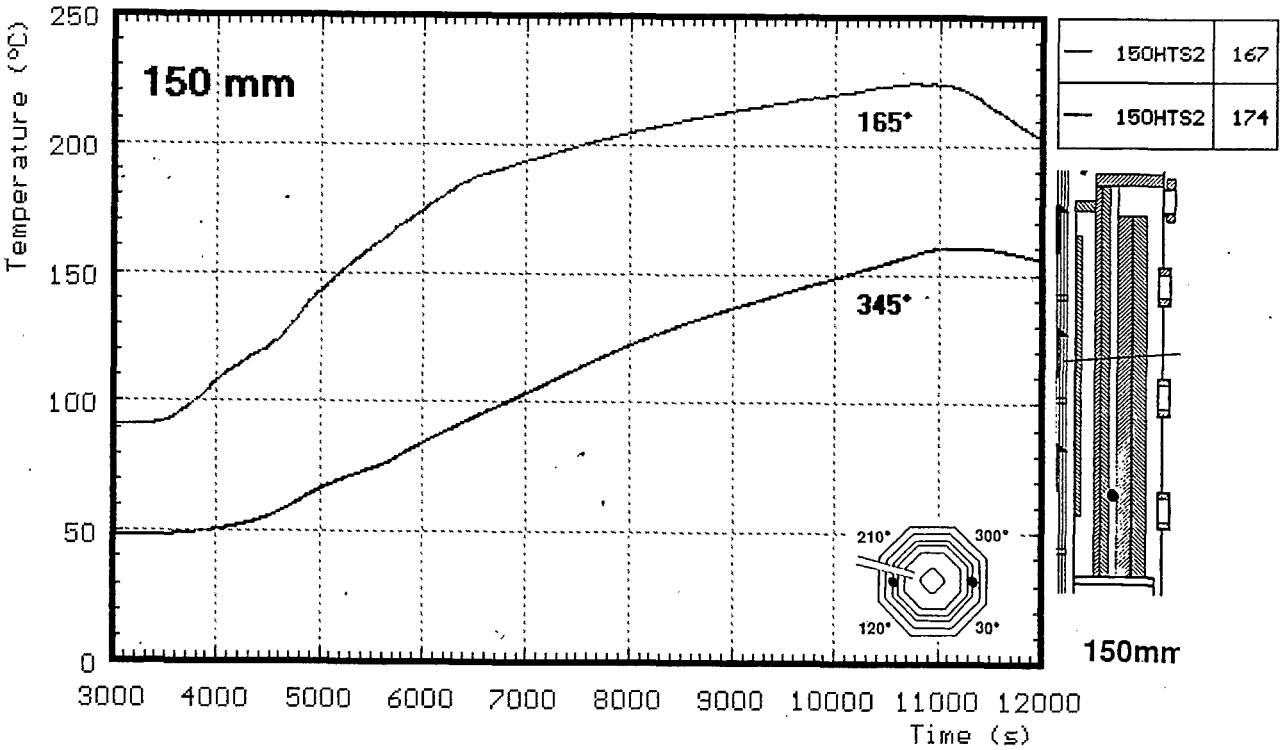

Fig. 62: CORA-30; Temperatures of HTS, Comparison in HT-shield at 192 mm radius and 150 mm elevation

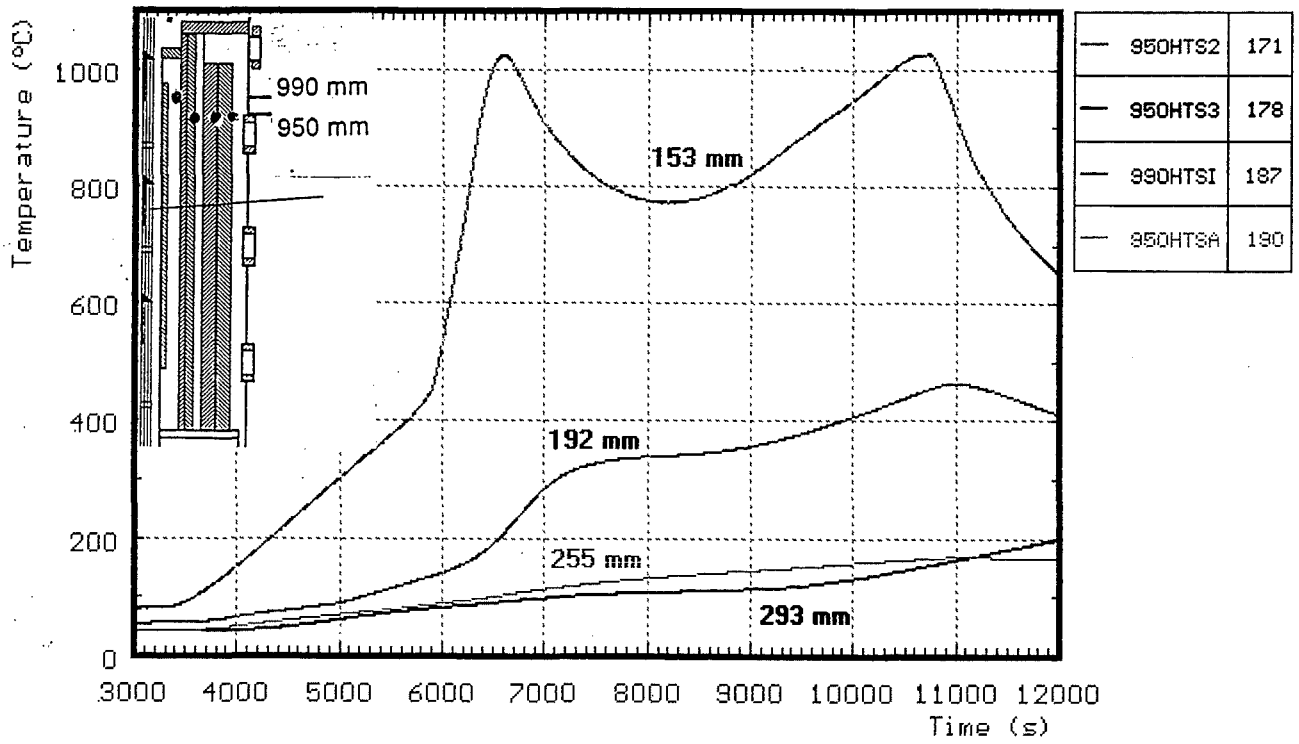

Fig. 63: CORA-30; Temperatures of HTS, Radial dependence at 950 mm elevation

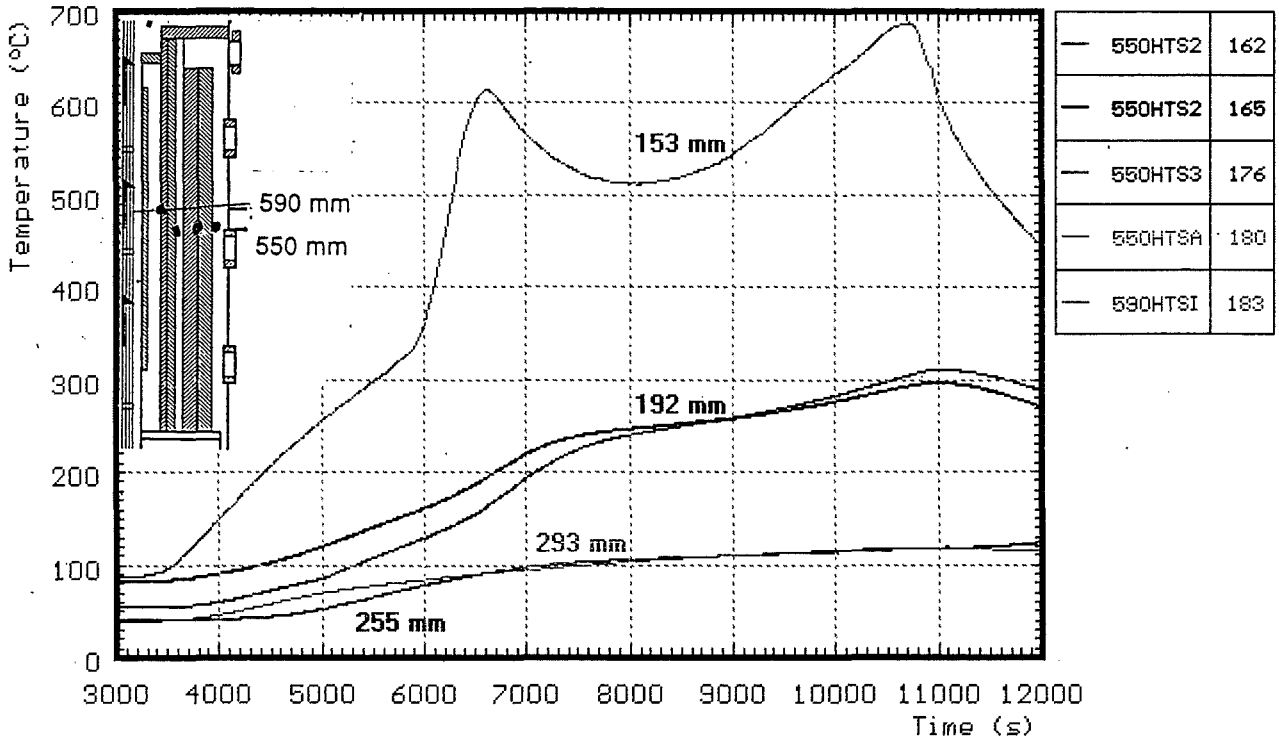

Fig. 64: CORA-30; Temperatures of HTS, Radial dependence at 550 mm elevation

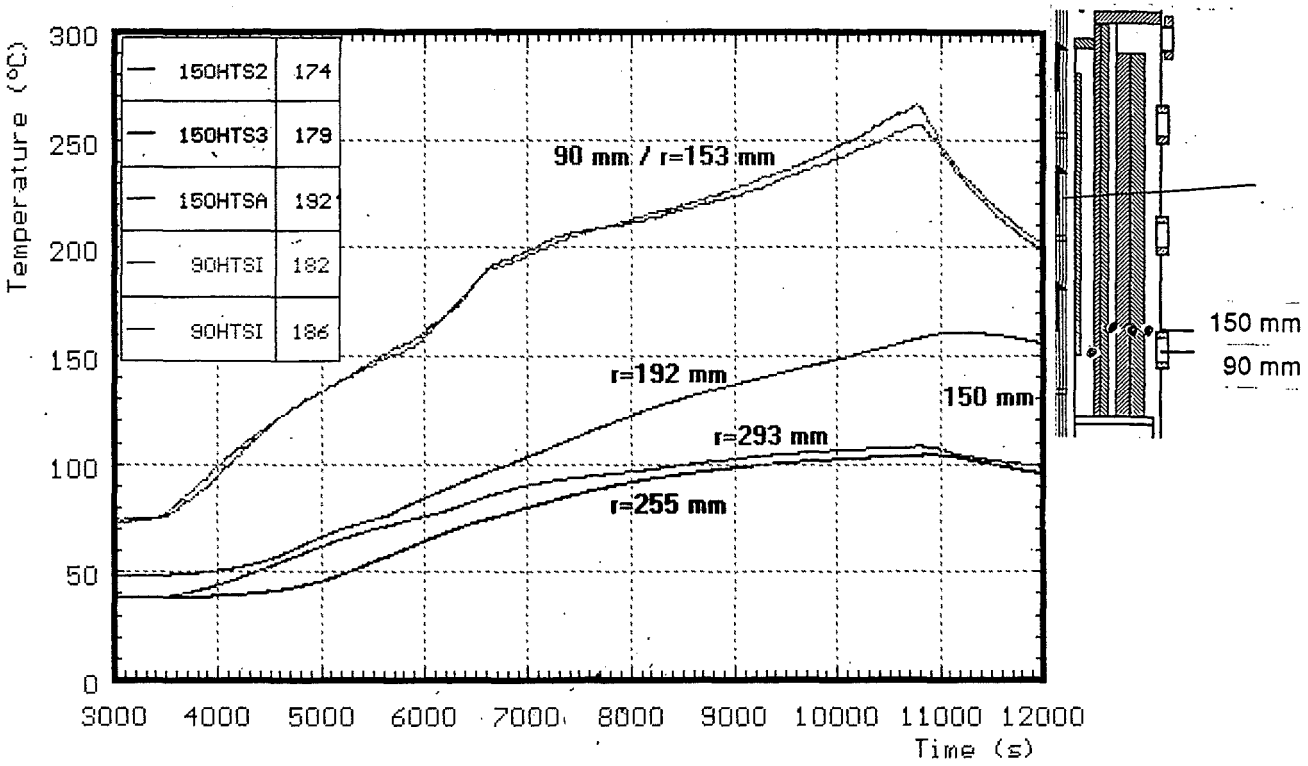

Fig. 65: CORA-30; Temperatures of HTS, Radial dependence at about 100 mm elevation

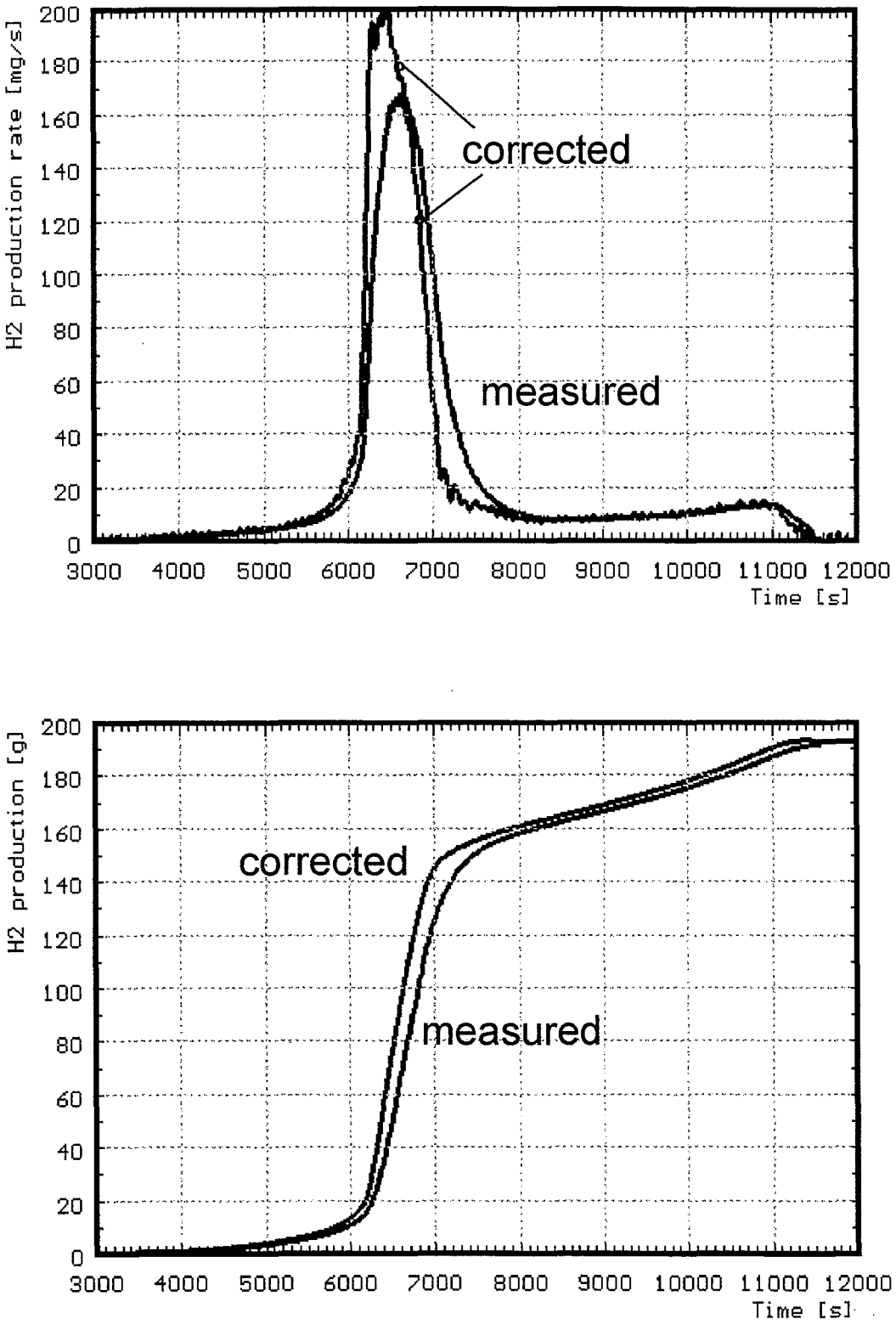

Fig. 66: Hydrogen production in test CORA-30; production rate (top) and integral values (bottom)

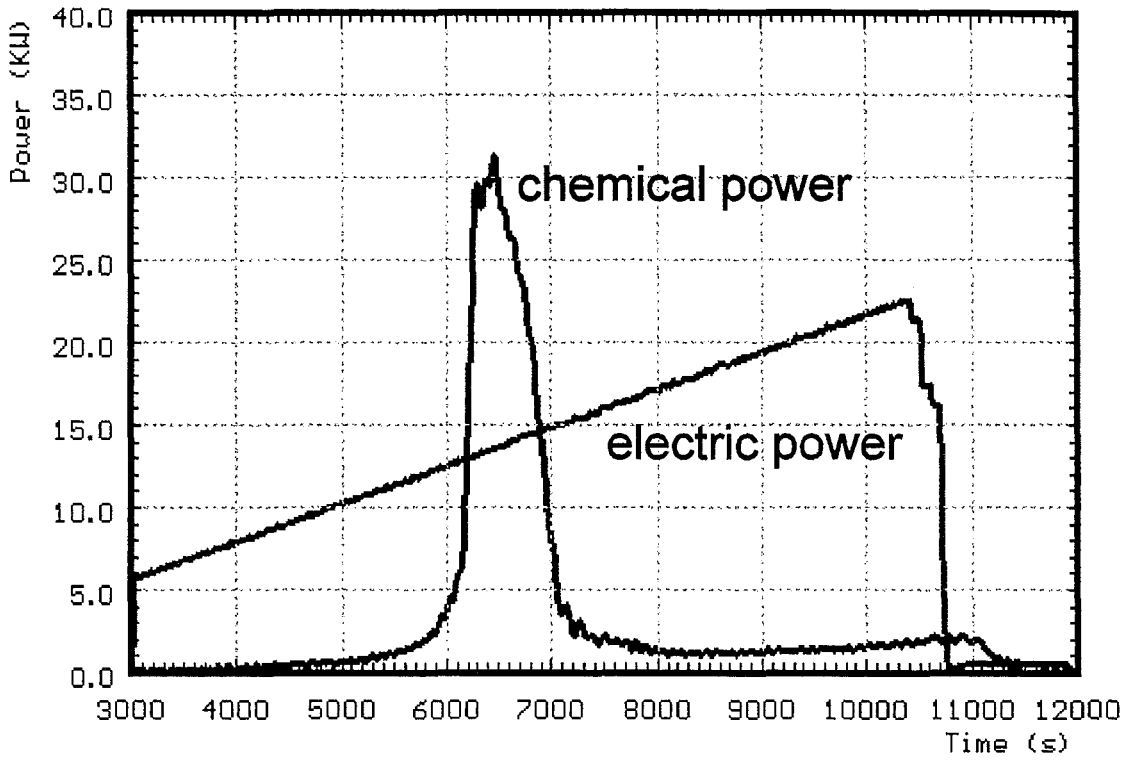

Fig. 67: CORA-30; Comparison of chemical and electric power

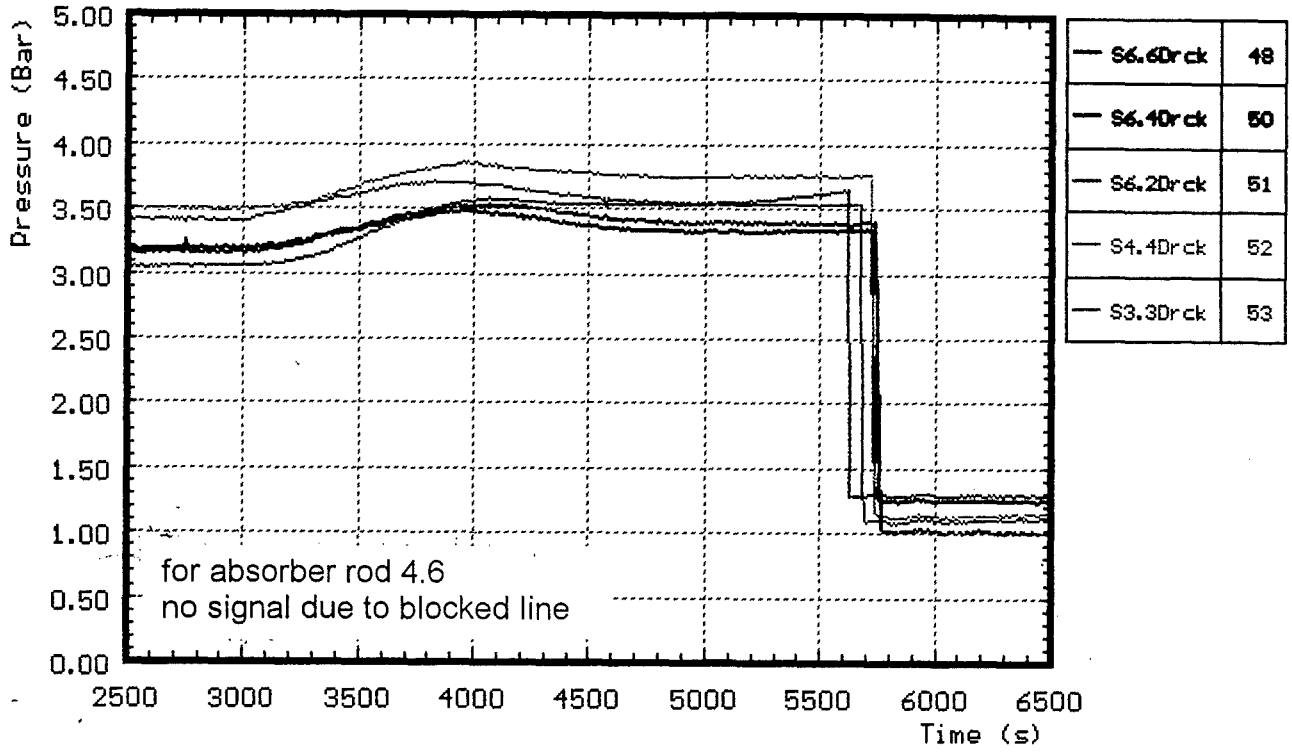

Fig. 68: CORA-30; Internal pressure of fuel rod simulators and absorber rods

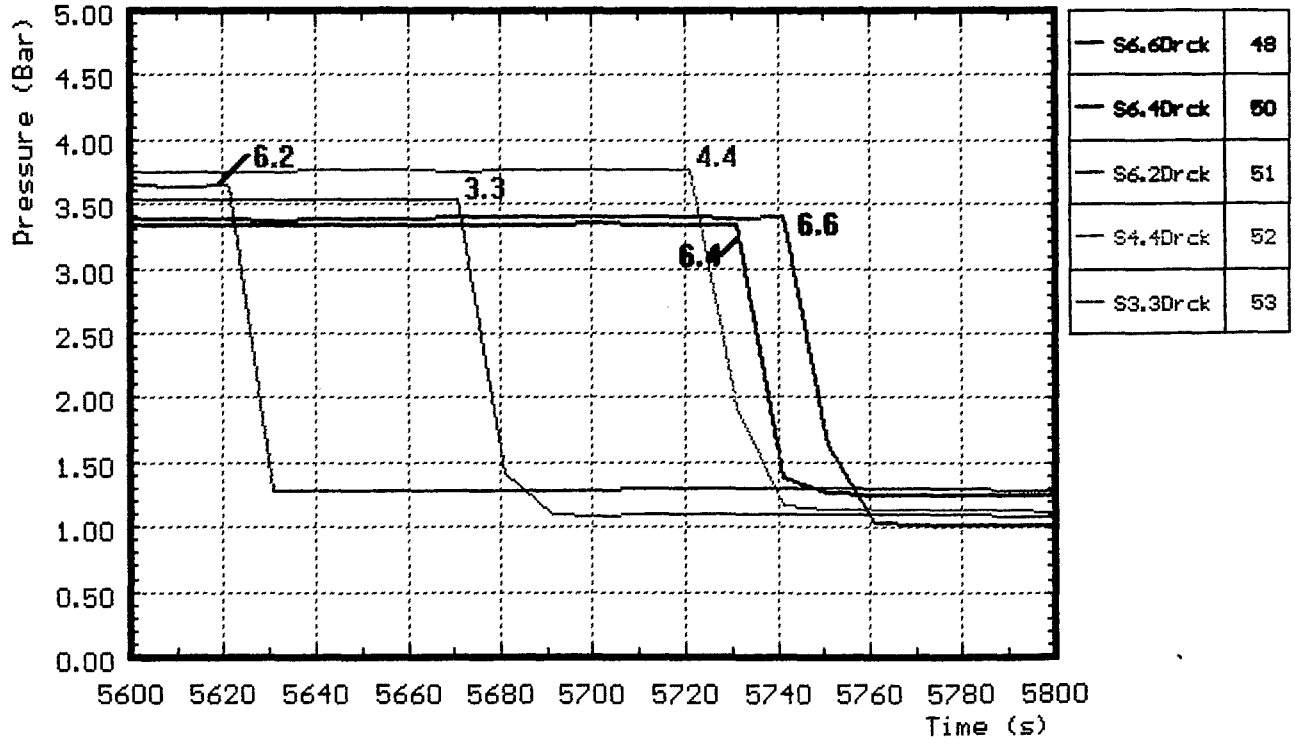

Fig. 69: CORA-30; Determination of failure time by pressure loss measurement

Pressure Loss Measurement		Video Measurement	
Failure of rods		Start of Melt Movement	
Absorber rod 6.2	5620 s		
		5644 s	800 mm
		5645 s	600 mm
		5650 s	700 mm

Fig. 70: CORA-30; Comparison of failure time determined by pressure loss measurement or first melt movement due to video inspection

Failure temperature rod 6.2: < 1330°C
Failure temperature rod 4.6: > 1180°C

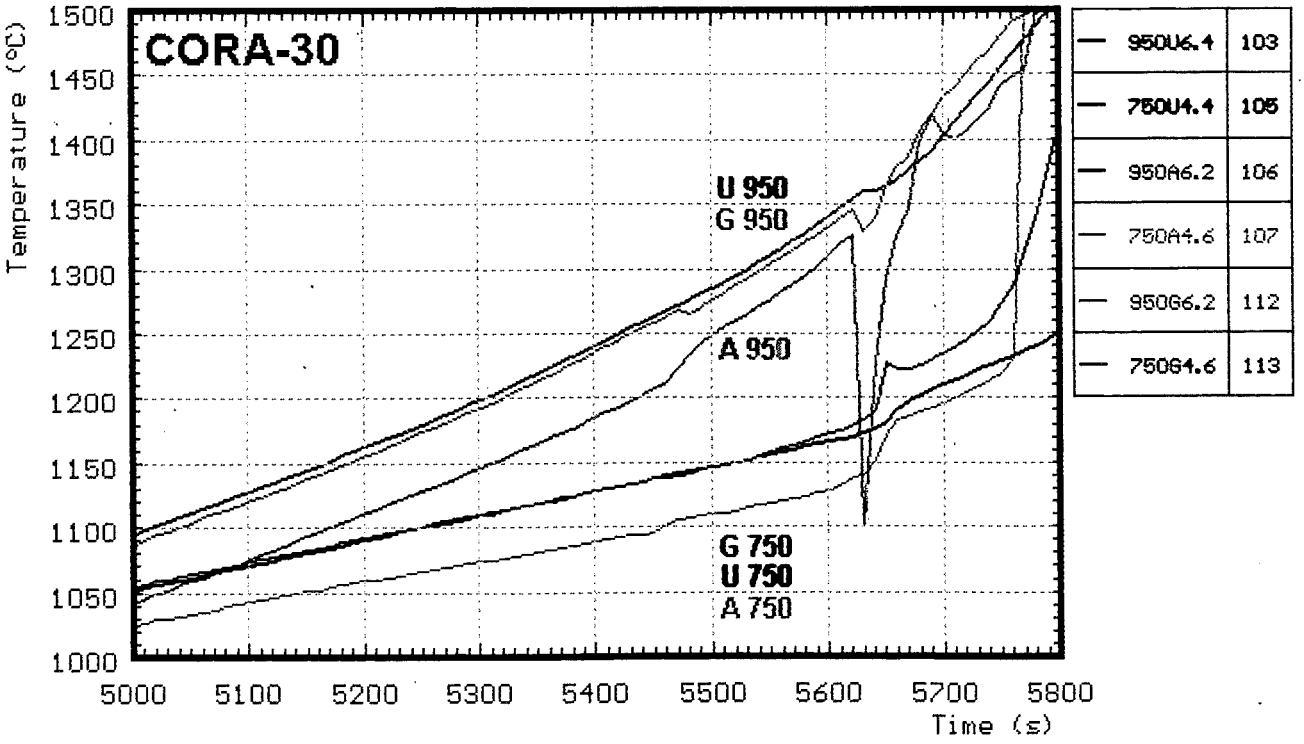

Fig. 71: CORA-30: Determination of failure of absorber rods 6.2 and 4.6 by irregularities in absorber and guide tube temperature measurement

		Failure time	Failure temperature
Heated rod	3.3	5670 s	<1410°C
Unheated rod	4.4	5720 s	<1420°C
Unheated rod	6.4	5730 s	<1430°C
Unheated rod	6.6	5740 s	<1440°C

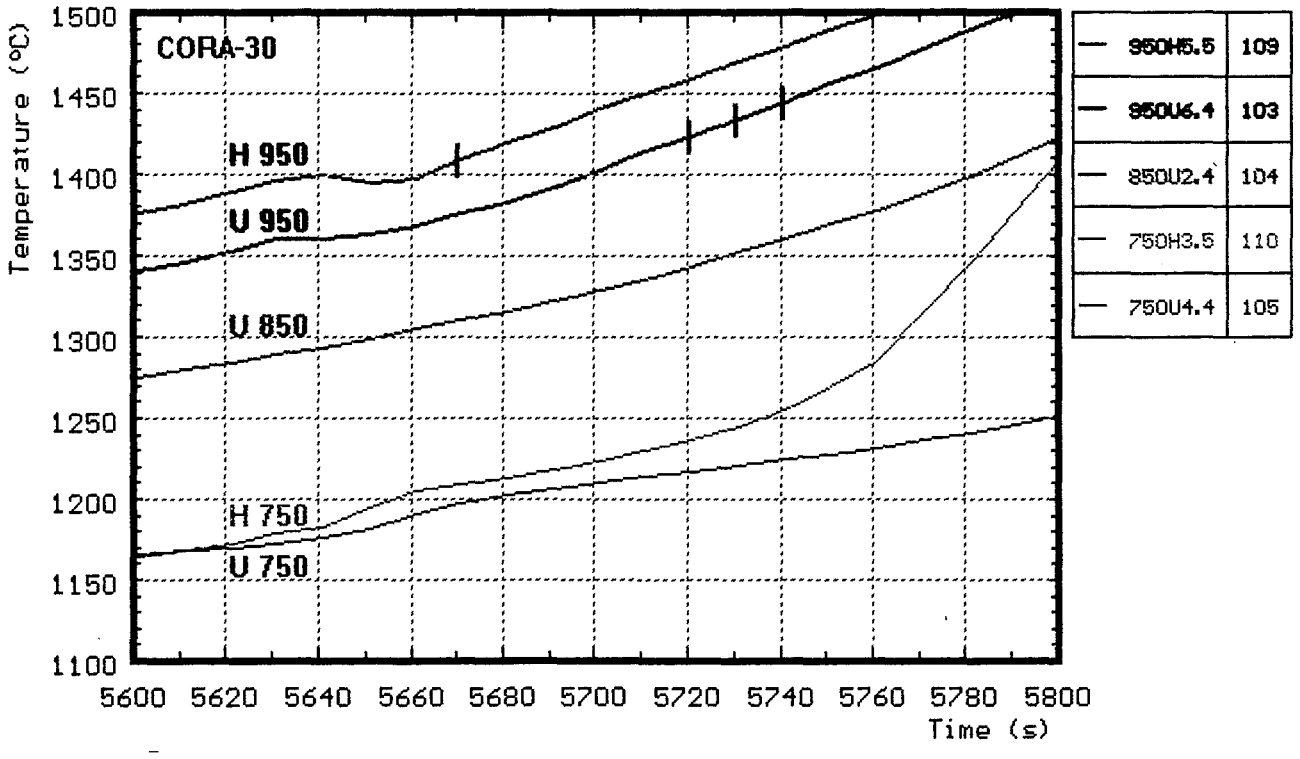

Fig. 72: CORA-30; Temperatures at failure times of fuel rod simulators determined by pressure loss measurement (Fig.69)

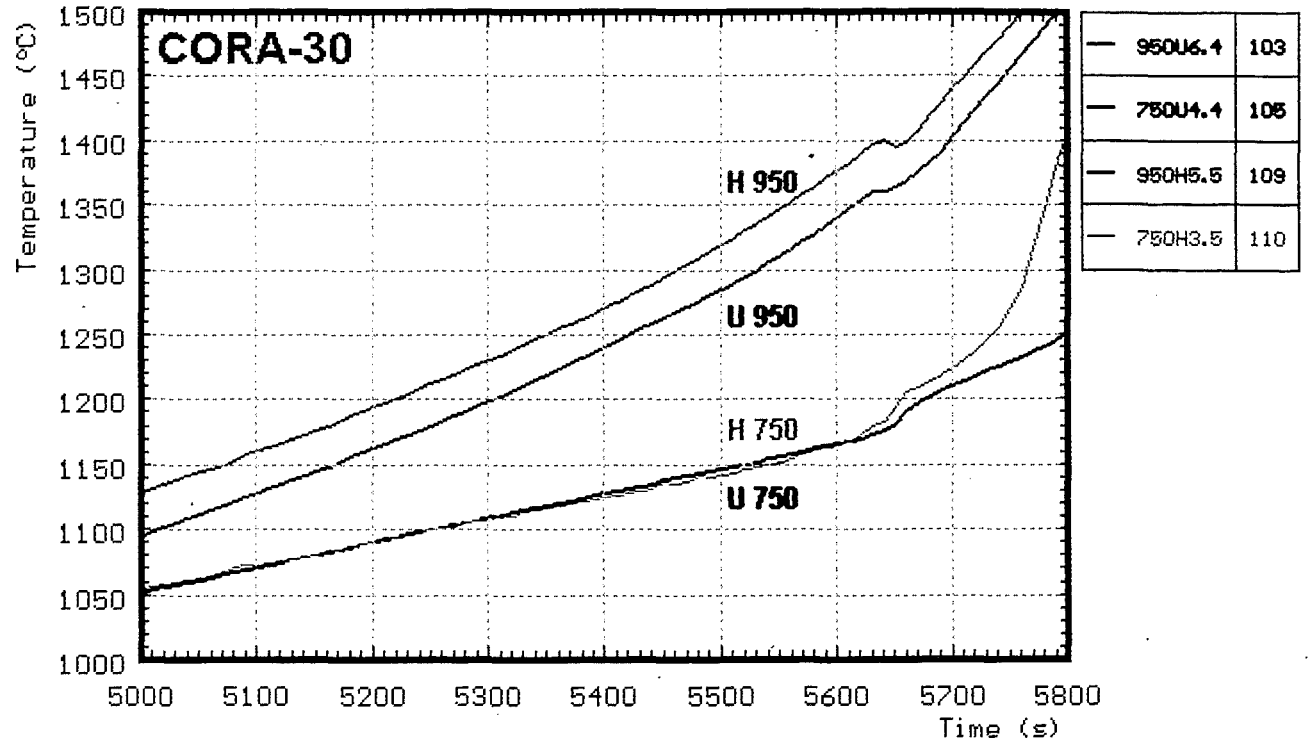

Fig. 73: CORA-30; Comparison of temperatures on heated and unheated fuel rods at absorber failure time

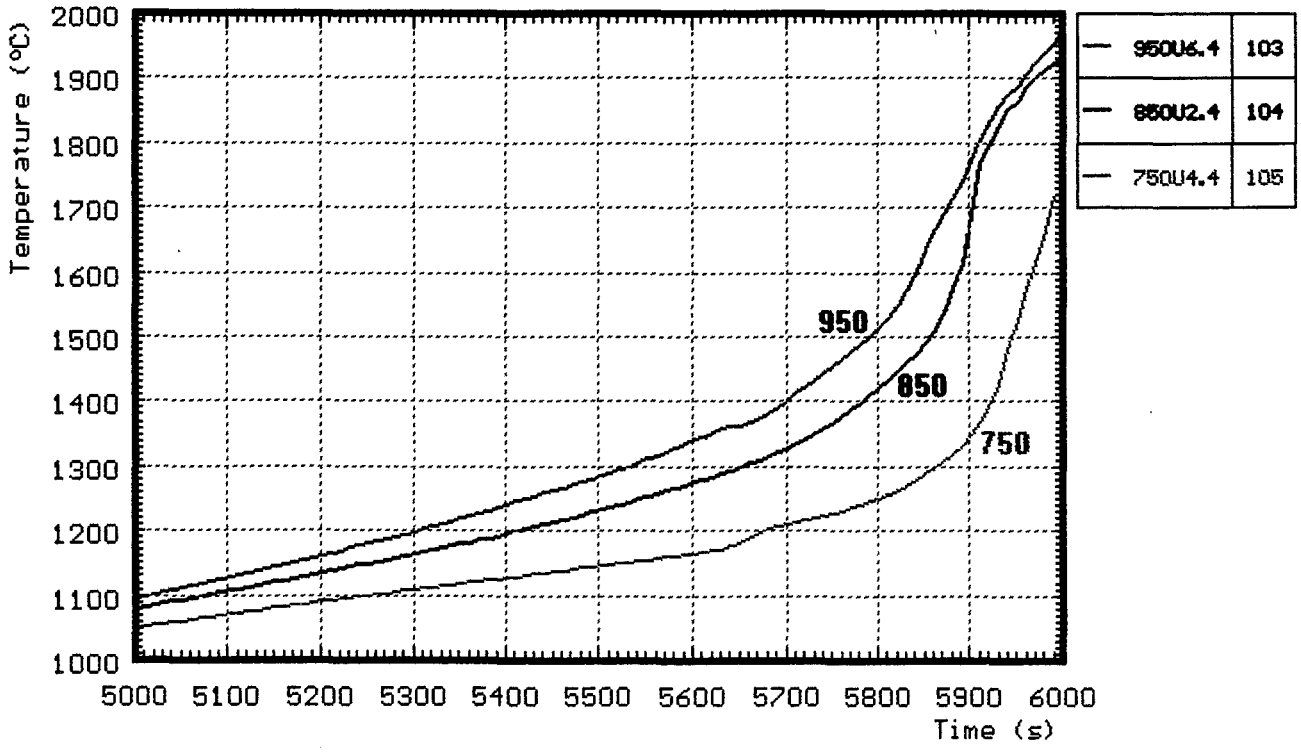

Fig. 74: CORA-30; Temperatures of unheated fuel rods

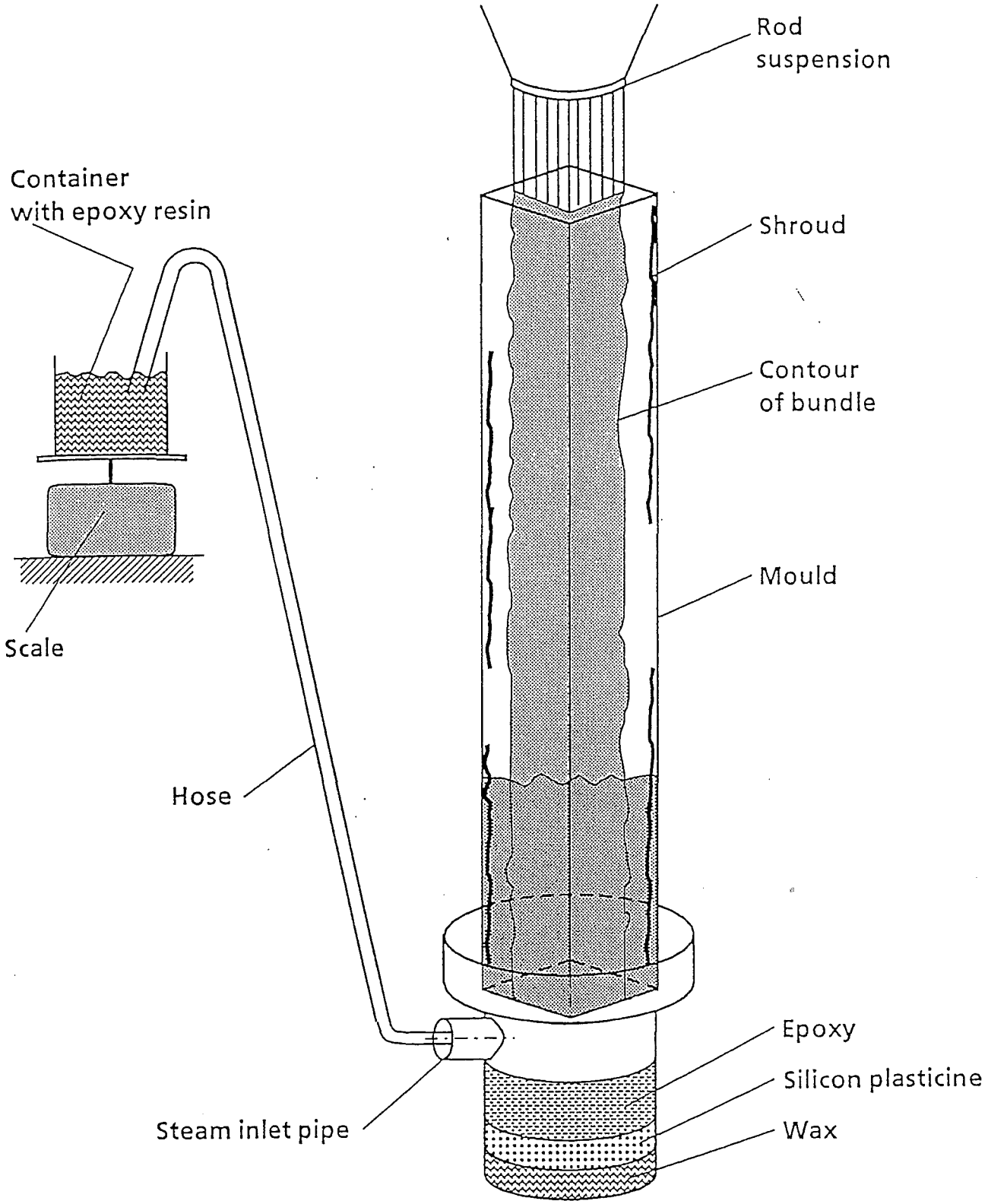

Fig. 75: CORA-30; Epoxing process of the test bundle

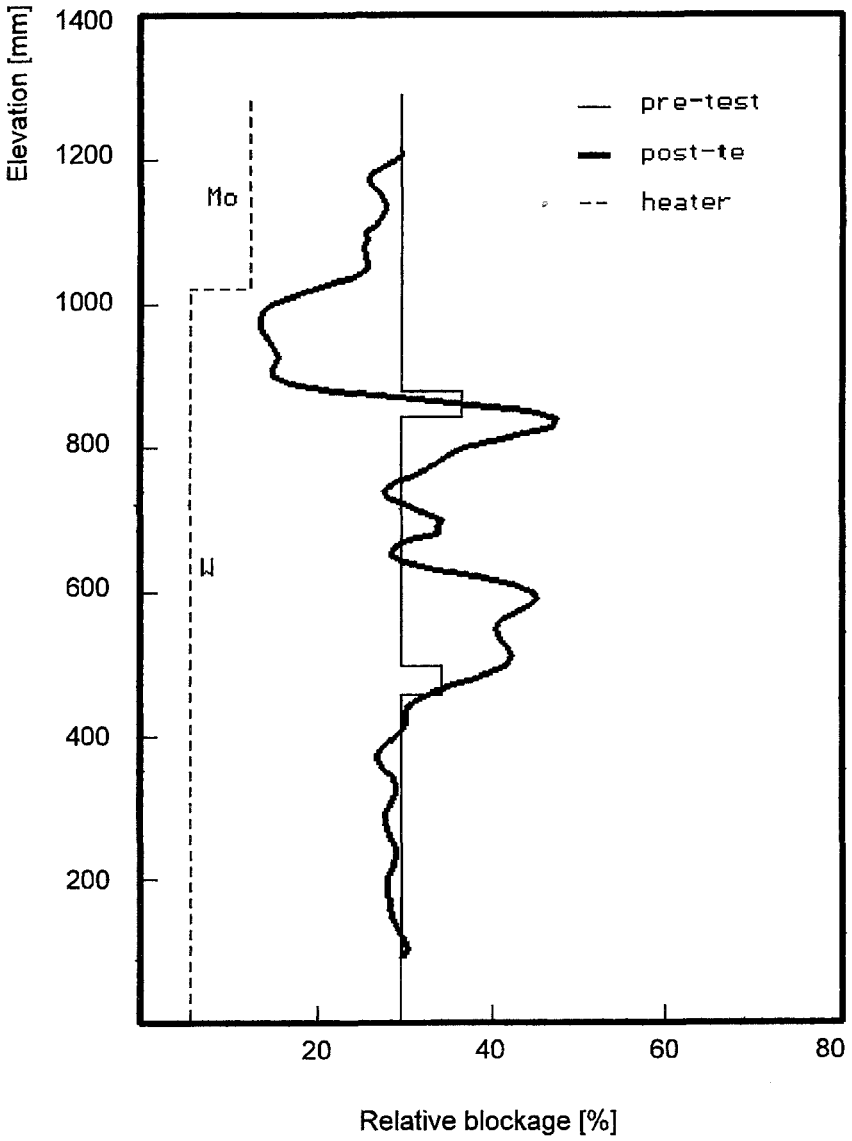

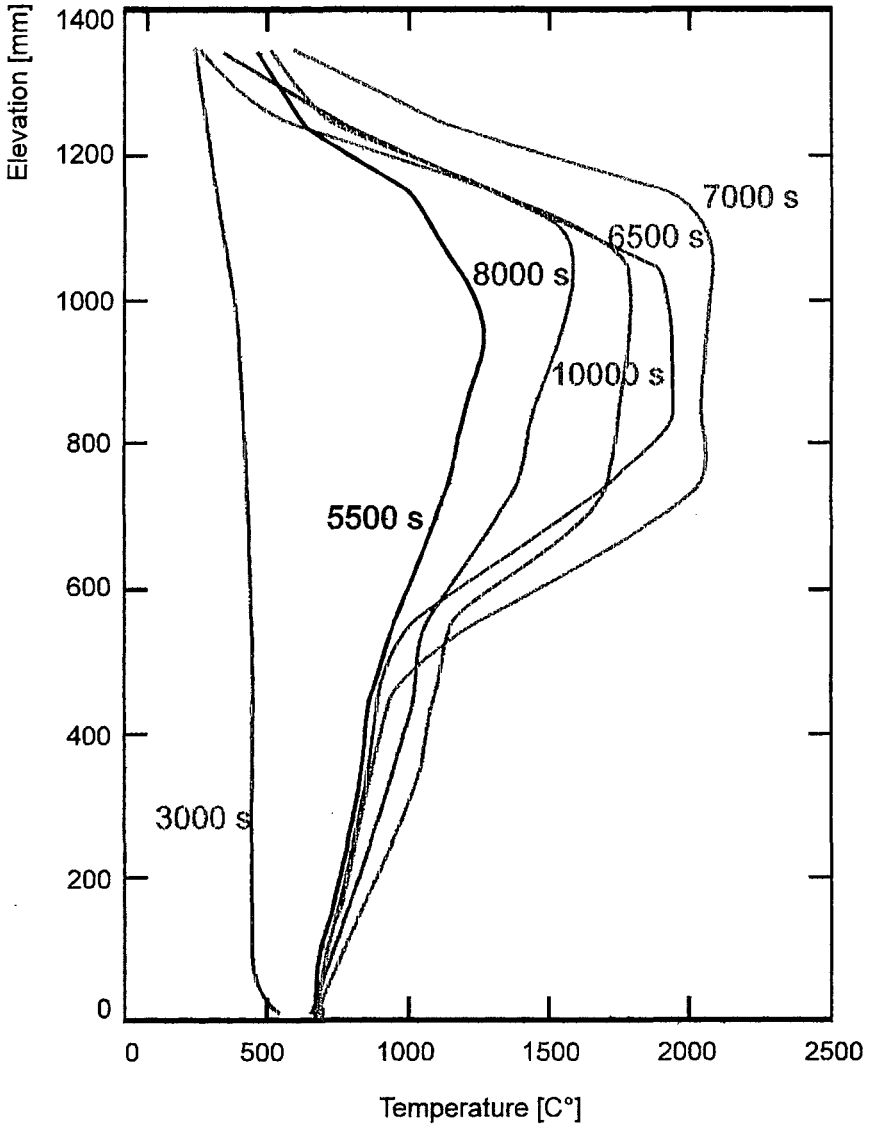

Fig. 76: CORA-30; Axial volume distribution after the test compared to the axial temperature distribution during the test

c30f76.cdr

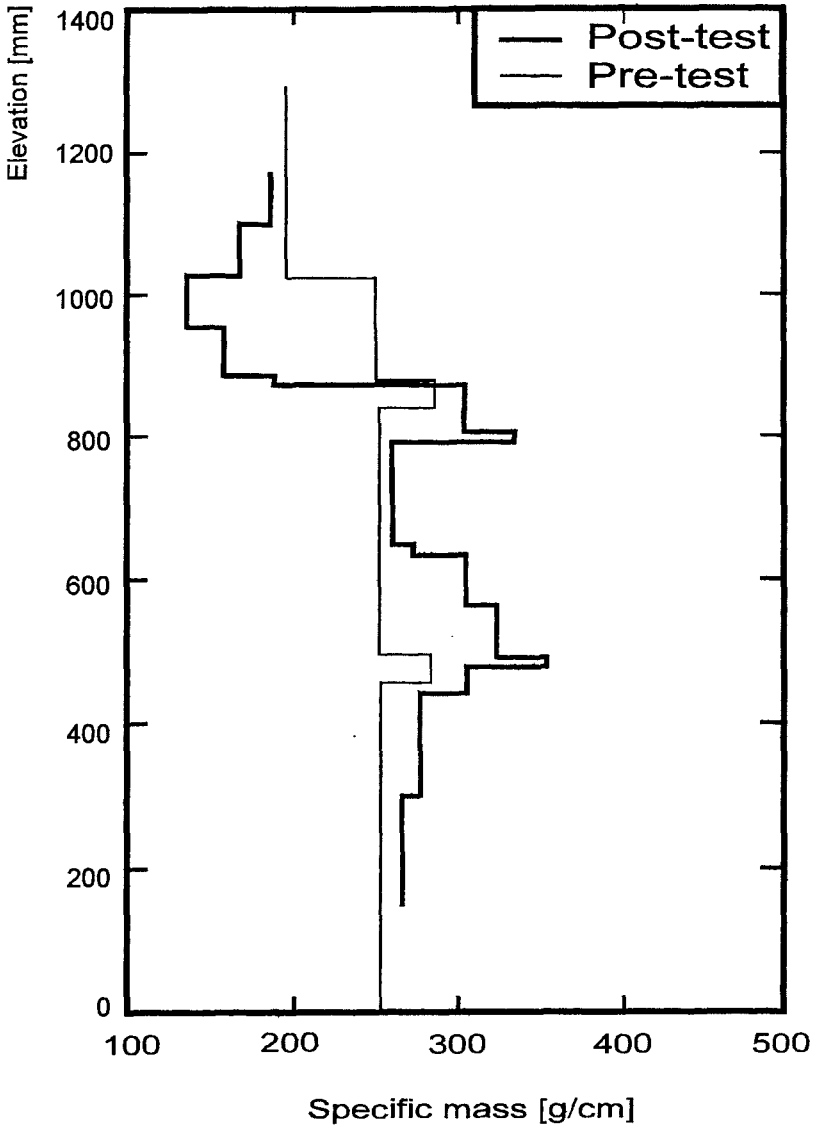

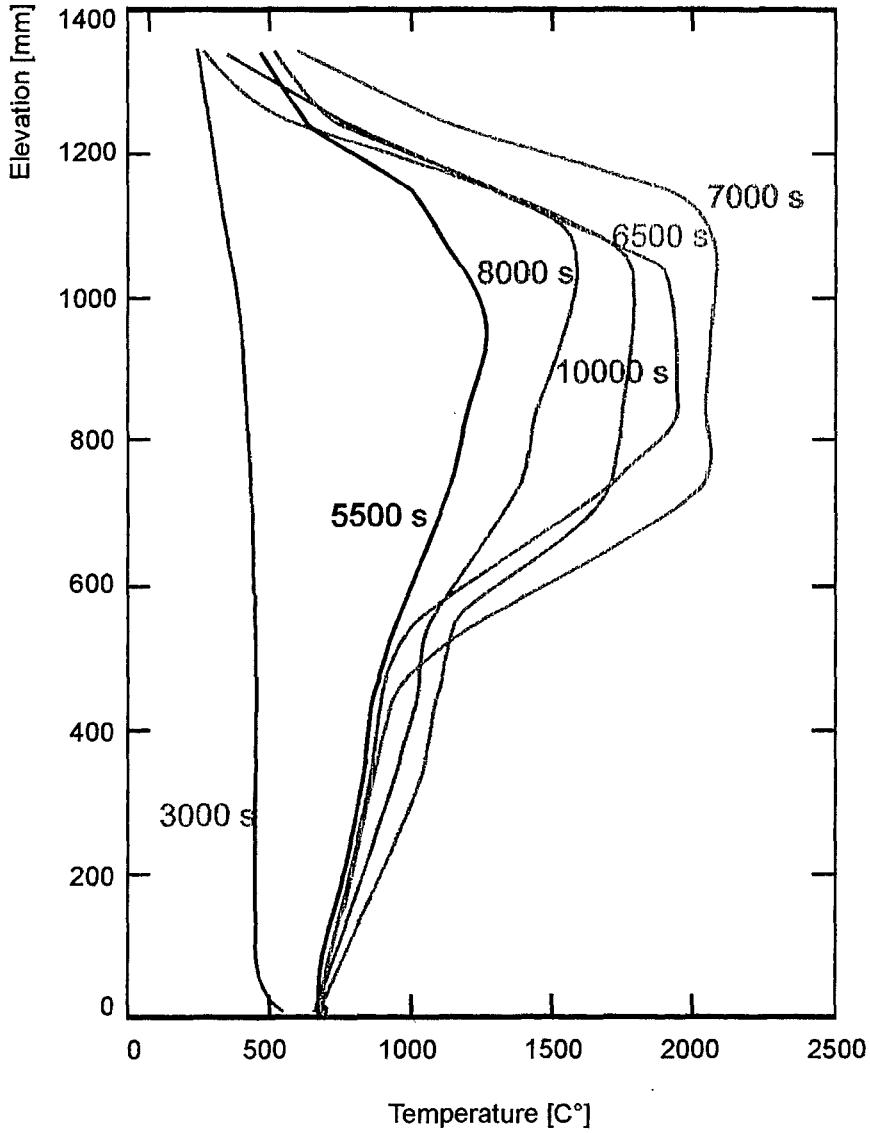

Fig. 77: CORA-30; Axial mass distribution after the test compared to the axial temperature profiles during the test

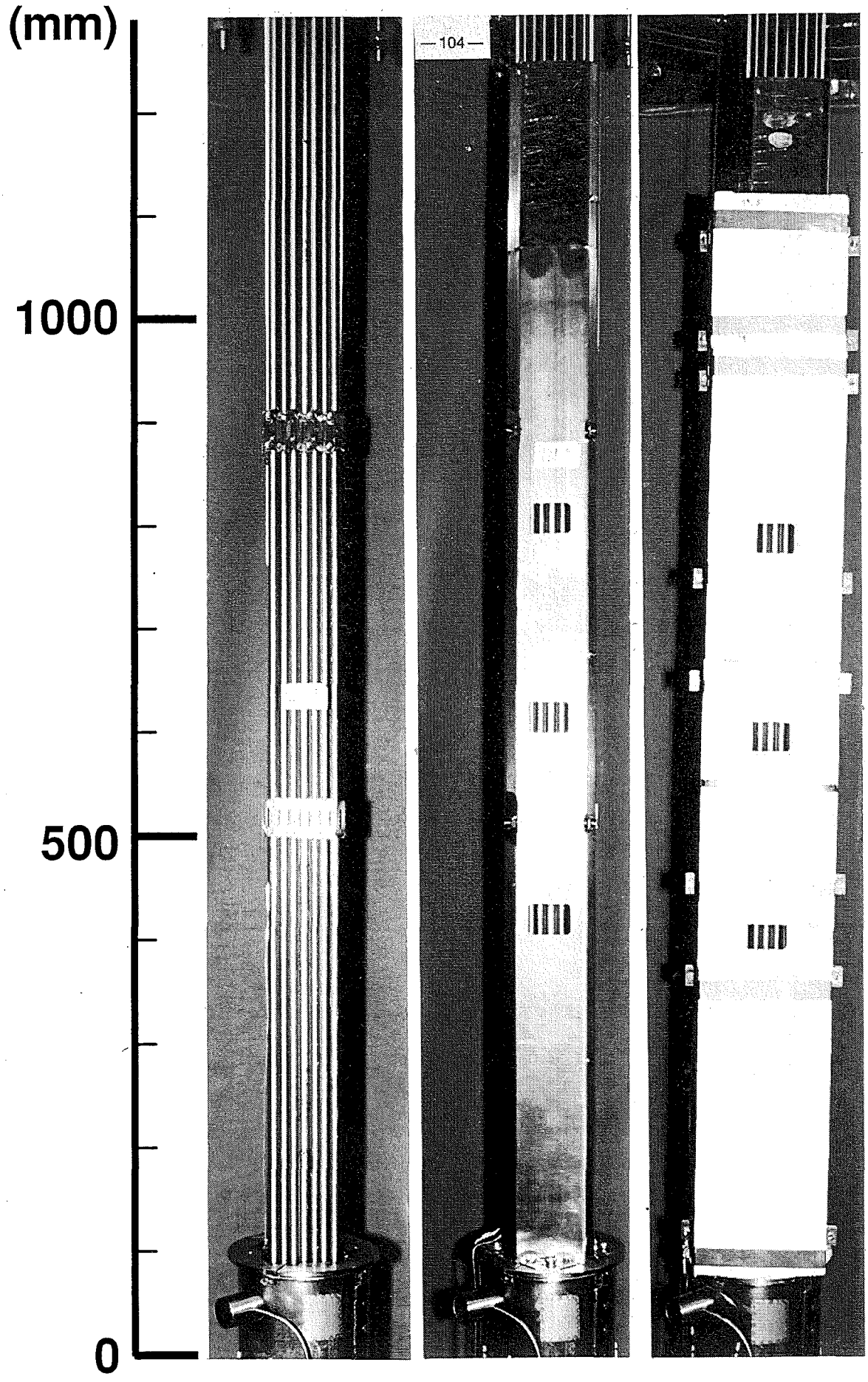

Fig. 81: CORA-30; Pretest appearance of bundle, shroud and shroud insulation

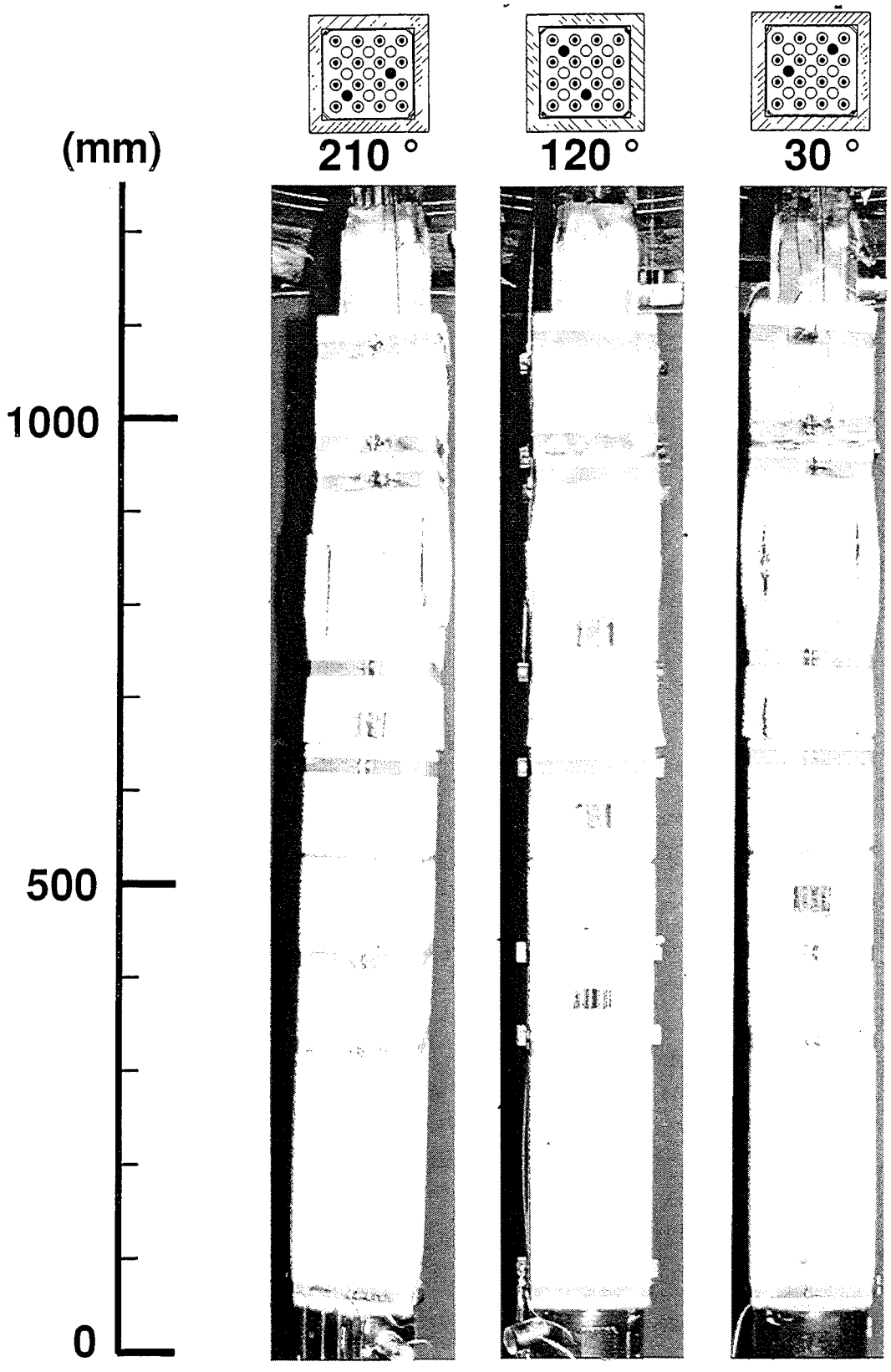

Fig. 82: CORA-30; Posttest appearance of the entire bundle length with shroud insulation; 210°, 120°, 30°

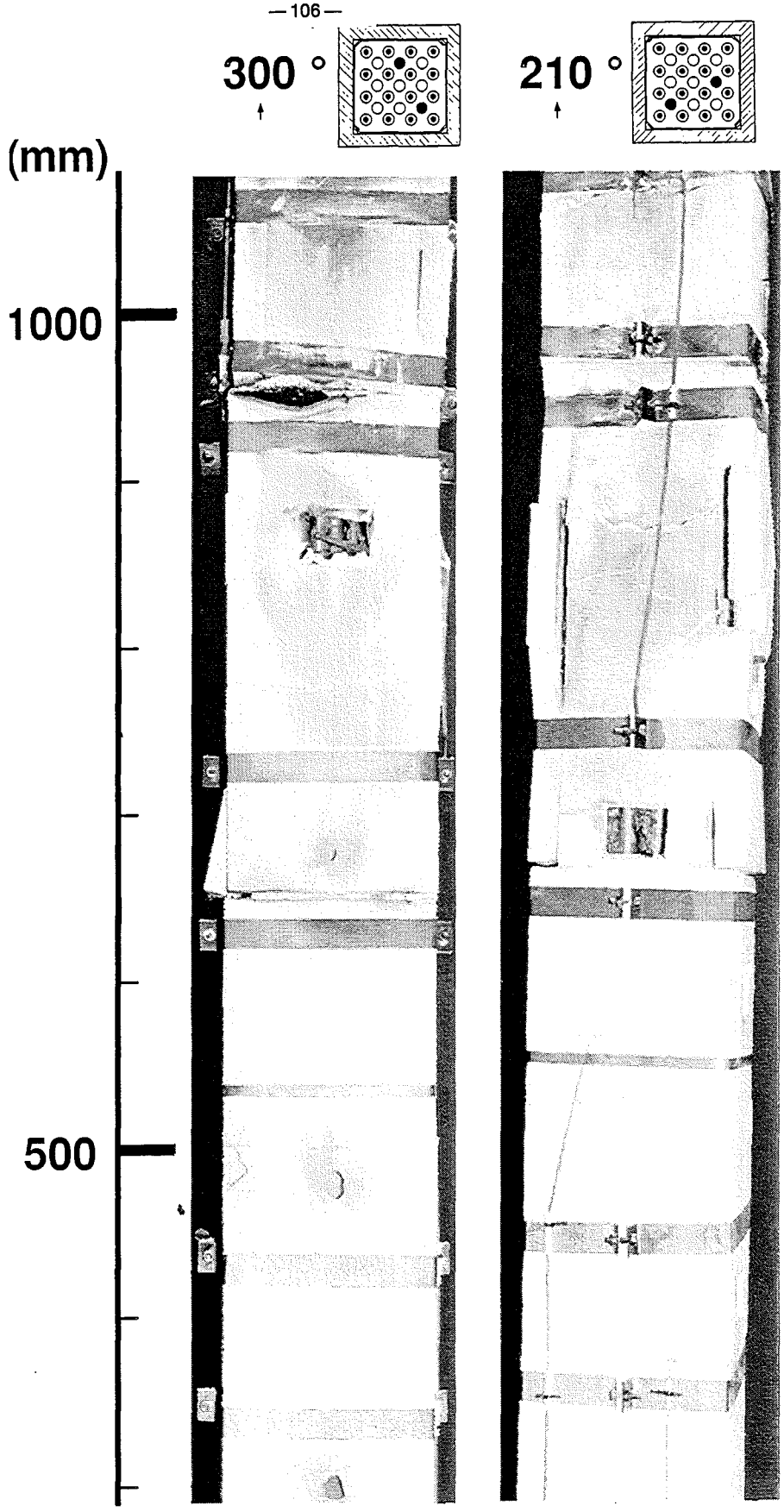

Fig. 83: CORA-30; Posttest appearance of the bundle with shroud insulation; 300°, 210° orientation; 300-1100 mm

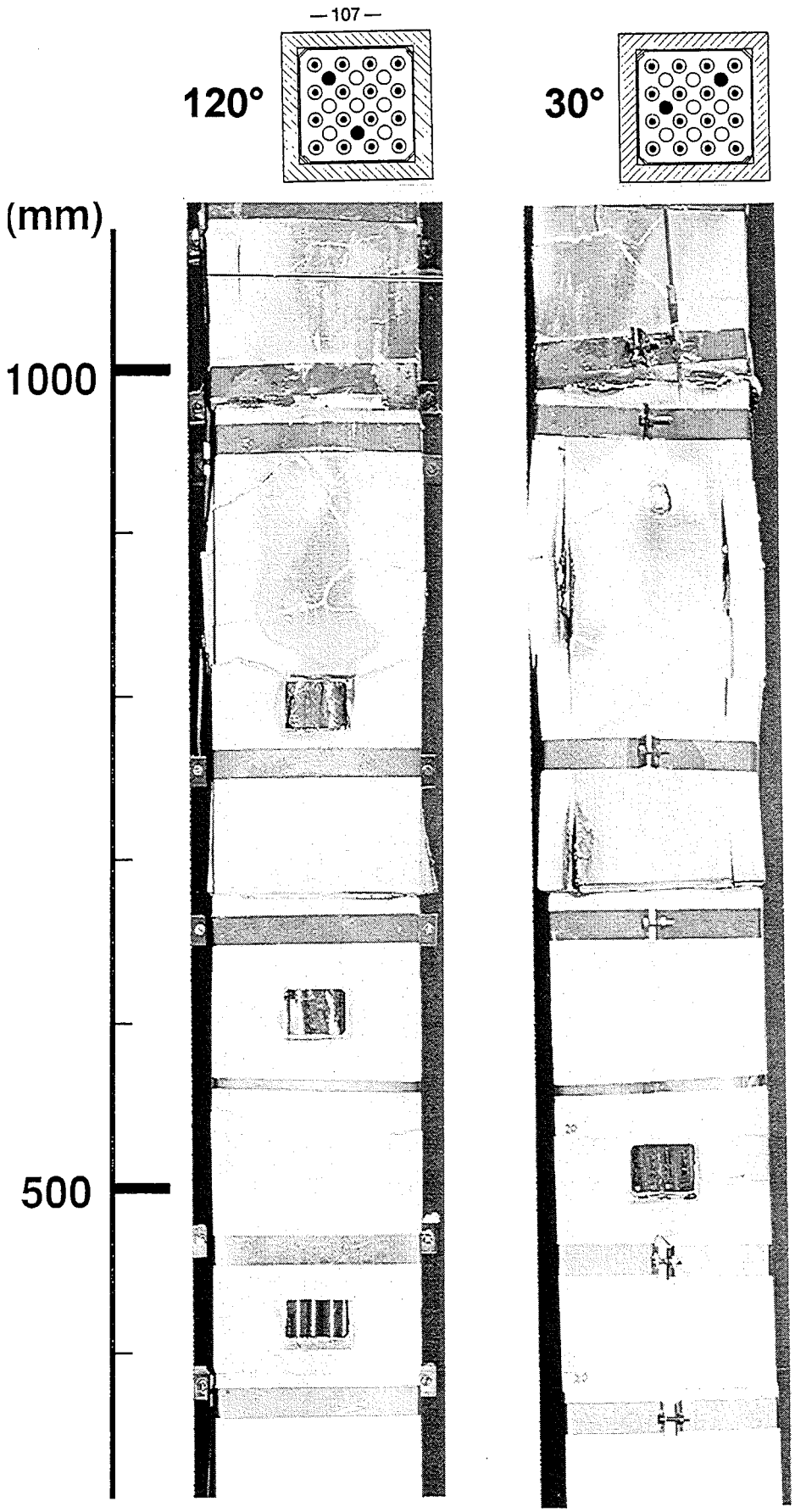

Fig. 84: CORA-30; Posttest appearance of the bundle with shroud insulation; 120°, 30° orientation; 300-1100 mm

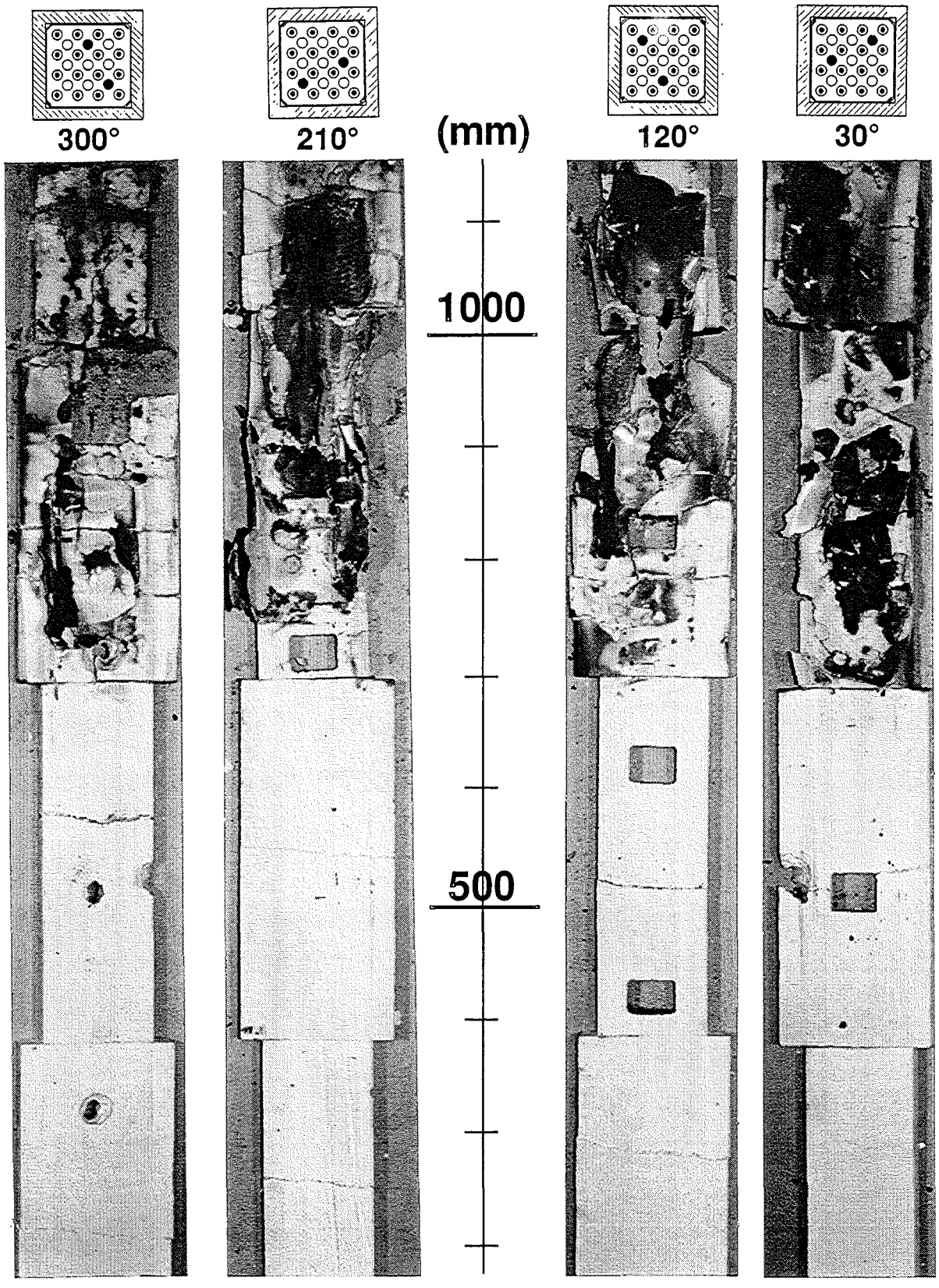

Fig. 85: CORA-30; Posttest view of the inner side of shroud insulation; 300°, 210°, 120°, 30° orientation

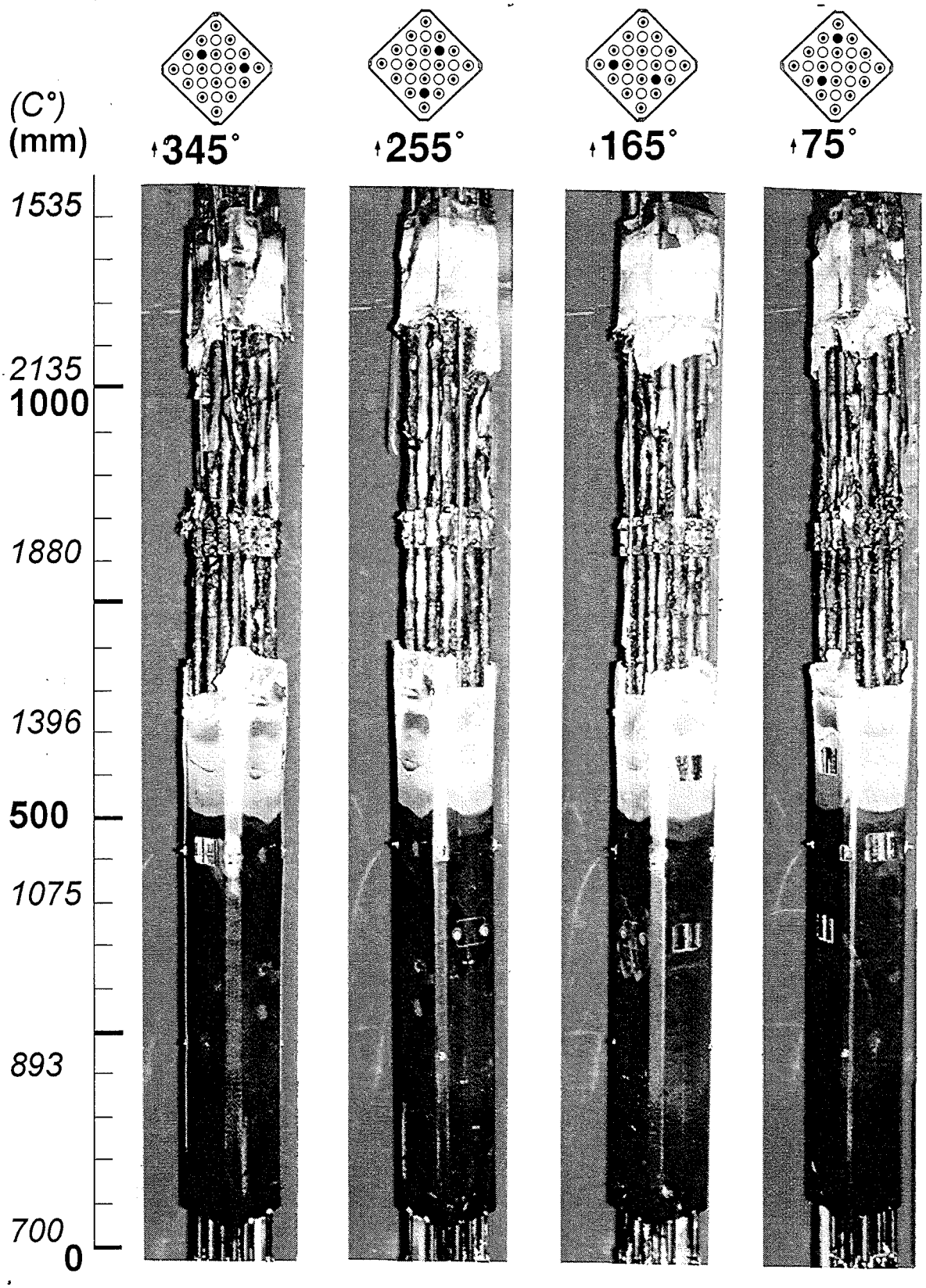

Fig. 86: Posttest view of bundle CORA-30 after partial removal of shroud; 345°, 255°, 165°, 75° orientation

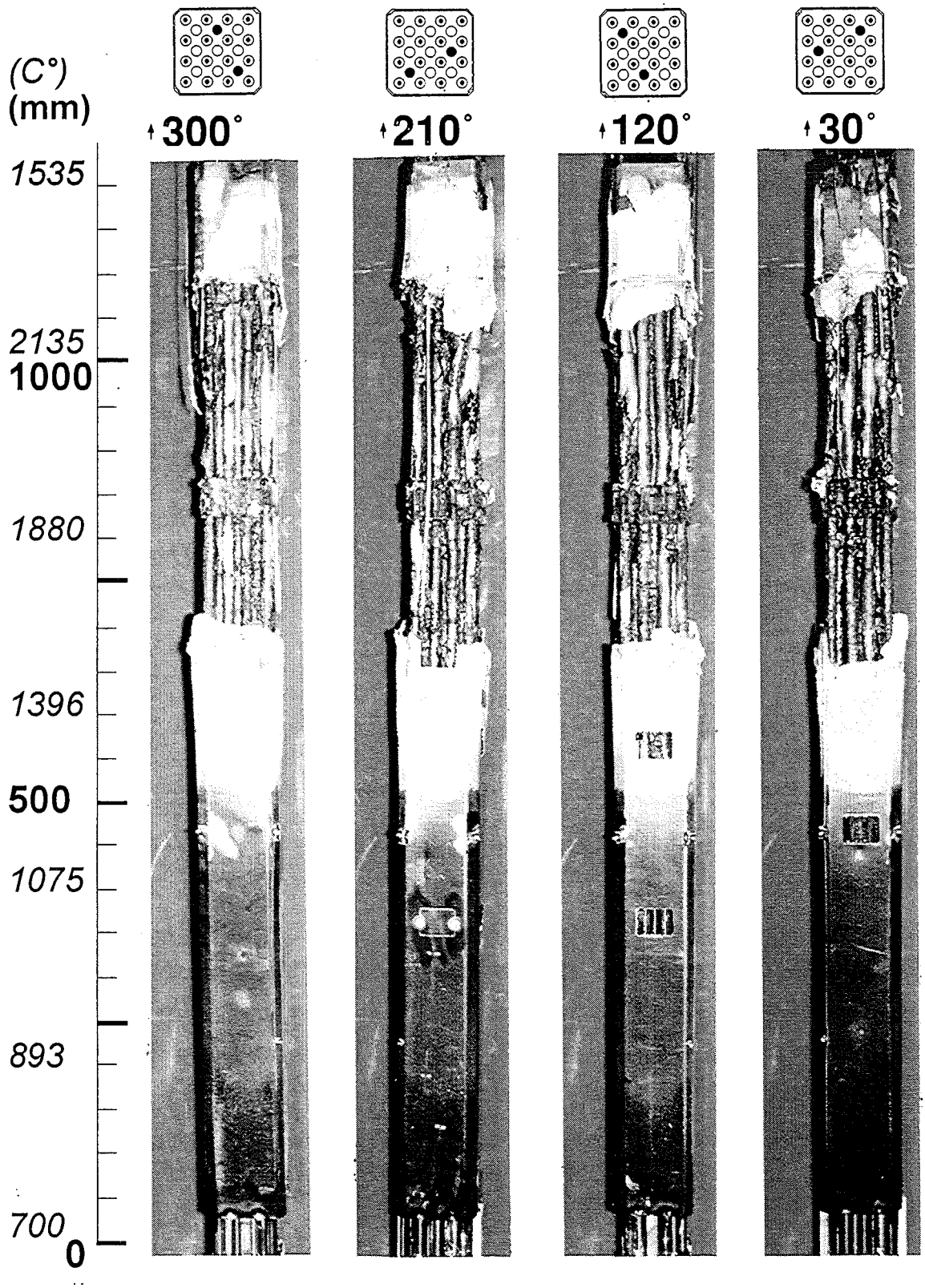

Fig. 87: Posttest view of bundle CORA-30 after partial removal of shroud; 300°, 210°, 120°, 30° orientation

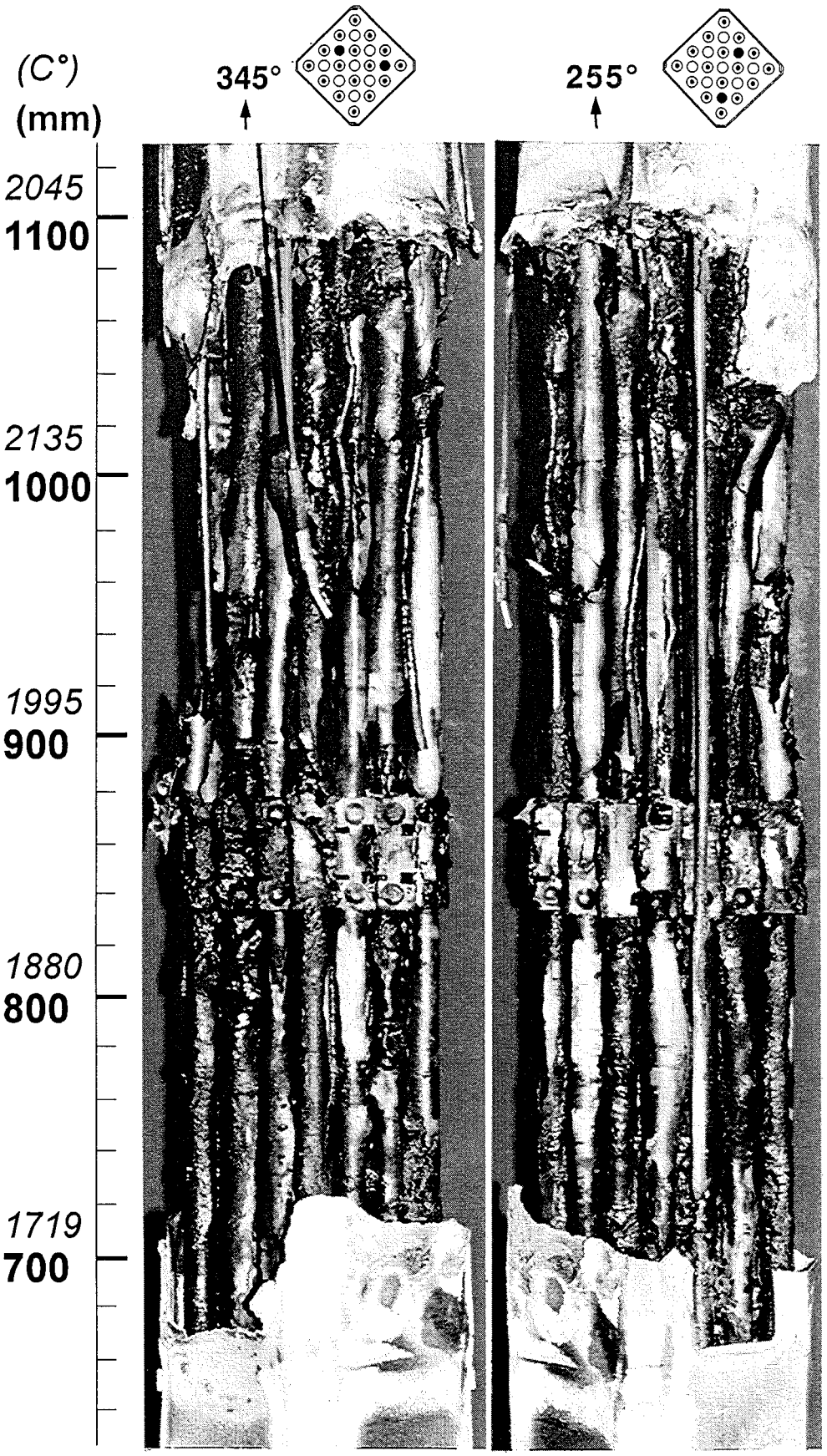

Fig. 88: CORA-30; Posttest view; 345° and 255° orientation; 650 - 1100 mm elevation

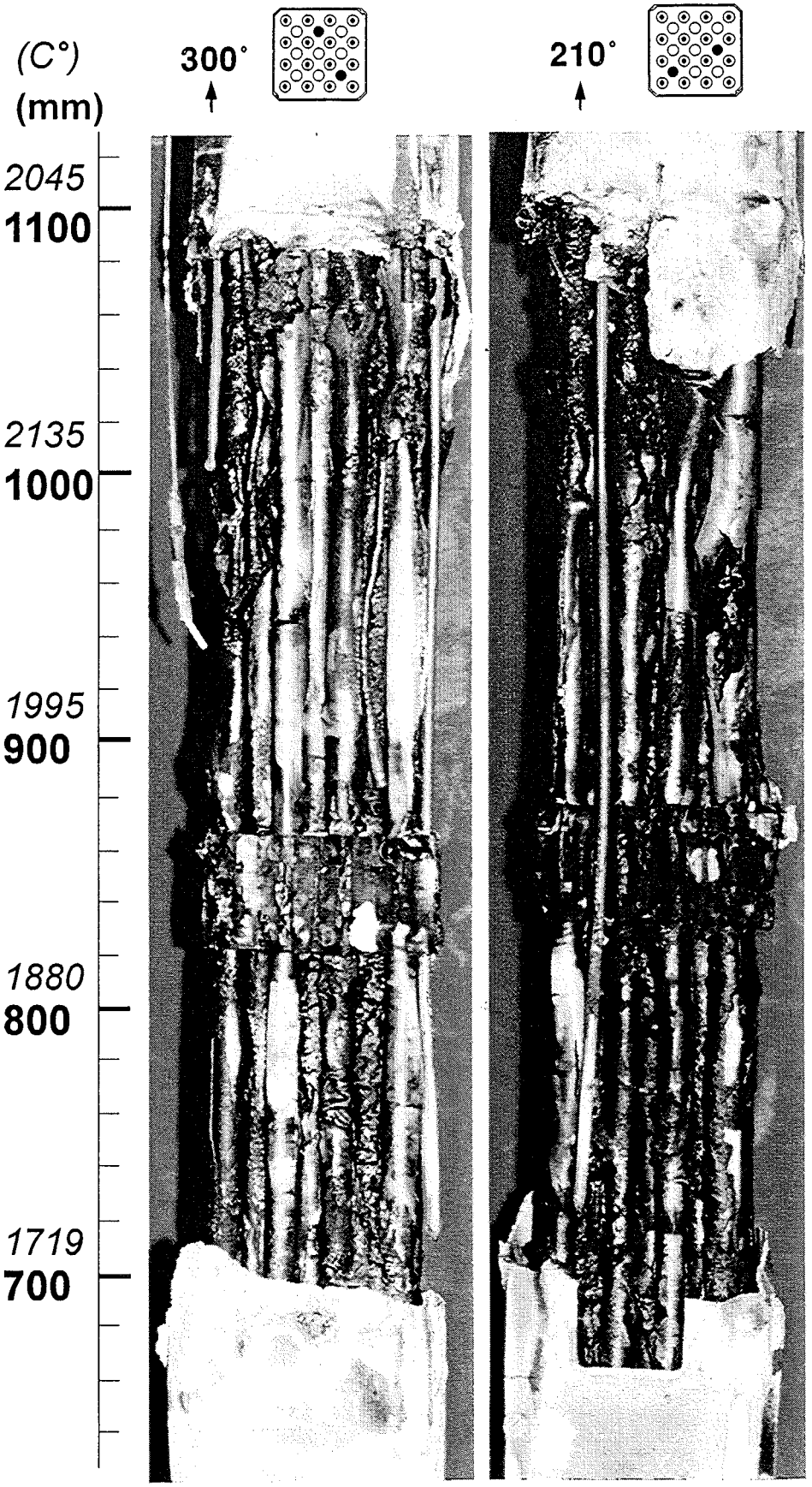

Fig. 89: CORA-30; Posttest view; 300° and 210° orientation; 650 - 1100 mm elevation

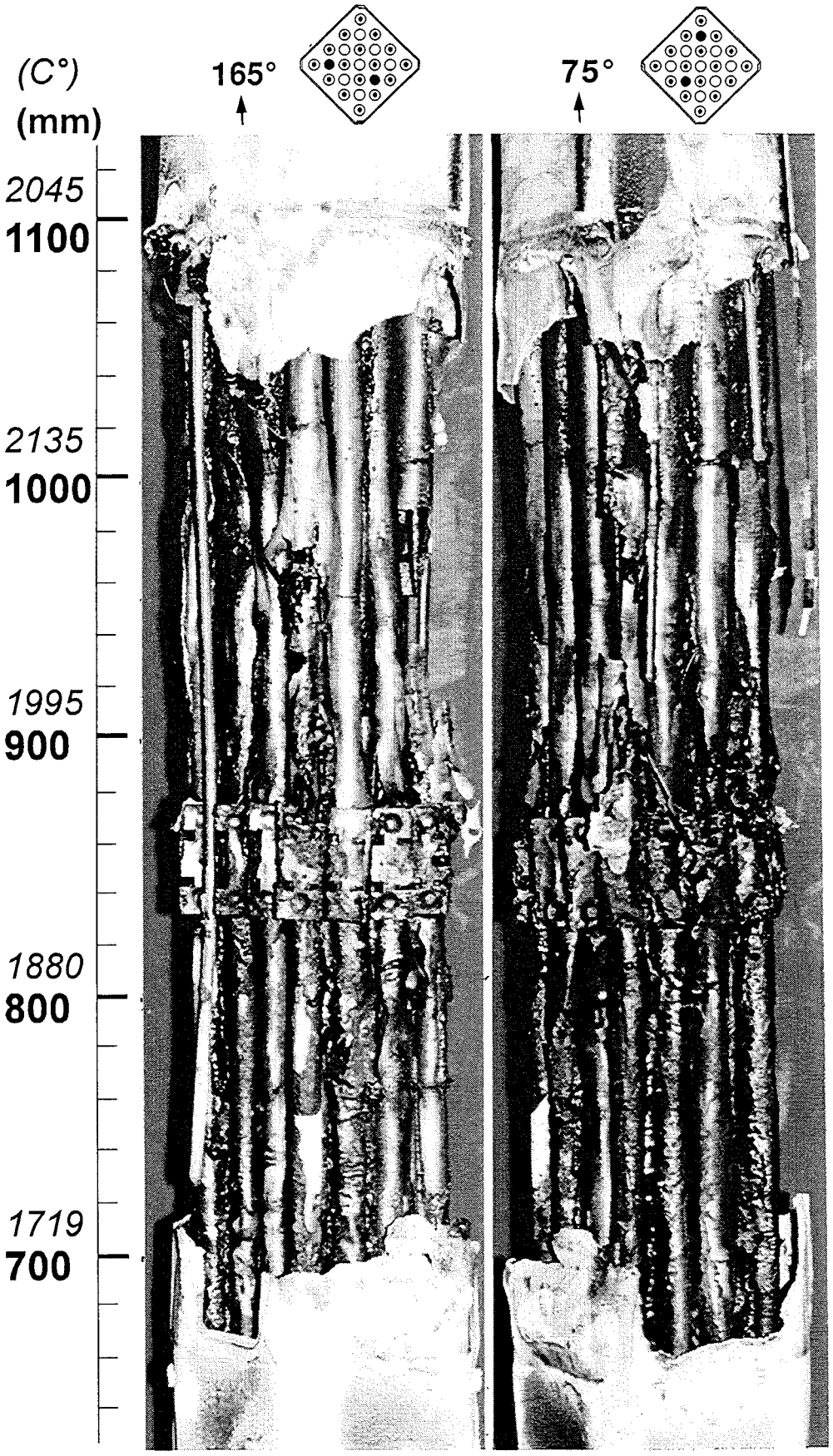

Fig. 90: CORA-30; Posttest view; 165° and 75° orientation; 650 - 1100 mm elevation

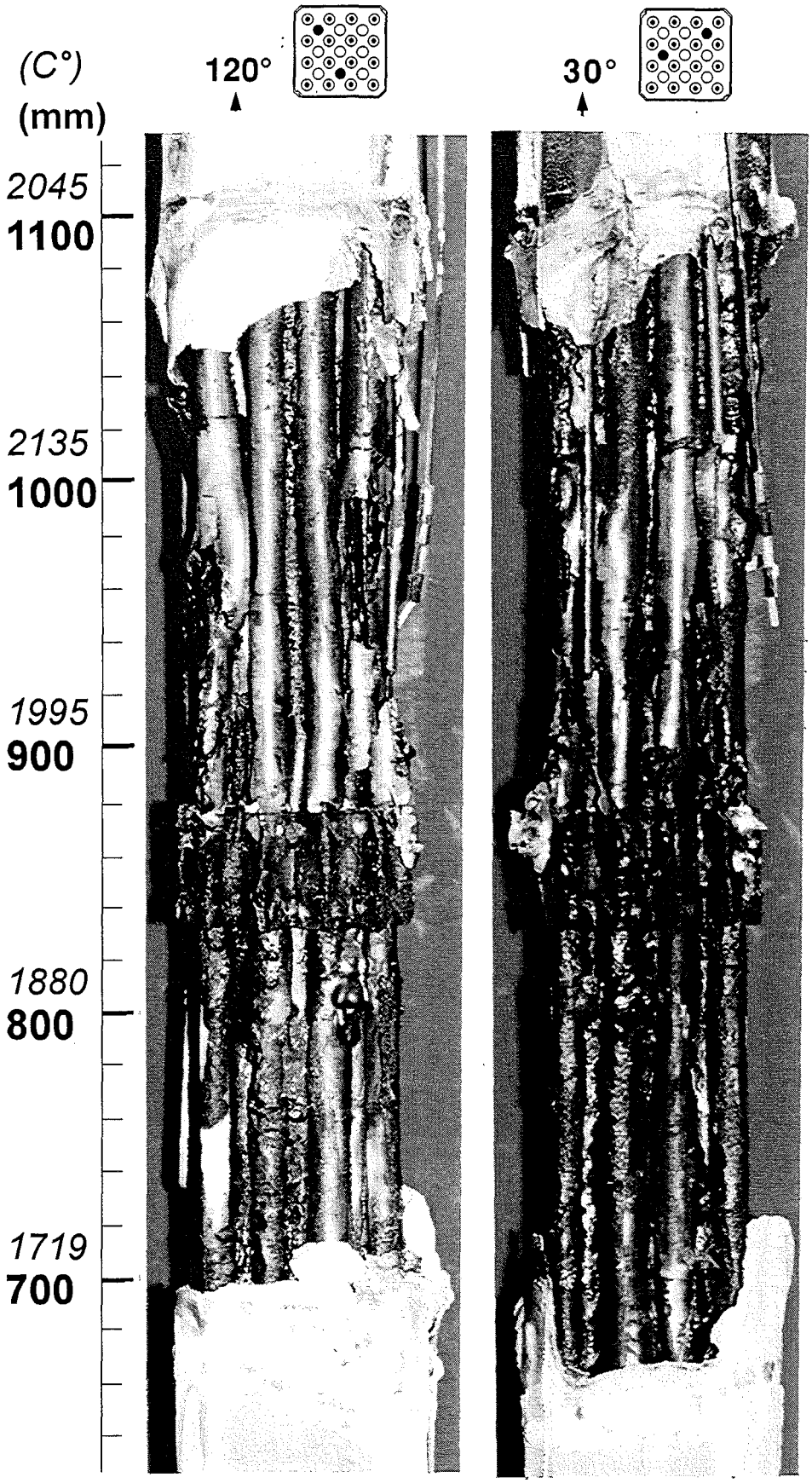

Fig. 91: CORA-30; Posttest view; 120° and 30° orientation; 650 - 1100 mm elevation

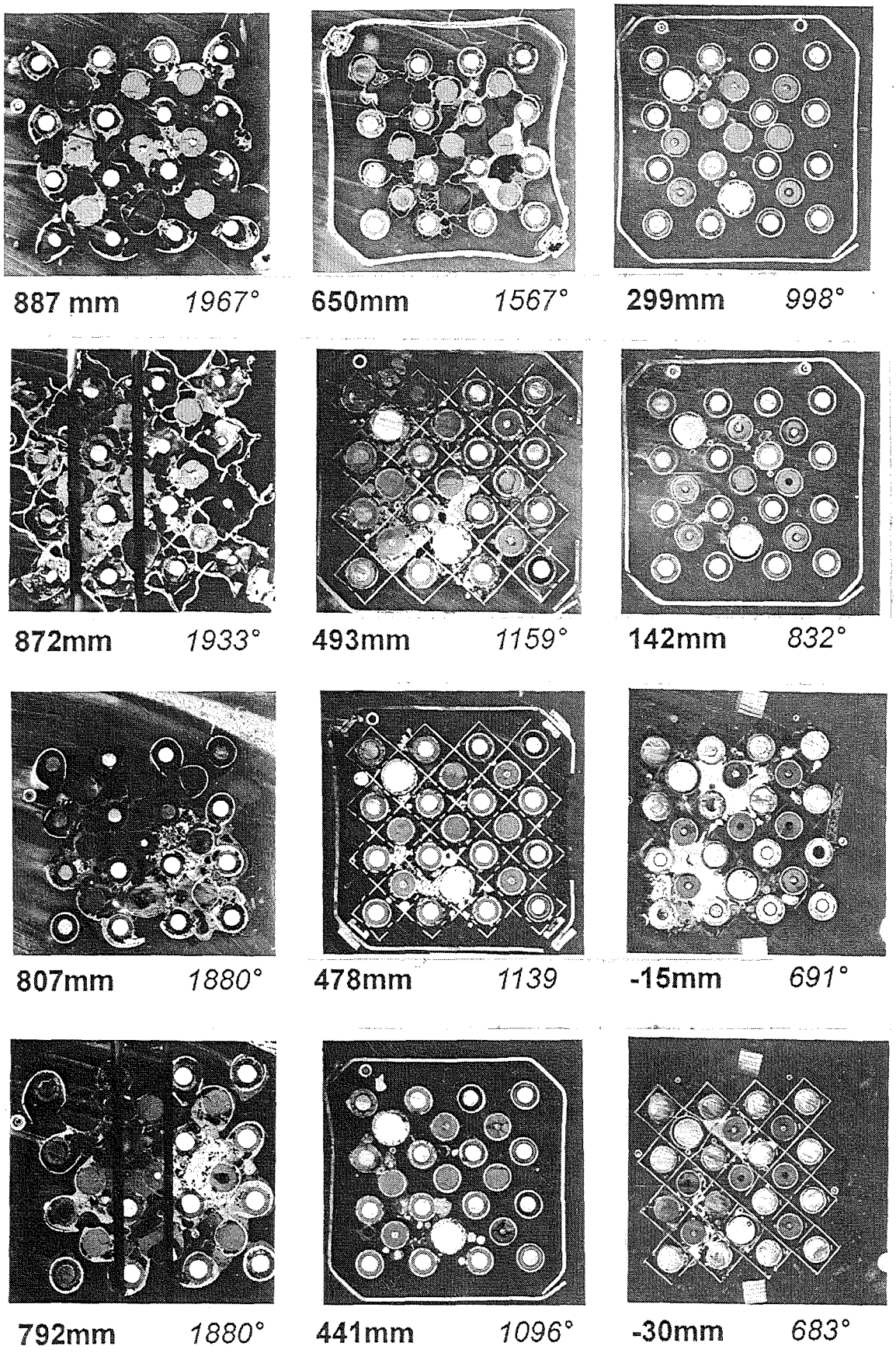

Fig. 92: CORA-30: Horizontal cross sections of bundle, top view (887- -30 mm)

Absorberrod 6.2

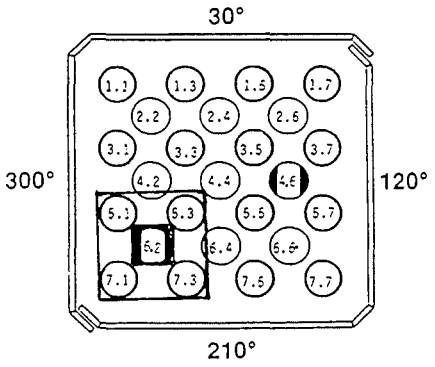

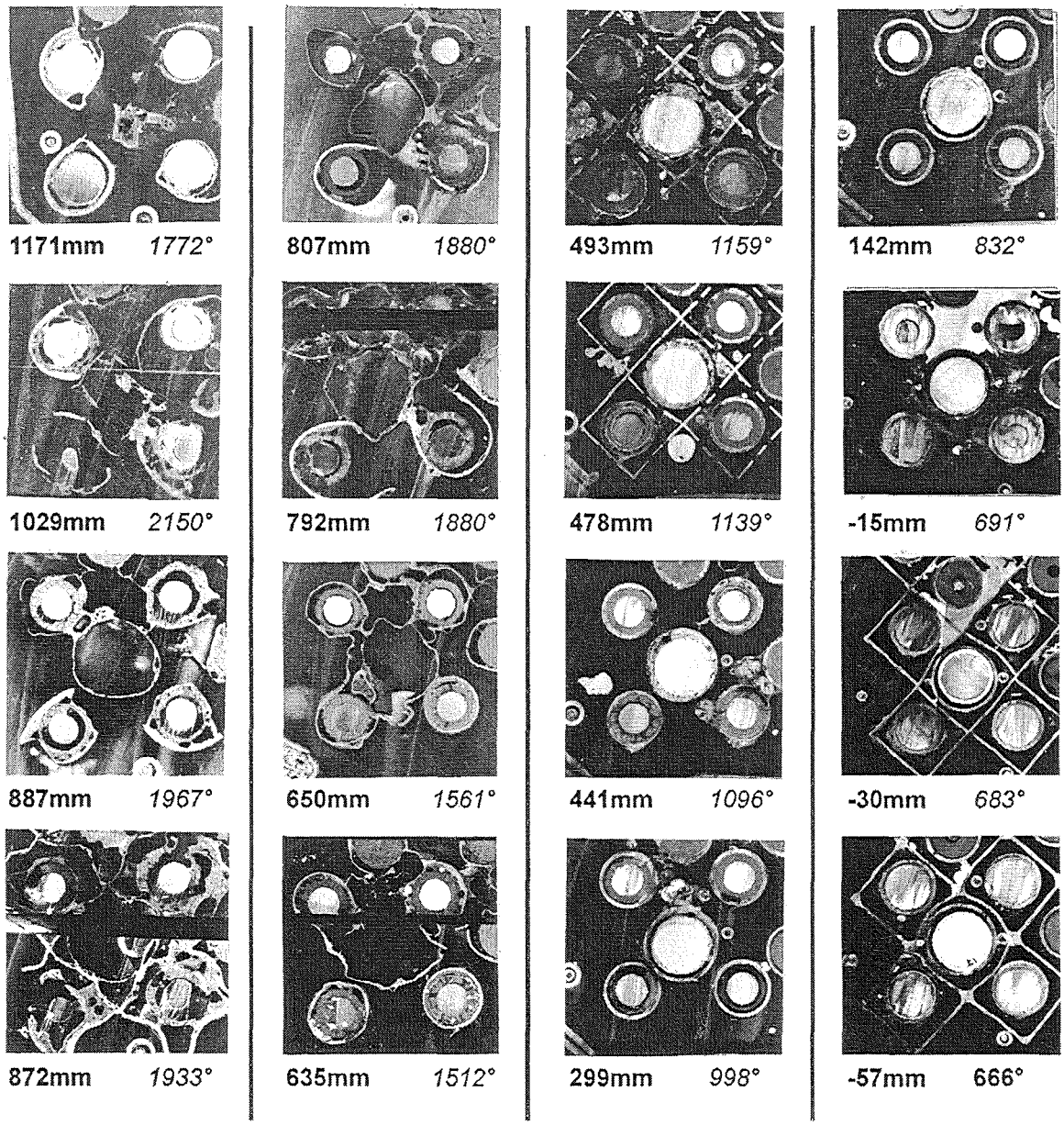

Fig. 93: CORA-30; Horizontal cross sections of the region of absorber rod 6.2, top view (1171 - 57 mm)

Absorberrod 4.6

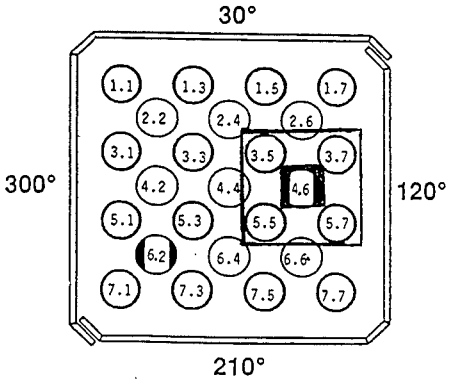

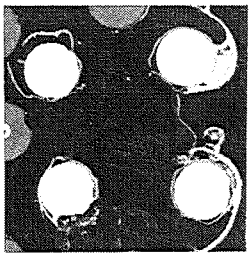
1171mm 1772°

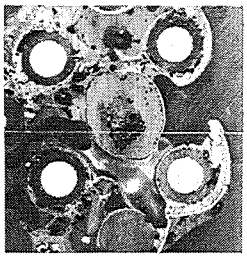
807mm 1880°

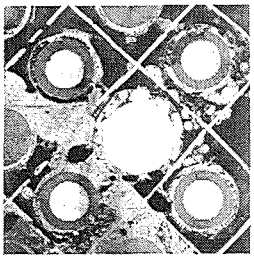
493mm 1159°

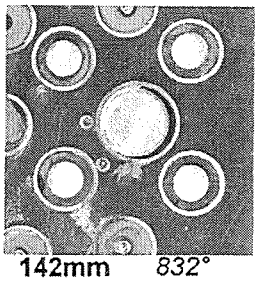
142mm 832°

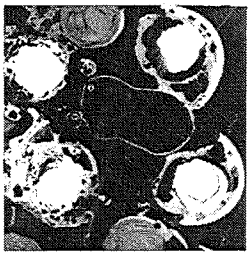
1029mm 2150°

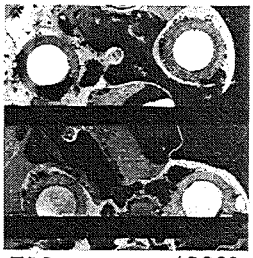
792mm 1880°

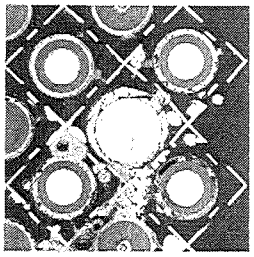
478mm 1139°

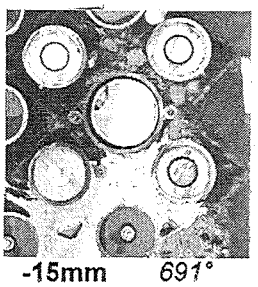
-15mm 691°

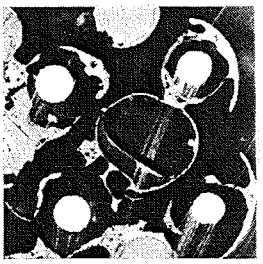
887mm 1967°

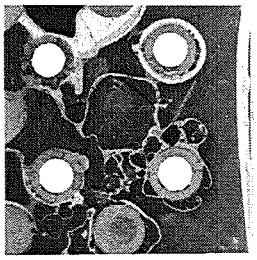
650mm 1561°

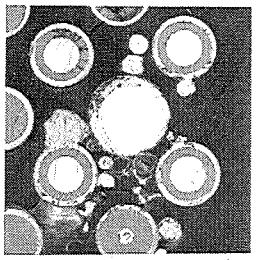
441mm 1096°

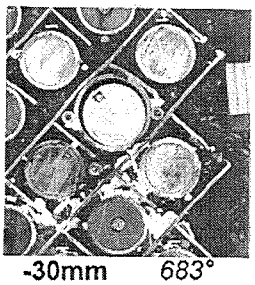
-30mm 683°

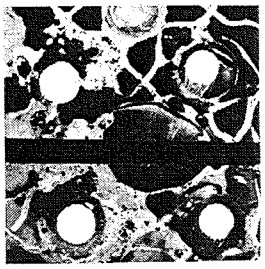
872mm 1933°

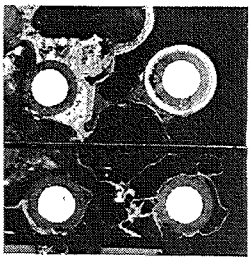
635mm 1512°

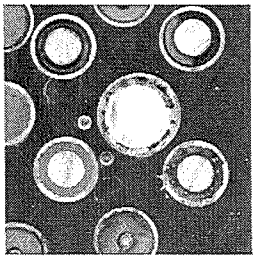
299mm 998°

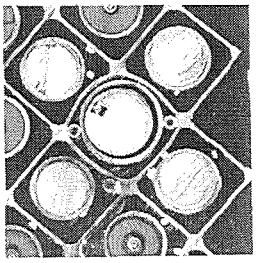
-57mm 666°

Fig. 94: CORA-30; Horizontal cross sections of the region of absorber rod 4.6, top view (1171 - -57 mm)

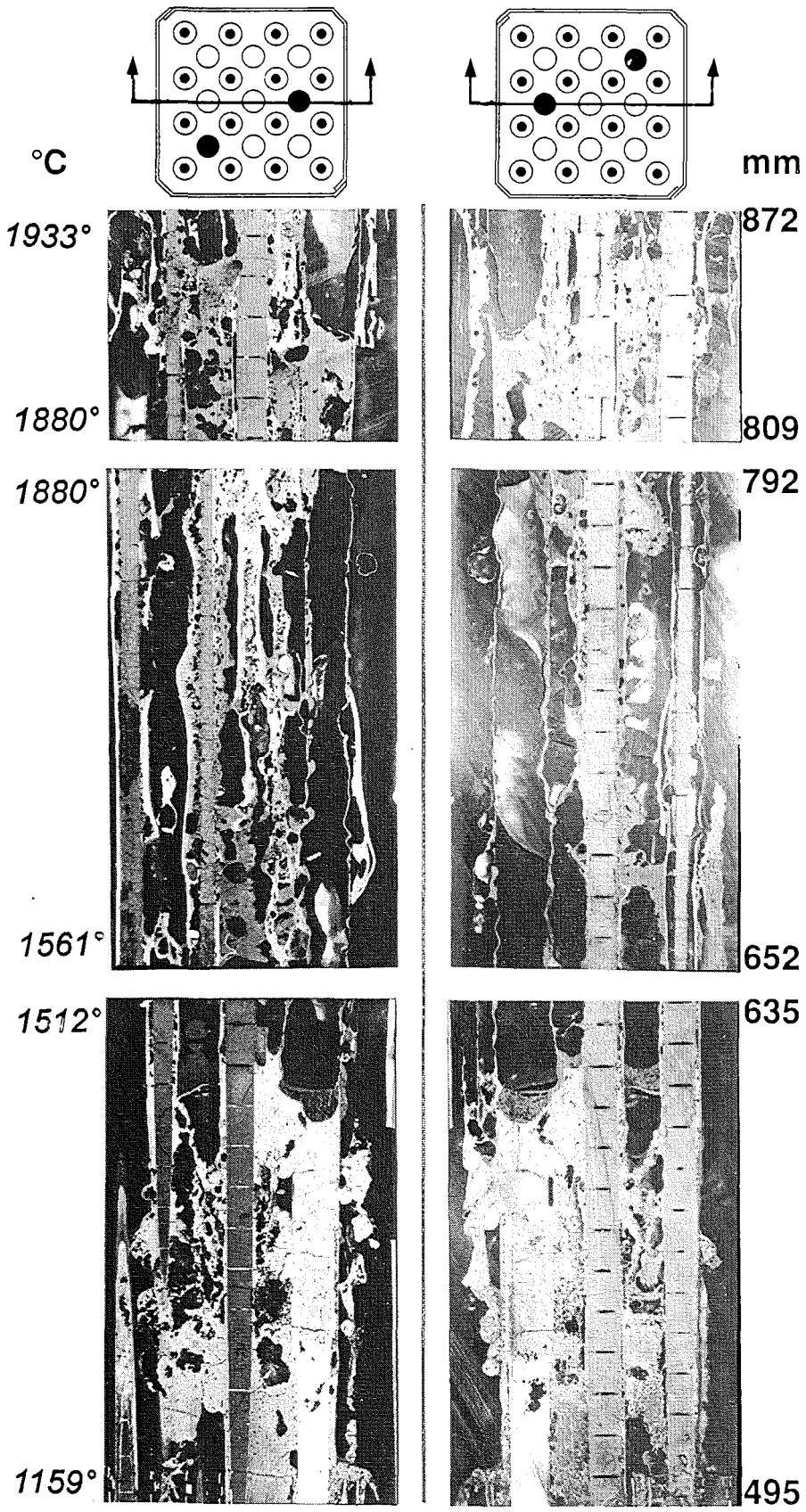

Fig. 95: CORA-30; Vertical cross sections through absorber rod 4.6, both sides of the cut (495 - 872 mm)

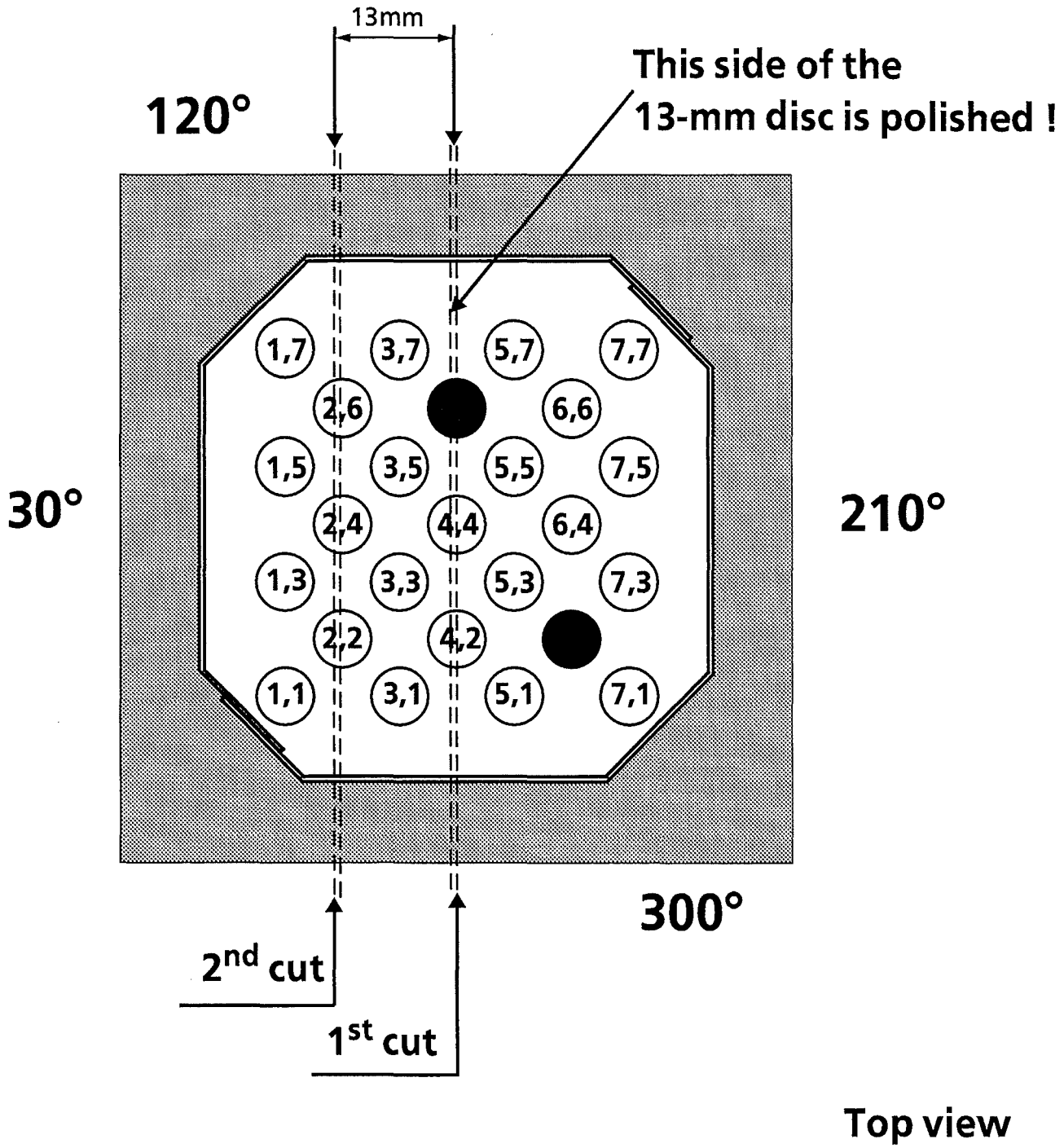

Fig. 95a: Locations of the vertical cuts through samples CORA - 30-f, 30-g, 30-h

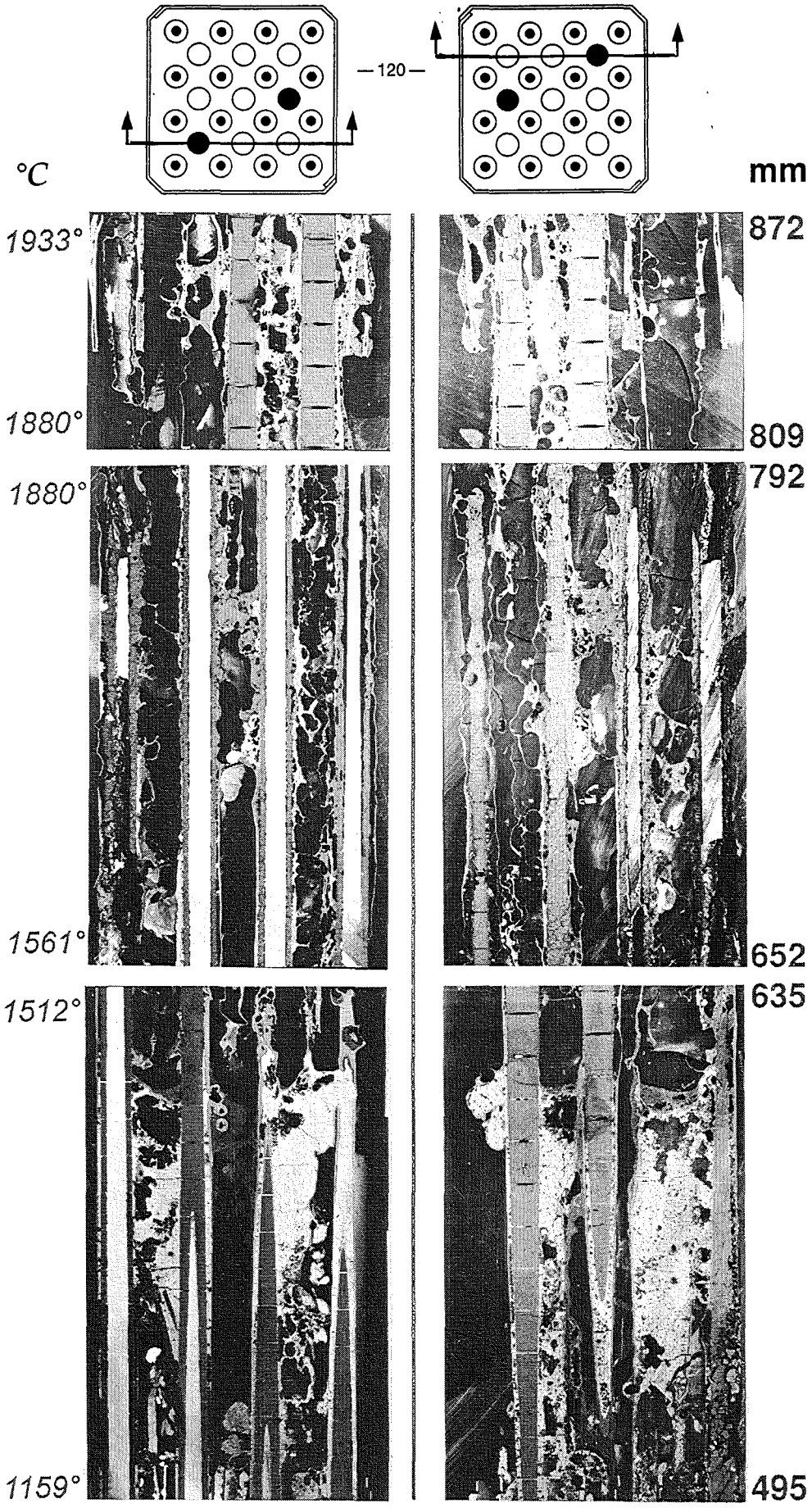

Fig. 96: CORA-30; Vertical cross sections through absorber rod 6.2, both sides of the cut (495 - 872 mm)

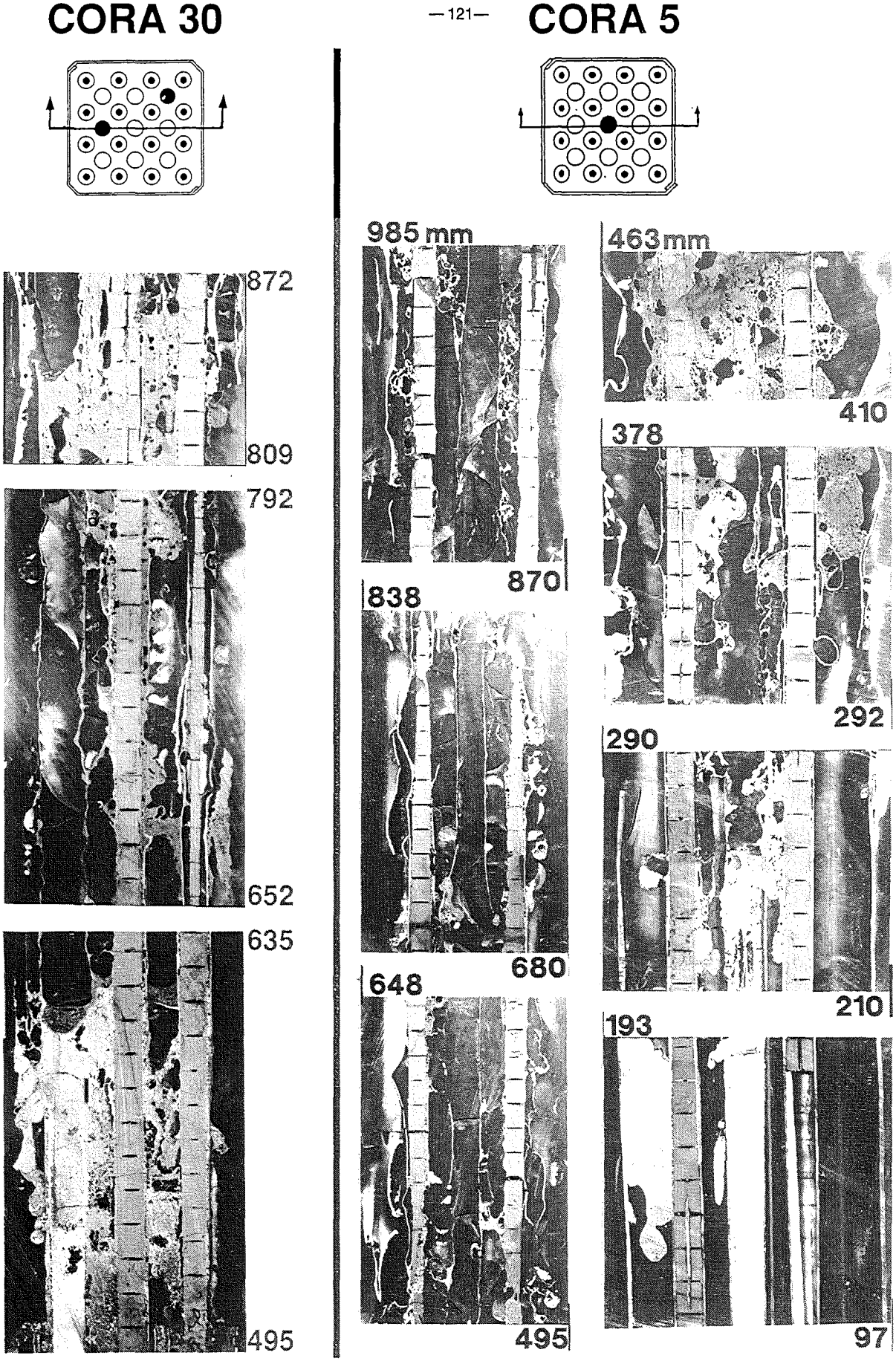

Fig. 97: Comparison of vertical cross sections CORA-30 /CORA-5

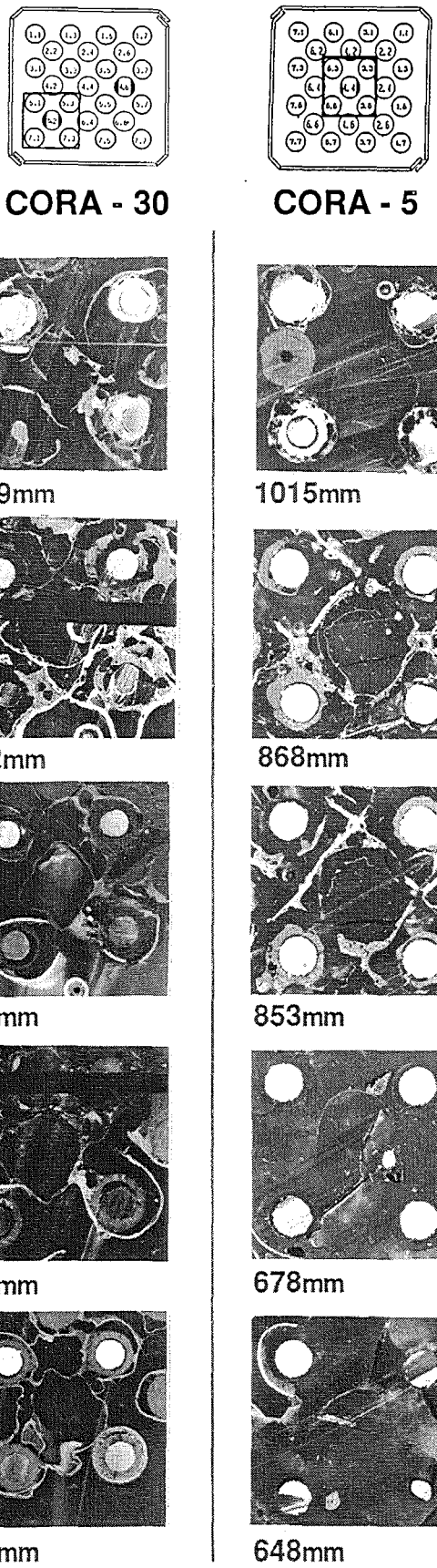

Fig. 98: Comparison of cross sections of absorber regions CORA-30/ CORA-5

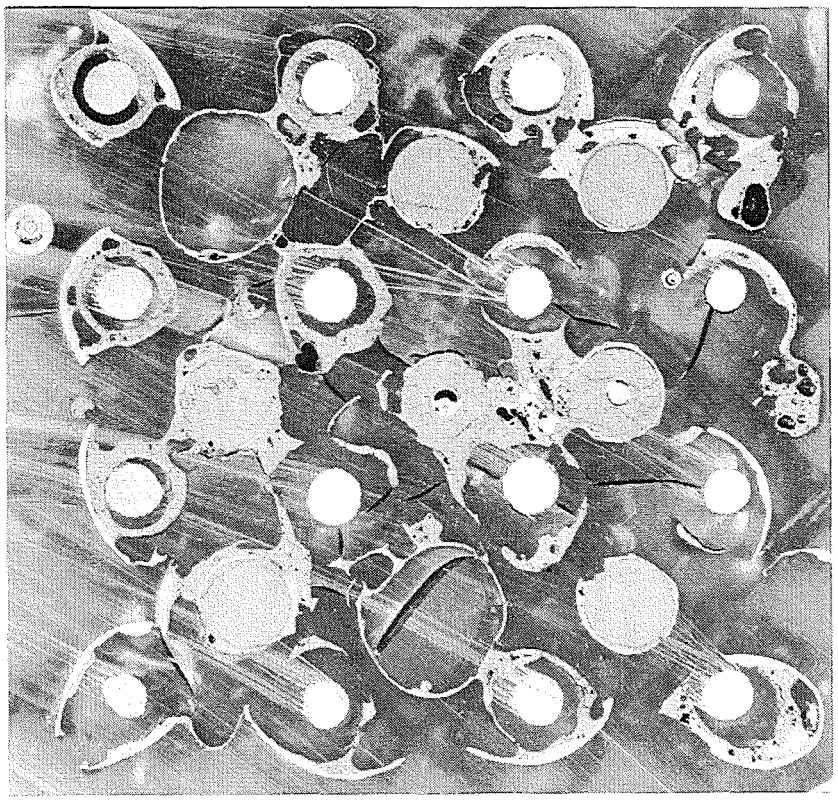

887 mm

CORA-30

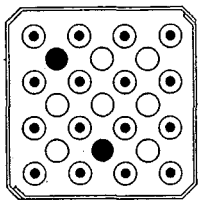

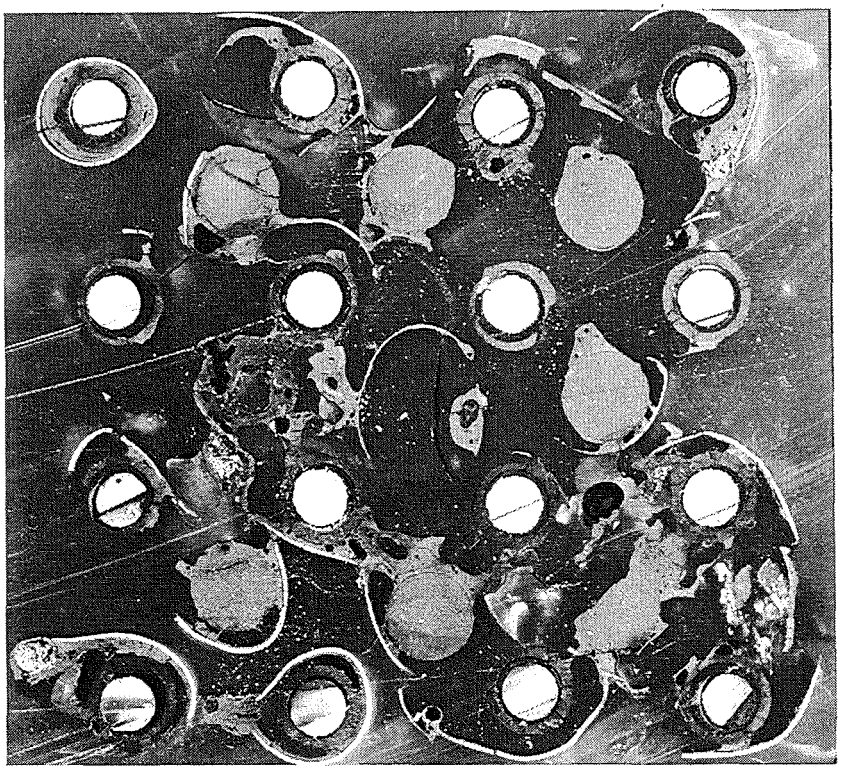

663 mm

CORA-5

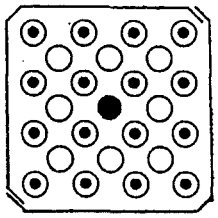

(top view)

Fig. 99: Comparison of horizontal cross sections CORA-30/ CORA-5 (887, 663 mm)

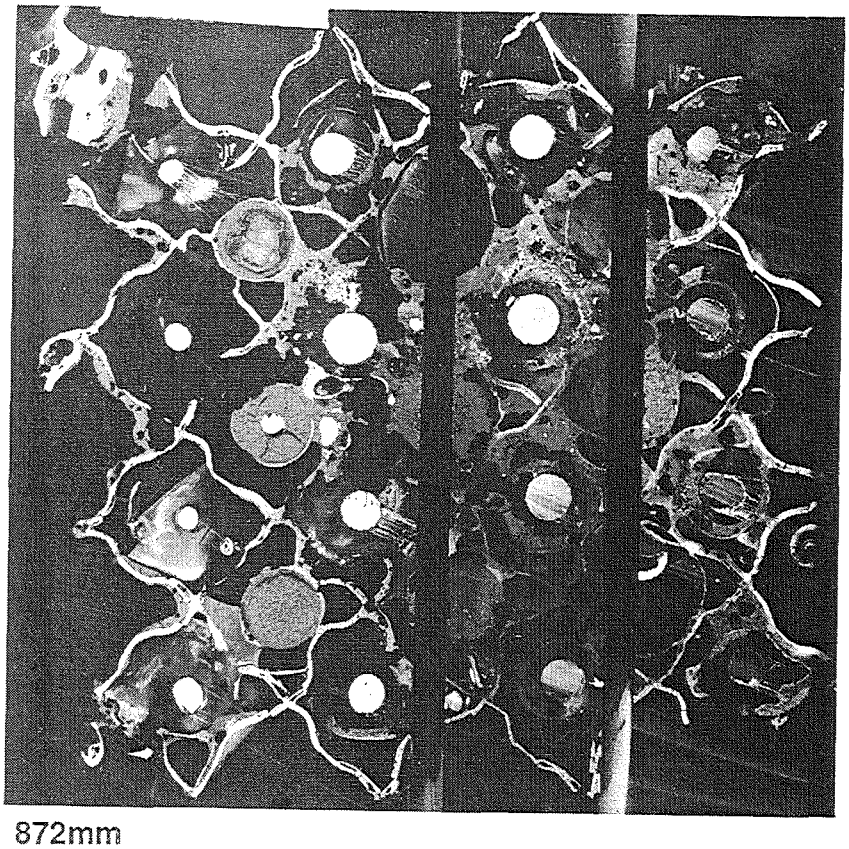

CORA-30

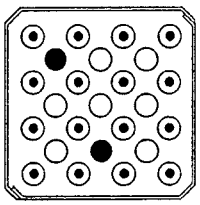

872mm

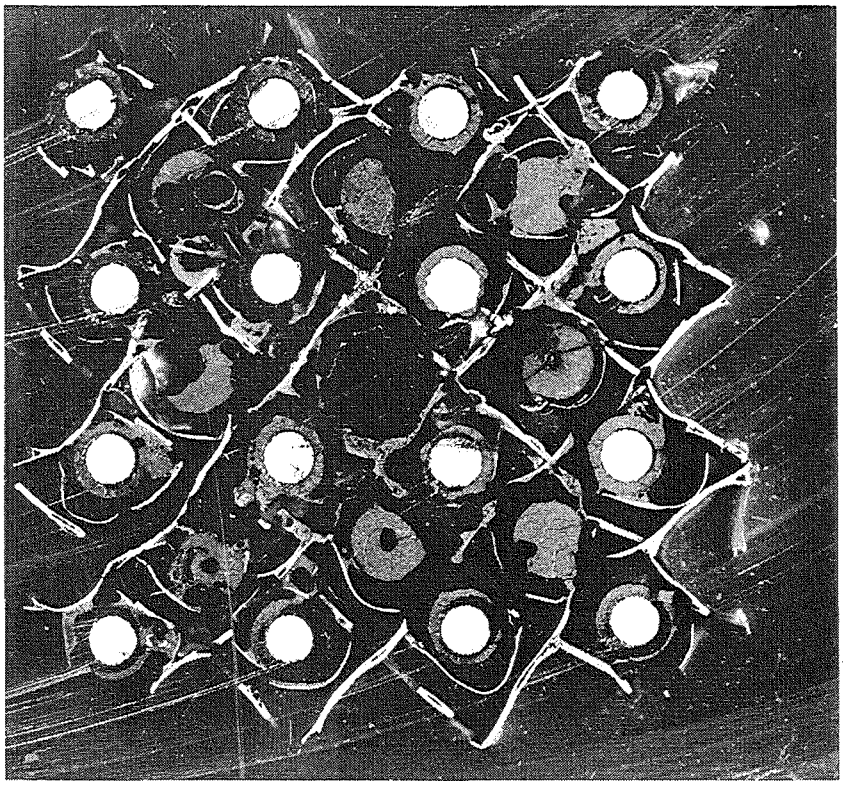

CORA-5

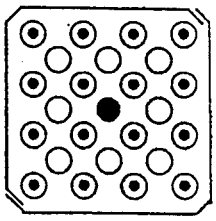

853mm

Fig. 100: Comparison of horizontal cross sections CORA-30/ CORA-5 (872, 853 mm)

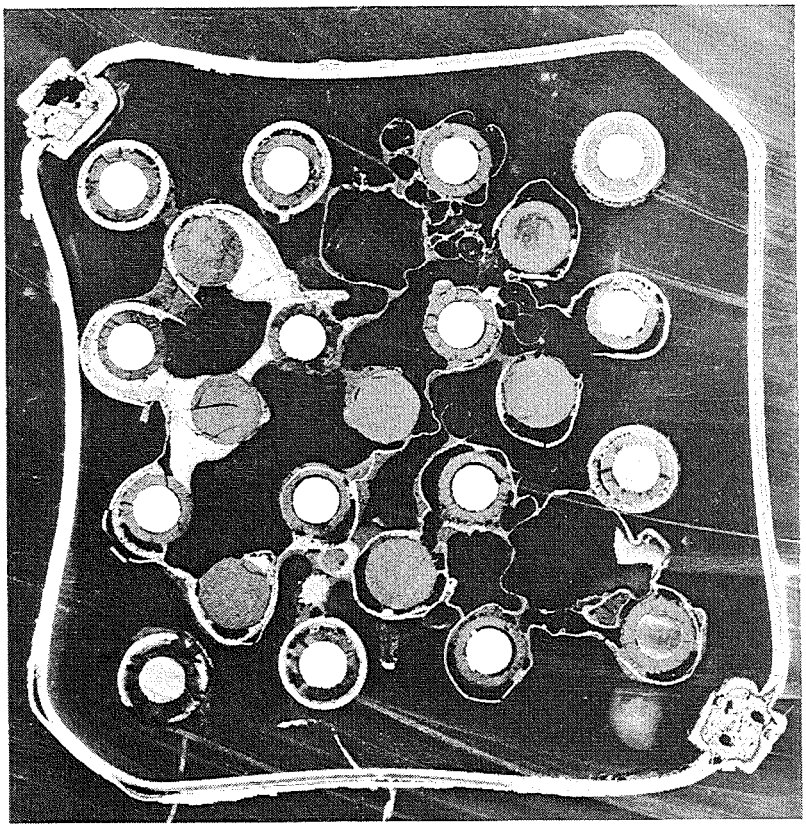

650mm

CORA-30

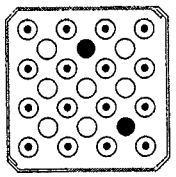

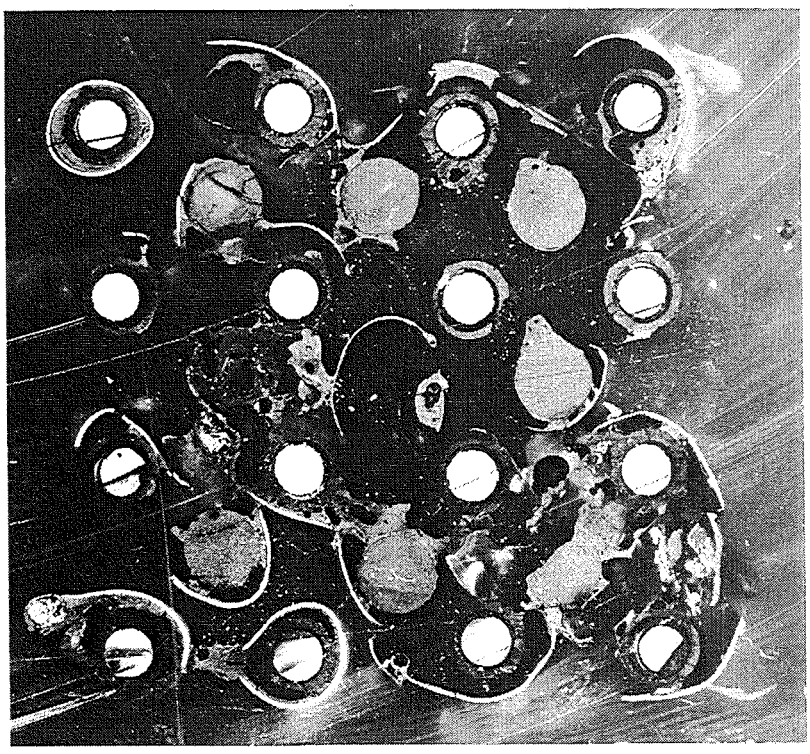

663mm

CORA-5

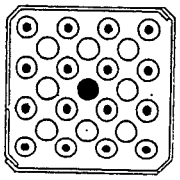

Fig. 101: Comparison of horizontal cross sections CORA-30/ CORA-5 (650, 663 mm)

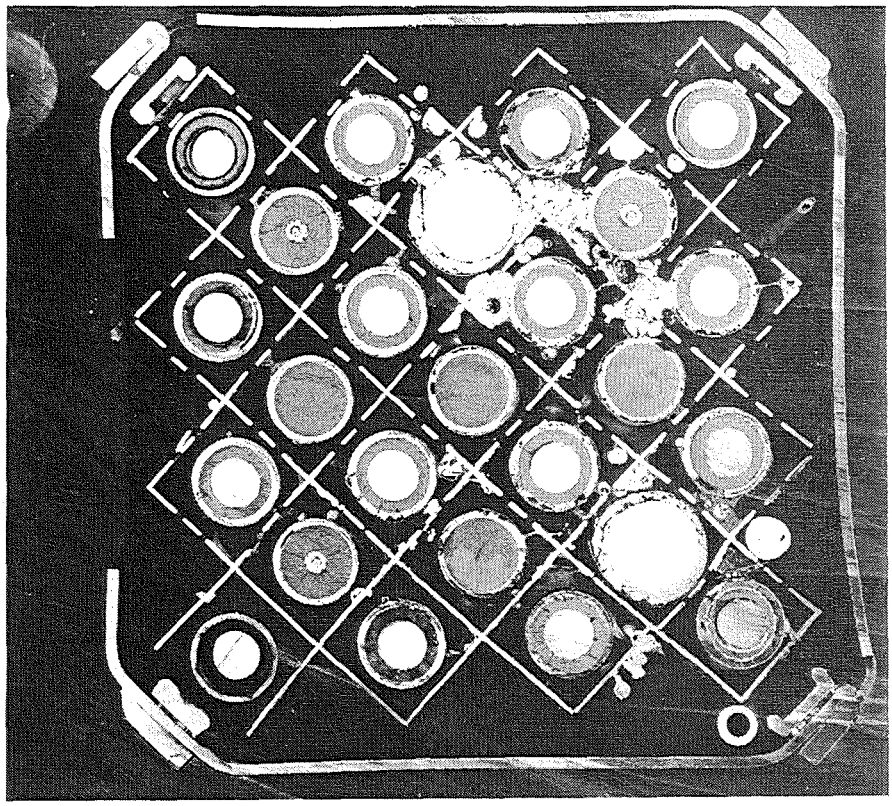

478mm

CORA-30

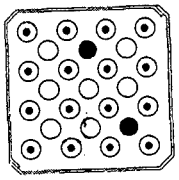

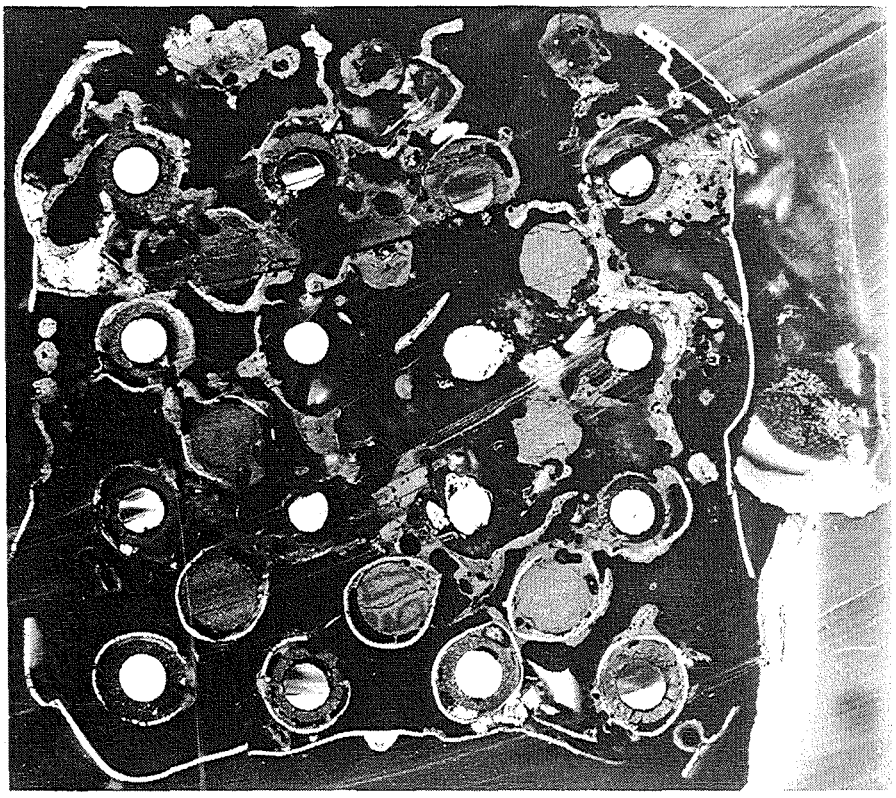

478mm

CORA-5

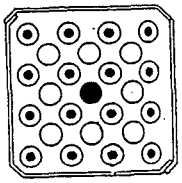

Fig. 102: Comparison of horizontal cross sections CORA-30/ CORA-5 (478 mm)

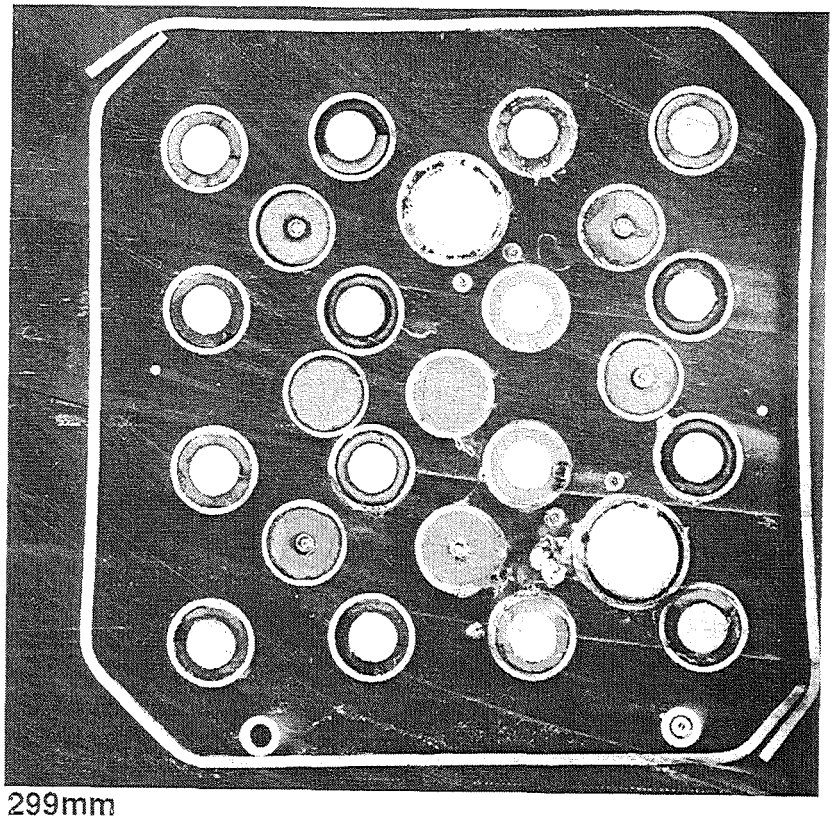

299mm

CORA-30

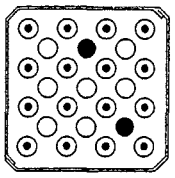

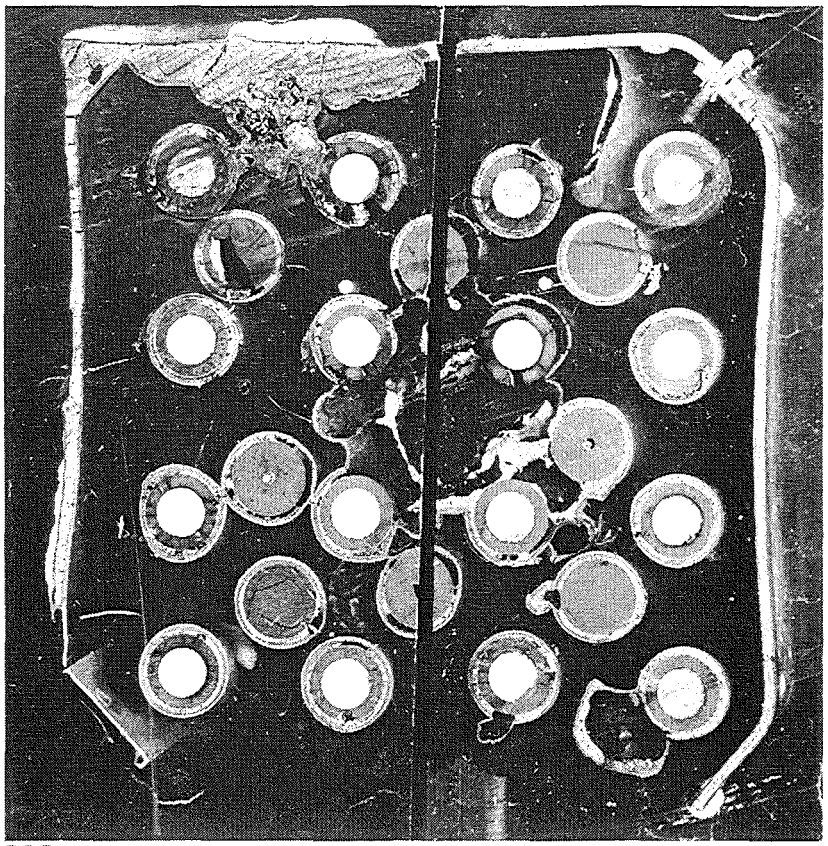

290mm

CORA-5

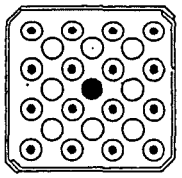

Fig. 103: Comparison of horizontal cross sections CORA-30/ CORA-5 (299, 290 mm)

Appendix A

Test data of the initial heating phase (3000 - 7000s)

Figures A1 - A24

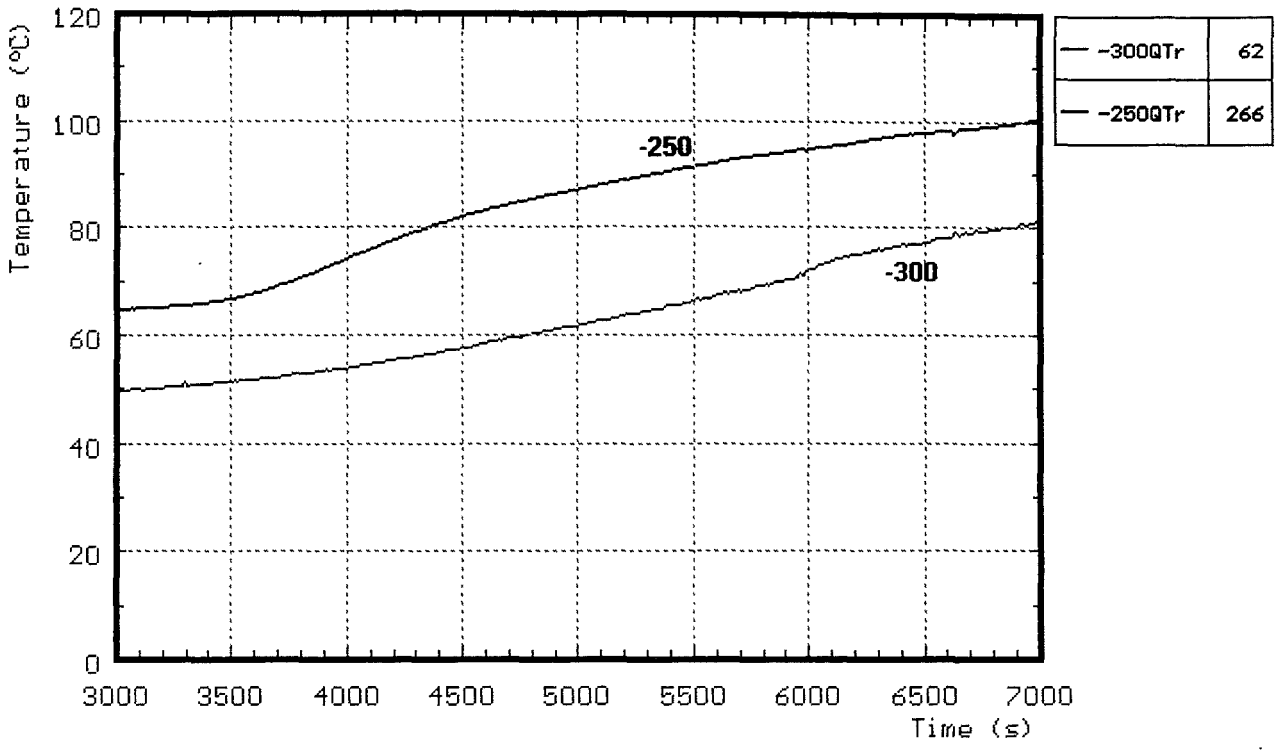

Fig. A1: CORA-30; Water temperature in the quench cylinder; initial heating phase

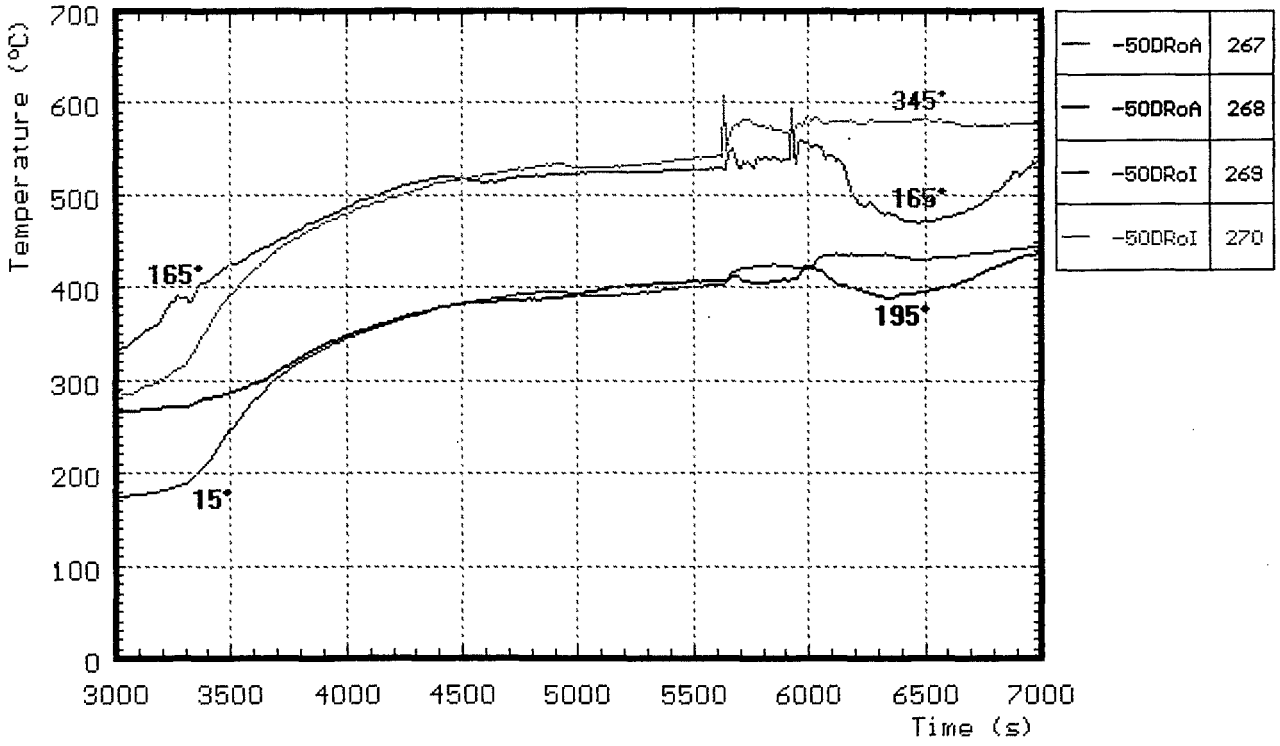

Fig. A2: CORA-30; Temperature in and on steam tube at -50mm elevation; initial heating phase

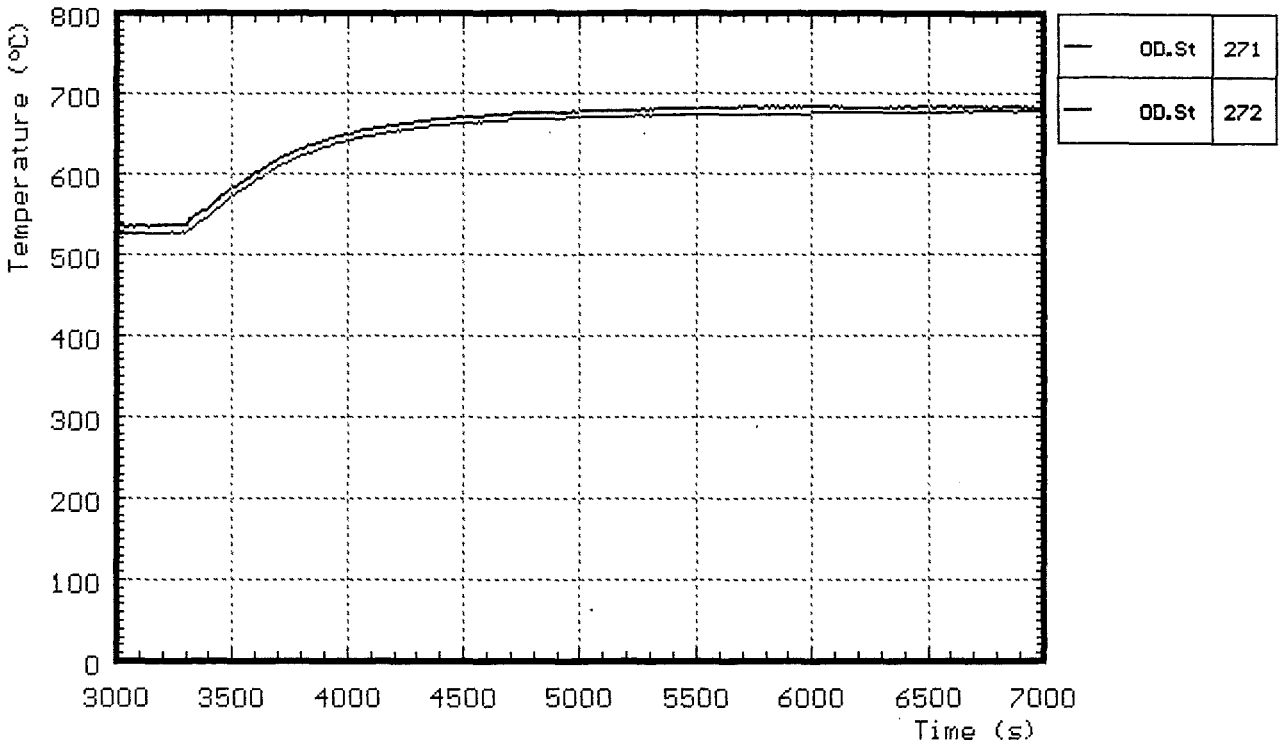

Fig. A3: CORA-30; Temperatures at the steam inlet; initial heating phase

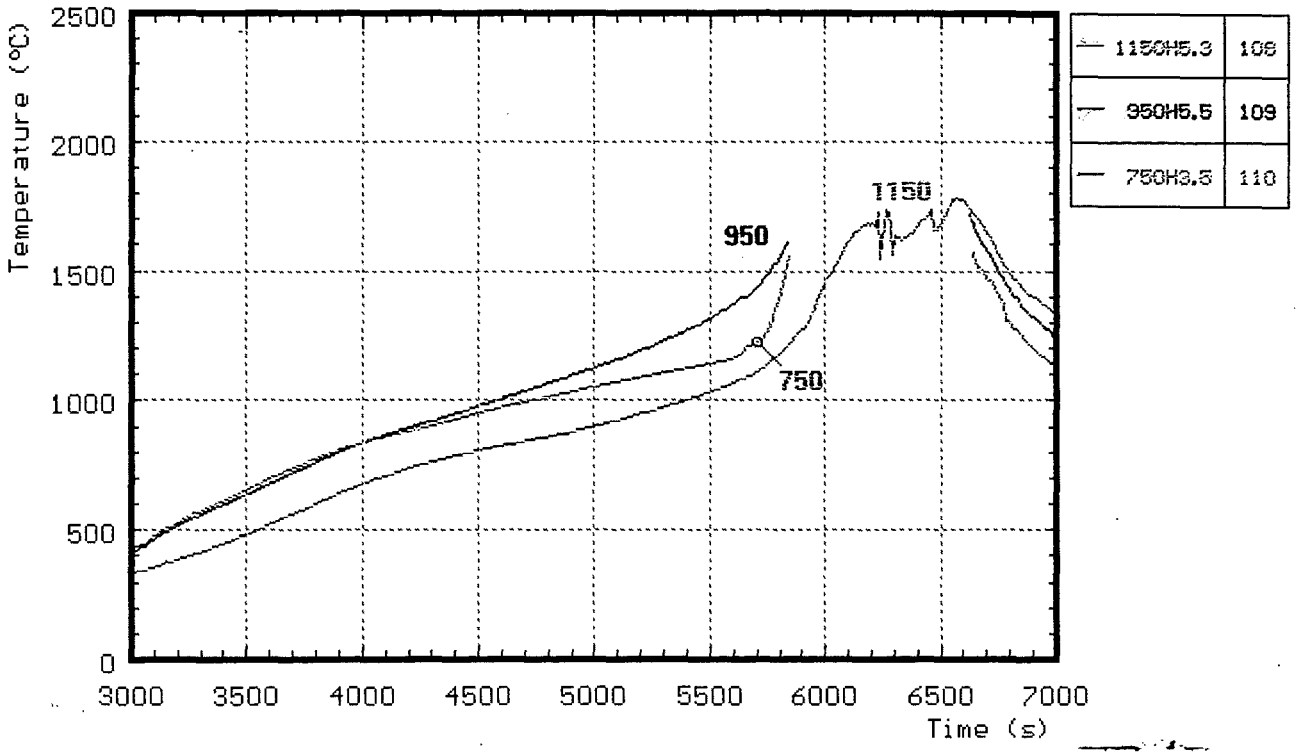

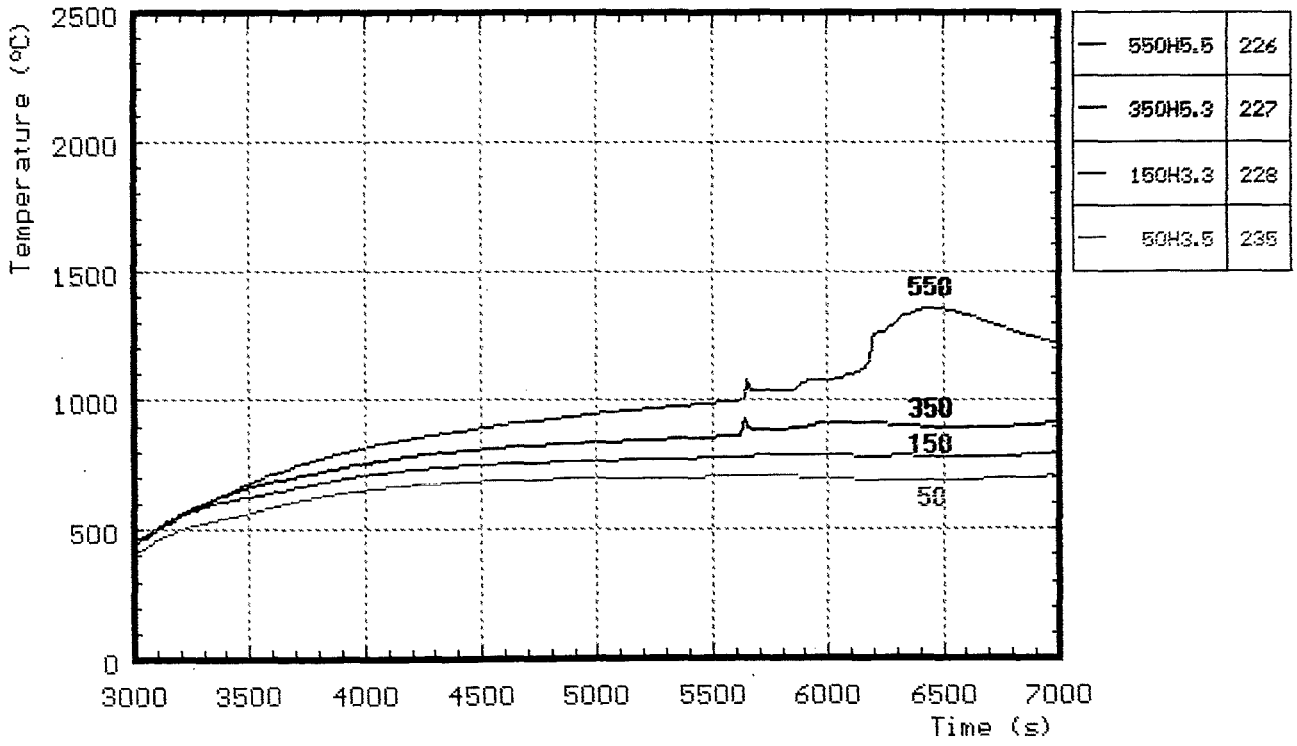

Fig. A4: CORA-30; Temperatures of heated rods; initial heating phase

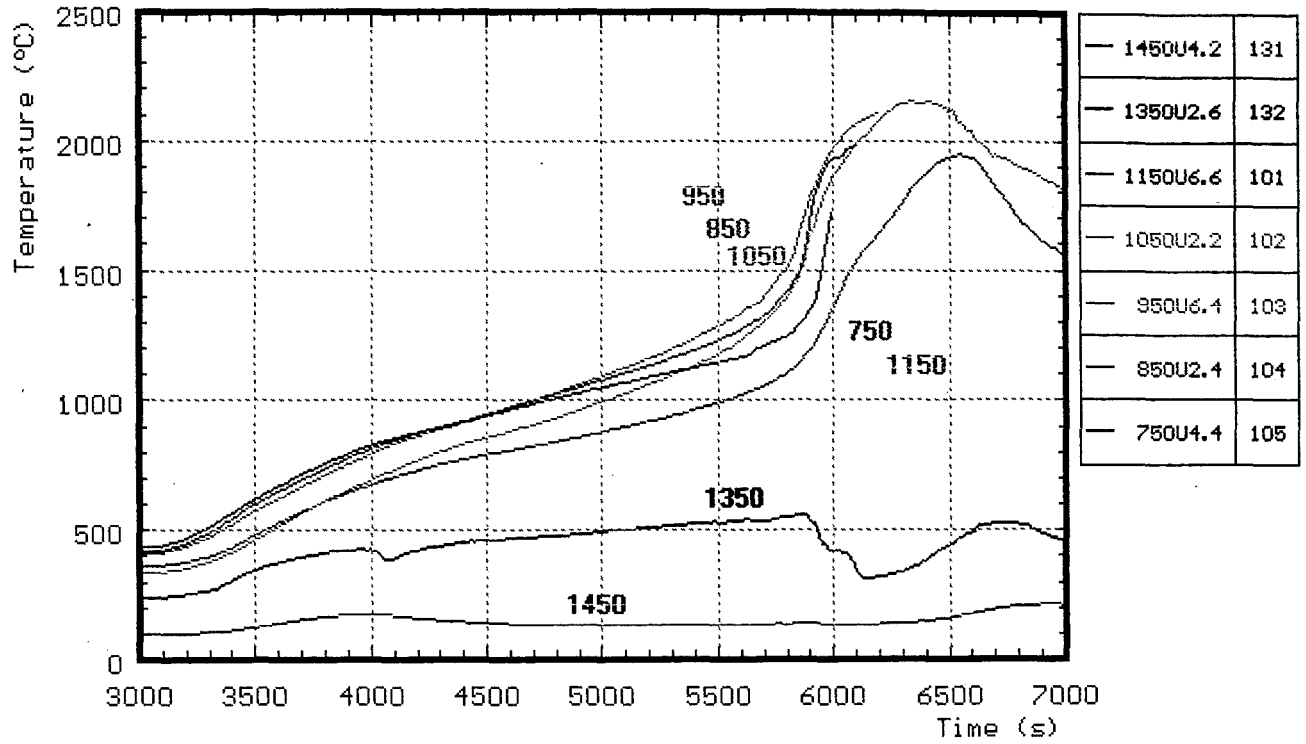

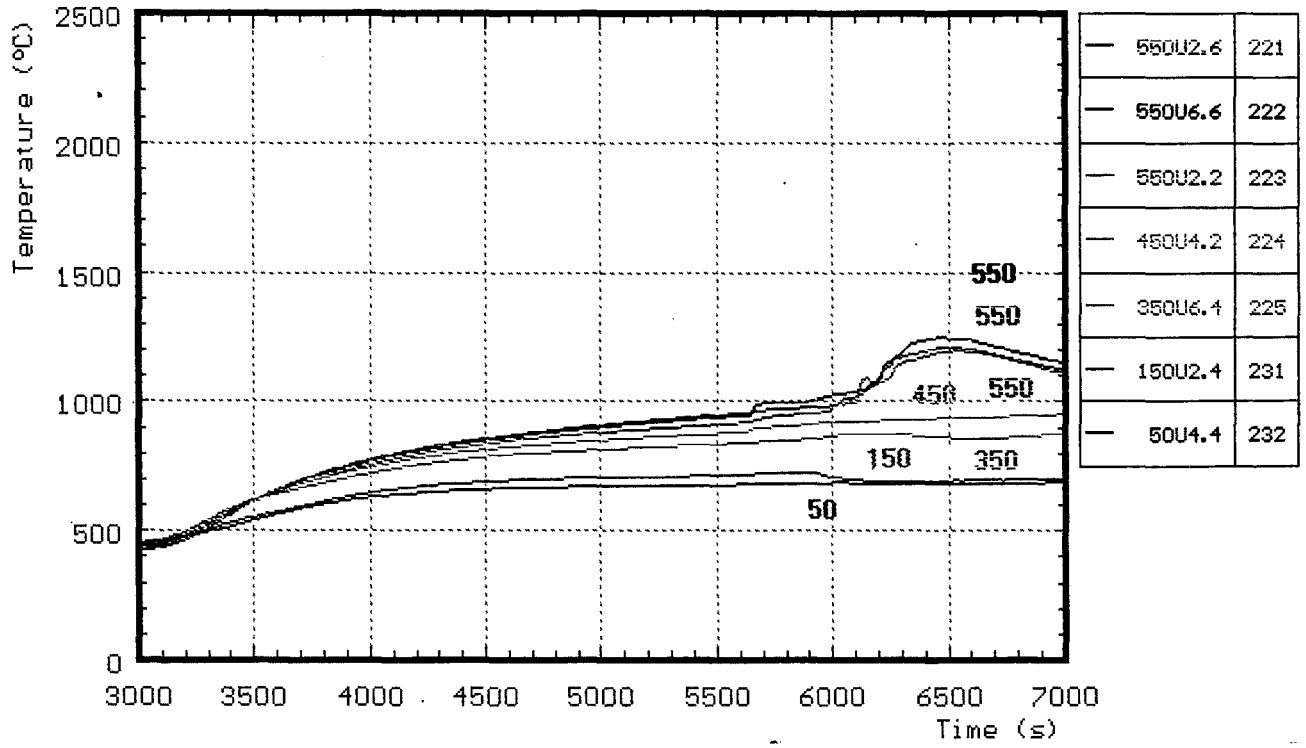

Fig. A5: CORA-30; Temperatures of unheated rods; initial heating phase

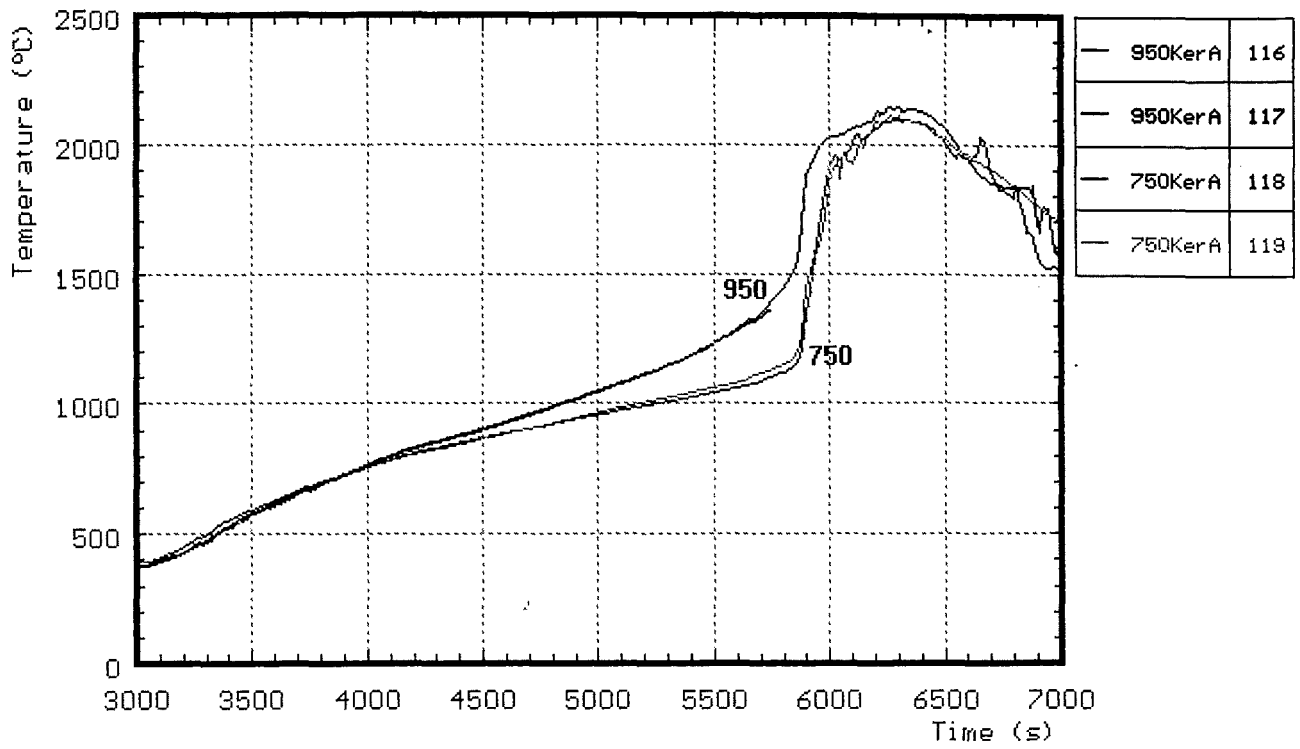

Fig. A6: CORA-30; Temperatures between bundle and shroud measured with ceramic protected TCs; initial heating phase

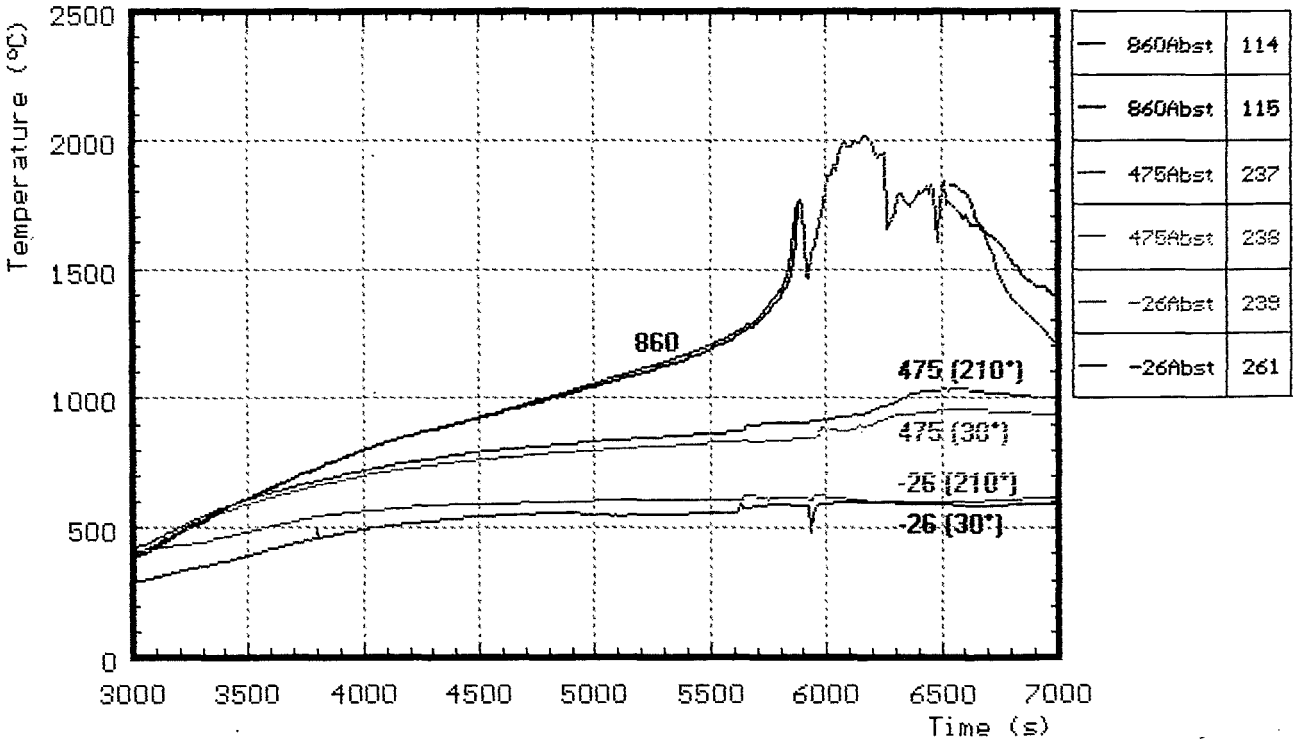

Fig. A7: CORA-30; Temperatures of the spacers; initial heating phase

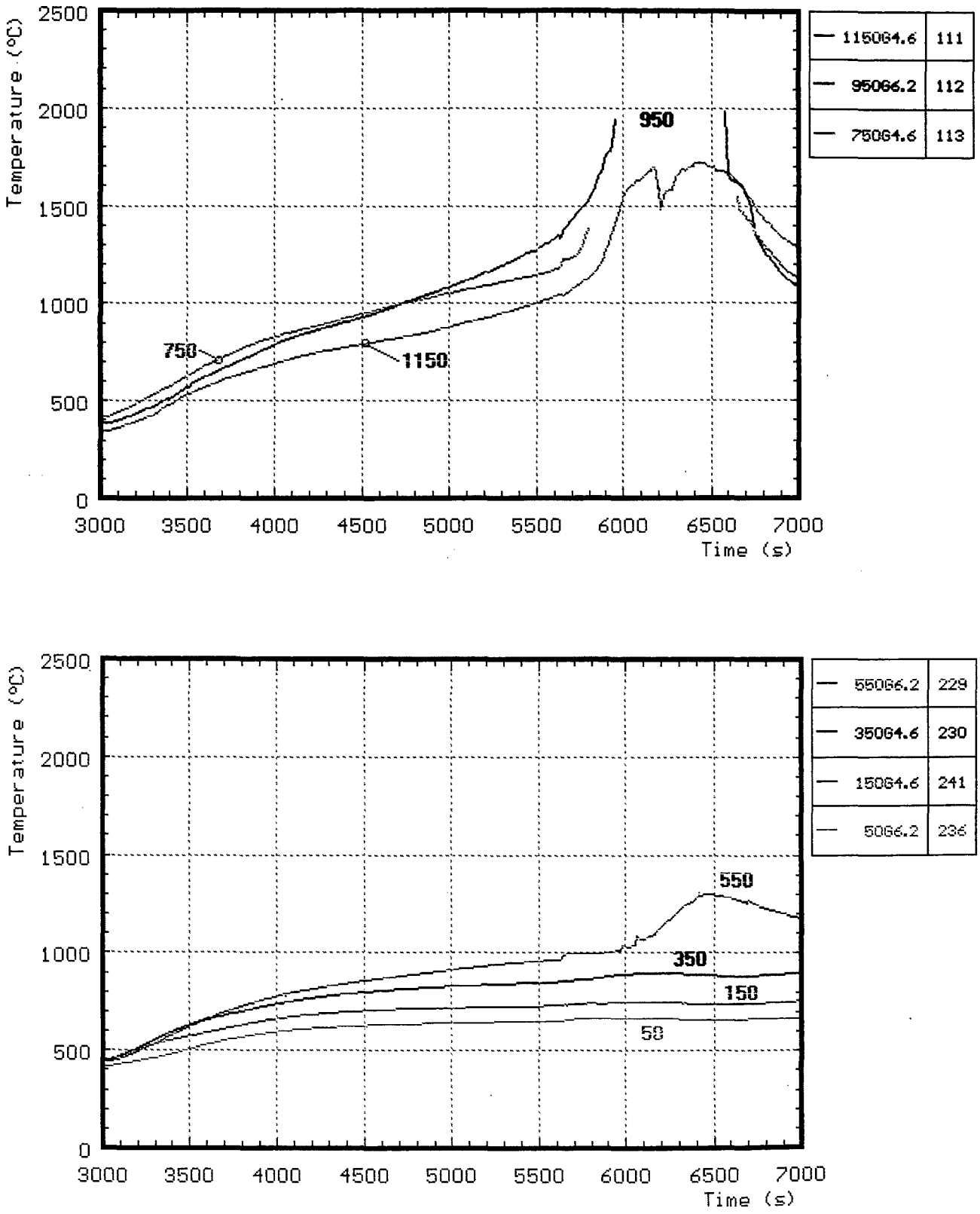

Fig. A8: CORA-30; Temperatures of the guide tubes of absorber rods; initial heating phase

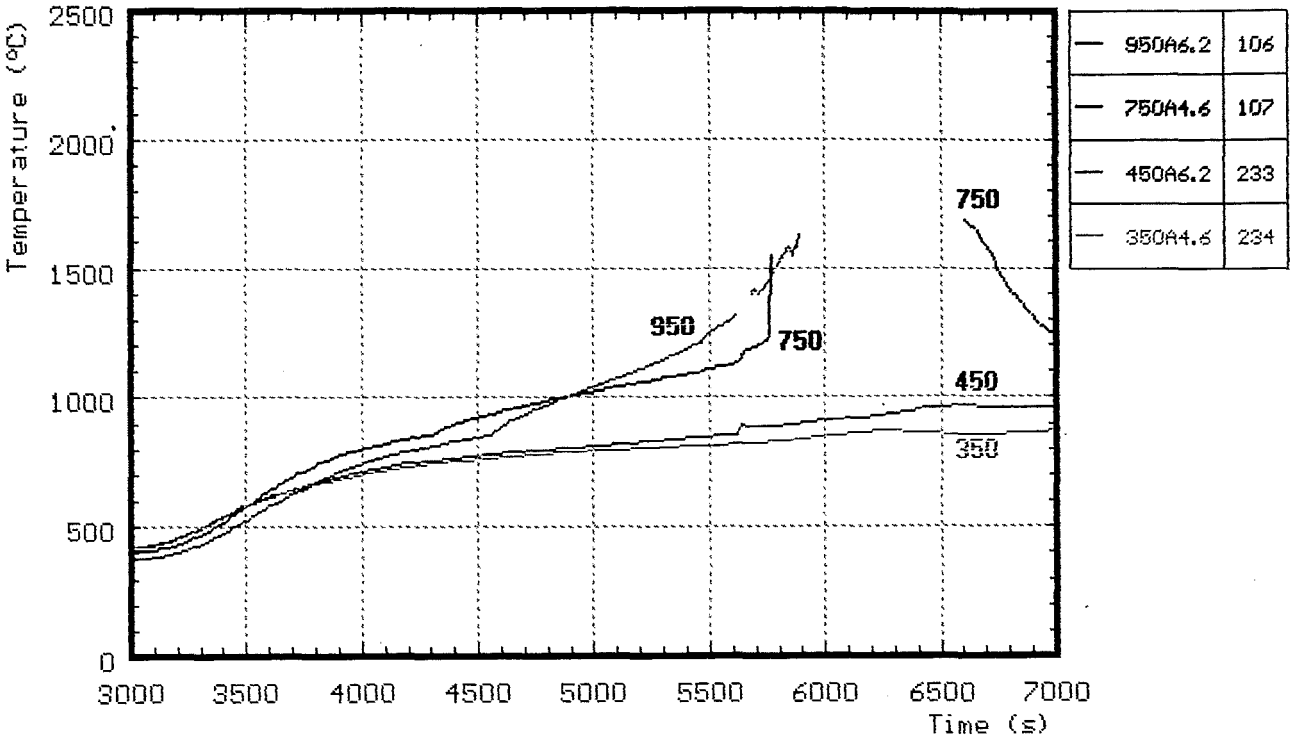

Fig. A9: CORA-30; Temperatures in the absorber; initial heating phase

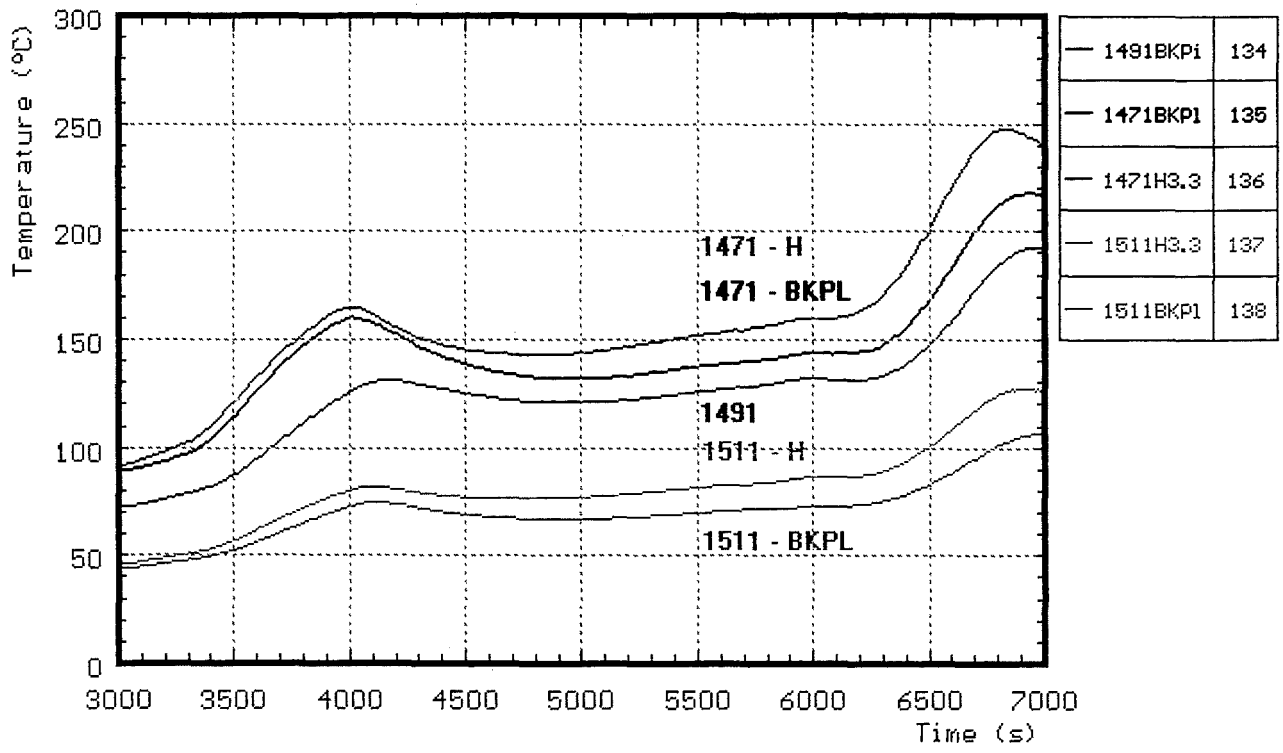

Fig. A10: CORA-30; Temperatures at the bundle head plate; initial heating phase

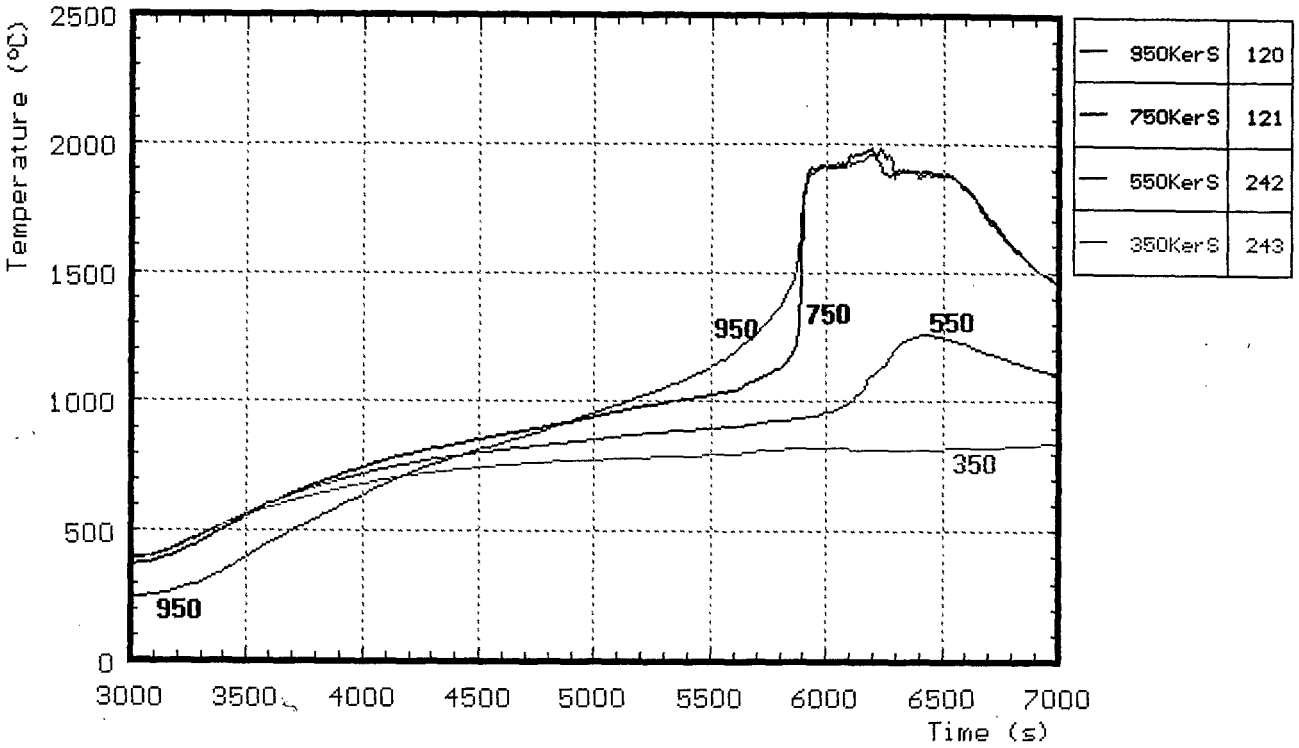

Fig. A11: CORA-30; Temperatures of inner side of shroud measured with ceramic protected TCs; initial heating phase

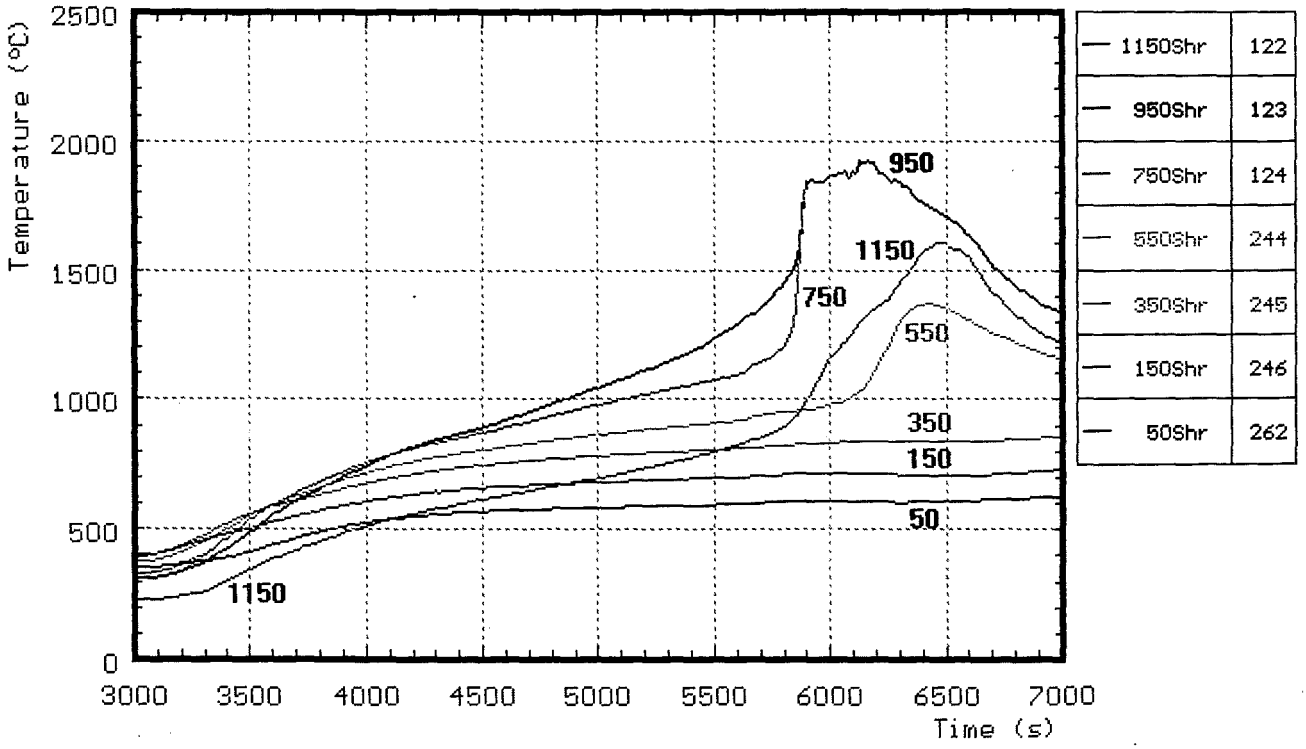

Fig. A12: CORA-30; Temperatures of outer side of shroud; initial heating phase

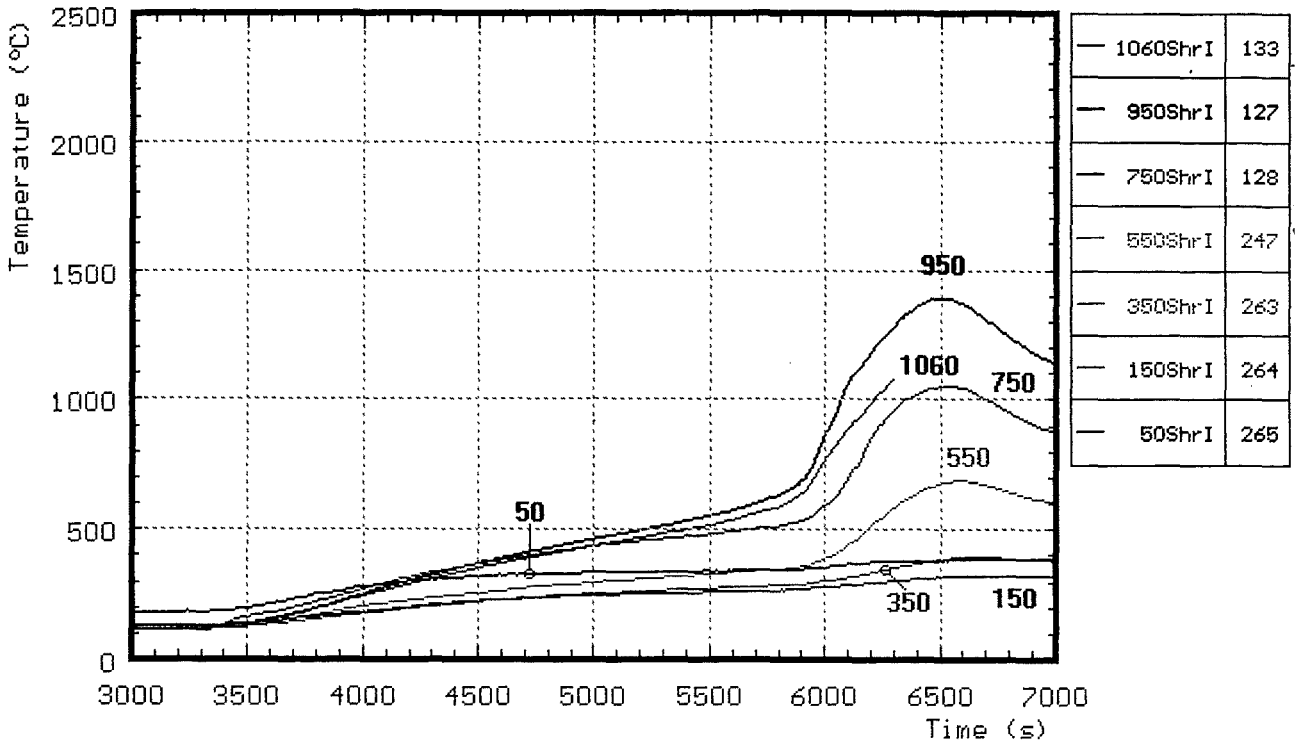

Fig. A13: CORA-30; Temperatures of the shroud insulation; initial heating phase

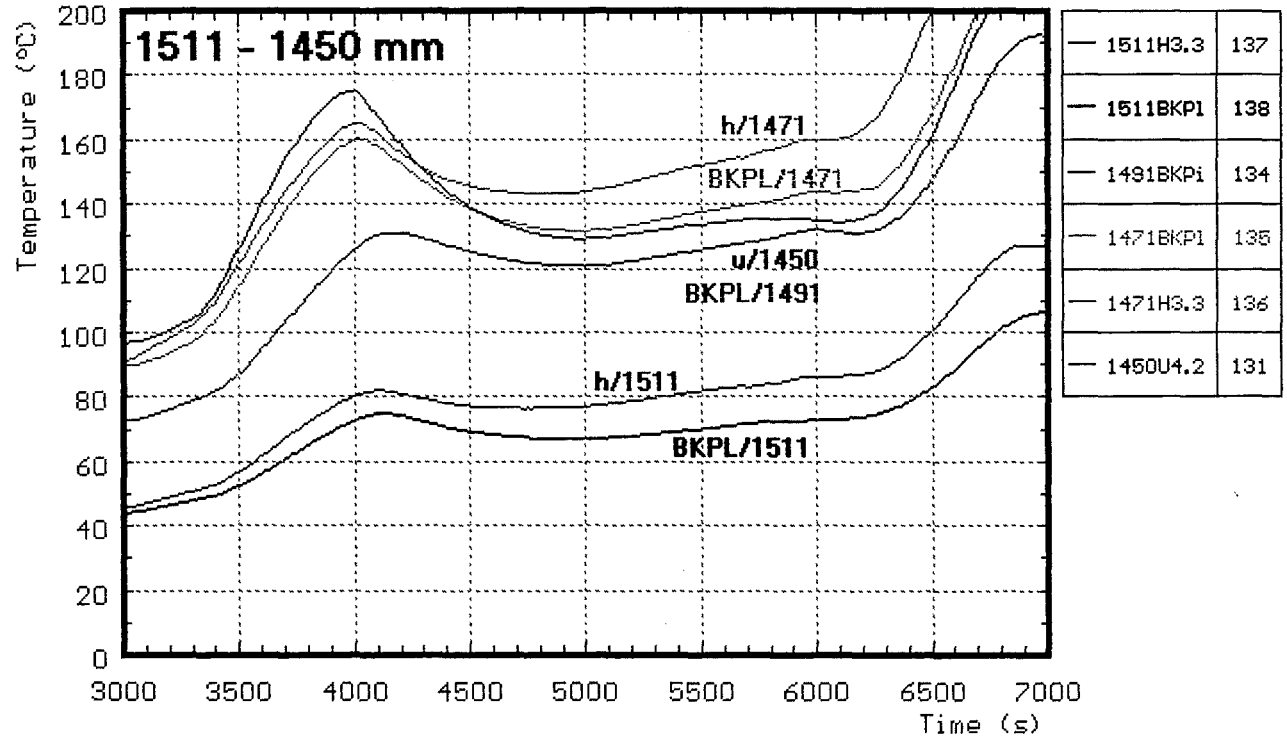

Fig. A14: CORA-30; Temperatures at elevations given; initial heating phase (1511-1450 mm)

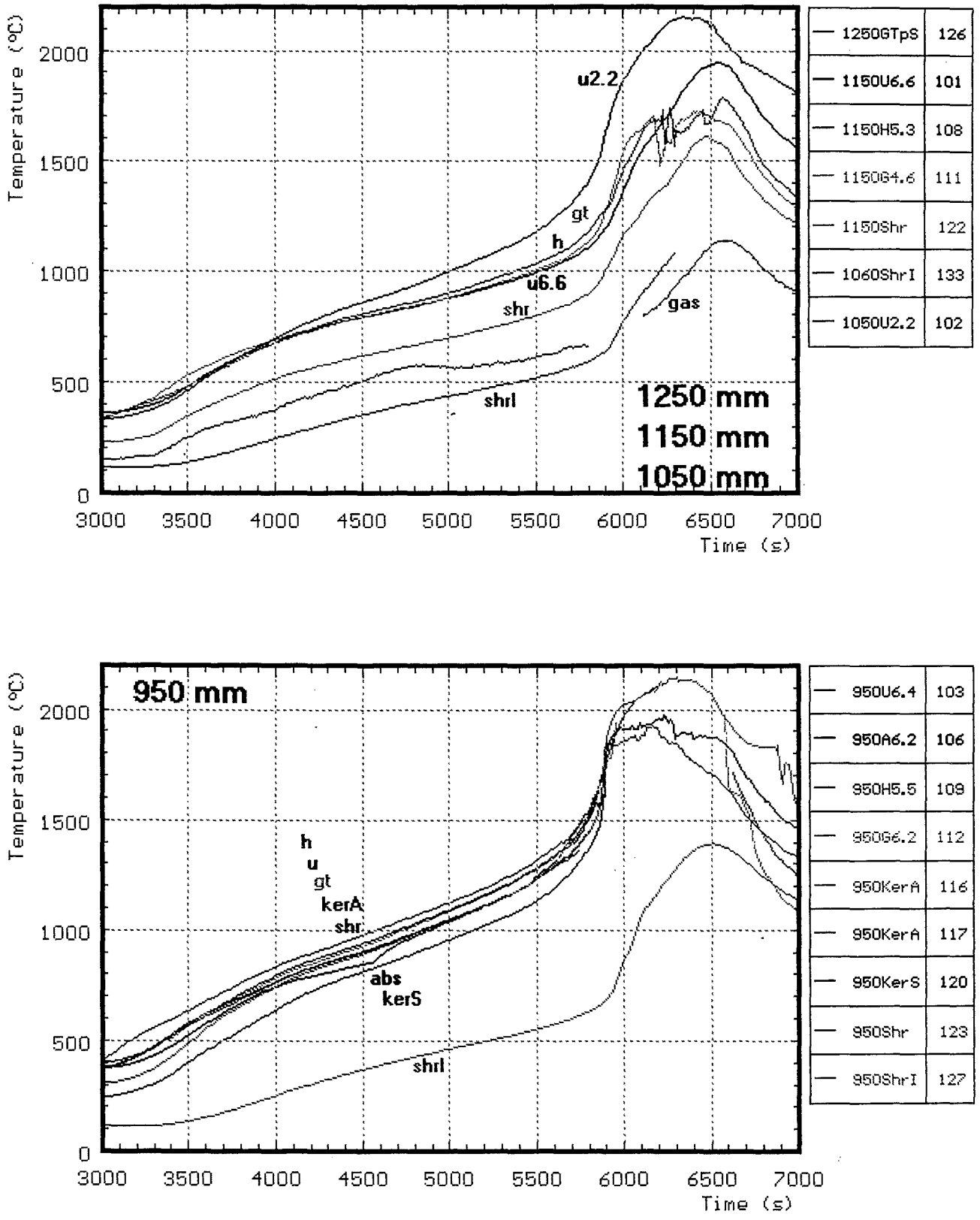

Fig. A15: CORA-30; Temperatures at elevations given; initial heating phase (1250-1050, 950 mm)

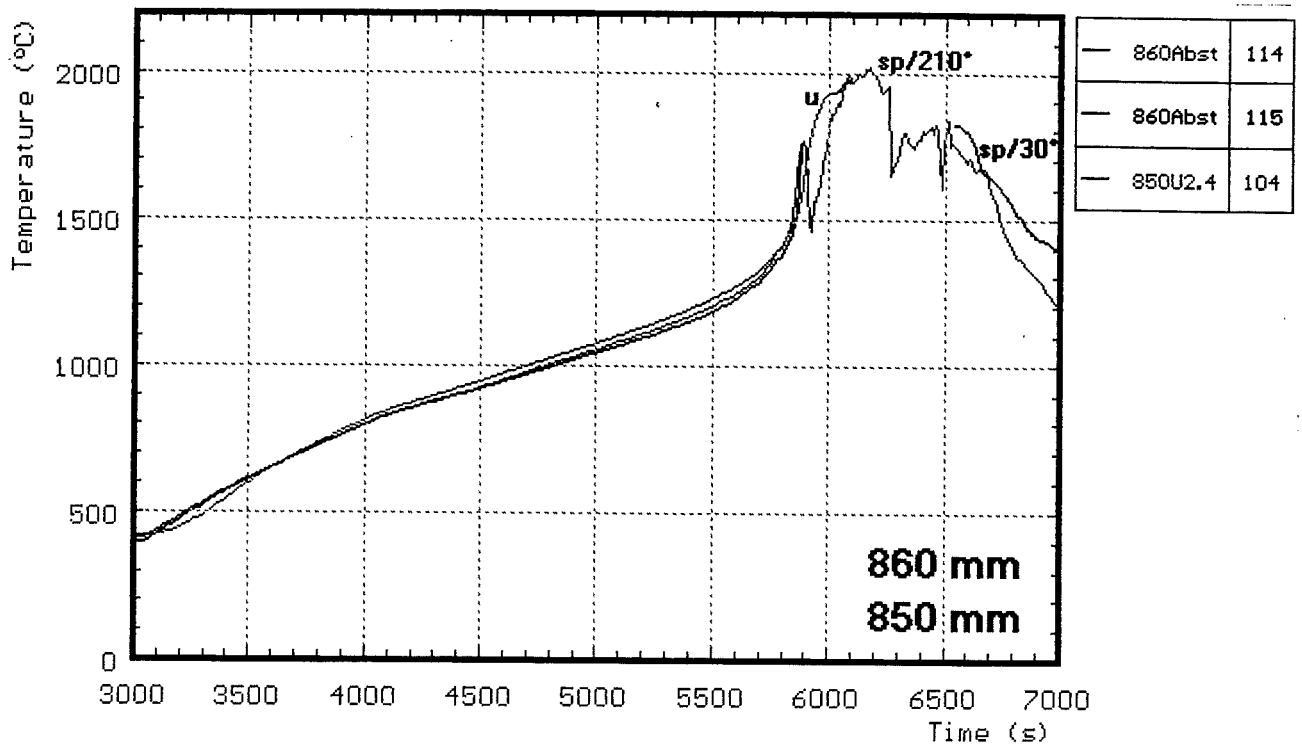

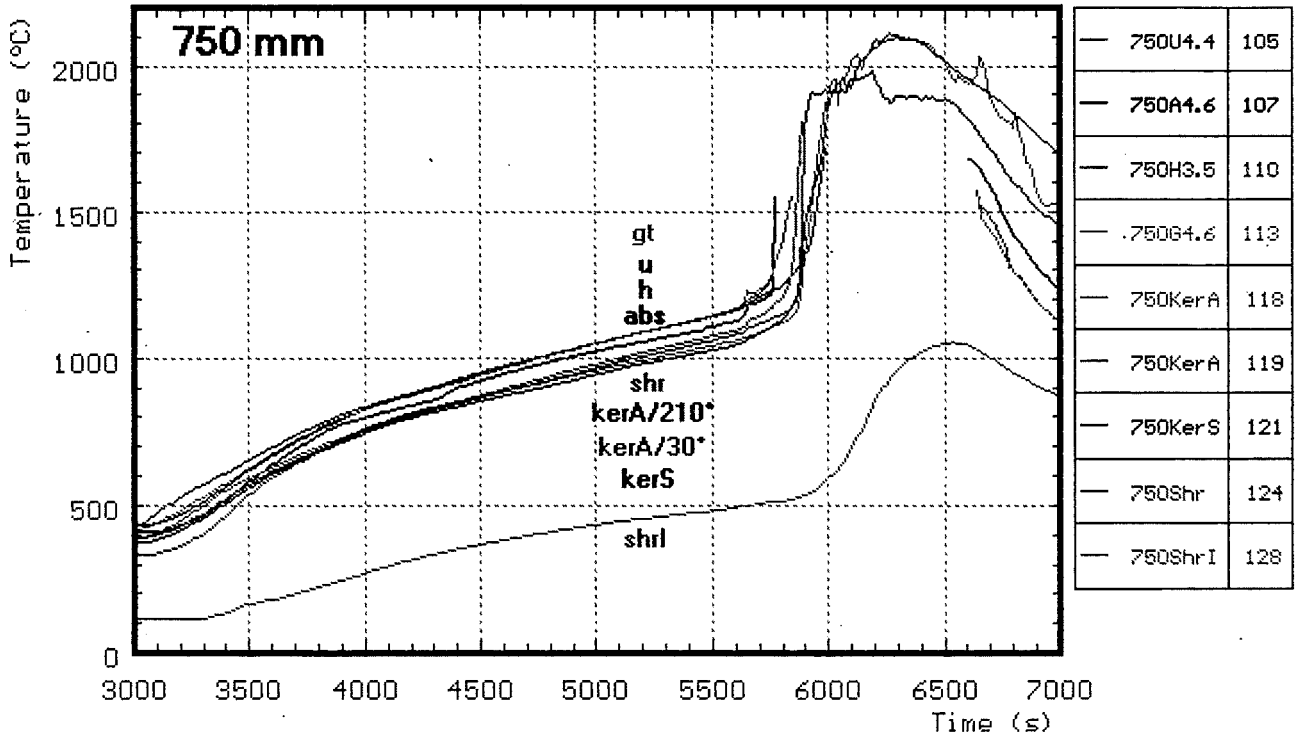

Fig. A16: CORA-30; Temperatures at elevations given; initial heating phase (860, 850, 750 mm)

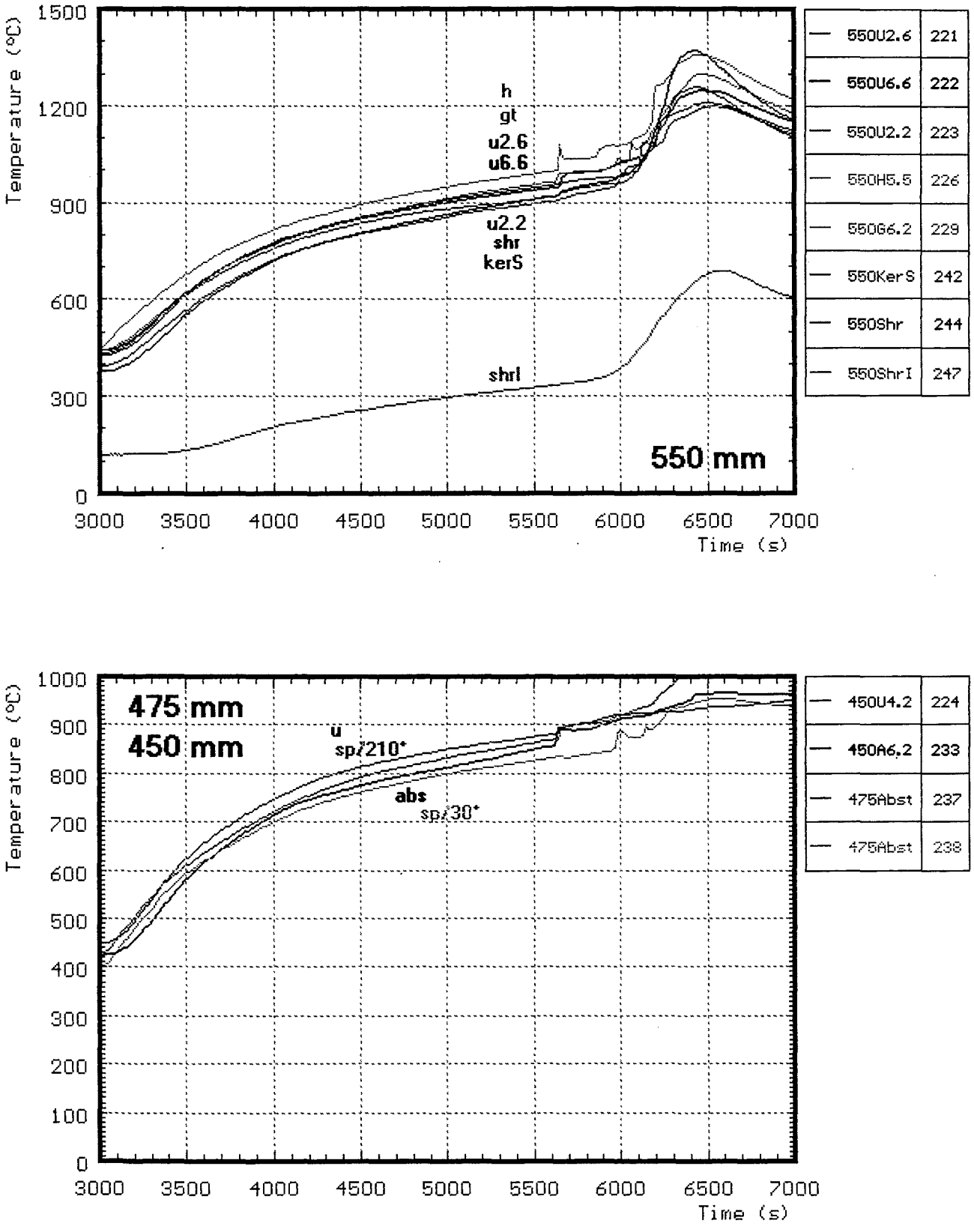

Fig. A17: CORA-30; Temperatures at elevations given; initial heating phase (550, 475, 450 mm)

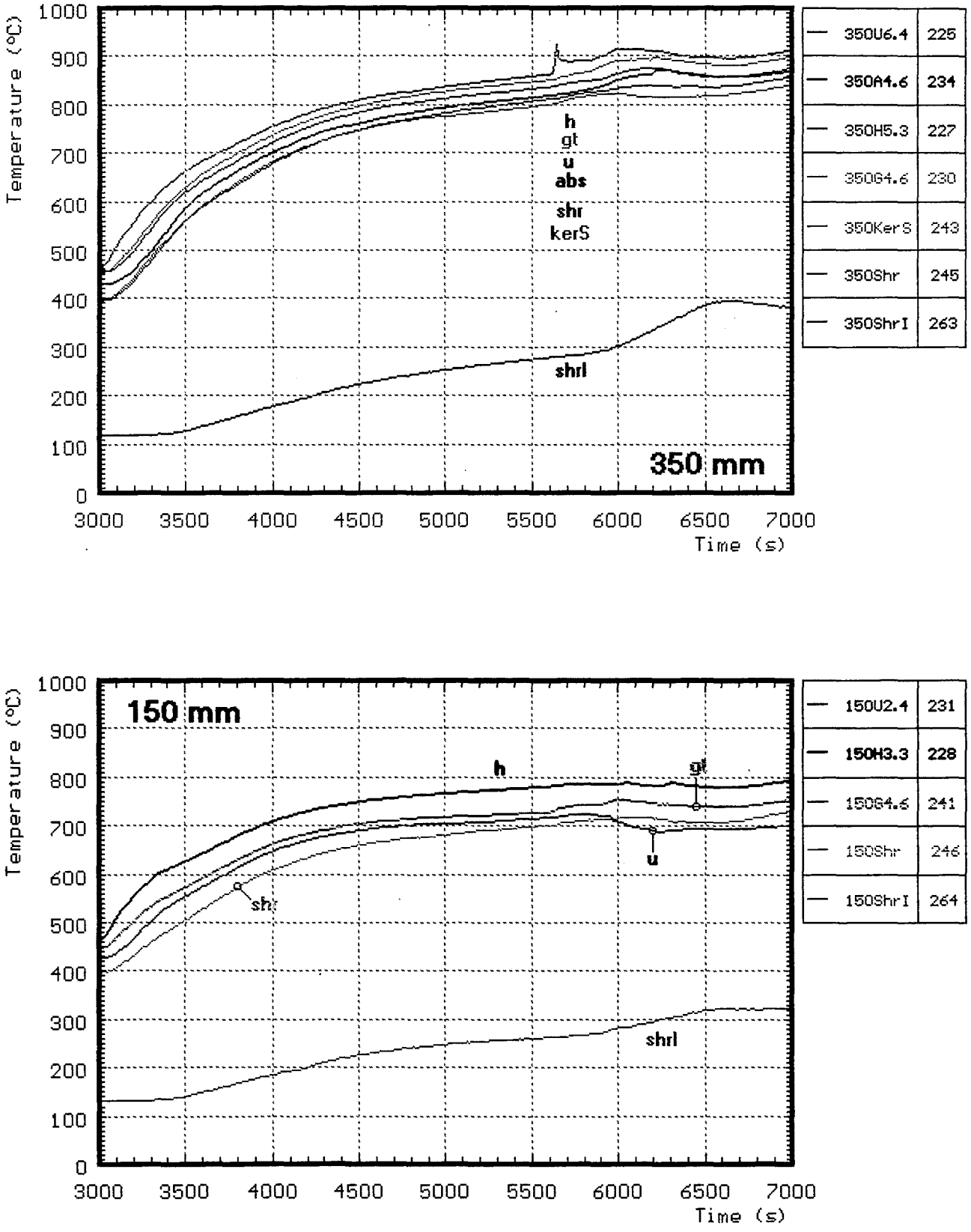

Fig. A18: CORA-30; Temperatures at elevations given; initial heating phase (350, 150 mm)

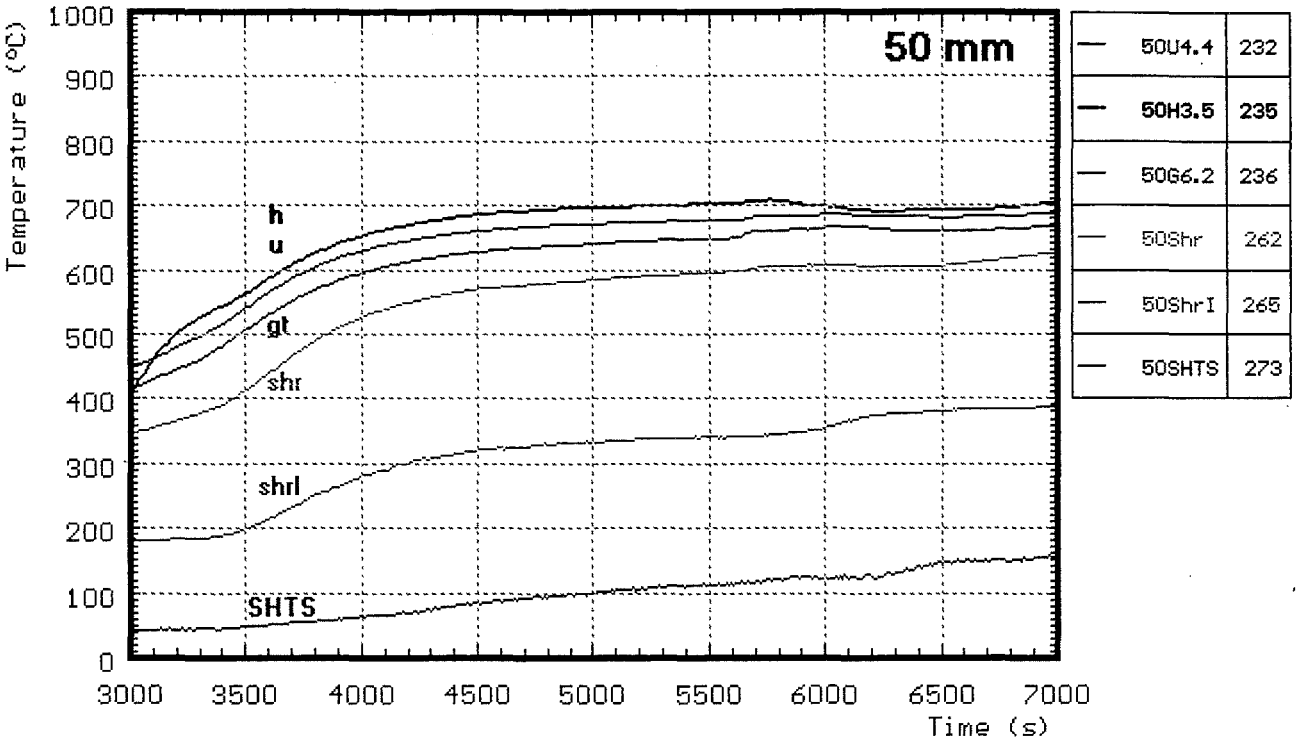

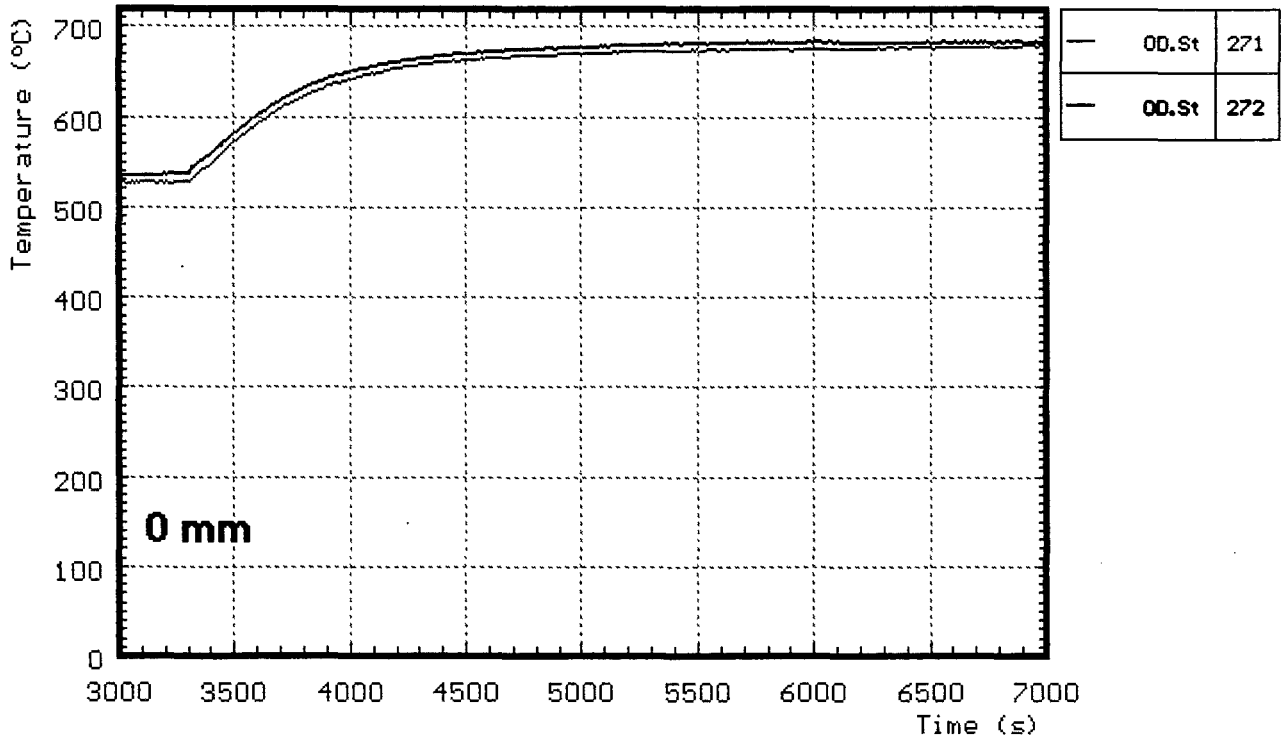

Fig. A19: CORA-30; Temperatures at elevations given; initial heating phase (50, 0 mm)

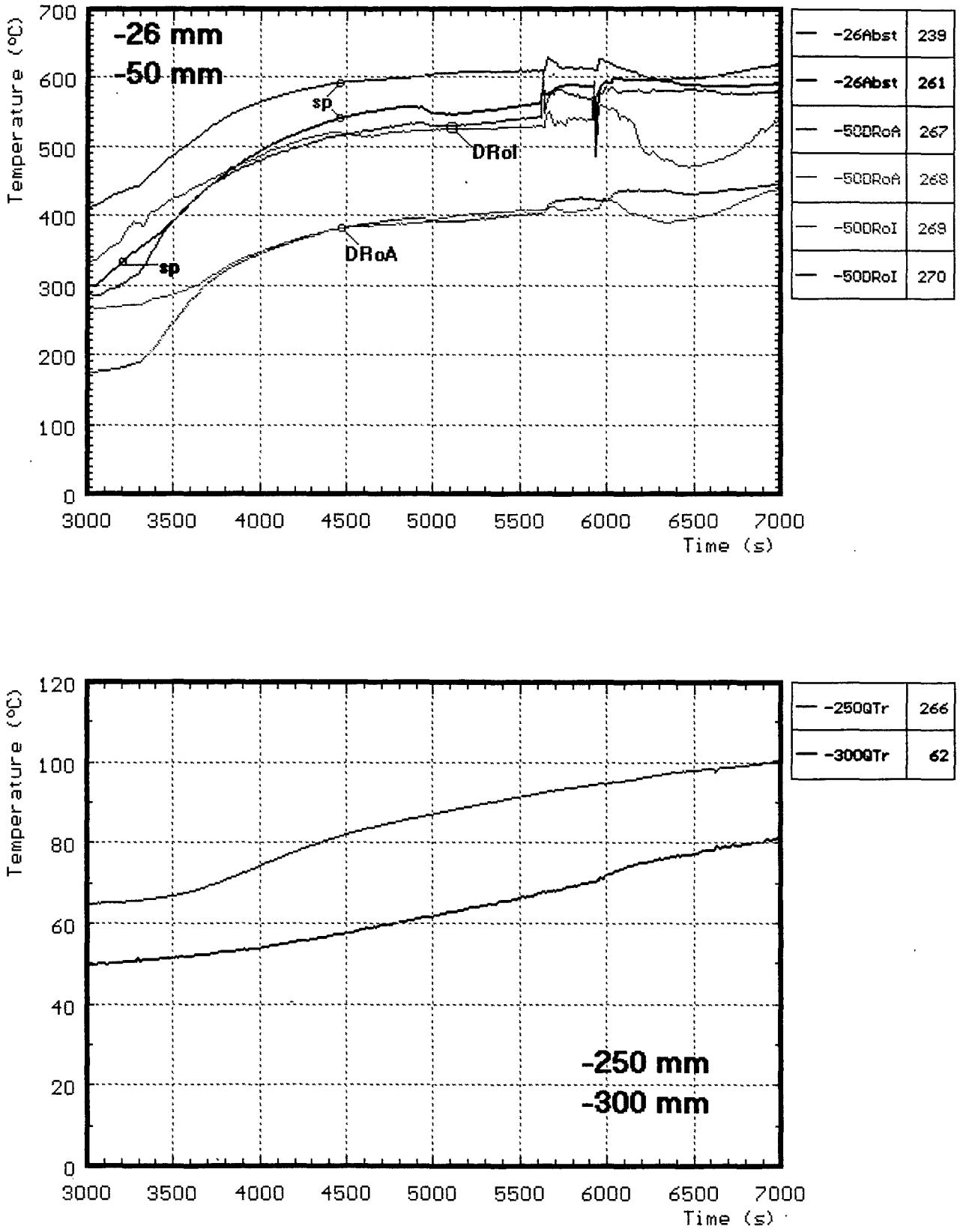

Fig. A20: CORA-30; Temperatures at elevations given; initial heating phase (-26, -50, -250, -300 mm)

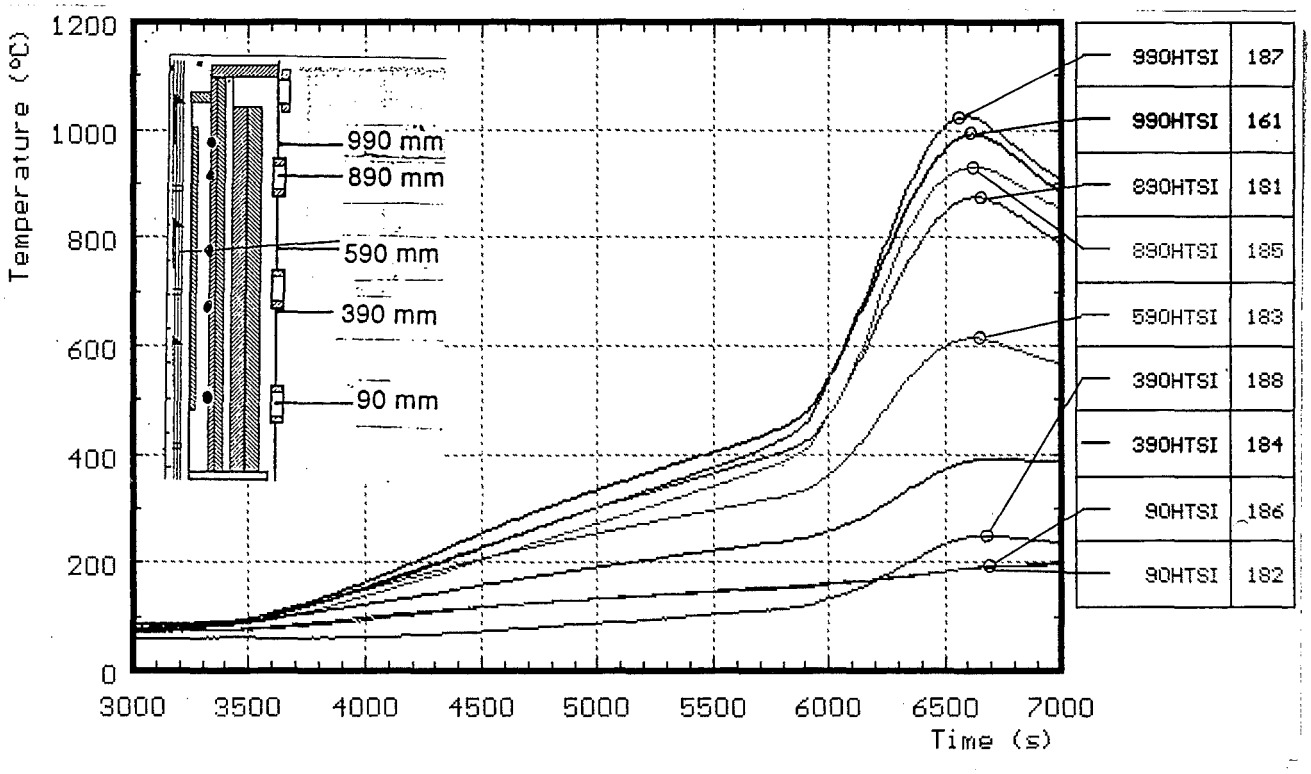

Fig. A21: CORA-30; Temperatures of HTS, Inner surface at153 mm radius; initial heating phase

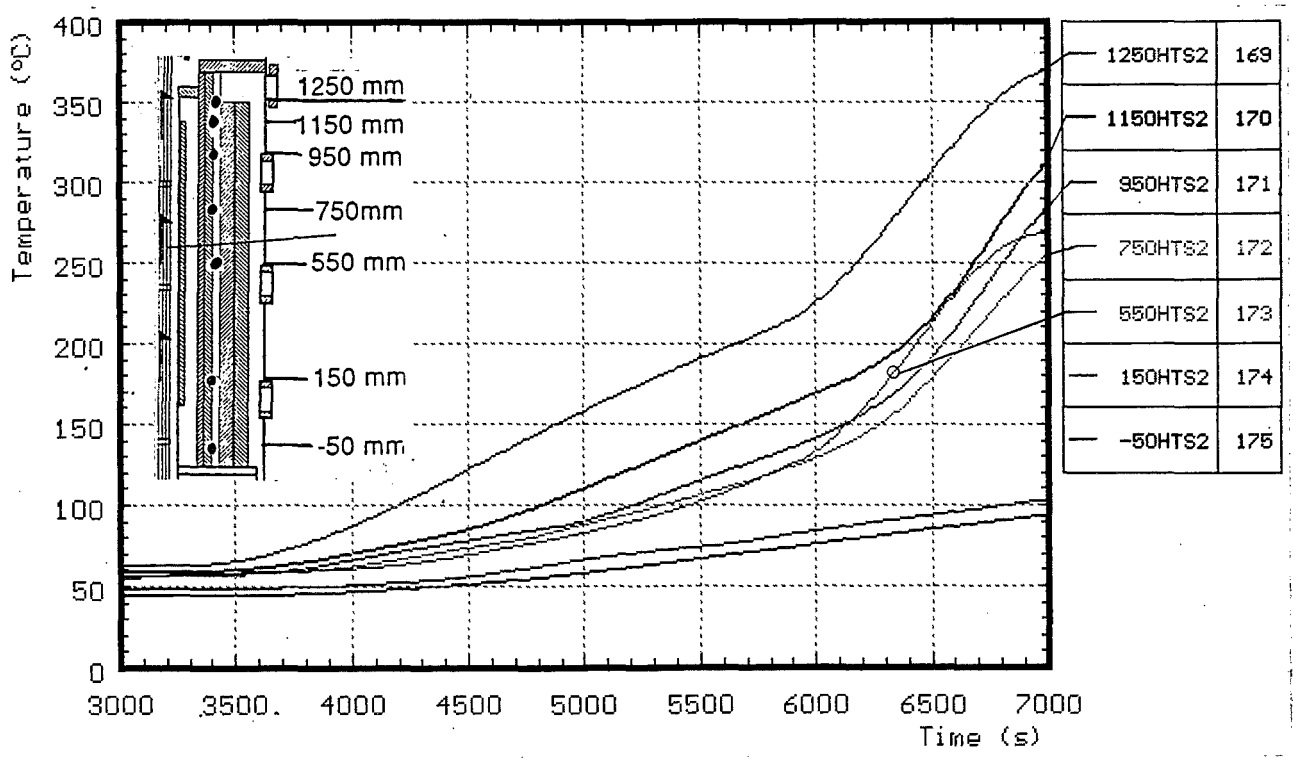

Fig. A22: CORA-30; Temperatures of HTS, Temperatures in HT shield at 192 mm radius, 345°; initial heating phase

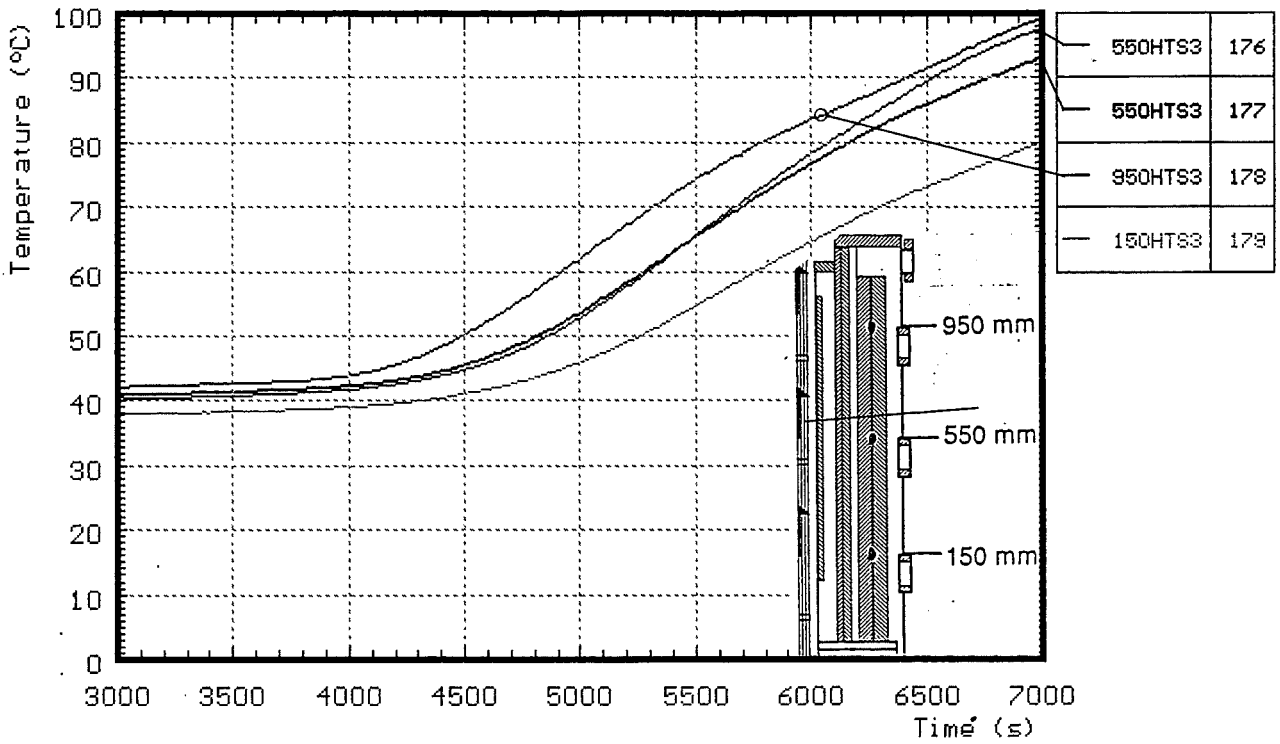

Fig. A23: CORA-30; Temperatures of HTS, Temperatures in HT shield at 255 mm radius; initial heating phase

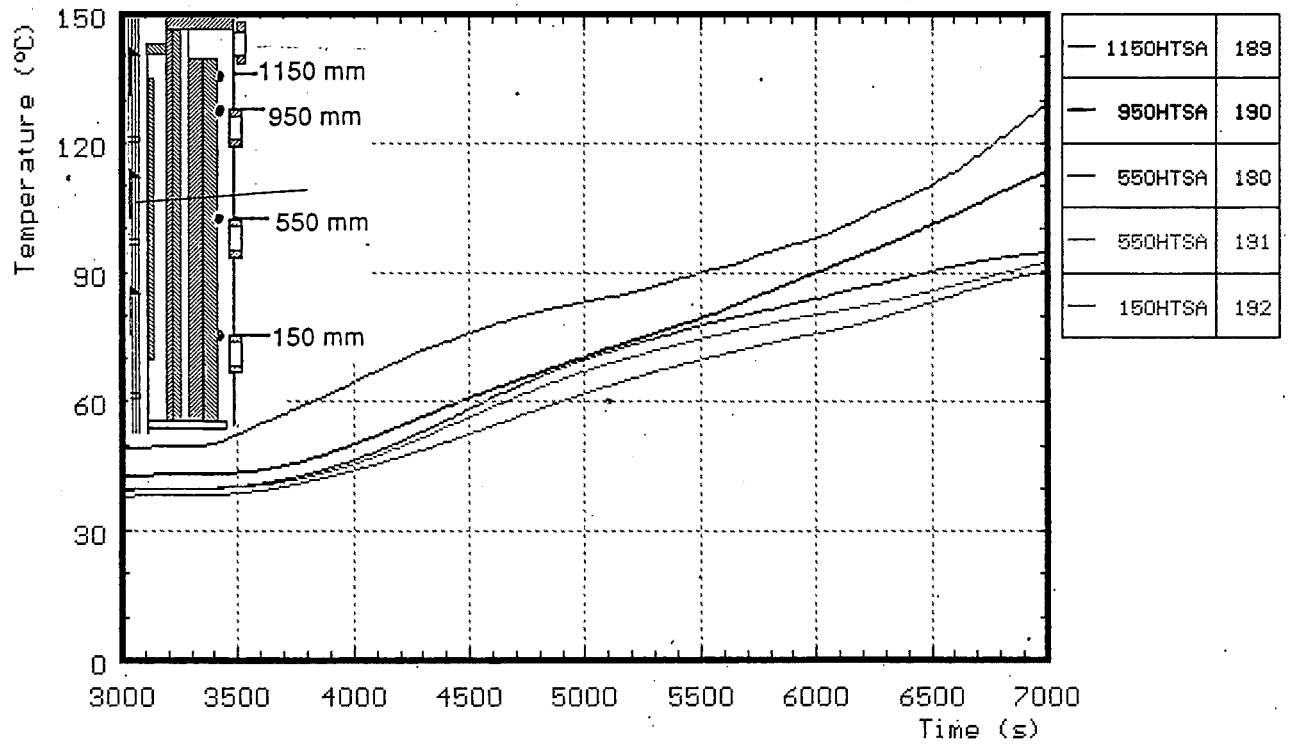

Fig. A24: CORA-30; Temperatures of HTS, Temperatures in HT shield at 293 mm radius; initial heating phase

Appendix B

Test data of the pre-heat phase (-12000 - 3000s)

Figures B1 - B22

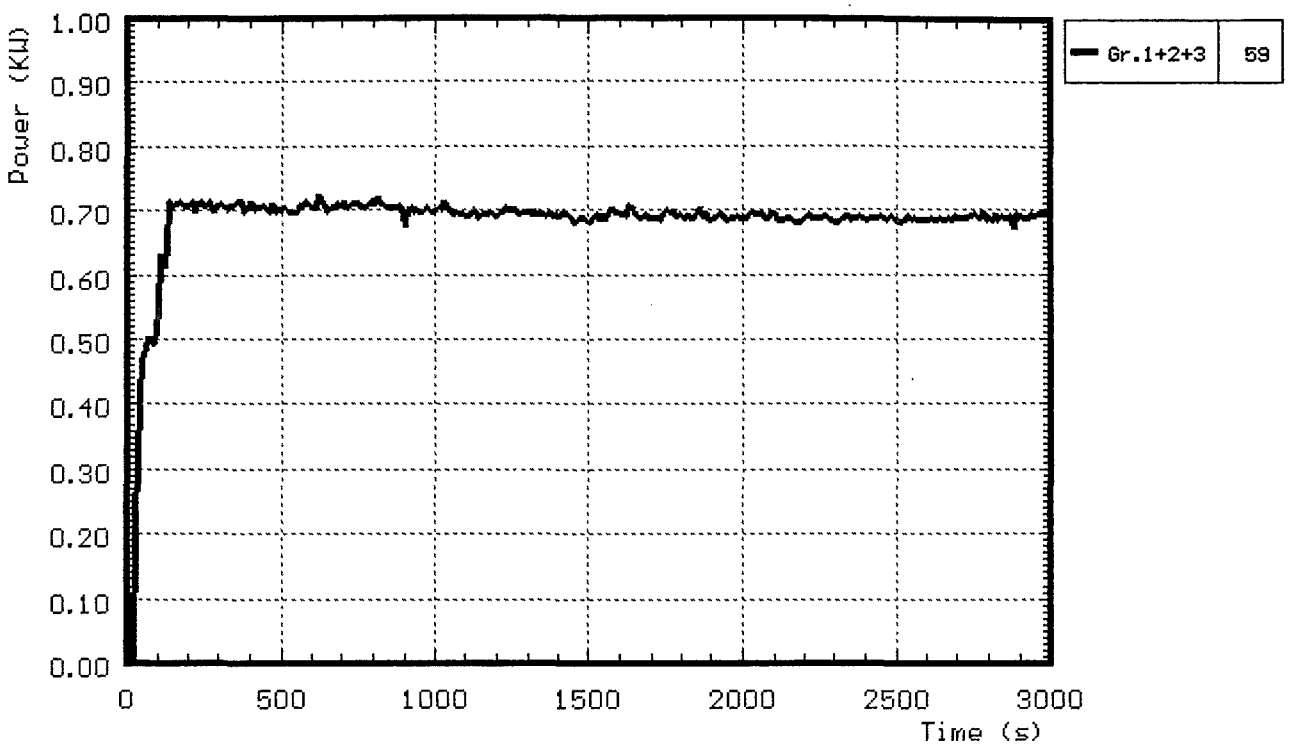

Fig. B1: CORA-30; Power input during pre-heat phase

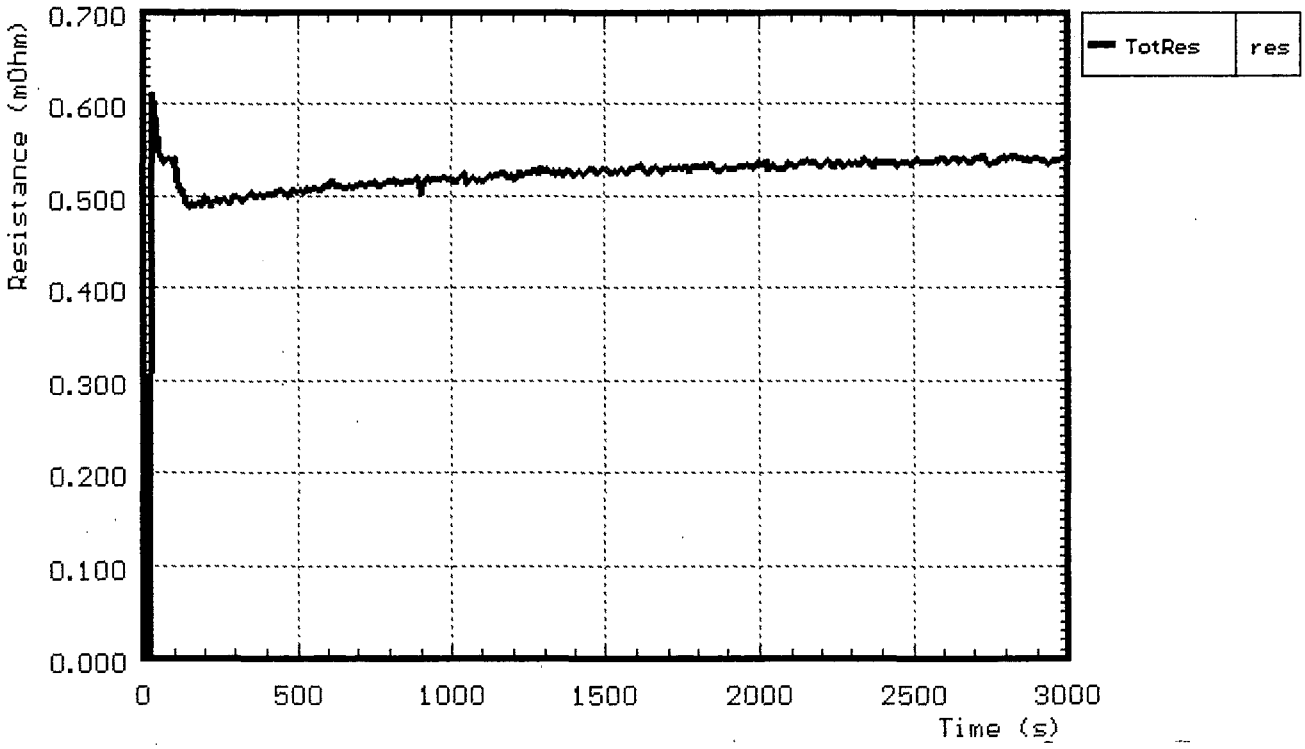

Fig. B2: CORA-30; Resistance of bundle during pre-heat phase

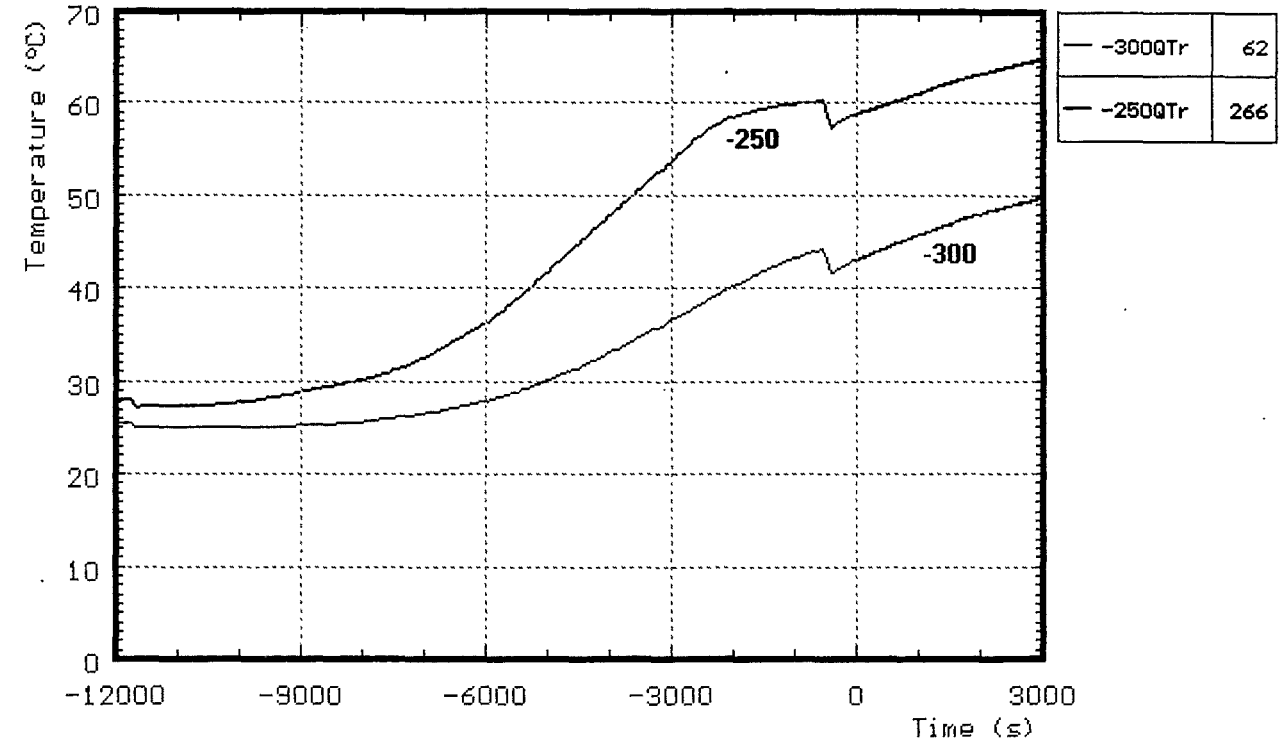

Fig. B3: CORA-30; Watertemperature in the quench cylinder; pre-heat phase

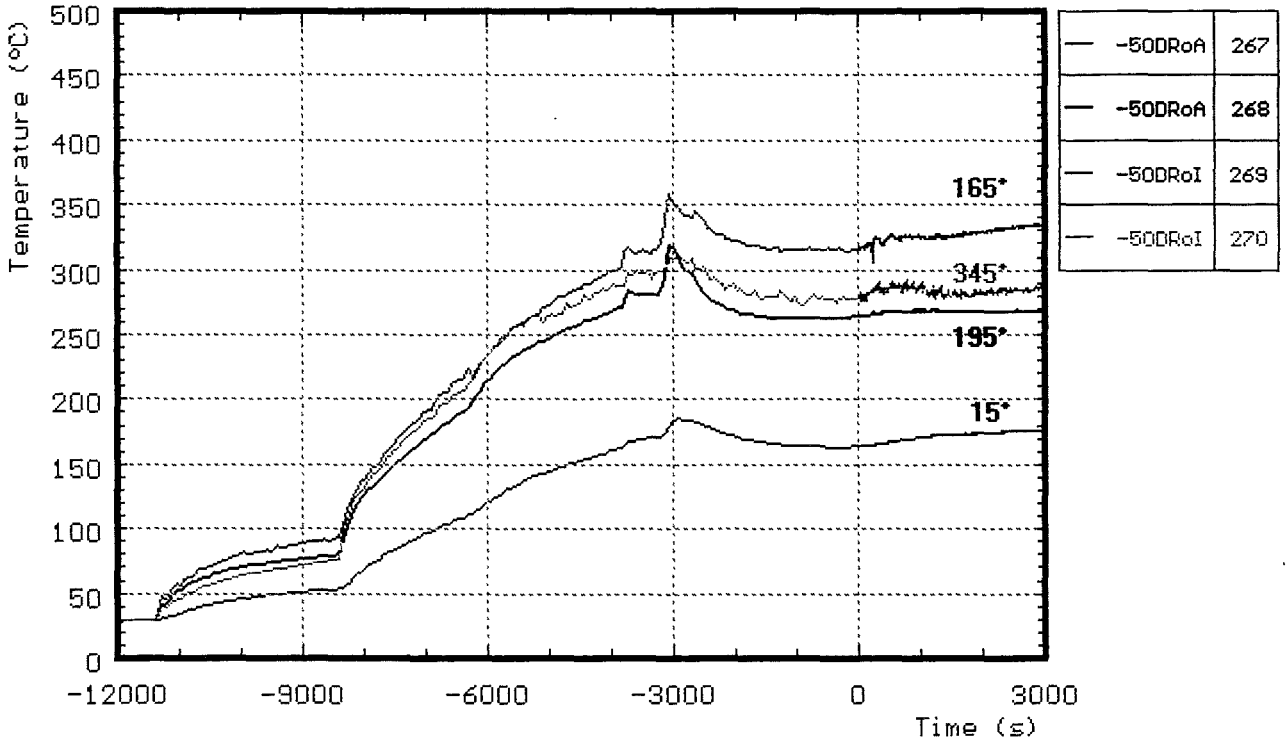

Fig. B4: CORA-30; Temperature in and on steam tube at -50 mm elevation; pre-heat phase

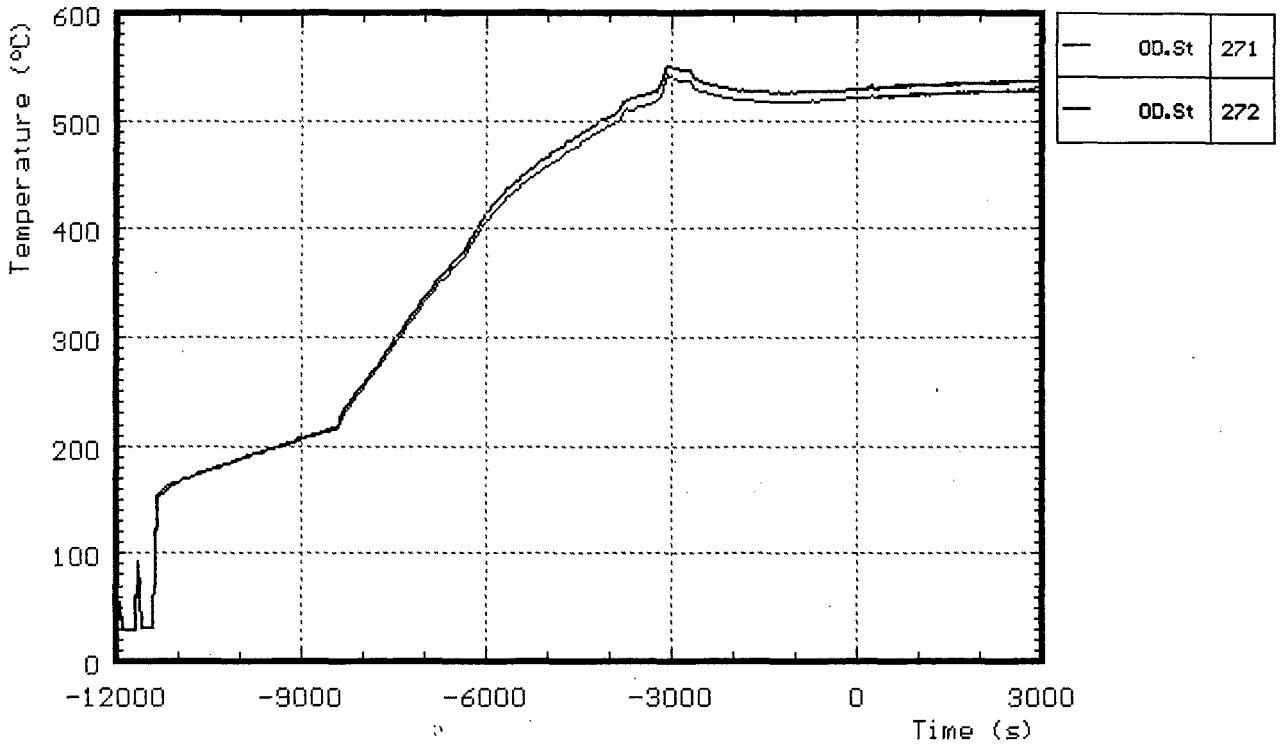

Fig. B5: CORA-30; Temperatures at steam inlet; pre-heat phase

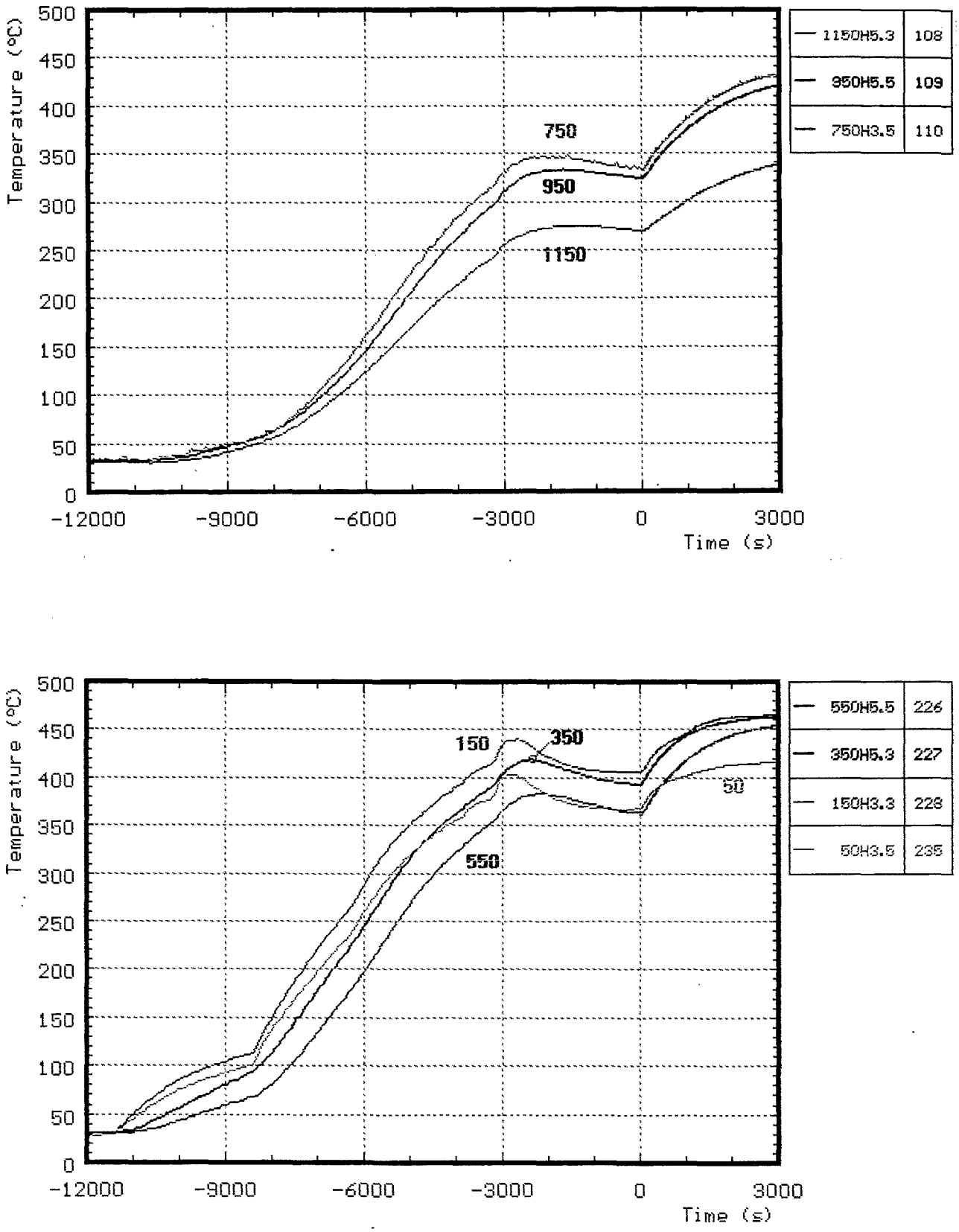

Fig. B6: CORA-30; Temperatures of heated rods; pre-heat phase

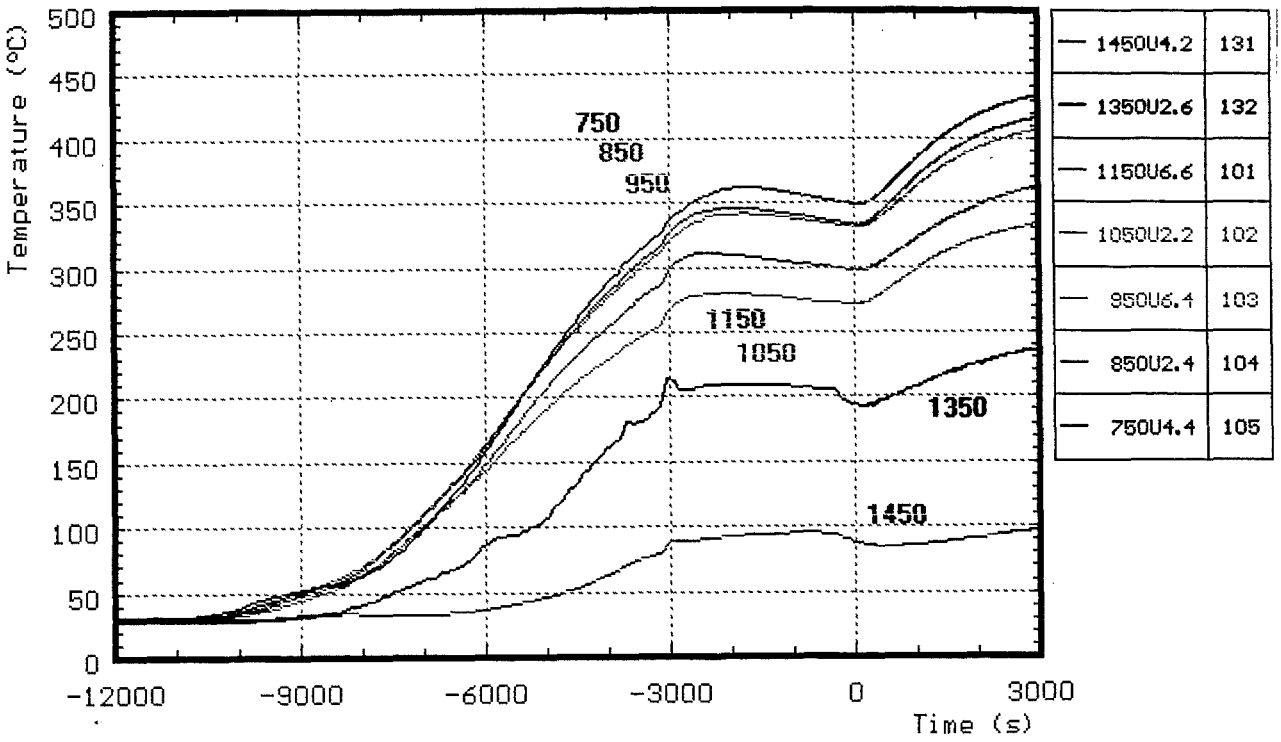

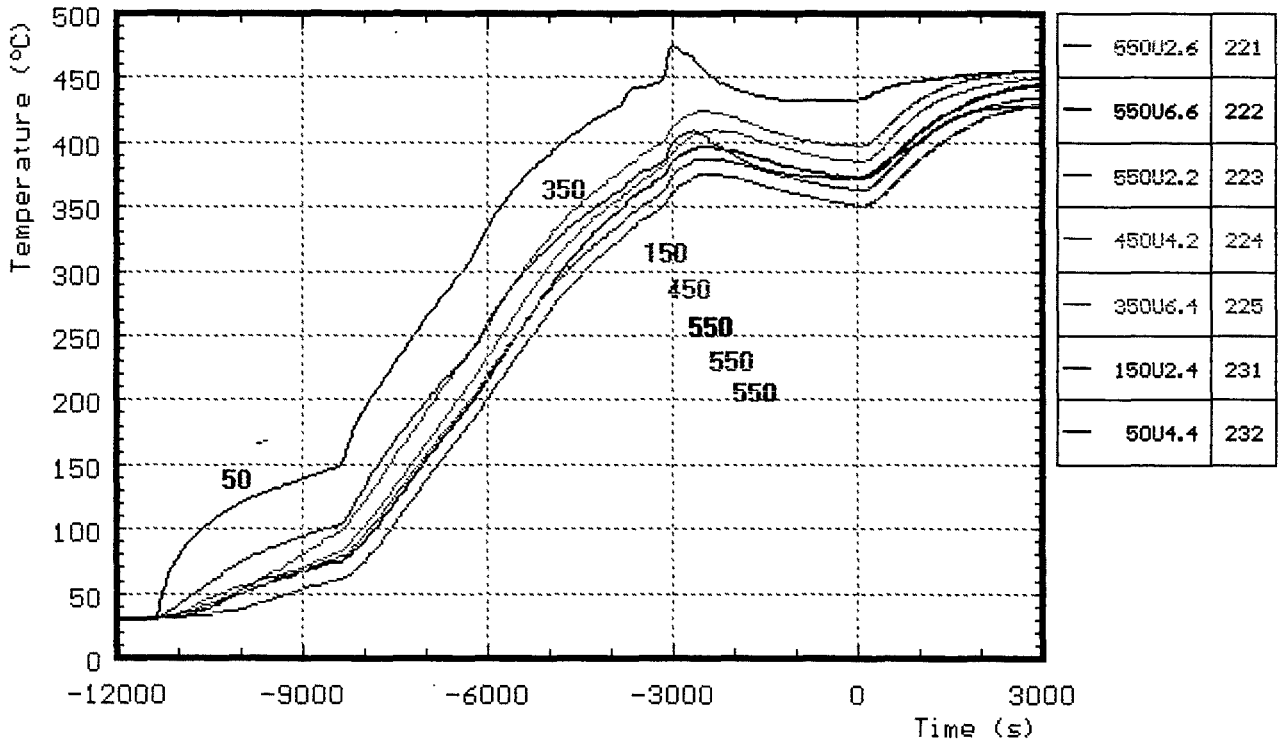

Fig. B7: CORA-30; Temperatures of unheated rods; pre-heat phase

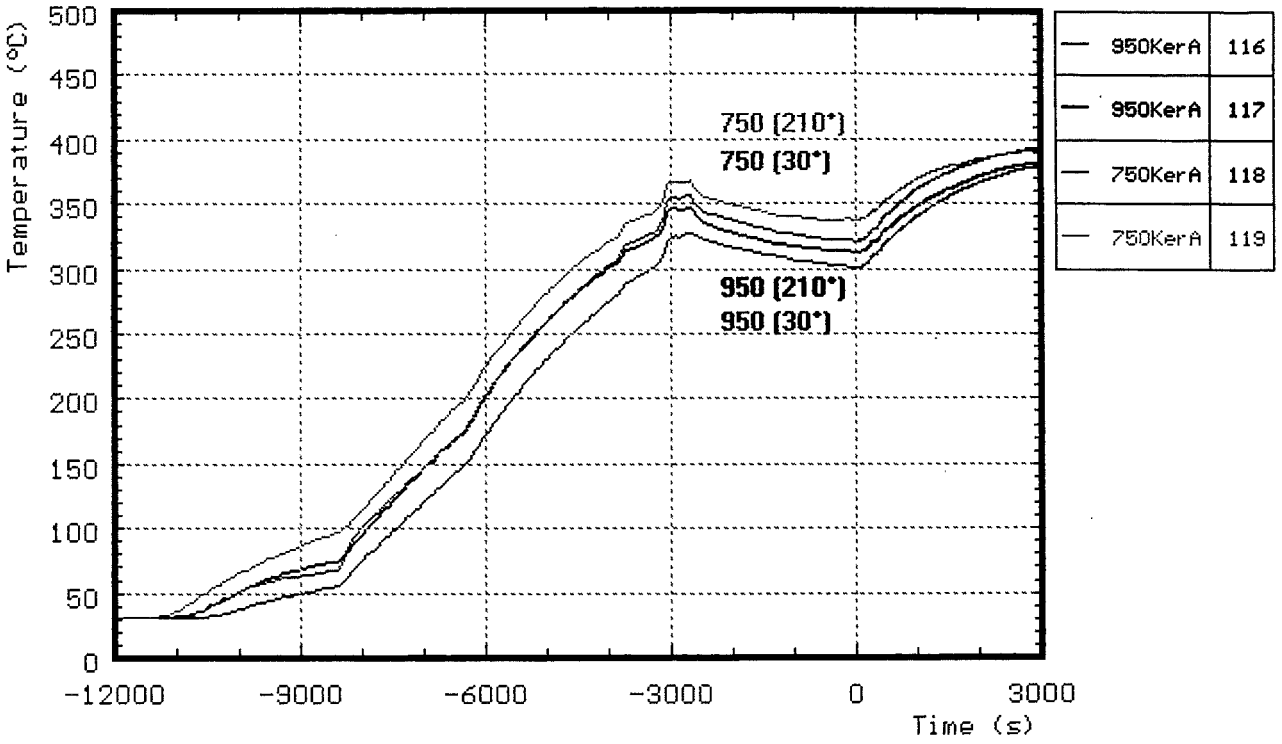

Fig. B8: CORA-30; Temperatures between bundle and shroud measured with ceramic protected TCs; pre-heat phase

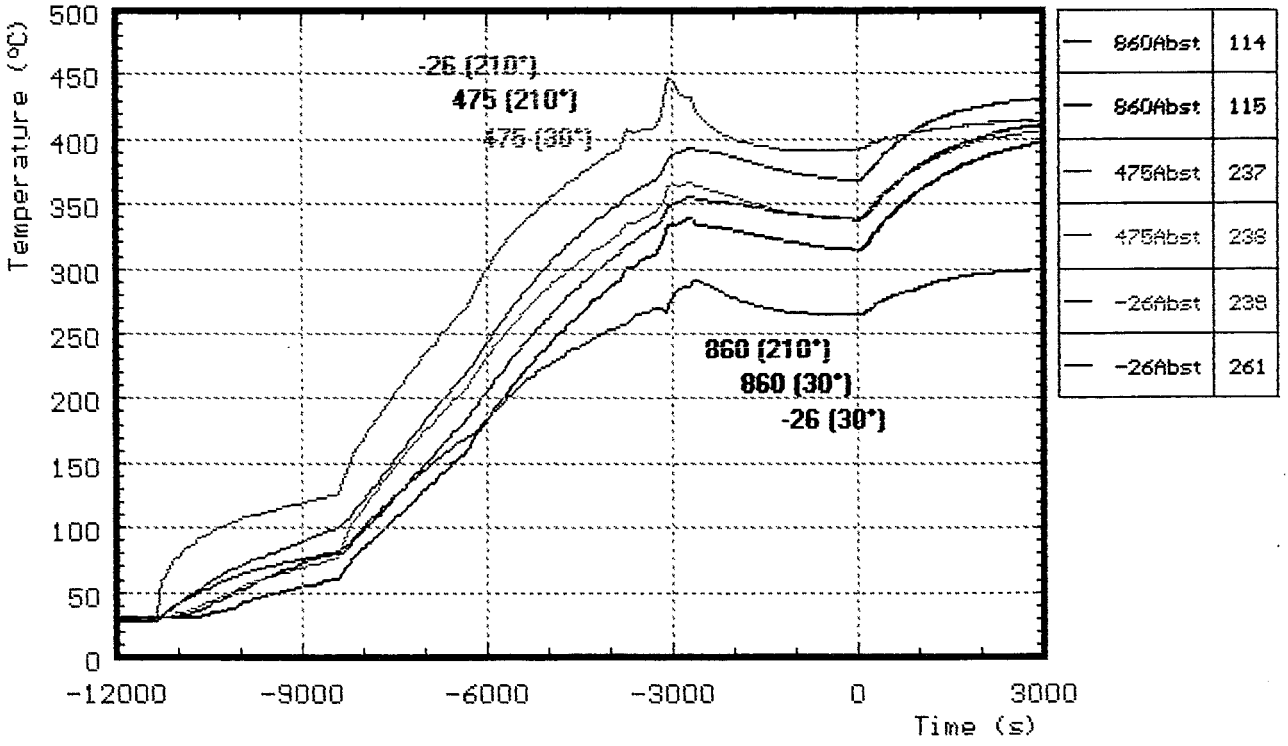

Fig. B9: CORA-30; Temperatures of the spacers; pre-heat phase

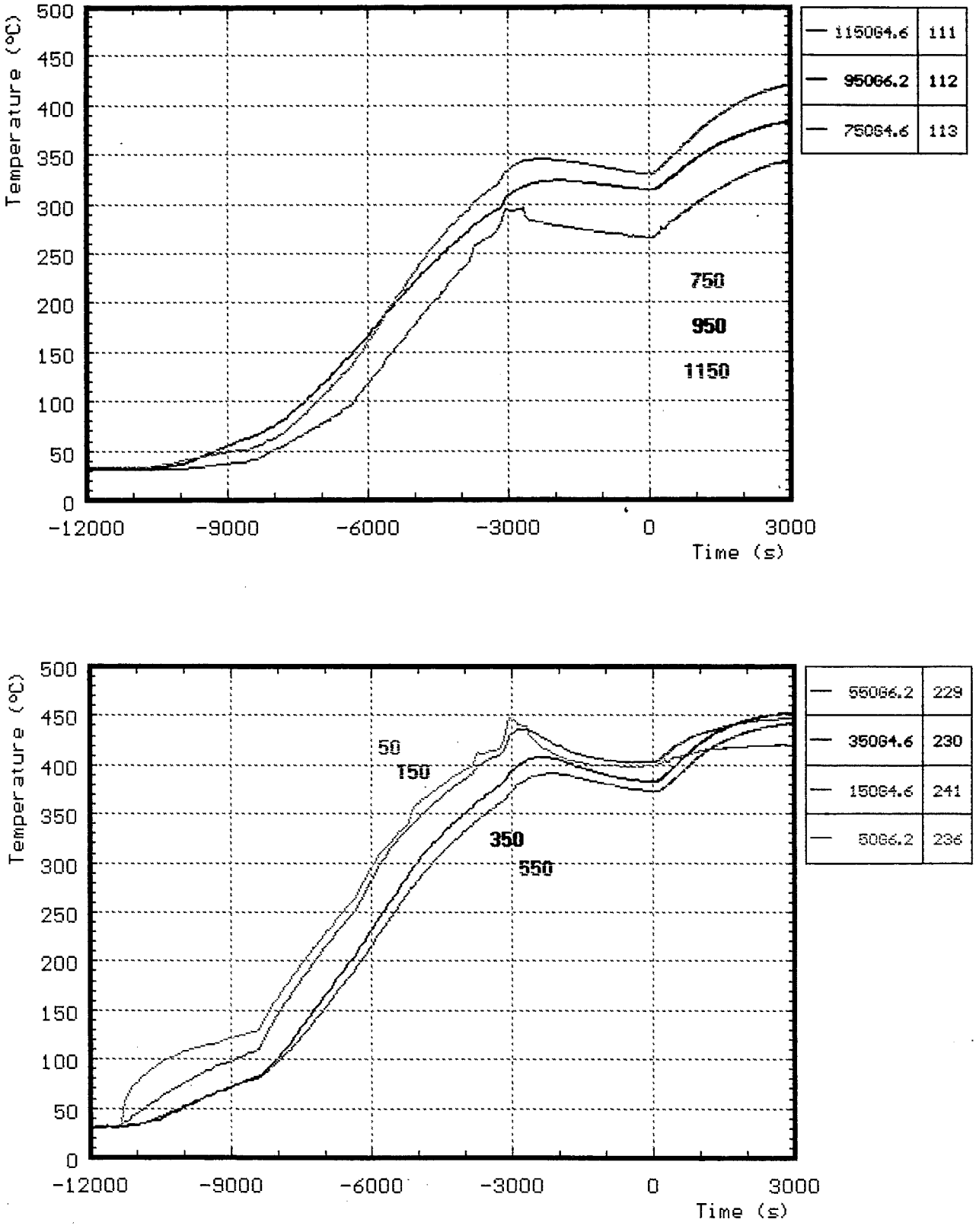

Fig. B10: CORA-30; Temperatures of the guide tubes of absorber rods; pre-heat phase

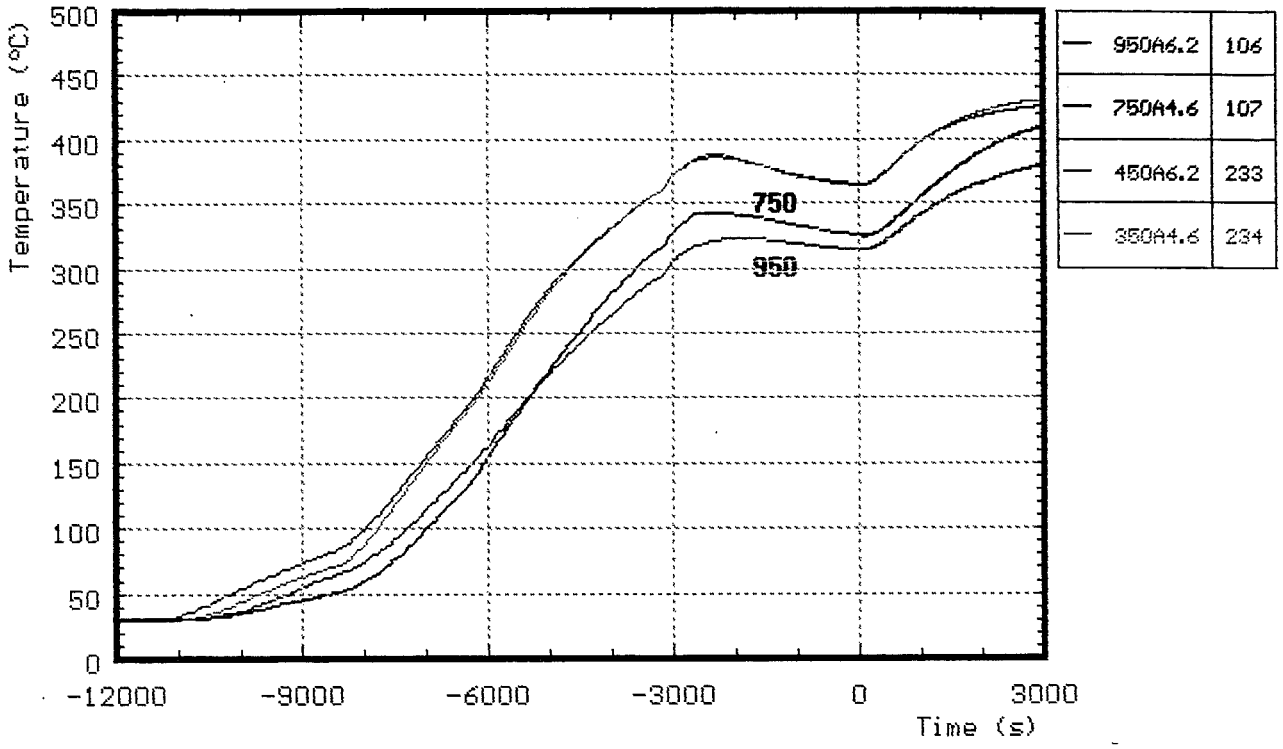

Fig. B11: CORA-30; Temperatures in the absorber; pre-heat phase

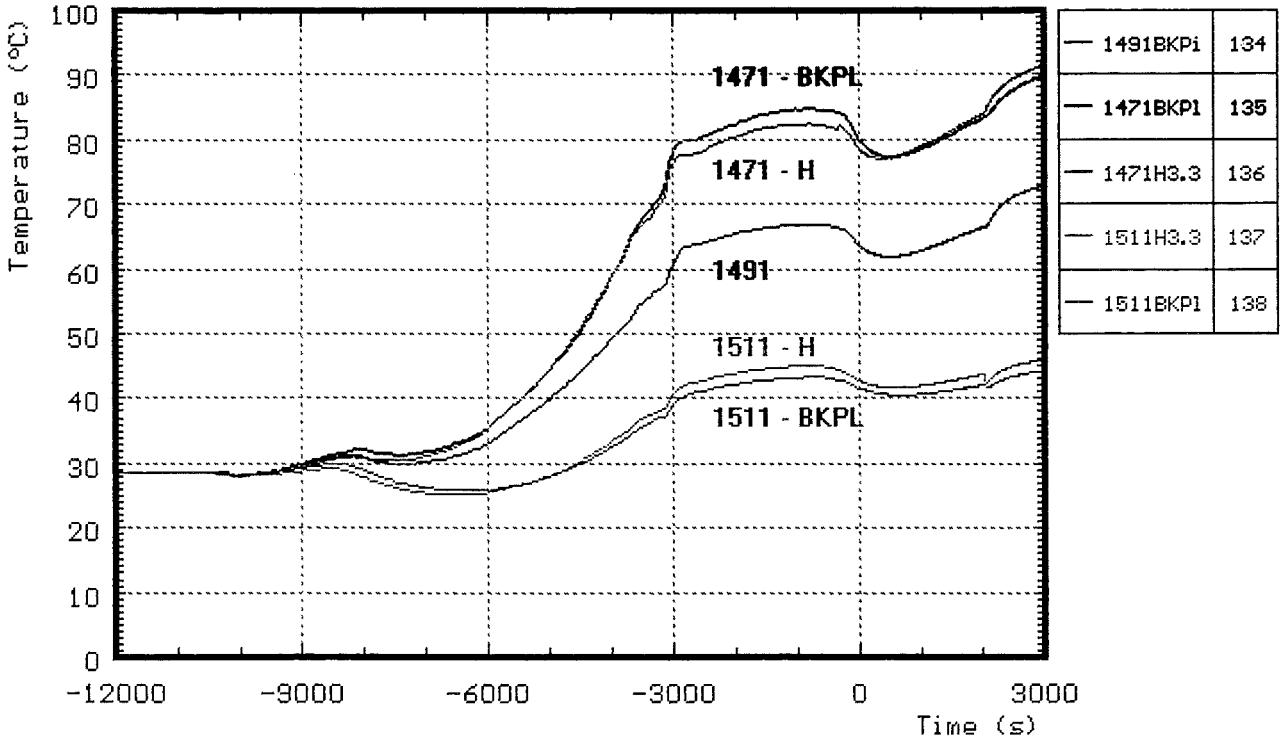

Fig. B12: CORA-30; Temperatures at the bundle head plate; pre-heat phase

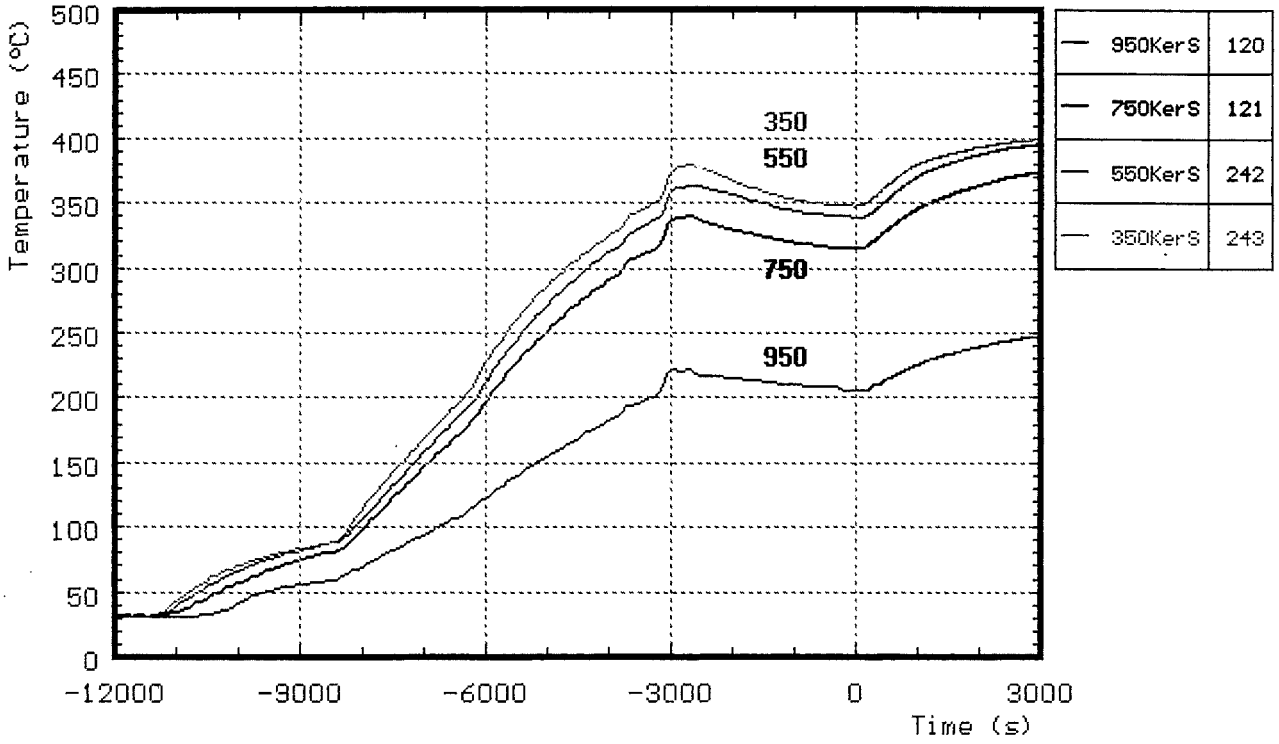

Fig. B13: CORA-30; Temperatures of inner side of shroud measured with ceramic protected TCs; pre-heat phase

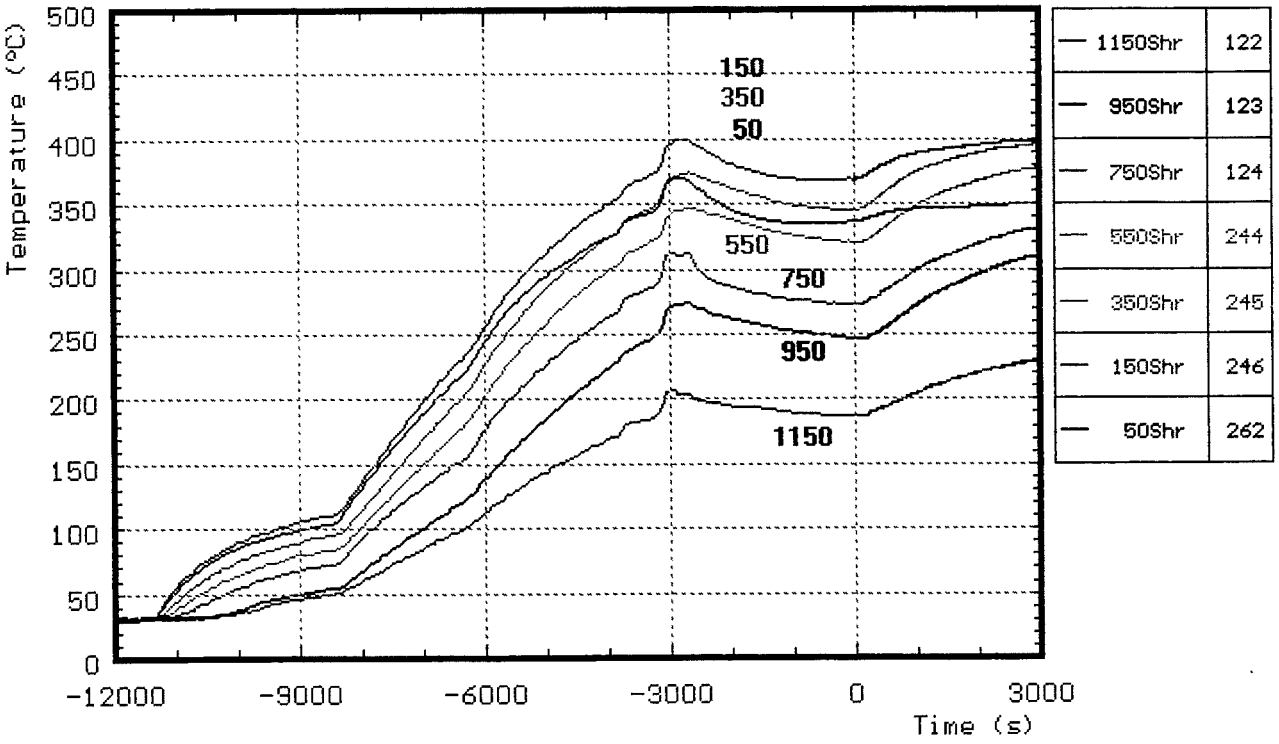

Fig. B14: CORA-30; Temperatures of outer side of shroud; pre-heat phase

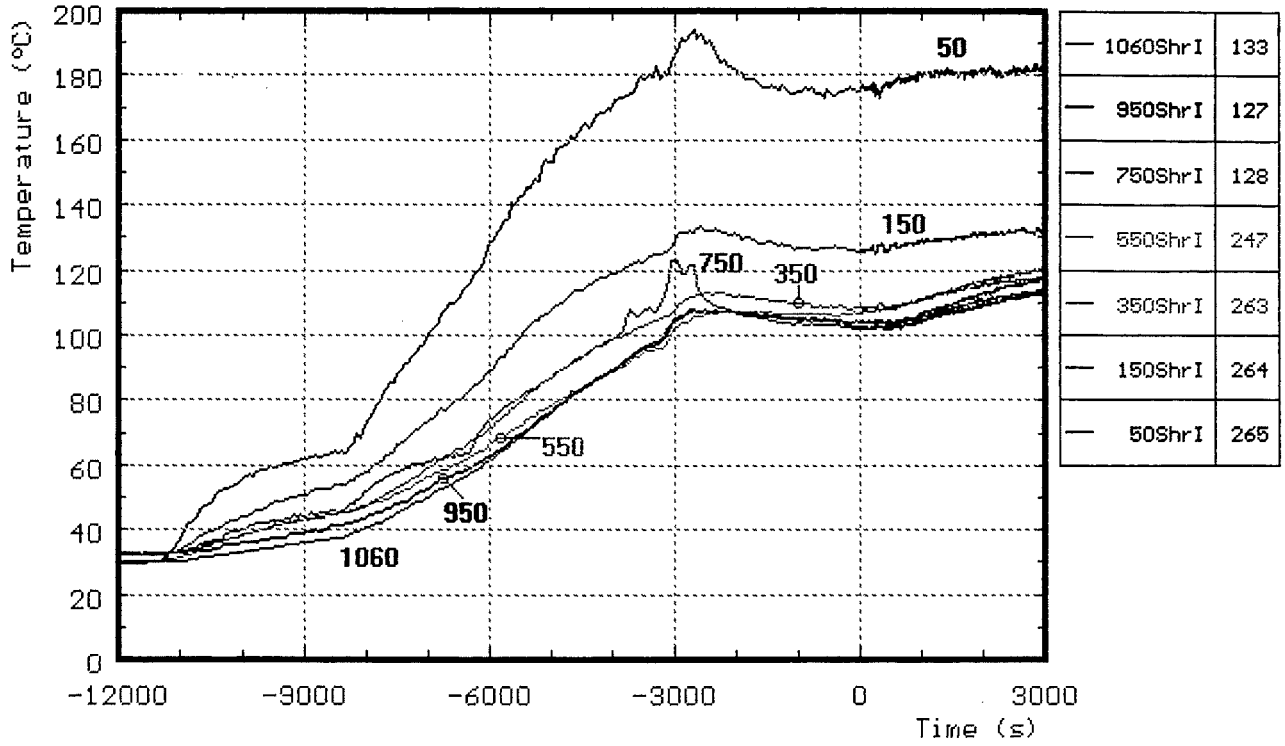

Fig. B15: CORA-30; Temperatures of the shroud insulation; pre-heat phase

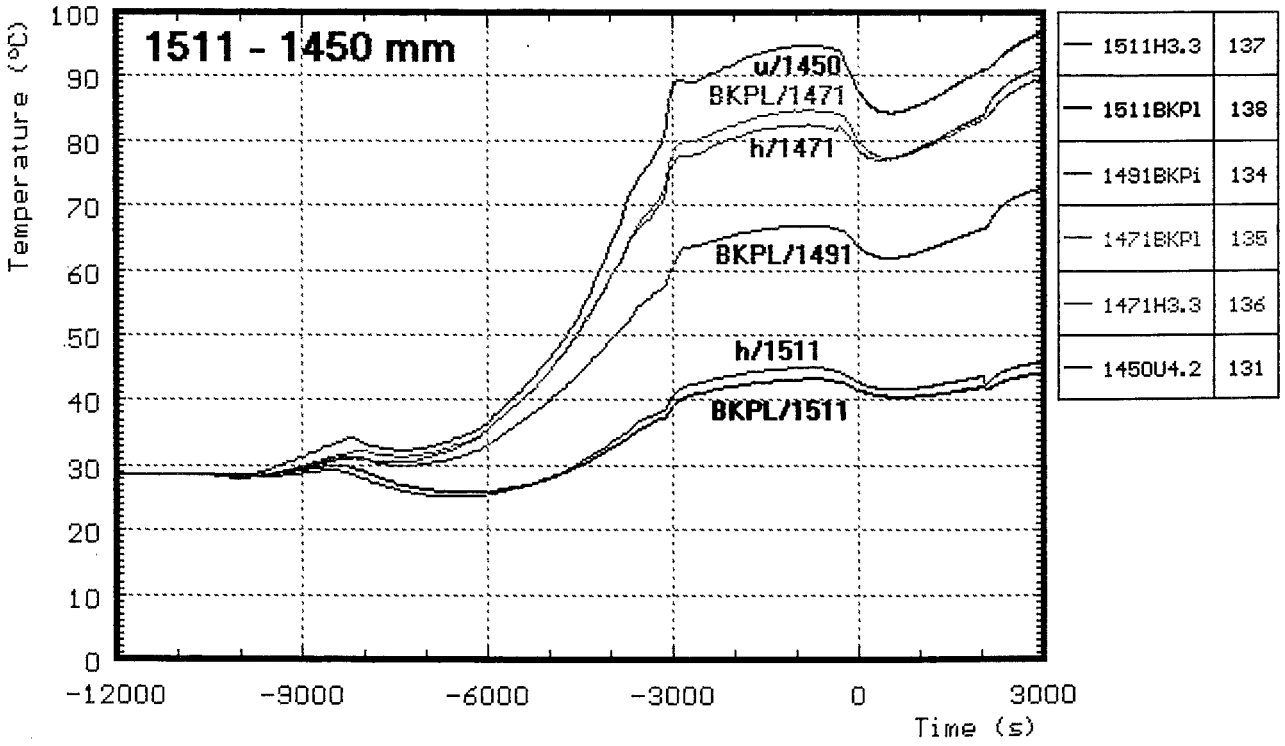

Fig. B16: CORA-30; Temperatures at elevations given; pre-heat phase (1511-1450 mm)

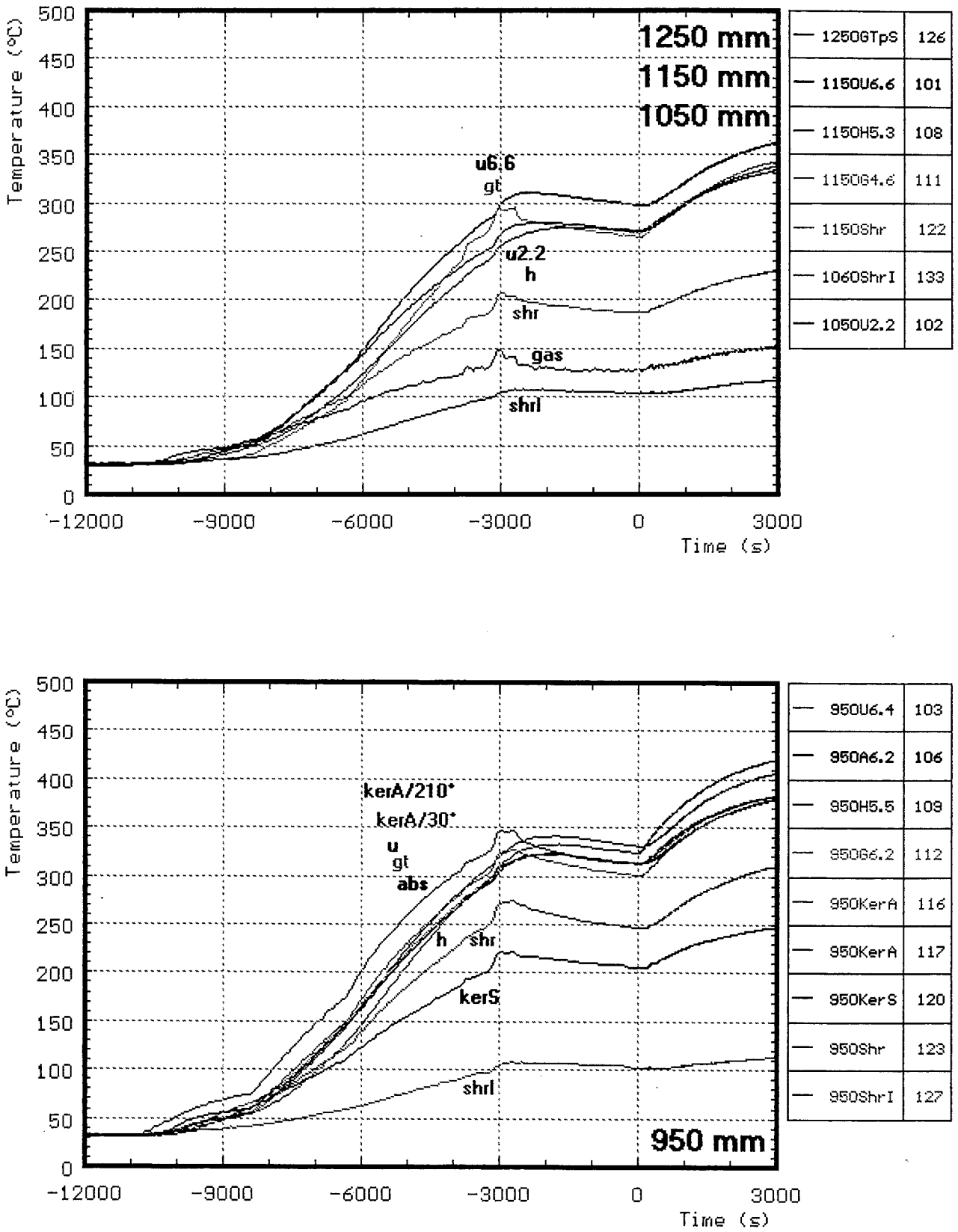

Fig. B17: CORA-30; Temperatures at elevations given; pre-heat phase (1250-1050,950 mm)

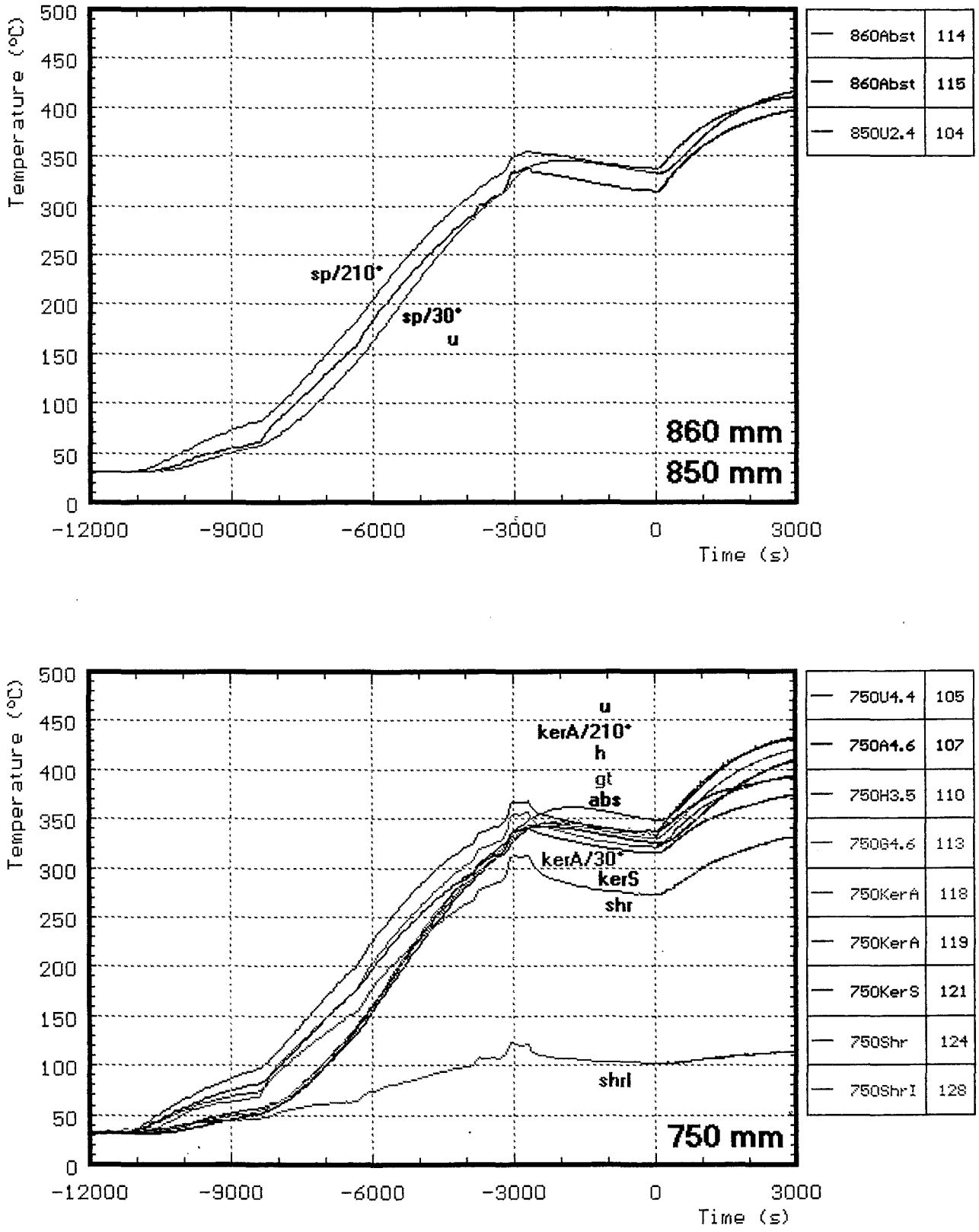

Fig. B18: CORA-30; Temperatures at elevations given; pre-heat phase (860,850,750 mm)

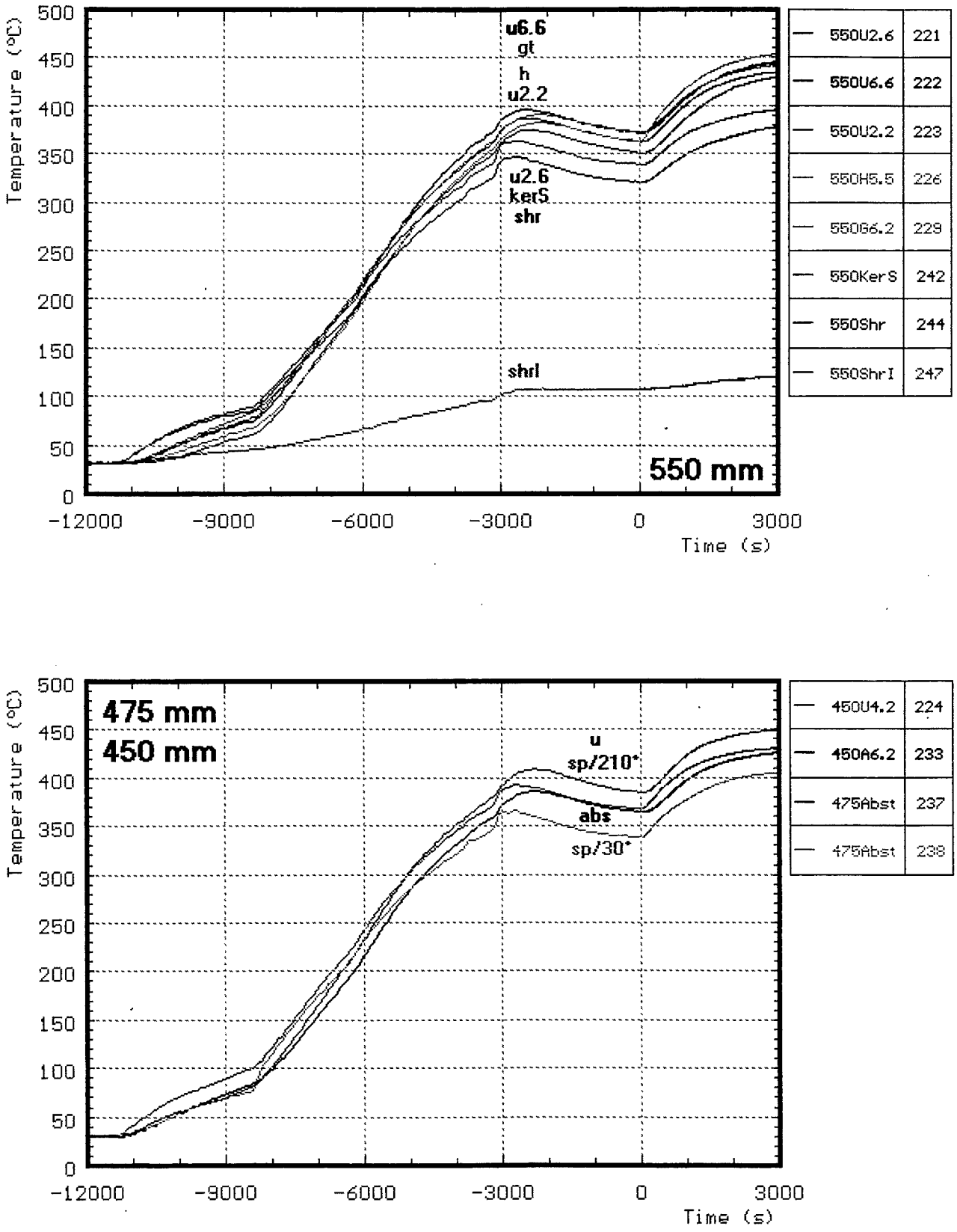

Fig. B19: CORA-30; Temperatures at elevations given; pre-heat phase (550, 475, 450 mm)

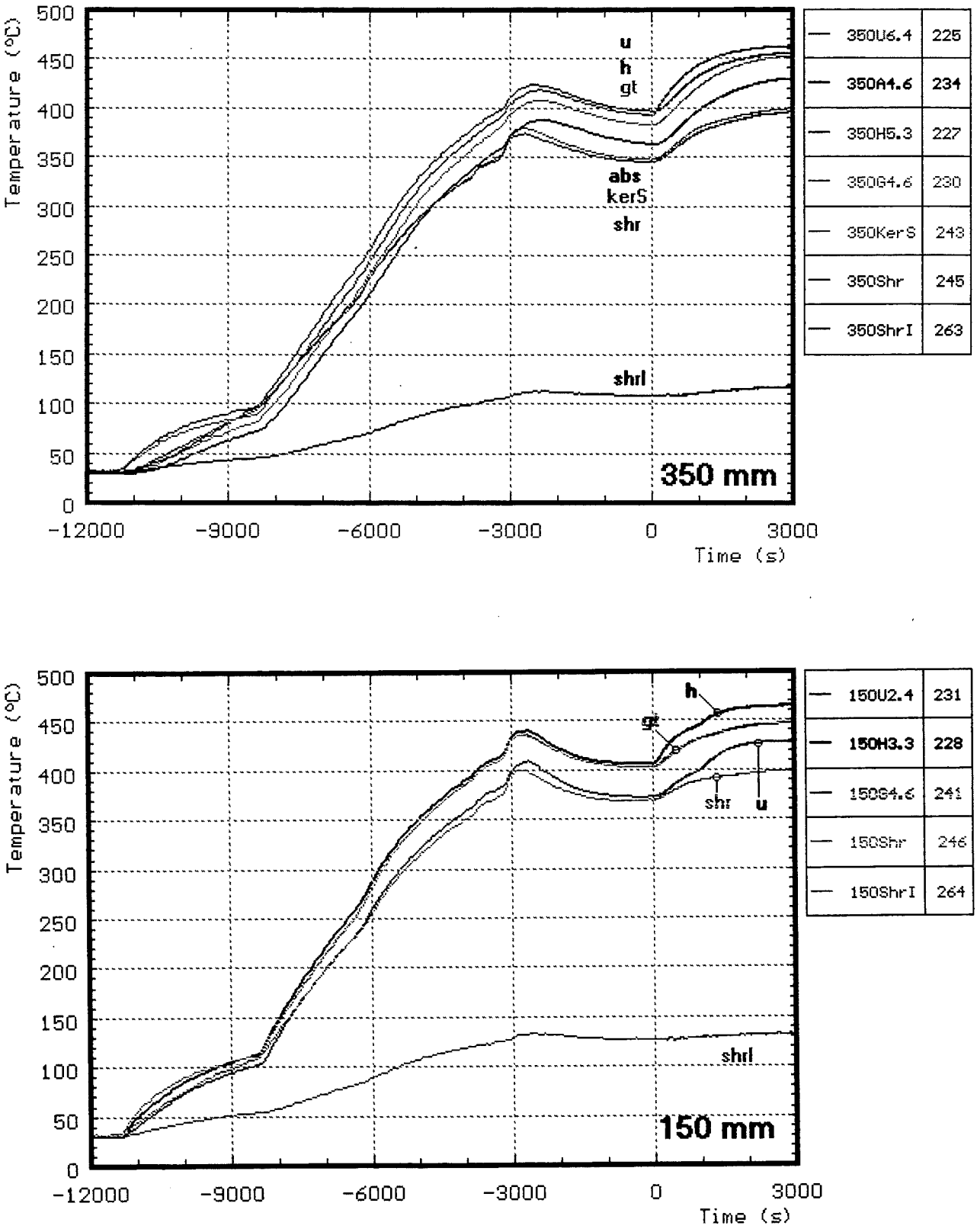

Fig. B20: CORA-30; Temperatures at elevations given; pre-heat phase (350, 150 mm)

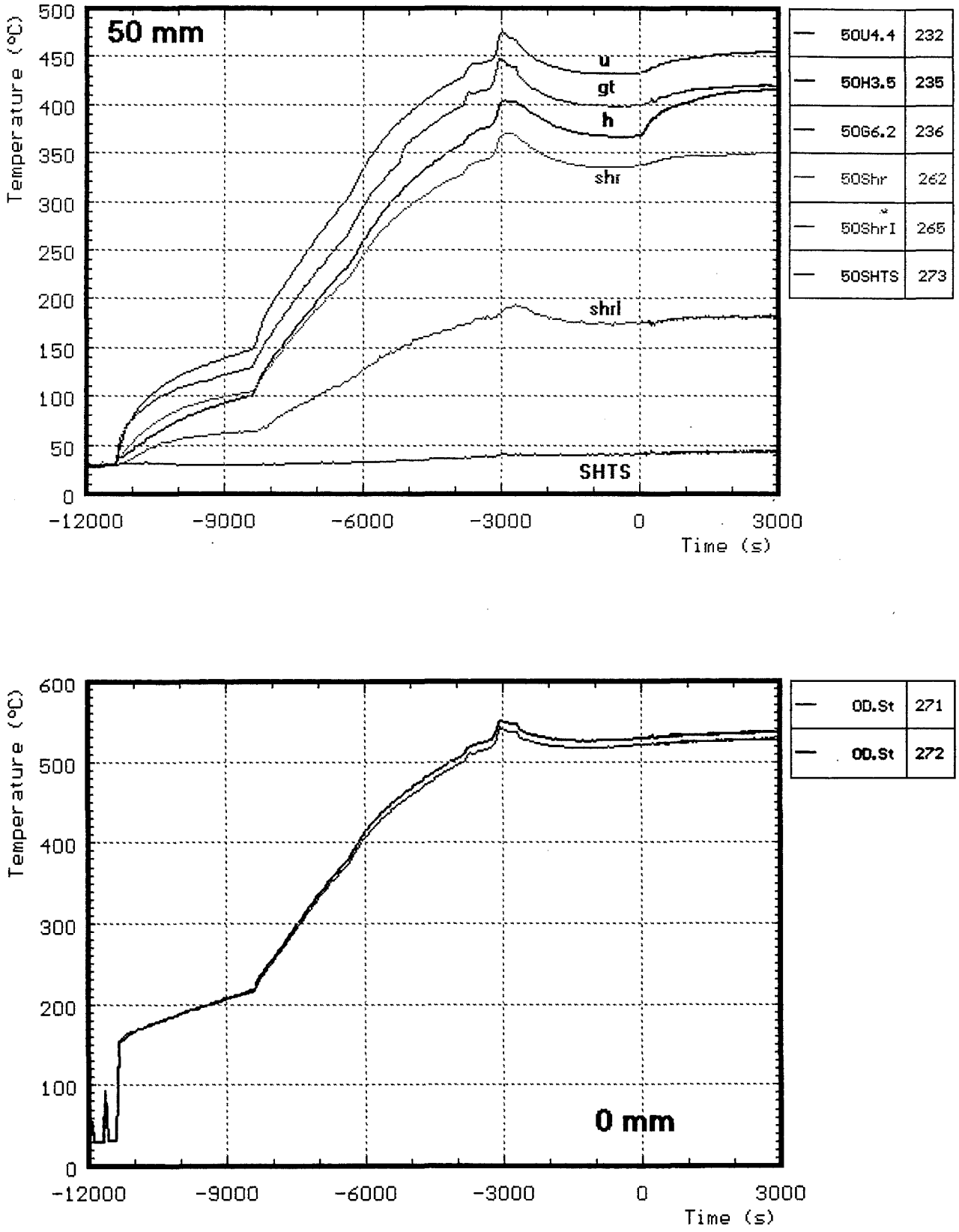

Fig. B21: CORA-30; Temperatures at elevations given; pre-heat phase (50, 0 mm)

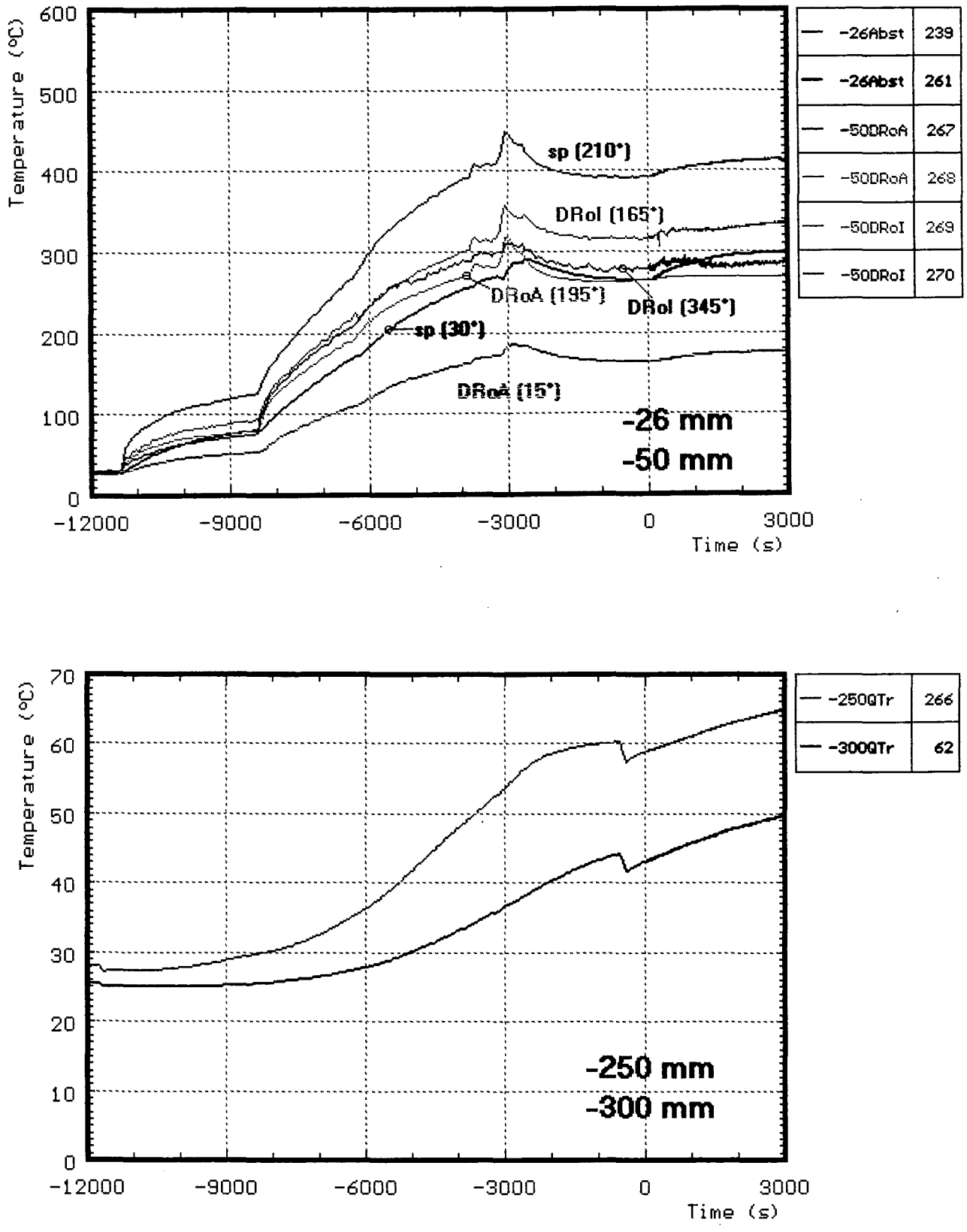

Fig. B22: CORA-30; Temperatures at elevations given; pre-heat phase (-26, -50, -250, -300 mm)

Appendix C

Complete set of cross sections

Figures C1 - C9

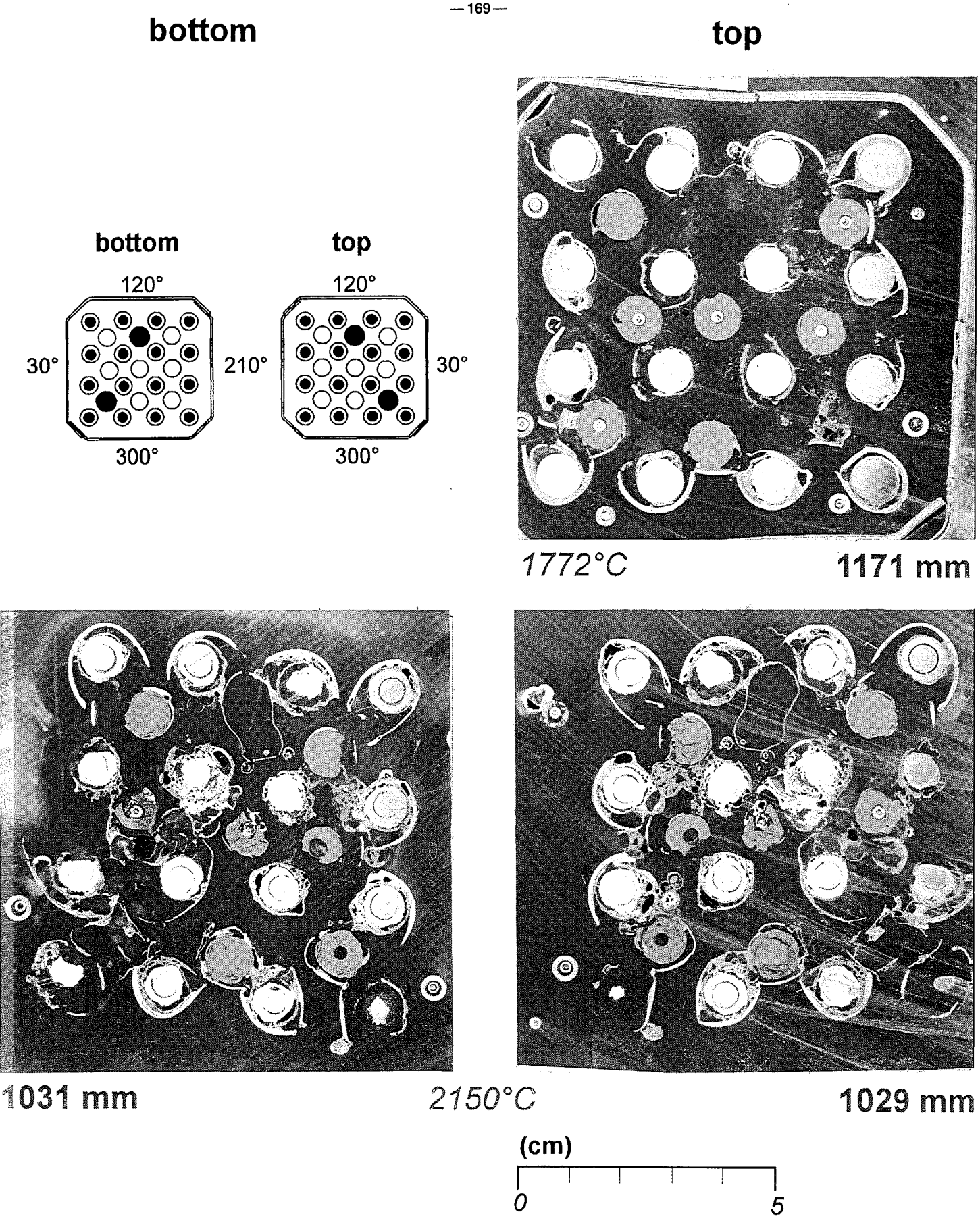

Fig. C1: Horizontal cross sections of bundle CORA-30 (1171, 1029 mm)

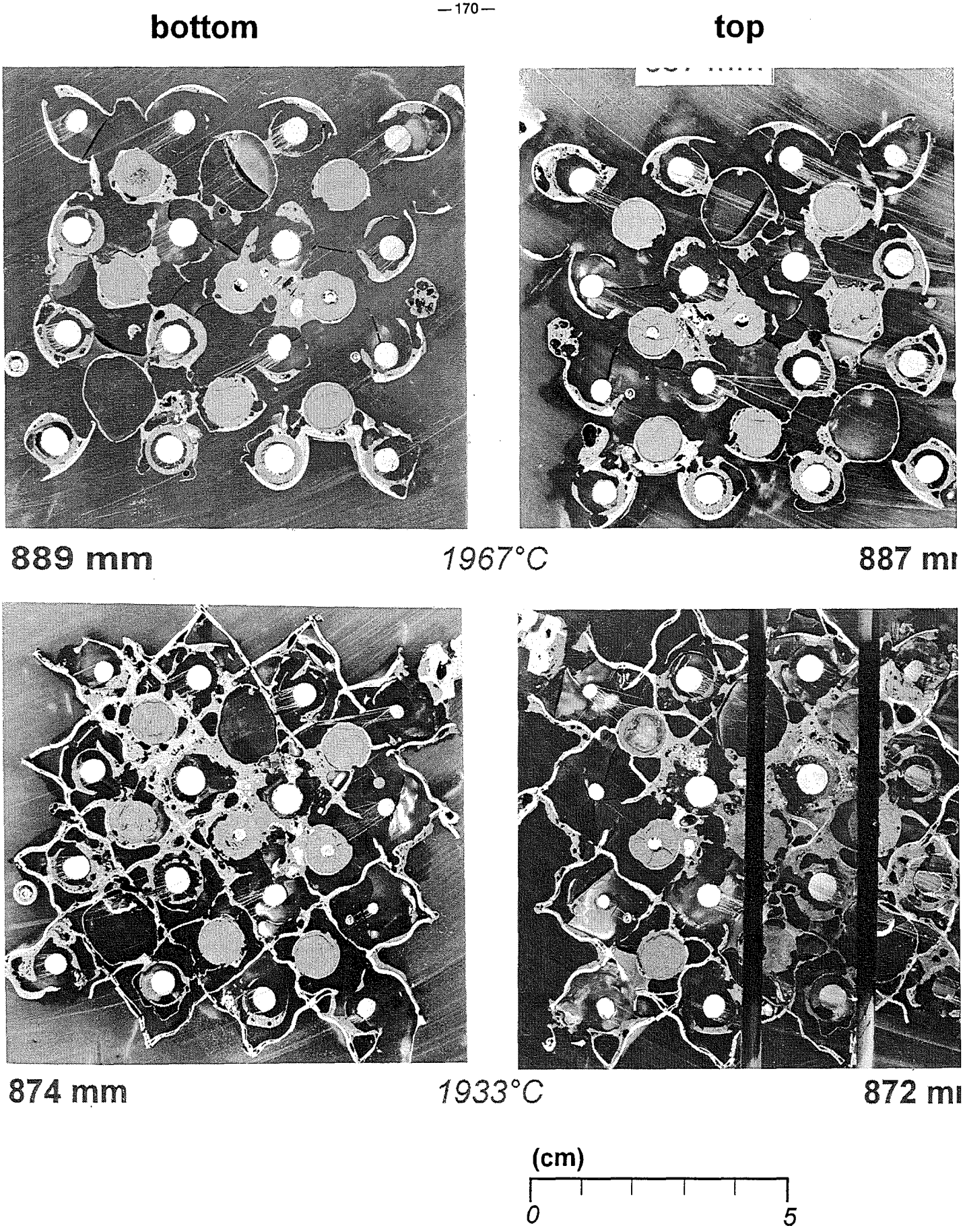

Fig. C2: Horizontal cross sections of bundle CORA-30 (887, 872 mm)

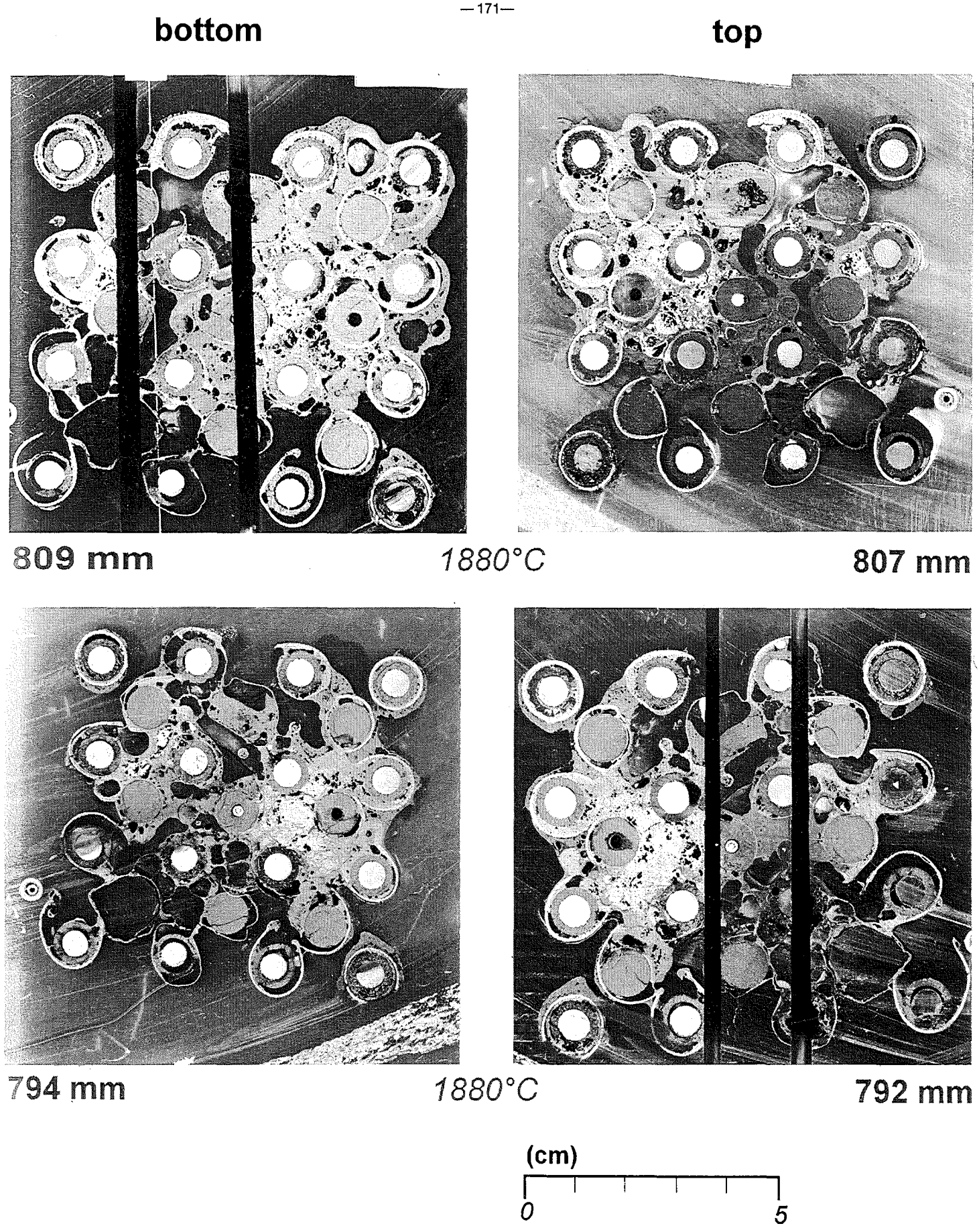

Fig. C3: Horizontal cross sections of bundle CORA-30 (807, 792 mm)

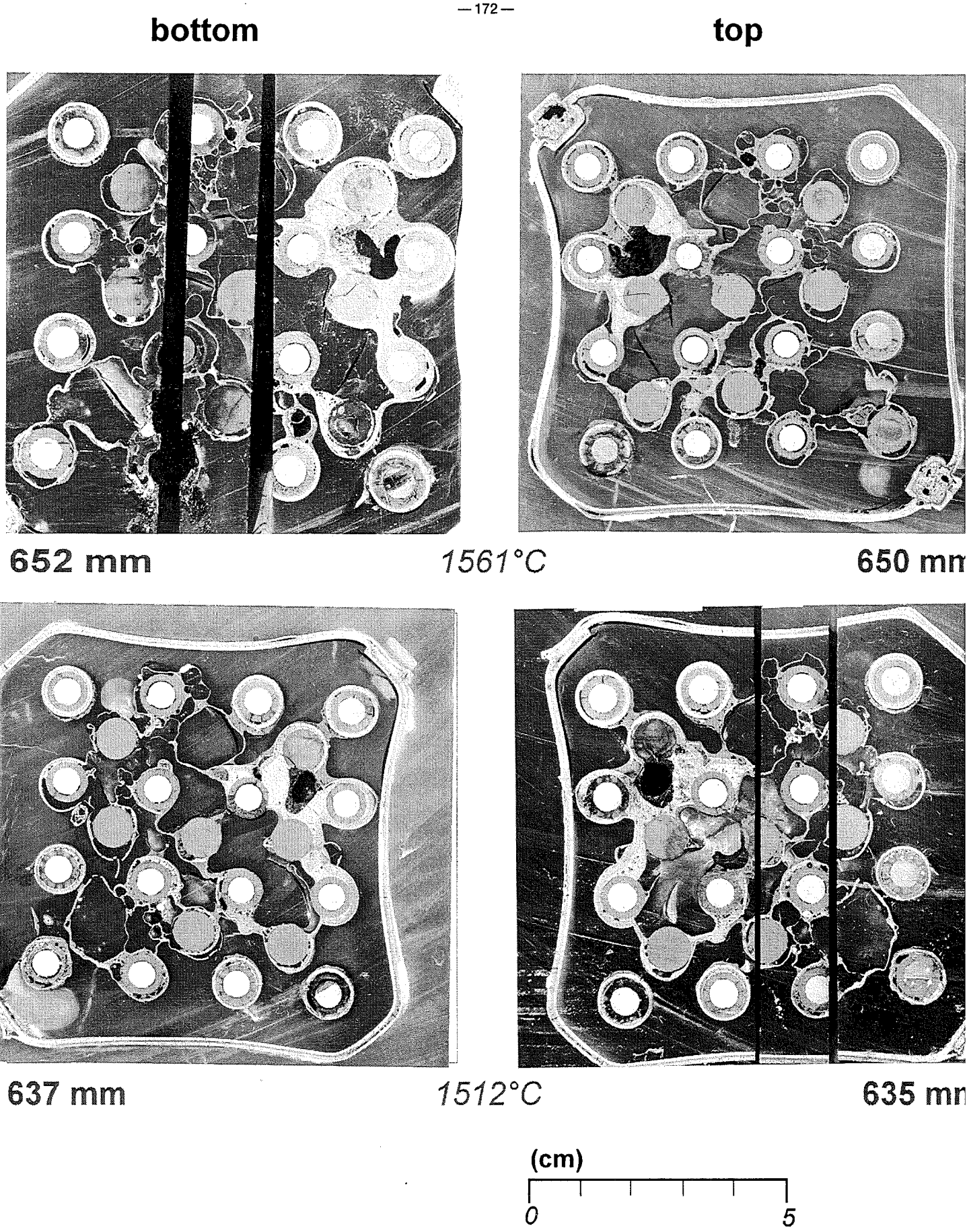

Fig. C4: Horizontal cross sections of bundle CORA-30 (650, 635 mm)

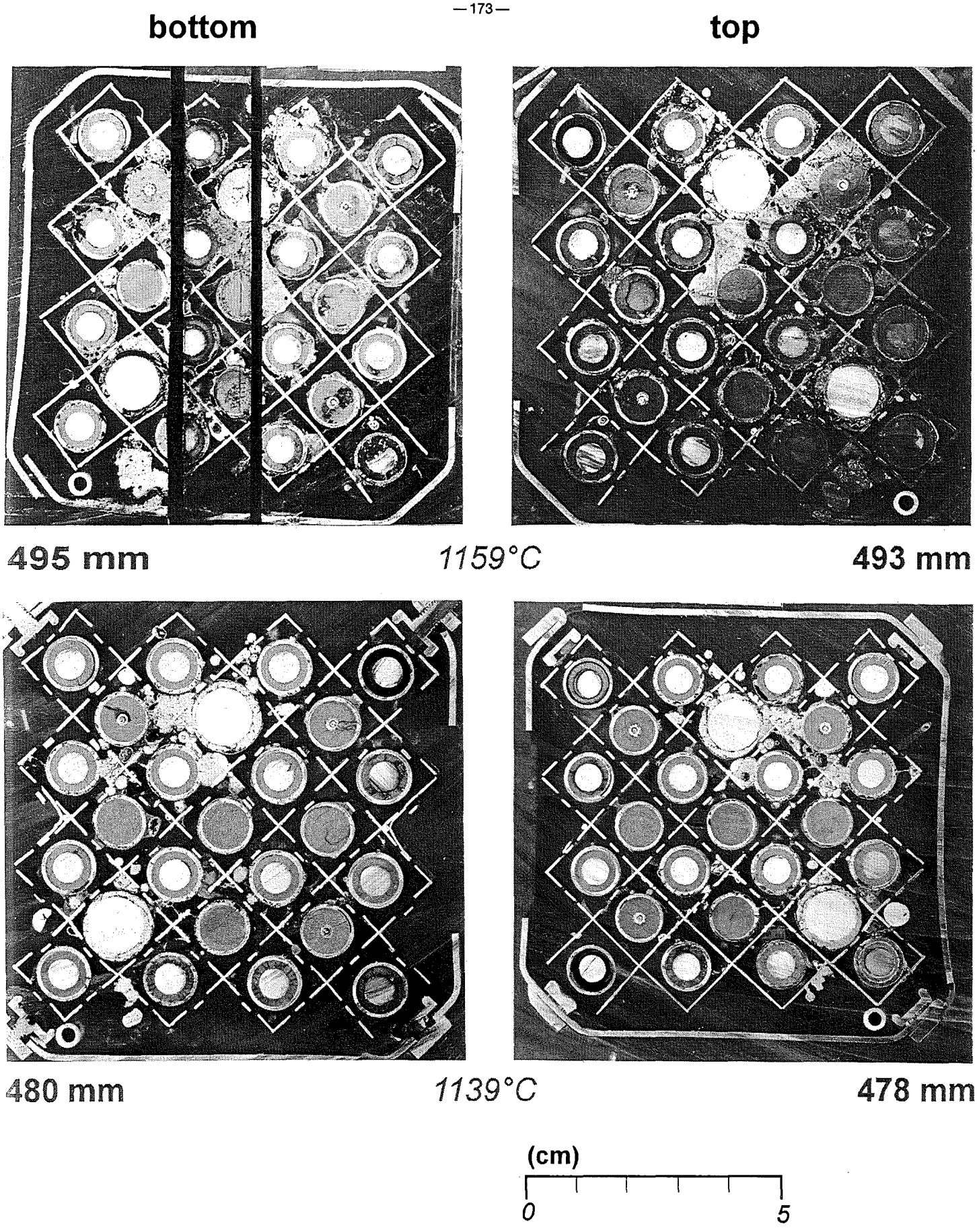

Fig. C5: Horizontal cross sections of bundle CORA-30 (493, 478 mm)

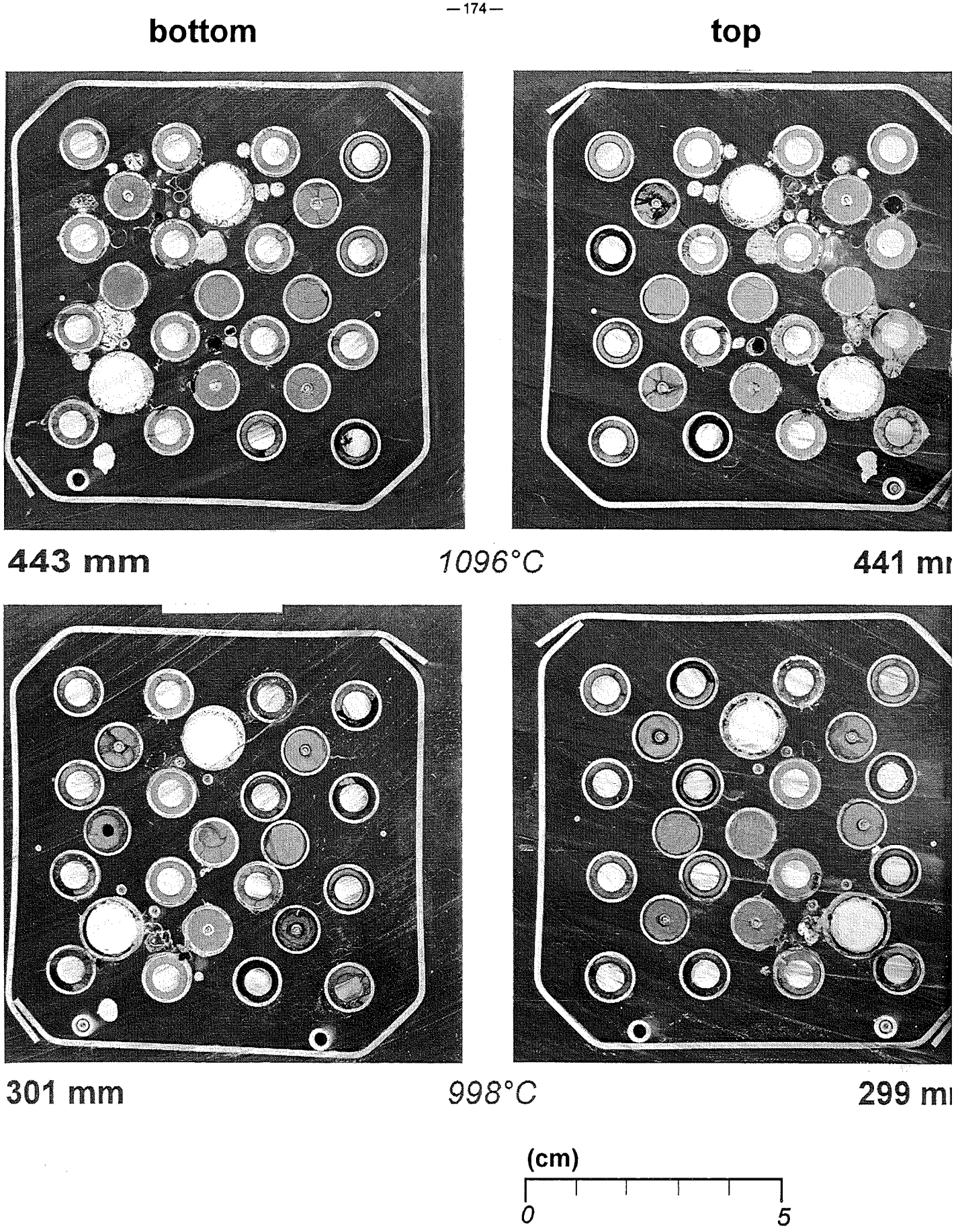

Fig. C6: Horizontal cross sections of bundle CORA-30 (441, 299 mm)

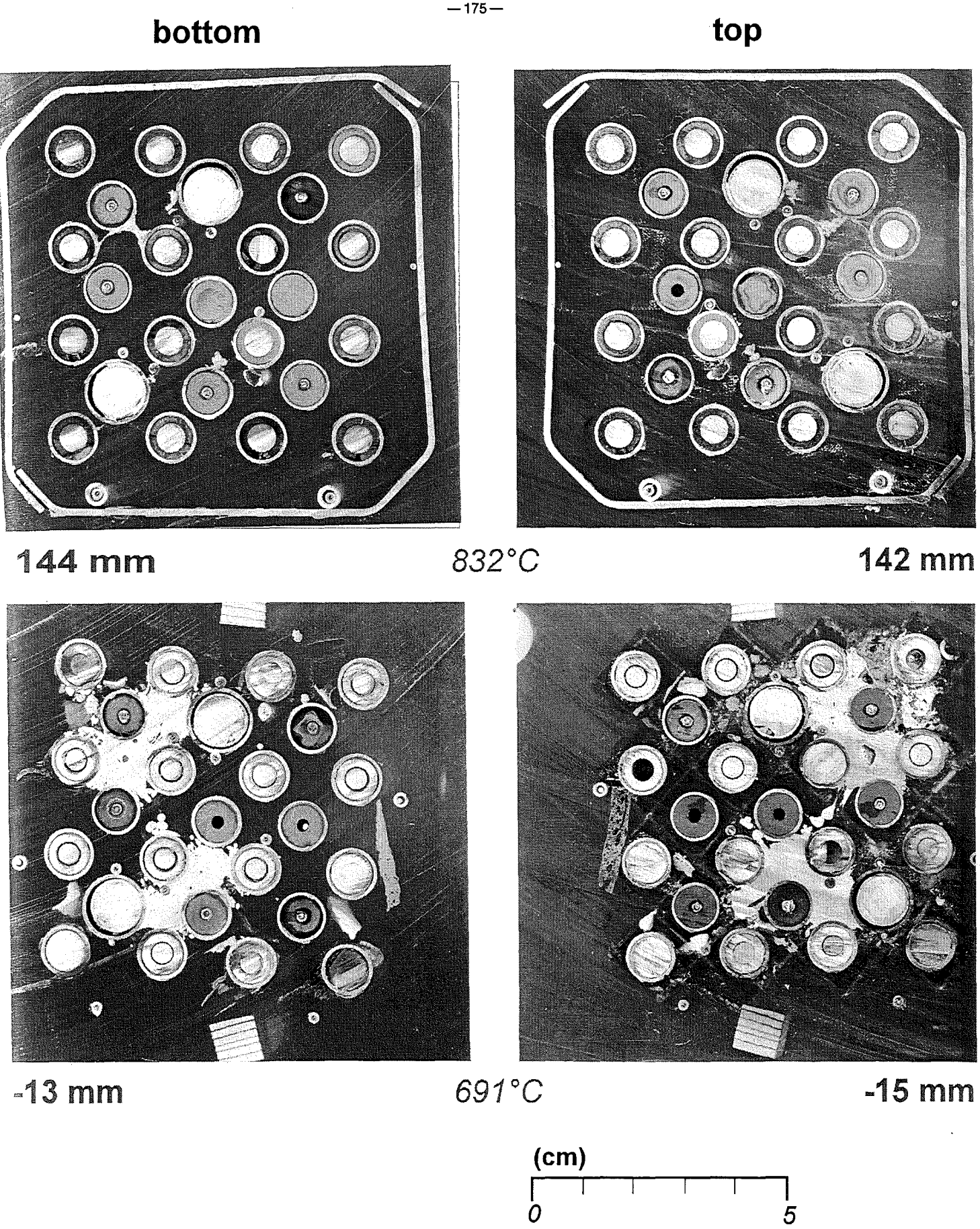

Fig. C7: Horizontal cross sections of bundle CORA-30 (142, -15 mm)

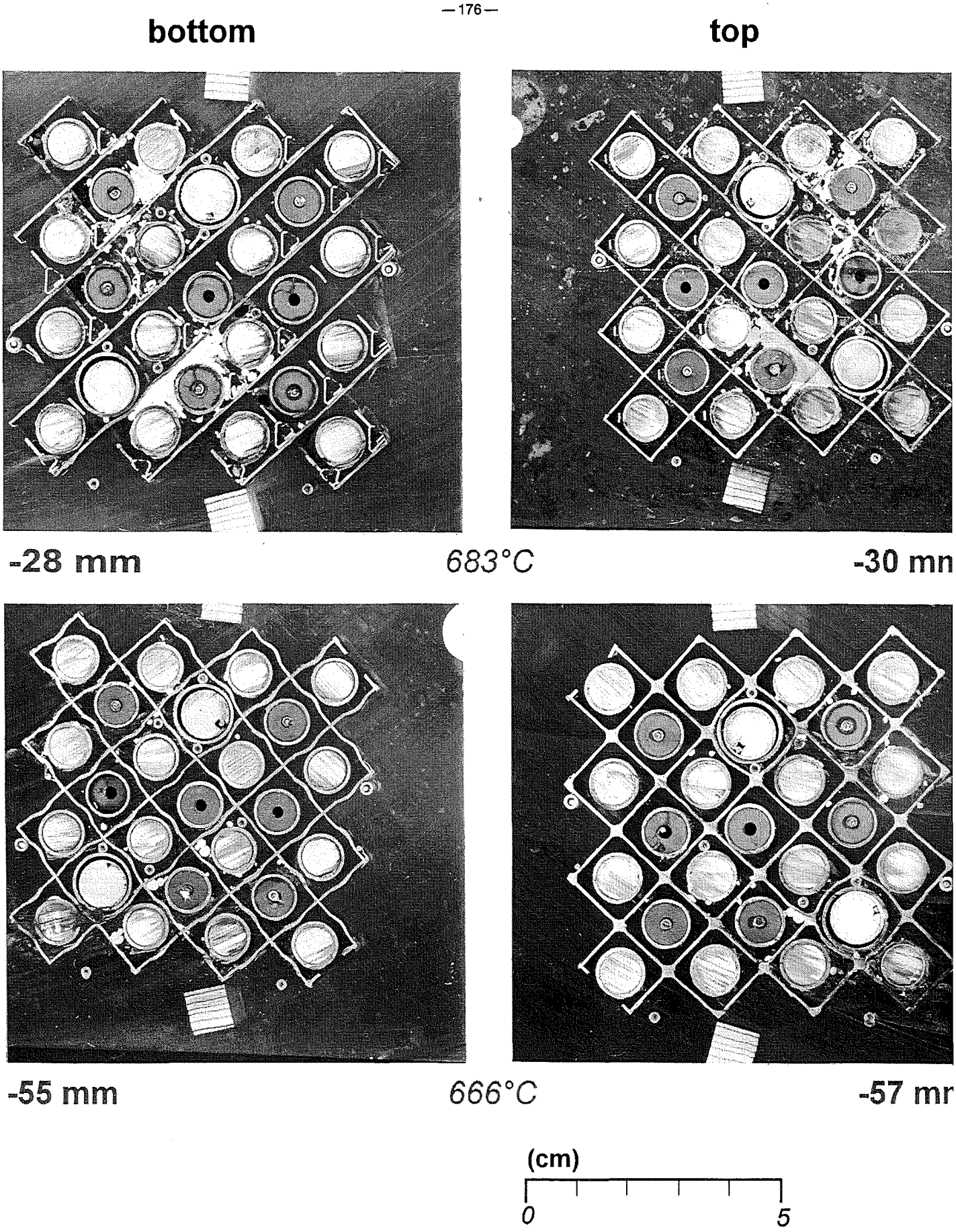

Fig. C8: Horizontal cross sections of bundle CORA-30 (-30, -57 mm)

bottom

-157 mm *410°C*

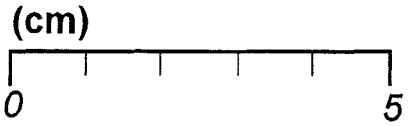

Fig. C9: Horizontal cross sections of bundle CORA-30 (-157 mm)